Symmetry restoration in mean-field approaches

J.A. Sheikh

Cluster University Srinagar,
Jammu and Kashmir,
Srinagar,
190 008,
India

Department of Physics,
University of Kashmir,
Srinagar, 190 006,
India

J. Dobaczewski

Department of Physics,
University of York,
Heslington,
York YO10 5DD,
United Kingdom

Department of Physics,
P.O. Box 35 (YFL),
University of Jyväskylä,
FI-40014 Jyväskylä,
Finland

Institute of Theoretical Physics,
Faculty of Physics,
University of Warsaw,
ul. Pasteura 5,
PL-02-093 Warsaw,
Poland

Helsinki Institute of Physics, P.O. Box 64,
FI-00014 University of Helsinki,
Finland

P. Ring

Physik-Department,
Technische Universität München,
D-85747 Garching,
Germany

State Key Laboratory of Nuclear Physics and Technology,
School of Physics,
Peking University, Beijing 100871,
China

L. M. Robledo

Center for Computational Simulation,
Universidad Politécnica de Madrid,
Campus de Montegancedo,
Boadilla del Monte,
28660-Madrid,
Spain

Departamento de Física Teórica,
Facultad de Física,
Universidad Autónoma de Madrid,
E-28049 Madrid,
Spain

C. Yannouleas

School of Physics,
Georgia Institute of Technology,
Atlanta, Georgia 30332-0430,
USA

The mean-field approximation based on effective interactions or density functionals plays a pivotal role in the description of finite quantum many-body systems that are too large to be treated by ab initio methods. Examples are strongly interacting atomic nuclei and mesoscopic condensed matter systems. In this approach, the linear Schrodinger equation for the exact many-body wave function is mapped onto a non-linear density-dependent one-body potential problem. This approximation, not only provides computationally very simple solutions even for systems with many particles, but due to the non-linearity, it also allows for obtaining solutions that break essential symmetries of the system, often connected with phase transitions. However, mean-field approach suffers from the drawback that the corresponding wave functions do not have sharp quantum numbers and, therefore, many results cannot be compared directly with experimental data. In this article, we discuss general group theoretical techniques to restore the broken symmetries, and provide detailed expressions on the restoration of translational, rotational, spin, isospin, parity and gauge symmetries, where the latter corresponds to the restoration of the particle number. In order to avoid the numerical complexity of exact projection techniques, various approximation methods available in the literature are examined. We present applications of the projection methods to simple nuclear models, realistic calculations in relatively small configuration spaces, nuclear energy density functional theory, as well as in other mesoscopic systems. We also discuss applications of projection techniques to quantum statistics in order to treat the averaging over restricted ensembles with fixed quantum numbers. Further, unresolved problems in the application of the symmetry restoration methods to the energy density functional theories are highlighted.

CONTENTS

I. INTRODUCTION

Mean-field approaches play a central role in the description of quantum many-body problems in areas like quantum chemistry, atomic, molecular, condensed matter and nuclear physics. The simplicity of the associated wave functions, both in the fermion and the boson cases, is the reason behind the popularity of the mean-field approaches. These product-type wave functions allow, on the one hand, an easy implementation of the symmetrization principle of quantum mechanics required for identical particles, and, on the other hand, permit the application of techniques used in the field theory, like the Wick's theorem, which enormously simplify the evaluation of the matrix elements of the many-body operators.

The optimal mean field, generating the single-particle orbitals, is usually determined through the application of the variational principle. In the fermion case, the variational principle, performed in the space of Slater determinants, leads to the familiar Hartree-Fock (HF) method. It is common to find situations where short-range attractive interactions induce correlations leading to the superfluidity or superconductivity phenomena that are well described by the BCS theory. The quasiparticles introduced in the BCS theory can be combined with the concepts of the HF theory to give the Hartree-Fock-Bogoliubov (HFB) mean-field theory, which is widely employed in nuclear physics.

Another facet of the mean-field approach is revealed within the Density Functional Theory (DFT). By using one-body densities as efficient and relevant degrees of freedom, DFT aims to map the exact wave functions of many-body systems onto the product states, which leads to the dynamical equations becoming formally identical to those given by the HF method. Although the foundations and approximations leading to HF and DFT methods are different, the similar structure of dynamical equations allows us to use for both, HF and DFT, the common name of mean-field approach.

One of the most salient characteristics of mean-field approaches is the fact that solutions often spontaneously break symmetries of the Hamiltonian. This is the case,

for instance, in the BCS and HFB theories, where the associated mean-field wave functions, which are the vacua of the corresponding quasiparticle operators, do not represent states with good particle number. The spontaneous symmetry-breaking mechanism provides a way to incorporate nontrivial dynamic correlations on top of the simple Slater determinants, while preserving the simplicity of the mean-field description.

It is the nonlinearity of the mean-field equations that favors the spontaneous symmetry-breaking mechanism, and may constitute the simplest description of the symmetry-breaking effects occurring at a more fundamental level. In this way, the mean-field symmetry breaking leads to interesting perspectives to understand the physics of a given problem. For example, it leads to an easy and efficient description of different collective effects, such as the appearance of rotational bands being the result of the rotational-symmetry breaking, so common in nuclear or molecular physics. Symmetry breaking can also be a useful concept in the presence of stationary degenerate symmetry-conserving states, whereupon the famous Jahn-Teller effect becomes effective.

Nevertheless, advantages of the spontaneous mean-field symmetry breaking come at a price: the resulting wave functions are not invariant or covariant with respect to broken-symmetry groups and, therefore, they cannot be labeled with the symmetry quantum numbers such as angular momentum, parity, etc. This represents a serious drawback if quantities like electromagnetic transition probabilities, with their selection rules, are to be computed. Another drawback of the symmetry-breaking mechanism is connected with sharp transitions observed between the symmetry-conserving and symmetry-breaking solutions, which may occur as a function of some parameters of the Hamiltonian. Such sharp transitions are typical for infinite systems, but cannot characterize finite many-body or mesoscopic systems.

A way to overcome the disadvantages of the symmetry-breaking mean field is to restore the broken symmetries, which is the subject matter of this review article. A general idea of such a restoration is to take linear combinations, properly weighted, of wave functions obtained by applying the elements of the symmetry group to the symmetry-breaking (often called "deformed") mean-field wave function. As a consequence of the symmetry of the Hamiltonian, these "rotated" deformed wave functions are degenerate, and linear combinations, thereof, are expected to have lower energies. In addition, if the weights of the linear combination are chosen according to the rules of group theory, the obtained wave functions become invariant or covariant with respect to the underlying symmetry group and can be labeled with proper quantum numbers. This procedure is denoted in the literature as "symmetry restoration" or "projection". As it leads to linear combinations of product states, it can be understood as introducing correlations beyond the mean-

field approach.

The theory behind the projection method is rooted in group theory as the weights of the linear combination are given by the irreducible representations of the symmetry group. In most of the cases, the symmetry group is a continuous Lie group (rotation, translation, particle number gauge, etc.) while in other cases it is a discrete group (parity).

Once the structure of the projector operator is fixed, two alternatives are available to determine the deformed intrinsic state. The simplest one is to restore the symmetry of the deformed state obtained after solving the HF, HFB, or Kohn-Sham equations. This procedure is called "projection after variation", where variation refers to the minimization of the mean-field energy. Another approach, fully self-consistent and variational, called "variation after projection", determines the deformed state through minimization of the projected energy, separately for each quantum numbers. In this way, different deformed states are obtained for a given quantum number. It turns out that extra flexibility brought in by the variation after projection method is able to smear out the sharp transitions mentioned before.

To compute basic quantities involved in the symmetry restoration, one takes advantage of the generalized Wick's theorem, which allows for calculating matrix elements of operators between mean-field states. This theorem can be applied to projection, because the rotated mean-field states are mean-field states again – they simply correspond to rotated (quasi)particles. This property is a direct consequence of the Thouless theorem, and of the fact that the Lie algebras of the relevant symmetry groups can be represented in terms of one-body operators.

The program to perform the projected calculations can be directly implemented when the problem is defined in terms of a Hamiltonian operator. However, this is not always the case, and in many applications the Hamiltonian is replaced by a density functional in the spirit of the Hohenberg-Kohn or Kohn-Sham approach. In this situation, one is forced to introduce some sort of prescriptions on how to compute the energy kernels. However, these recepies are plagued with conceptual problems that have not been resolved yet in the most general case.

Further, it is also common to use different interactions for each of the three contributions to the energy coming from a two body operator, namely the direct, exchange, and pairing contributions (the most typical case is probably the use of the Slater approximation for the Coulomb exchange contribution and the neglect of the Coulomb antipairing field). In this case, a naive use of the generalized Wick's theorem can lead to spurious contributions and specific ways to deal with this problem have to be devised. These difficulties represent serious impediments for the practical implementation of the symmetry-restoration methods in nuclear physics.

Due to the characteristic features of the nuclear bare interaction, it cannot be directly used in the calculation of a typical nucleus using HF techniques. This fact is a direct consequence of the strong short-range repulsion leading to the so-called "saturation property" of the nuclear interaction, which is at the heart of many basic nuclear properties. Instead of using the bare nuclear interaction one is forced to use "effective interactions" to take into account not only the short-range repulsion but also the effects of Pauli blocking in nuclear medium. Early attempts to derive such effective interactions using nonrelativistic Brueckner-like method failed, and alternative phenomenological effective interactions had to be devised.

As these phenomenological effective interactions usually contain density-dependent terms, the corresponding mean-field approaches are referred to as based on the energy density functionals (EDFs). The main benefit of such approaches is their applicability over the whole periodic chart. Very successful phenomenological effective interactions have been developed over the years with great success in describing the bulk nuclear properties. The success of the EDF methods motivated the introduction of the symmetry restoration (beyond mean field step) aimed to gain access to symmetry-conserving observables and to increase the accuracy of the bulk properties.

The present review article is organized in the following manner. Basic ideas regarding the symmetry breaking and restoration are presented in Sec. II. Section III outlines the general formalism of the symmetry restoration and Sec. IV discusses the applicability of the approximate projection methods. Symmetry restoration methods in simple nuclear models are discussed in Sec. V, nuclear DFT in Sec. VI, and other mesoscopic systems in Sec. VII. A brief description of the projection in statistical approaches is given in Sec. VIII and finally we provide summary and concluding remarks in Sec. IX.

II. SYMMETRY BREAKING IN SIMPLE MODELS

In this Section, we introduce the subject matter of symmetry breaking and restoration by presenting three very simple examples, First, in Sec. II.A, we discuss a solution of a one-particle problem in one dimension, where neither mean-field nor many-body complications appear. Second, in Sec. II.B, we move to a two-particle problem in two dimensions, where one can illustrate the role of the mean-field approximation. And third, in Sec. II.C, we discuss the case of a many-body setting. All three simple models are exactly solvable, which allows us to analyze the problem of symmetry breaking and restoration in the quantum mechanical context and to clearly delineate the role of approximations that unavoidably have to be made in realistic situations.
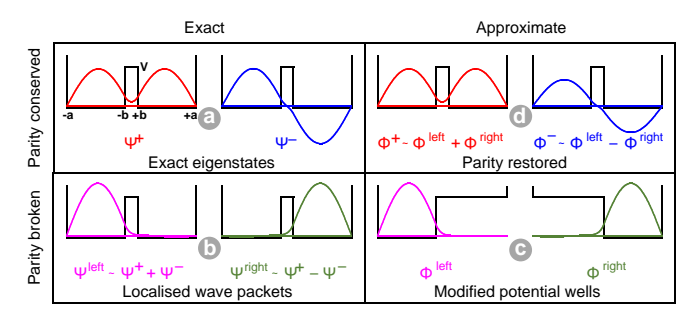
FIG. 1 (Color online) Wave functions of the two lowest eigenstates of a particle moving in the double symmetric potential well. Left (right) panels show exact (approximate) solutions of the Schrödinger equation. Top (bottom) panels show parity-conserving (broken-parity) solutions. The approximate broken-parity wave functions shown in the bottom-right panel are obtained by filling in one of the wells.

A. Doubly symmetric potential well

Consider the doubly symmetric potential well (Sakurai, 1994), that is, a one-dimensional infinite potential well of width $2a$ with a step-like potential barrier of width $2b$ and height V placed in the middle. To link this example to nuclear-physics scales of mass, distance, and energy, let us use the parameters of $\hbar^2/2m = 20\,\mathrm{MeV\,fm^2}$, $a = 10\,\mathrm{fm}$, $b = 1\,\mathrm{fm}$, and $V = 40\,\mathrm{MeV}$. In this model, exact wave functions can be very easily determined; those of the two lowest eigenstates are plotted in Fig. 1(a).

The model is symmetric with respect to the middle of the well, and thus the eigenstates are either symmetric or antisymmetric, $\hat{P}|\Psi^\pm\rangle = \pm|\Psi^\pm\rangle$, where $\hat{P}$ is the inversion operator $x \to -x$. The parameters of the model are chosen in such a way that the two lowest states reside predominantly within the left and right well, and not in the barrier region.

The two lowest eigenstates of opposite parity can be expressed as linear combinations of two localized configurations, that is,

$$|\Psi^\pm\rangle = \tfrac{1}{\sqrt{2}}\left(|\Psi^{\mathrm{left}}\rangle \pm |\Psi^{\mathrm{right}}\rangle\right), \qquad (1)$$

for

$$|\Psi^{\mathrm{left}}\rangle = \tfrac{1}{\sqrt{2}}\left(|\Psi^+\rangle + |\Psi^-\rangle\right), \qquad (2)$$

$$|\Psi^{\mathrm{right}}\rangle = \tfrac{1}{\sqrt{2}}\left(|\Psi^+\rangle - |\Psi^-\rangle\right), \qquad (3)$$

see Fig. 1(b). That is, the localized configurations are wave packets built of the two lowest eigenstates of the system. In these configurations, the particle resides either in the left or in the right well. The four states are pairwise orthogonal, and both, the pair of exact states, $|\Psi^+\rangle$ and $|\Psi^-\rangle$, and that of localized wave packets, $|\Psi^{\mathrm{left}}\rangle$ and $|\Psi^{\mathrm{right}}\rangle$, span the same subspace of the two lowest eigenstates.

It is now very important to realize that by breaking the symmetry of the problem, we can build a very reasonable model of the localized wave packets, see Fig. 1(c).

Indeed, by keeping only the left or right potential well, we obtain the left and right *broken-symmetry* states, $|\Phi^{\mathrm{left}}\rangle$ and $|\Phi^{\mathrm{right}}\rangle$. The broken-symmetry states are the exact eigenstates in the modified potential wells, but at the same time they are approximate eigenstates in the original doubly symmetric potential well. In the scale of Fig. 1, they cannot really be distinguished from the exact wave packets $|\Psi^{\mathrm{left}}\rangle$ and $|\Psi^{\mathrm{right}}\rangle$. Note that $|\Phi^{\mathrm{left}}\rangle$ and $|\Phi^{\mathrm{right}}\rangle$ are stationary in the modified potential wells, whereas we use them to model non-stationary wave packets $|\Psi^{\mathrm{left}}\rangle$ and $|\Psi^{\mathrm{right}}\rangle$ of the original doubly symmetric potential well.

At this point, we arrive at the very heart of the subject matter of this article. Namely, the symmetry-broken solutions, which pertain to a different problem than the original one, can serve us as approximate solutions of the original problem. This is achieved by restoring their symmetry, that is, by considering the symmetric and antisymmetric combinations of $|\Phi^{\mathrm{left}}\rangle$ and $|\Phi^{\mathrm{right}}\rangle$,

$$|\Phi^\pm\rangle = \tfrac{1}{\sqrt{2\pm2\epsilon}}\left(|\Phi^{\mathrm{left}}\rangle \pm |\Phi^{\mathrm{right}}\rangle\right), \qquad (4)$$

see Fig. 1(d), where ϵ is the scalar product of $|\Phi^{\mathrm{left}}\rangle$ and $|\Phi^{\mathrm{right}}\rangle$. Since the inversion transforms the two broken-symmetry states one into another, $\hat{P}|\Phi^{\mathrm{left}}\rangle = |\Phi^{\mathrm{right}}\rangle$ and $\hat{P}|\Phi^{\mathrm{right}}\rangle = |\Phi^{\mathrm{left}}\rangle$, states (4) have correct symmetry properties of $\hat{P}|\Phi^\pm\rangle = \pm|\Phi^\pm\rangle$.

Figure 2 summarizes the logic of the construction presented above and depicts energies of all discussed states. In the left panel, we show how the pair of exact eigenstates, $|\Psi^+\rangle$ and $|\Psi^-\rangle$, is transformed into the pair of exact localized wave packets, $|\Psi^{\mathrm{left}}\rangle$ and $|\Psi^{\mathrm{right}}\rangle$. In our model, the exact eigenstates are split in energy by $\delta E = 75.6\,\mathrm{keV}$, whereas the average energies of both wave packets E^{loc} are, of course, the same and located exactly in the middle between the two eigenenergies,

$$\delta E = E^- - E^+, \qquad E^{\mathrm{loc}} = \tfrac{1}{2}\left(E^+ + E^-\right). \qquad (5)$$

In the right panel of Fig. 2, we show how the pair of approximate localized states, $|\Phi^{\mathrm{left}}\rangle$ and $|\Phi^{\mathrm{right}}\rangle$, is by the symmetry restoration transformed into the pair of approximate eigenstates $|\Phi^+\rangle$ and $|\Phi^-\rangle$. It is gratifying to see that the model energies of approximate localized states $\mathcal{E}^{\mathrm{loc}}$ are only 1.6 keV higher than the average energies of the localized exact wave packets E^{loc} (5). It is even more gratifying to see that energies of the symmetry-restored states,

$$\mathcal{E}^\pm = \frac{\mathcal{E}^{\mathrm{loc}} \pm \Delta}{1 \pm \epsilon}, \qquad (6)$$

are only 1.8 and 1.7 keV above their exact counterparts. These energies depend on the matrix element Δ of the original Hamiltonian between the approximate localized states, $|\Phi^{\mathrm{left}}\rangle$ and $|\Phi^{\mathrm{right}}\rangle$ and on the overlap ϵ between
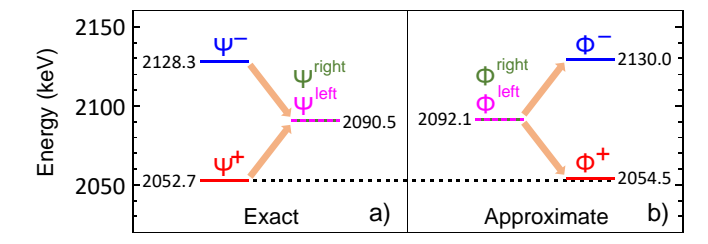
FIG. 2 (Color online) Energies of the exact (left) and approximate (right) states shown in Fig. 1.

them. The energy splitting between the two symmetry-restored states,

$$\delta\mathcal{E} = \mathcal{E}^- - \mathcal{E}^+ = \frac{2\epsilon\mathcal{E}^{\text{loc}} - 2\Delta}{1-\epsilon^2}, \tag{7}$$

which equals 75.5 keV, almost exactly reproduces the exact result.

We should mention at this point that the exact localized wave packets, $|\Psi^{\text{left}}\rangle$ and $|\Psi^{\text{right}}\rangle$, which represent non-stationary solutions of the Schrödinger equation in the doubly symmetric potential well, evolve in time in such a way that after the time of $T = \pi\hbar/\delta E$, the left wave packet will appear on the right-hand side and vice versa. For the selected parameters of the model, this left-right quantum oscillation time is very short, $T \simeq 3 \times 10^{-21}$ s, and thus, a localized particle created in the left or right well will not really keep its identity. However, if the barrier width is increased from 2 to 45 fm, this oscillation time becomes $T \simeq 40$ days, and the particle created in one of the wells would remain there like a classical system would do. In the case of the wide barrier, the approximate localized states, $|\Phi^{\text{left}}\rangle$ and $|\Phi^{\text{right}}\rangle$, become extremely good representations of the localized exact wave packets, and the symmetry restoration becomes an extremely efficient method to obtain perfect approximations of the symmetry-conserving exact eigenstates.

The simple model discussed in this section shows that the symmetry breaking and restoration is a useful concept of describing physical reality of quantum mechanics, and that it is not inherent to complicated many-body systems. Nevertheless, it is for these complicated and difficult systems that it finds its most prominent and successful applications.[1] In particular, in nuclear and molecular physics, there is an overwhelming evidence that symmetry-restored mean-field states provide for a global understanding of multiple phenomena and experimental observations.

At this point, to relate the symmetry restoration to the rigorous DFT (Bartlett, 2010; Becke, 2014; Hohenberg

---

[1] Analyses performed in schematic models can be found, e.g., in (Robledo, 1992; Yannouleas and Landman, 2002a,b).

and Kohn, 1964; Jones, 2015; Kohn and Sham, 1965), a few comments are in order. The basis for existence theorems of exact DFT is the variational principle, whereby one reaches the exact ground-state of the system and its density. Within our simple example above, it would mean that the DFT is bound to yield the exact, symmetry conserving, positive-parity ground-state wave function $\Psi^+(x) = \langle x|\Psi^+\rangle$ and its density $\rho(x) = |\Psi^+(x)|^2$, and not the localized wave functions $\Psi^{\text{left}}(x) = \langle x|\Psi^{\text{left}}\rangle$ or $\Psi^{\text{right}}(x) = \langle x|\Psi^{\text{right}}\rangle$ and their respective densities.

However, it is obvious that densities (be they average or maximum) of exact and localized wave functions differ by about a factor of two, compare Figs. 1(a) and (b). This simple observation creates an important issue for systems, like nuclei, for which the equilibrium local density (the so-called saturation density of about $0.16\,\text{fm}^{-3}$) is an important physical parameter determined by the nature of the underlying interaction. Indeed, for such systems we build (or derive) functionals that describe infinite saturated systems, which leads to the local density approximation, or finite self-bound systems, within a single potential well (typical for a drop of matter). Such functionals then have minimum energies at saturation density and thus can properly work only for localized wave functions and not for the exact symmetry-conserving ones.

To bring the discussion above away from the simple example, which we introduced only to illustrate basic concepts, and towards a realistic case, consider a positive-parity ground state of an alpha-particle emitting nucleus. Before the decay, the density of nucleons is almost constant within the nucleus and equal to the saturation density. After the decay, the exact parity-conserving wave function would correspond to a symmetric combination of a recoil nucleus moving right, with the alpha particle moving left, and that of the recoil moving left and the alpha moving right. It is obvious that such a state cannot be modelled by the same density functional as that used to model the nucleus before the decay, because densities are now twice smaller than the saturation density. However, it is also obvious that a symmetry-broken state, e.g., the one with the recoil moving left and alpha moving right, is entirely within the remit of that functional, because both subsystems do have similar local densities, not very different from the saturation density.

The case of the alpha-emitting nucleus illustrates crucial points of nuclear DFT, whereupon the symmetry breaking plays a fundamental role. It also tells us that the symmetry restoration is an equally fundamental piece of the description. Indeed, after modelling the DFT state of the recoil moving left and alpha moving right, we must symmetrize the obtained solution, because the alpha-particle detectors will, of course, never see any left-right asymmetry of the decay process. In this sense, the DFT description of many-body systems gives us immediate access to physical localized states describing specific

configurations, by which we mean specific arrangements of constituents of composite objects. However, it is now clear that these configurations should never be confused with exact eigenstates, as they simply represent specific wave packets thereof, whereas a reasonable modeling of the exact eigenstates is then accessible via the symmetry restoration.

There remains, nevertheless, one troubling element of the link between the DFT and symmetry restoration. Indeed, to restore the symmetry, we need to have access not only to the average energies of the localized broken-symmetry states $|\Phi^{\text{left}}\rangle$ or $|\Phi^{\text{right}}\rangle$, which are within the remit of DFT, but also to the overlaps, $\epsilon = \langle \Phi^{\text{left}}|\Phi^{\text{right}}\rangle$, and matrix elements, $\Delta = \langle \Phi^{\text{left}}|\hat{H}|\Phi^{\text{right}}\rangle$, thereof, neither of which is. Within the nuclear-DFT applications, there is an overwhelming evidence that ϵ and Δ can be evaluated using the corresponding Kohn-Sham states and generalized Wick's theorem, see Appendix A. This gives us a rich and reasonable description of numerous experimental data. However, such an approach constitutes a hybrid mix of the DFT and wave-function approaches and, to our knowledge, it has as yet no justification in any solid formalism. It appears that the many-body-physics community has executed a spectacular triple Axle jump into a pool without really verifying whether the water is there or not. Nevertheless, the obtained excellent results indicate that we may rather worry about finding a justification than about questioning the method itself.

The reader is begged to excuse us for partly simplistic and partly philosophical narrative of this introductory section. We thought that exposing these basic notions could constitute a useful background of the following sections, where we move right on to the forefront description pertaining to the subject matter of this review. However, the advanced discussion that is coming up should not obscure the vision of the forest behind trees.

B. Dissociation of the natural molecular hydrogen and other similar 2D artificial dimers

The dissociation of the natural Hydrogen molecule H_2 is a well-known example that illustrates the symmetry dilemma facing the mean-field approach, namely, the fact that the restricted Hartree Fock (RHF), see Sec. VII, provides wave functions that conserve the symmetries of the many-body Hamiltonian, but the corresponding total energy is higher than that of the unrestricted Hartree Fock (UHF). The UHF lowers the total energy by breaking the symmetries of total spin and parity with respect to the dissociation axis. However, the resulting UHF wave function does not preserve the required symmetries.

The dissociation of H_2 in both the RHF and the UHF level and the correct-symmetry/higher-energy versus lower-energy/wrong-symmetry dilemma have been described in detail in Ch. 3.8.7. of (Szabo and Ostlund,

1989). It is remarkable that the total energy of the wrong-symmetry UHF solution is twice the energy of each separated atom as expected on grounds of physical intuition.

As illustrated in (Yannouleas and Landman, 2001, 2002a,b) for two electrons trapped in a two-dimensional quantum dot molecule (an artificial system denoted as H_2-QDM), the symmetry dilemma can be overcome by using symmetry restoration. The H_2-QDM system consists of two electrons trapped inside two parabolic quantum dots (each with a harmonic-potential confinement specified by a frequency $\hbar\omega_0$) separated by a distance d and interdot barrier V_b. A large value of V_b suppresses the tunneling between the dots and mimics an increase in the separation distance d.

Figure 3 displays the RHF and UHF results for the singlet state, and for the interdot distance of $d = 30$ nm and barrier of $V_b = 4.95$ meV. In the RHF (Fig. 3, left), both the spin-up and spin-down electrons occupy the same bonding (σ_g) molecular orbital. In contrast, in the UHF result the spin-up electron occupies an optimized $1s$ (or $1s_L$) atomic-like orbital in the left quantum dot, while the spin down electron occupies the corresponding $1s'$ (or $1s_R$) atomic-like orbital in the right quantum dot. Concerning the total energies, the RHF yields $E_{\text{RHF}} = 13.68$ meV, while the UHF energy is $E_{\text{UHF}} = 12.83$ meV representing a gain in energy of 0.85 meV. Since the energy of the triplet is $E_{\text{UHF}} = 13.01$ meV, the singlet conforms to the requirement that for two electrons at zero magnetic field the singlet is always the ground state; on the other hand the RHF molecular-orbital solution fails in this respect.

To make further progress, we utilize the spin projection technique to restore the broken symmetry of the UHF determinant,

$$\sqrt{2}\Psi_{\text{UHF}}(1,2) = \begin{vmatrix} u(\mathbf{r}_1)\alpha(1) & v(\mathbf{r}_1)\beta(1) \\ u(\mathbf{r}_2)\alpha(2) & v(\mathbf{r}_2)\beta(2) \end{vmatrix}$$
$$\equiv |u(1)\bar{v}(2)\rangle, \qquad (8)$$

where $u(\mathbf{r})$ and $v(\mathbf{r})$ are the $1s$ (left) and $1s'$ (right) localized orbitals of the UHF solution displayed in the right column of Fig. 3; α and β denote the up and down spins, respectively. In Eq. (8) we also define a compact notation for the Ψ_{UHF} determinant, where a bar over a space orbital denotes a spin-down electron; absence of a bar denotes a spin-up electron.

$\Psi_{\text{UHF}}(1,2)$ is an eigenstate of the projection S_z of the total spin $\mathbf{S} = \mathbf{s}_1 + \mathbf{s}_2$, but not of $\mathbf{S}^2$. One can generate a many-body wave function which is an eigenstate of S^2 with eigenvalue $s(s+1)$ by applying the projection operator defined in Sec. VII.G below, i.e.,

$$\mathcal{P}_{\text{spin}}^{s,t} = 1 \mp \varpi_{12} , \qquad (9)$$

where the operator ϖ_{12} interchanges the spins of the two electrons, provided that their spins are different
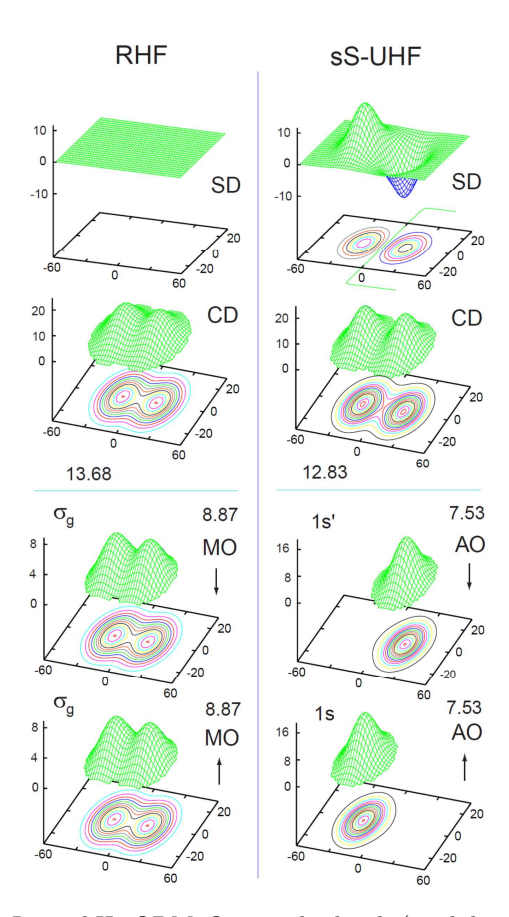
FIG. 3 Lateral H_2-QDM: Occupied orbitals (modulus square, bottom half), spin densities (SD, difference of partial spin-up and spin-down densities, top row), and total charge densities (CD, sum of spin-up and spin-down densities, second row) for the spin unpolarized case. Left column: Restricted Hartree-Fock (RHF) results. Right column: spin and space unrestricted Hartree-Fock (sS-UHF) results exhibiting a breaking of the space symmetry (parity). The numbers displayed with each orbital are their eigenenergies in meV, while the up and down arrows indicate an electron with an up or down spin. The RHF orbitals are delocalized and extend over both quantum dots; they are denoted as molecular orbitals (MO). The UHF orbitals are localized on one quantum dot (either left or right), and are denoted as atomic orbitals (AO). The numbers displayed with the charge densities are the total energies in meV. Distances along the x and y axes are in nm and the electron densities are in 10^{-4} nm^{-2}. The choice of parameters is: effective mass of the electron $m^* = 0.067m_e$ (m_e is the free-electron mass), trapping frequency for each quantum dot $\hbar\omega_0 = 5$ meV, interdot separation $d = 30$ nm, interdot barrier $V_b = 4.95$ meV, and material dielectric constant $\kappa = 20$. [Reprinted with permission from (Yannouleas and Landman, 2001)].

The singlet state of two electrons (with $s = 0$) is approximated as follows:

$$\sqrt{2}\mathcal{P}^s_{\text{spin}}\Psi_{\text{UHF}}(1,2) = (1 - \varpi_{12})\sqrt{2}\Psi_{\text{UHF}}(1,2)$$
$$= |u(1)\bar{v}(2)\rangle - |\bar{u}(1)v(2)\rangle. \quad (10)$$

In contrast to the single-determinant wave functions of the RHF and UHF methods, the projected many-body

wave function (10) is a linear superposition of two Slater determinants, and thus represents a corrective step beyond the mean-field approximation.

Expanding the determinants in Eq. (10), one finds the equivalent expression

$$\sqrt{2}\mathcal{P}^s_{\text{spin}}\Psi_{\text{UHF}}(1,2) = (u(\mathbf{r}_1)v(\mathbf{r}_2) + u(\mathbf{r}_2)v(\mathbf{r}_1))\chi(0,0) , \quad (11)$$

where the spin eigenfunction for the singlet is given by

$$\chi(s = 0, S_z = 0) = (\alpha(1)\beta(2) - \alpha(2)\beta(1))/\sqrt{2} . \quad (12)$$

Eq. (11) has the form of a Heitler-London (Heitler and London, 1927) or valence bond wave function. However, unlike the Heitler-London scheme which uses the orbitals $\phi_L(\mathbf{r})$ and $\phi_R(\mathbf{r})$ of the separated (left and right) atoms, expression (11) employs the UHF orbitals which are self-consistently optimized for any separation d and potential barrier height V_b. As a result, expression (11) can be characterized as a generalized-valence-bond wave function. Taking into account the normalization of the spatial part, we arrive at the following improved wave function for the singlet state exhibiting all the symmetries of the original many-body hamiltonian,

$$\Psi^s_{GVB}(1,2) = N_+\mathcal{P}^s_{\text{spin}}\Psi_{\text{UHF}}(1,2)/\sqrt{2} , \quad (13)$$

where the normalization constant is given by

$$N_+ = 1/\sqrt{1 + S^2_{uv}} , \quad (14)$$

S_{uv} being the overlap integral of the $u(\mathbf{r})$ and $v(\mathbf{r})$ orbitals,

$$S_{uv} = \int u(\mathbf{r})v(\mathbf{r})d\mathbf{r} . \quad (15)$$

The total energy of the generalized-valence-bond state is given by

$$E^s_{GVB} = N^2_+[h_{uu} + h_{vv} + 2S_{uv}h_{uv} + J_{uv} + K_{uv}] , \quad (16)$$

where h is the single-particle part of the total hamiltonian defined in Sec. VII.B, and J and K are the direct and exchange matrix elements associated with the $e - e$ repulsion $e^2/\kappa r_{12}$, where κ is the material dielectric constant. For comparison, we give also here the corresponding expression for the HF total energy either in the RHF ($v = u$) or UHF case,

$$E^s_{HF} = h_{uu} + h_{vv} + J_{uv} . \quad (17)$$

For the triplet, the projected wave function coincides with the original HF determinant, so that the corresponding energies in all three approximation levels are equal, i.e., $E^t_{GVB} = E^t_{RHF} = E^t_{UHF}$.

A major test for the suitability of different methods is their ability to properly describe the dissociation limit
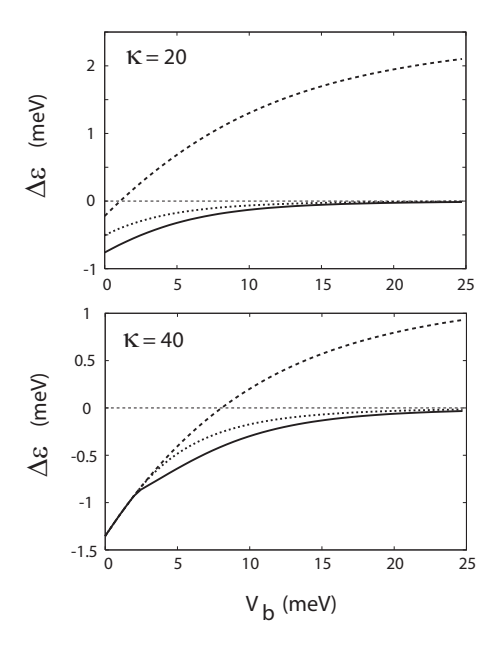
FIG. 4 Lateral H_2-QDM: The energy difference between the singlet and triplet states according to the RHF (molecular-orbital theory, top line), the UHF (broken symmetry, middle line), and the generalized-valence-bond approach (Projection Method, bottom line) as a function of the interdot barrier V_b. For $V_b = 25$ meV complete dissociation has been clearly reached. Top frame: dielectric constant $\kappa = 20$. Bottom frame: dielectric constant $\kappa = 40$. The choice of the remaining parameters is: electron effective mass $m^* = 0.067 m_e$, trapping frequency $\hbar\omega_0 = 5$ meV, and interdot distance $d = 30$ nm. [Reprinted with permission from (Yannouleas and Landman, 2001)].

of the molecule. The H_2-QDM dissociates into two non-interacting quantum-dot hydrogen atoms with arbitrary spin orientation. As a result, the energy difference, $\Delta\varepsilon = E^s - E^t$, between the singlet and the triplet states of the molecule must approach the zero value from below as the molecule dissociates. To theoretically generate such a dissociation process, we keep the separation d constant and vary the height of the interdot barrier V_b; an increase in the value of V_b reduces the coupling between the individual dots and for sufficiently high values we can always reach complete dissociation.

Figure 4 displays the evolution in zero magnetic field of $\Delta\varepsilon$ as a function of V_b and for all three approximation levels, i.e., the RHF (molecular-orbital theory, top line), the UHF (middle line), and the generalized-valence-bond approach (bottom line). The interdot distance is the same as in Fig. 3, i.e., $d = 30$; the case of $\kappa = 20$ is shown at the top panel, while the case of a weaker $e - e$ repulsion is displayed for $\kappa = 40$ at the bottom panel.

First we observe that the molecular-orbital approach fails to describe the dissociation of the H_2-QDM, since it predicts a strongly stabilized ferromagnetic ordering in contradiction to the expected singlet-triplet degeneracy upon full separation of the individual dots. The sec-

ond observation is that both the UHF and generalized-valence-bond solutions describe the energetics of the dissociation limit ($\Delta\varepsilon \to 0$ for $V_b \to \infty$) rather well. In particular, in both the UHF and generalized-valence-bond methods, the singlet state remains the ground state for all values of the interdot barrier. Between the two singlets, the generalized-valence-bond one is always the lowest, As a result, the generalized-valence-bond method presents an improvement over the UHF method both at the level of symmetry preservation and at the level of energetics.

C. The seniority model

So far we discussed symmetry breaking and restoration for one or two particles. However, an essential point of the symmetry breaking discussed in this article is the approximate treatment of correlations in a many-body system by introducing the mean-field approximation, that is, by describing the many-body system in terms of a product state $|\Phi\rangle$ of uncorrelated particles (or quasi-particles) moving in a single-particle potential with a broken symmetry. To elaborate this aspect in more detail, we now briefly discuss the seniority model introduced by Kerman (Kerman, 1961) as an example. We consider N fermions in a degenerate single j-shell (with $\Omega = j + \frac{1}{2}$) interacting through a monopole paring force with the corresponding many-body Hamiltonian $\hat{H}$,

$$\hat{H} = -G\hat{S}_+\hat{S}_-, \tag{18}$$

where G is the strength of the interaction and operator $\hat{S}_+$,

$$\hat{S}_+ = (\hat{S}_-)^\dagger = \sqrt{\frac{\Omega}{2}}[a^\dagger a^\dagger]_{J=0}, \tag{19}$$

creates a Cooper-pair of particles coupled to angular momentum $J = 0$. Together with the operator $\hat{S}_0$ connected with the particle number operator $\hat{N}$ by the relation

$$\hat{S}_0 = \frac{1}{2}(\hat{N} - \Omega), \tag{20}$$

operators $\hat{S}_+, \hat{S}_0$, and $\hat{S}_-$ form the algebra of the group $SU(2)$ of the quasi-spin. It has the Casimir operator $\hat{\mathbf{S}}^2$,

$$\hat{\mathbf{S}}^2 = \hat{S}_+\hat{S}_- + \hat{S}_0^2 - \hat{S}_0, \tag{21}$$

with the eigenvalue $S(S + 1)$. Hamiltonian (18) can be expressed as

$$\hat{H} = -G(\hat{\mathbf{S}}^2 - \hat{S}_0^2 + \hat{S}_0), \tag{22}$$

and thus it is diagonal in the basis characterized by the quantum numbers S, S_0 or S, N. The particle vacuum $|-\rangle$ with $N = 0$ is given by $S = \frac{\Omega}{2}$ and $S_0 = -\frac{\Omega}{2}$. Starting from this vacuum $|-\rangle$, and applying the raising operator

$\hat{S}_+$, one finds the exact ground states of the system with even particle numbers N (Hara, 1967),

$$|\frac{\Omega}{2}, N\rangle \propto \hat{S}_+^{N/2}|-\rangle. \tag{23}$$

This is a condensate of $n = \frac{N}{2}$ Cooper pairs. In terms of the original fermions this is a highly correlated state.

We now use the mean-field approximation for the operator (18) and find the BCS Hamiltonian,

$$\hat{H}_{BCS} = -\Delta(\hat{S}_+ + \hat{S}_-), \tag{24}$$

with $\Delta = G\langle\Phi|S_+|\Phi\rangle$, where $|\Phi\rangle$ is a BCS-state, that is, the eigenstate of $\hat{H}_{BCS}$. It has a form of a generalized product state,

$$|\Phi\rangle = \prod_{m>0}(u_m + v_m a_{jm}^\dagger a_{j\bar{m}}^\dagger)|-\rangle \propto \prod_m \alpha_{jm}|-\rangle, \tag{25}$$

which is a quasiparticle vacuum for the quasiparticle operators $\alpha_{jm}^\dagger = u_m a_{jm}^\dagger - v_m a_{j\bar{m}}$ determined by the diagonalization of the mean-field Hamiltonian $\hat{H}_{BCS}$.

It is evident that $\hat{H}_{BCS}$ breaks the particle-number symmetry; therefore one looks for eigenfunctions of $\hat{H}'_{BCS} = \hat{H}_{BCS} - \lambda\hat{N}$, where the Lagrange parameter λ is determined by the subsidiary condition $\langle\Phi|\hat{N}|\Phi\rangle = N$. Since the BCS Hamiltonian depends on the gap parameter Δ, one ends up with is a non-linear problem, which has to be solved iteratively. In the seniority model discussed here, the single-particle part ($\sim a^\dagger a$) of $\hat{H}_{BCS}$ vanishes and thus does not depend on the quantum number m, and hence the BCS amplitudes u_m and v_m do not depend on m either.

The BCS Hamiltonian $\hat{H}_{BCS}$ breaks the particle-number symmetry, and so it also breaks the gauge symmetry, which is defined as the rotation in the gauge space given by the operator $\hat{R}(\varphi)$,

$$\hat{R}(\varphi) = \exp(-i\varphi\hat{N}). \tag{26}$$

Through this symmetry breaking, it is possible to represent the wave function as a product state in terms of quasiparticles. In the exact solution, these quasiparticles are not independent and there are additional correlations, which are not taken into account in the product state. However, we can bring these correlations back by the restoration of the symmetry. This is achieved by the particle-number projection, that is, by neglecting in the wave function $|\Phi\rangle$ all the contributions with particle numbers different from N. For this purpose we express the BCS state $|\Phi\rangle$ (25) in terms of the operator $\hat{S}_+$ as

$$|\Phi\rangle \propto \exp(\frac{v}{u}\sum_{m>0} a_m^\dagger a_{\bar{m}}^\dagger)|-\rangle \propto \exp(\frac{v}{u}\hat{S}_+)|-\rangle, \tag{27}$$

and the particle-number projection then leads to

$$P^N|\Phi\rangle \propto \hat{S}_+^{N/2}|-\rangle. \tag{28}$$

We find that the restoration of the symmetry leads to the exact solution (23) of the system. Of course, this is a very specific model and the fact, that symmetry restoration brings us back to the exact solution, depends definitely on the fact, that the operator $\hat{S}_+$ does not depend on the particle number nor on other properties of the model such as the strength parameter G. Nonetheless, also in more general cases, where the symmetry restoration does not lead to the exact solution, we will find that by restoring symmetries, one can improve the mean-field approximation considerably.

III. SYMMETRY RESTORATION - GENERAL FORMALISM

As discussed in the previous section, mean-field solutions may break symmetries that the original many-body Hamiltonian obeys. For strong symmetry breaking, approximate methods can be used to restore the broken symmetries, and these are discussed in Sec. IV. For weak symmetry breaking, wave functions defined in the intrinsic frame of reference should have their broken symmetries restored. In the sixties and seventies of the last century, considerable efforts were made to decouple the total Hamiltonian in terms of intrinsic and collective degrees of freedom. As we discuss below, owing to the Galilean invariance, this method works well for the simplest case of the linear-momentum, but the technique becomes quite cumbersome for the restoration of other symmetries.

Moreover, the popular terminology referring to the intrinsic and laboratory reference frames can be either confusing, or useless, or both. Indeed, in the language of the symmetry restoration, no reference frame is ever changed, namely, both the broken-symmetry and restored-symmetry wave functions reside in the same unique Hilbert space with one unique reference frame conveniently predefined and used. Then, the restored-symmetry wave function is obtained from the broken-symmetry one by acting on it with a specific symmetry-restoration operator, which does not change any reference frame either, but rather rotates the broken-symmetry wave function in the predefined reference frame.

In this article we use the notion of an *active* rotation, whereby not the reference frame but states and operators are rotated. However, even if we used a *passive* rotation scheme, whereby the wave function stays the same and the reference frame is rotated, this would not have been equivalent to any change of the reference frame from intrinsic to laboratory. Although we may occasionally slip into the traditional terminology of the intrinsic and laboratory frames, but the reader should always follow the correct description by translating the term "wave function in the intrinsic (laboratory) frame" as "broken-symmetry (restored-symmetry) wave function".

Symmetry breaking leads to an ambiguity in the solution of the variational problem. For a continuous symme-

try group, an infinite number of solutions, obtained by applying the generators of the Lie group on the intrinsic state, have the same expectation value of the energy. For instance, all Nilsson intrinsic states that differ only by rotation in space have the same energy. Peierls and Yoccoz (Peierls and Yoccoz, 1957) employed a linear superposition of these degenerate wave functions with the weight functions determined through a second variational procedure. In the first variational problem, the intrinsic wave function is determined and in the second a subspace of the first is constructed which is invariant under the symmetry group due to its very construction. Since the two variations are performed independent of one another, this double variational approach, which is referred to as projection after variation, is inconsistent with the full variational approach.

Indeed, for a robust treatment of the symmetry breaking by including correlations going beyond the mean-field approach, the variational principle is employed by considering the trial wave function only from the subspace corresponding to the symmetry eigenvalue. In the case of rotational symmetry this corresponds to first projecting the intrinsic wave function onto a state with well-defined angular-momentum and then performing the variational procedure. This variation after projection method, proposed originally by Zeh (Zeh, 1965), can be shown to lead to practically exact results for a degenerate model (Sheikh and Ring, 2000). The difference between the two approaches becomes quite obvious for the case of particle permutational symmetry, with the method of Peierls and Yoccoz giving rise to an approximate antisymmetrized Hartree solution, while the method of Zeh leading to the correct HF solution.

Projection methods developed to restore the symmetries can be divided into those pertaining to abelian and non-abelian symmetry groups (Ring and Schuck, 1980). Restoration of the linear-momentum symmetry, gauge symmetry associated with the particle number, and parity symmetry pertain to the abelian groups. For this class, projection operators have expected mathematical properties of idempotency and hermiticity. For the class of non-abelian symmetry groups, which includes three-dimensional rotation, and corresponds to restoration of angular-momentum or isospin, the projection operators do not have properties of idempotency and hermiticity. However, as we discuss below, such operators project out the relevant quantum numbers from the intrinsic wave function, and that is what is important from physical considerations.

In the following, we first construct the projection operators using the group theoretical and generator coordinate methods. As is evident, all the projection operators can be expressed as basis transformations in some representation. Projection methods for various symmetries, such as linear-momentum, three-dimensional angular-momentum, particle number, and parity are discussed in

Sec. III.B. For the simplest case of linear-momentum, it is shown that the method of redundant variables can be employed to separate out the intrinsic and the collective motion (center of mass). It is further shown that for the non-abelian three-dimensional angular-momentum case, the operator is not a true projection operator in the mathematical sense, but it projects out the angular-momentum quantum numbers. The projection operators for particle number and for discrete parity symmetry are also briefly discussed in this section.

The projection formalism using the generalized HFB basis is discussed in Sec. III.C. In this section, the expressions for the norm and the Hamiltonian kernels between the HFB transformed and the initial basis are obtained using the generalized Wick's theorem, see Appendix A. Methods for performing variation after projection are then discussed in this section. In particular, it is demonstrated that variation after projection of an arbitrary symmetry-projected energy leads to the HFB equations, as is the case for the unprojected energy, with the only difference that the pairing and HF fields get modified and depend on the projected quantum numbers as well.

A. Projection Operator - Mathematical Basis

The mathematical structure of the projection operators is constructed in this subsection using the group theoretical approach and the generator coordinate method.

1. Group Theoretical Approach

A projection operator, $\hat{P}^\mu$ can be constructed such that for an arbitrary wave function $|\Psi\rangle$, $\hat{P}^\mu|\Psi\rangle$ is the component of $|\Psi\rangle$ in the irreducible subspace μ. In the following, we construct the mathematical structure of such an operator using the group theoretical approach and closely follow the textbook of Hamermesh (Hamermesh, 1962).

Let us suppose that $\{|\Psi^\mu\rangle\}$ span an irreducible subspace, transforming according to the irreducible representation μ of the group transformations $\{\hat{R}(g)\}$, i.e.,

$$\hat{R}(g) |\Psi_j^\mu\rangle = \sum_i |\Psi_i^\mu\rangle \ D_{ij}^\mu(g), \qquad (29)$$

where g denotes the group element. The matrix functions $D_{ij}^\mu(g)$ are the continuous single-valued representations of the group, which for the group of three-dimensional rotations are called Wigner D-functions (Edmonds, 1957; Varshalovich et al., 1988). The functions $D_{ij}^\mu(g)$ obey the orthogonality theorem of representation theory

$$\sum_g D_{i'j'}^{\mu'\,*}(g) \ D_{ij}^\mu(g) = \frac{V}{n_\mu}\delta_{\mu\mu'} \ \delta_{ii'} \ \delta_{jj'}, \qquad (30)$$

where n_μ denotes the dimension of the irreducible representation. For finite groups, V is the order of the group and the sum in (30) runs over all group elements, whereas for continuous groups, V is the volume of the parameter space of the group, and the sum over the group elements should be replaced by an integral over the group parameters.

Multiplying equation (29) by $D_{i'j'}^{\mu'*}(g)$ and summing over the group elements, we have

$$\sum_g D_{i'j'}^{\mu'*}(g) \; \hat{R}(g) \; |\Psi_j^\mu\rangle = \delta_{\mu\mu'} \; \delta_{jj'} \frac{V}{n_\mu} |\Psi_i^\mu\rangle \; . \qquad (31)$$

This allows us to define operators $\hat{P}_{ij}^\mu$,

$$\hat{P}_{ij}^\mu = \frac{n_\mu}{V} \sum_g D_{ij}^{\mu*}(g) \; \hat{R}(g), \qquad (32)$$

such that

$$\hat{P}_{ij}^\mu \; |\Psi_{j'}^{\mu'}\rangle = \delta_{\mu\mu'} \; \delta_{jj'} \; |\Psi_i^\mu\rangle \qquad (33)$$

and

$$\hat{P}_{ij}^\mu \hat{P}_{i'j'}^{\mu'} = \delta_{\mu\mu'} \; \delta_{ji'} \; \hat{P}_{ij'}^\mu, \qquad \left(\hat{P}_{ij}^\mu\right)^\dagger = \hat{P}_{ji}^\mu. \qquad (34)$$

It is evident from the above equation that the diagonal operators, $\hat{P}_i^\mu = \hat{P}_{ii}^\mu$, project out the i-th columns of the μ-th irreducible representation, and obey

$$\hat{P}_i^\mu \; \hat{P}_j^{\mu'} = \delta_{\mu\mu'} \; \delta_{ij} \; \hat{P}_i^\mu. \qquad (35)$$

It means that they are hermitian and idempotent, i.e., projection operators in the strict mathematical sense.

However, from physical considerations, these operators are only useful in the case of abelian groups, where all the matrices in the representation characterized by μ commute. For non-abelian groups, the wave functions $\hat{P}_i^\mu|\Psi\rangle$ are no longer tensors with respect to this group, i.e., under the operation $\hat{R}(g)$ they do not behave as wave functions $|\Psi_i^\mu\rangle$ shown in Eq. (29). In the following sections, we will see how this problem is solved through introducing the generalized projection operators $\hat{P}_{ij}^\mu$ of Eq. (32), which are not projection operators in the strict mathematical sense.

The derivation of projection operators was here presented for finite groups. As already mentioned above, for continuous Lie groups, the finite set of operators is replaced by a set of operators depending on continuous parameters. Then, the summation over the group elements in Eq. (31) is replaced by integration over these continuously varying parameters. For a compact Lie group, the domain over which these continuous parameters vary has a finite volume V in Eq. (32). For the case of the rotational group in three dimensions, where the group elements depend on three Euler angles $\Omega = (\alpha, \beta, \gamma)$, the volume is $V = \int d\Omega = 8\pi^2$ and the dimension of the representation characterized by the angular momentum $\mu = I$ is $n_\mu = 2I + 1$.

2. Generator Coordinate Method

The expression for the projection operator can also be obtained as a special case of the generator coordinate method (Hill and Wheeler, 1953; Ring and Schuck, 1980). In this method, the many-body Hamiltonian is diagonalized in a subspace spanned by a set of generating functions $|\Phi(\Omega)\rangle$, parametrized with the generator coordinate Ω. A generalization to a multidimensional space of generator coordinates is possible, but in what follows we consider only one dimension.

For a symmetry-breaking wave function $|\Phi\rangle$, we can construct the set $|\Phi(\Omega)\rangle$ by transforming it with the symmetry operator $\hat{R}(\Omega) \equiv \hat{R}(g(\Omega))$, where Ω parametrizes the continuous-group elements g. For different values of Ω, the transformed wave functions

$$|\Phi(\Omega)\rangle = \hat{R}(\Omega)|\Phi\rangle, \qquad (36)$$

have the same energy expectation values. Peierls and Yoccoz (Peierls and Yoccoz, 1957) employed these rotated states as the generating wave function in the generator-coordinate-method technique, i.e., considering the ansatz

$$|\Psi\rangle = \int d\Omega \; f(\Omega) \; |\Phi(\Omega)\rangle. \qquad (37)$$

Variation of the energy expectation value with respect to the weight function $f(\Omega)$ leads to the diagonalization of the Hamiltonian with the generating functions as nonorthogonal basis states. To restore the symmetry, the weight function is chosen in such a way that the resulting many-body wave function transforms as in Eq. (29). It can be shown that the collective subspace is invariant under the symmetry transformation, i.e.,

$$\hat{R}(\Omega)|\Psi\rangle = \int d\Omega' \; f(-\Omega + \Omega') \; |\Phi(\Omega')\rangle. \qquad (38)$$

where $(-\Omega + \Omega')$ is a short hand notation for the group element $\hat{R}^{-1}(\Omega)\hat{R}(\Omega')$. This implies that the projector $\hat{P}$ onto this subspace commutes with the symmetry operator $\hat{R}(\Omega)$ and it is possible to find simultaneous eigenstates of $\hat{P}\hat{H}\hat{P}$ and the symmetry operator. Thus, a function $f(\Omega)$ exists that not only minimizes the energy but also has the proper symmetry.

Function $f(\Omega)$ can be found by expanding it in terms of the representations of the group, characterized by eigenvalues of the Casimir operators. For abelian groups, the situation is particularly simple. For the one-dimensional case, discussed here, we concentrate on the example corresponding to the one-dimensional rotation around the z-axis, where Ω represents the angle of rotation, i.e.,

$$\hat{R}(\Omega)|\Phi\rangle = e^{-i\Omega\hat{J}_z}|\Phi\rangle. \qquad (39)$$

The irreducible representations of this group are one-dimensional and given by

$$D^M(\Omega) = e^{-iM\Omega}. \qquad (40)$$

Therefore expressing the weight function $f(\Omega)$ in terms of these irreducible representations corresponds to a Fourier transformation

$$f(\Omega) = \sum_M g_M D^{M*}(\Omega) = \sum_M g_M e^{iM\Omega}. \qquad (41)$$

Using the M-th component $D^{M*}(\Omega)$ as the generator-coordinate weight function in Eq. (37) we obtain in agreement with the ansatz (32)

$$\begin{aligned}
|\Psi^M\rangle &= \frac{1}{2\pi} \int_0^{2\pi} d\Omega D^{M*}(\Omega) e^{-i\Omega \hat{J}_z} |\Phi\rangle \\
&= \frac{1}{2\pi} \int_0^{2\pi} d\Omega e^{-i\Omega(\hat{J}_z - M)} |\Phi\rangle \\
&= \delta(\hat{J}_z - M) |\Phi\rangle = \hat{P}^M |\Phi\rangle.
\end{aligned} \qquad (42)$$

with the projector

$$\hat{P}^M = \frac{1}{2\pi} \int_0^{2\pi} d\Omega \ e^{-i\Omega(\hat{J}_z - M)}. \qquad (43)$$

As we see, the generator-coordinate-method result is in full agreement with the general expression for the projection operator derived in the previous subsection from group theoretical considerations.

B. Projection Methods For Various Symmetries

1. Linear Momentum

In the shell model approach, localized single-particle states are employed that are not eigenstates of the momentum operator. Conversely, the plane waves that are eigenstates of the momentum operator cannot describe a localized system of particles. In the following, we describe the Peierls-Yoccoz method (Peierls and Yoccoz, 1957) for projection of the linear-momentum eigenstates from the shell-model wave function.

Let us consider the operator $\hat{\mathbf{P}} = \sum_i \mathbf{p_i}$ of the total momentum and $|\mathbf{K}\rangle$ its eigenstate, $\hat{\mathbf{P}}|\mathbf{K}\rangle = \mathbf{K}|\mathbf{K}\rangle$, with the normalization condition, $\langle \mathbf{K}'|\mathbf{K}\rangle = \delta^3(\mathbf{K}' - \mathbf{K})$. Having in mind, that the operator

$$e^{-i\mathbf{a}\hat{\mathbf{P}}}\Phi(\mathbf{r}_1, \ldots, \mathbf{r}_A) = \Phi(\mathbf{r}_1 - \mathbf{a}, \ldots, \mathbf{r}_A - \mathbf{a})$$

produces a translation of the many-body wave function by the amount $\mathbf{a}$, it is evident that

$$\hat{P}_{\mathbf{K}} = \frac{1}{(2\pi)^3} \int d^3a \ e^{-i\mathbf{a}(\hat{\mathbf{P}} - \mathbf{K})} = \delta^3(\hat{\mathbf{P}} - \mathbf{K}), \qquad (44)$$

projects out the state with a definite value of the momentum $\mathbf{K}$. Let us consider an arbitrary wave function, $|\Phi\rangle$

which is expanded in terms of the momentum eigenstates as

$$|\Phi\rangle = \int d^3K \ \phi_{\mathbf{K}} |\mathbf{K}\rangle \quad . \qquad (45)$$

It can be easily shown that

$$\hat{\mathbf{P}}_{\mathbf{K}}|\Phi\rangle = |\mathbf{K}\rangle \ \phi_{\mathbf{K}} \quad , \qquad (46)$$

and, therefore, $\hat{\mathbf{P}}_{\mathbf{K}}$ projects the $\mathbf{K}$-th component of the wave function.

Symmetry breaking in mean-field models is associated with collective phenomena caused by long-range nucleon-nucleon correlations (Lipkin, 1960, 1961). Considerable efforts have been expended in the sixties and seventies (Lipkin, 1956, 1958; Lipkin et al., 1955; Villars, 1957; Villars and Cooper, 1970) to separate collective and intrinsic coordinates. In the following, we briefly describe the method of redundant coordinates for the translational motion to separate collective and intrinsic degrees of freedom. It is only in this special case where the collective variables, which are the center-of-mass coordinates, can be fully separated owing to the Galilean invariance.

Nevertheless, let us begin by considering a general case of separating the intrinsic and the collective degrees of freedom through a transformation from the $3A$ particle coordinates $(\mathbf{r}_1, \mathbf{r}_2, \ldots, \mathbf{r}_A)$ to collective coordinates $(q_1, q_2, \ldots, q_f)$ and intrinsic coordinates $(\chi_1, \chi_2 \ldots, \chi_{3A-f})$. Although there are many different types of collective motion in a correlated many-body system, we consider here only those connected with symmetry breaking, i.e., those corresponding to the Goldstone modes (Goldstone, 1961; Nambu, 1960). In this case it is quite easy to identify the collective coordinates since they are directly related to the symmetry breaking of the physical system and are canonical conjugate variables of the generators of the symmetry group (Marshalek and Weneser, 1969). For instance, in the case of translational motion, collective variables are the center-of-mass coordinates. However, in general, the specification of the intrinsic coordinates is a major problem. It is only in the case of relatively light systems where they can be treated explicitly, for instance, the relative coordinate $(\mathbf{r}_1 - \mathbf{r}_2)$ in two-body systems or Jacobi coordinates in three- and four-body systems.

The transformed Hamiltonian, obtained by separating collective and intrinsic coordinates, consists of the collective part, the intrinsic part, and the coupling term. The first problem in this approach is that this concept is only reasonable if the coupling term is relatively small. Only for the case of translations, it vanishes exactly, but in all other cases, the coupling term needs to be reduced considerably through a proper choice of the intrinsic coordinates. The next, even bigger, problem is that the intrinsic part does not depend on $3A$ coordinates, but only on $(3A - f)$ variables. This means that these co-

ordinates cannot be associated with independent single-particle states, as is the case in the intrinsic shell-model Hamiltonian.

A way to circumvent the above problem is to follow the method of redundant variables (Ring and Schuck, 1980). In this approach, the Hilbert space in $3A$ coordinates is embedded into a larger space with $3A + f$ coordinates, where f is the number of collective coordinates. The physical subspace is then defined by f additional conditions:

$$g_1 = g_2 = \cdots = g_f = 0. \qquad (47)$$

In the second stage, the redundant coordinate system in the laboratory frame is mapped onto the intrinsic coordinate system with collective coordinates $q_1, q_2, ..., q_f$ and particle coordinates $\mathbf{x_1}, \mathbf{x_2}, \ldots, \mathbf{x_A}$, i.e.,

$$\mathbf{r_i} = \mathbf{r_i}(q_1, q_2, ..., q_f, \mathbf{x_1}, \mathbf{x_2}, \ldots, \mathbf{x_A}),$$
$$i = 1, \ldots, A \qquad (48)$$

$$g_j = g_j(q_1, q_2, ..., q_f, \mathbf{x_1}, \mathbf{x_2}, \ldots, \mathbf{x_A}),$$
$$j = 1, ..., f. \qquad (49)$$

The transformed Hamiltonian in the intrinsic system can be separated into three parts:

$$\hat{H} = \hat{H}_{coll}(\mathbf{q}) + \hat{H}_{intr}(\mathbf{x}) + \hat{H}_{coup}(\mathbf{q}, \mathbf{x}). \qquad (50)$$

In general, it is a difficult problem to find a transformation such that the coupling term is small.

For the case of translational motion, the transformation from the laboratory redundant system to the intrinsic system is given by

$$\mathbf{r_i} = \mathbf{x_i} + \mathbf{R}, \qquad (51)$$

$$\mathbf{g} = \frac{1}{A}\sum_{j=1}^{A} \mathbf{x_j}, \qquad (52)$$

and the inverse transformation is

$$\mathbf{x_i} = \mathbf{r_i} - \mathbf{R}, \qquad (53)$$

$$\mathbf{R} = \frac{1}{A}\sum_{j=1}^{A} \mathbf{r_j} - \mathbf{g}. \qquad (54)$$

The method of redundant variables is now applied to a shell model Hamiltonian with the two-body interaction term depending on the relative coordinates, i.e.,

$$\hat{H} = -\frac{\hbar^2}{2m}\sum_i \left(\frac{\partial}{\partial \mathbf{r_i}}\right)^2 + \frac{1}{2}\sum_{i<j} V(|\mathbf{r_i} - \mathbf{r_j}|). \qquad (55)$$

Using the transformation given by Eqs. (51 - 54), we obtain

$$\hat{H} = \hat{H}_{coll}(\mathbf{R}) + \hat{H}_{intr}(\mathbf{x}), \qquad (56)$$

with

$$\hat{H}_{coll} = -\frac{\hbar^2}{2Am}\left(\frac{\partial}{\partial \mathbf{R}}\right)^2, \qquad (57)$$

$$\hat{H}_{intr} = \sum_i \frac{\hat{\mathbf{p}}_i^2}{2m} + V(|\mathbf{x_i} - \mathbf{x_j}|) - \frac{\hat{\mathbf{P}}^2}{2Am}, \qquad (58)$$

where $\hat{\mathbf{p}}_i = \frac{\hbar}{i}\frac{\partial}{\partial \mathbf{x_i}}$ and $\hat{\mathbf{P}} = \sum_i \mathbf{p_i}$. It is evident from the above expression that internal and the collective coordinates are completed decoupled. However, even here we are faced with the problem, that we have here $3A$ intrinsic coordinates $(\mathbf{x_1}, \mathbf{x_2}, \ldots, \mathbf{x_A})$ instead of $3A - 3$. This redundancy leads to spurious motions of the center of mass and the corresponding kinetic energy is subtracted in the well known center-of-mass correction $\hat{\mathbf{P}}^2/2Am$. For heavy nuclei, it decreases with $1/A$, but for light nuclei this term leads to an essential contribution and one is far from the exact solution of the center of mass problem. See (Messud, 2013) for an alternative solution to the center-of-mass problem.

For other symmetries, the method of redundant variables becomes exceedingly cumbersome (Gulshani, 2011; Villars and Cooper, 1970) and it is rarely applied.

2. Three Dimensional Rotation

Rotation in three dimensions is characterized by the Euler angles $\Omega = (\alpha, \beta, \gamma)$ and the corresponding group element is given by the operator

$$\hat{R}(\Omega) = e^{-i\alpha\hat{J}_z} \ e^{-i\beta\hat{J}_y} \ e^{-i\gamma\hat{J}_z} \quad . \qquad (59)$$

As discussed in Sec. III.A.1, the rotational group in three dimensions is non-abelian and therefore we have to introduce the generalized projection operators (32):

$$\hat{P}_{MK}^I = \frac{2I+1}{8\pi^2}\int d\Omega \ D_{MK}^{I*}(\Omega) \ \hat{R}(\Omega). \qquad (60)$$

Following (Lamme and Boeker, 1968), we define a complete and orthogonal set of many-body wave functions $|IM\alpha\rangle$ which are eigenstates of the angular momentum operators $\hat{\mathbf{J}}^2$ and $\hat{\mathbf{J}_z}$, and α combines all the remaining quantum numbers in the many-body Hilbert space. This yields

$$\hat{R}(\Omega)|IM\alpha\rangle = \sum_K D_{KM}^I(\Omega)|IK\alpha\rangle, \qquad (61)$$

where the $D-$matrices are the Wigner functions (Edmonds, 1957; Varshalovich *et al.*, 1988), constituting the representation of the rotational group[2]. Using the com-

---

[2] we have to keep in mind that we use throughout this article active rotations, whereby the states are rotated and not the reference frame. Therefore the Wigner functions are defined here as $D_{MK}^I = \langle IM|e^{-i\alpha\hat{J}_z} \ e^{-i\beta\hat{J}_y} \ e^{-i\gamma\hat{J}_z}|IK\rangle$ in contrast to the book of Edmonds which uses passive rotations with the Wigner functions $\langle IM|e^{i\alpha\hat{J}_z} \ e^{i\beta\hat{J}_y} \ e^{i\gamma\hat{J}_z}|IK\rangle$

pleteness relations for the states $|IM\alpha\rangle$, we can express the generalized projectors (60) in terms of these states and find after a simple derivation

$$\hat{P}^I_{MK} = \hat{1} \cdot \hat{P}^I_{MK} \cdot \hat{1} = \sum_\alpha |IM\alpha\rangle\langle IK\alpha|. \qquad (62)$$

This again shows that only the diagonal term $\hat{P}^I_{MM}$ is a projector onto the sub-space of the Hilbert space with the quantum numbers I and M. Obviously, these projectors provide for the full resolution of unity as in $\hat{1} = \sum_{IM} \hat{P}^I_{MM}$. However, individual states $\hat{P}^I_{MM}|\Phi\rangle$, projected on good quantum numbers I and M, cannot be identified with the basis states $|IM\alpha\rangle$, i.e., they do not obey Eq. (61).

To better understand the meaning of the additional[3] quantum number K in the projector $\hat{P}^I_{MK}$, we start from a deformed intrinsic (symmetry-breaking) wave function $|\Phi\rangle$ and use the generator-coordinate-method ansatz (37). We expand the weight function $f^I_M(\Omega)$ in terms of the Wigner functions

$$f^I_M(\Omega) = \frac{2I+1}{8\pi^2} \sum_K g_K D^{I*}_{MK}(\Omega), \qquad (63)$$

and obtain the projected many-body state

$$|\Psi^I_M\rangle = \sum_K \frac{2I+1}{8\pi^2} \int d\Omega\, g_K D^{I*}_{MK}(\Omega)\hat{R}(\Omega)|\Phi\rangle,$$
$$= \sum_K g_K \hat{P}^I_{MK}|\Phi\rangle. \qquad (64)$$

From Eq. (62) it is evident that this wave function has good quantum numbers

$$\hat{\mathbf{J}}^2|\Psi^I_M\rangle = I(I+1)|\Psi^I_M\rangle \text{ and } \hat{\mathbf{J}}_z|\Psi^I_M\rangle = M|\Psi^I_M\rangle, (65)$$

independently of the expansion coefficients g_K.

It turns out, that, in contrast to abelian groups, here the weight function $f^I_M(\Omega)$ for the generator-coordinate-method ansatz (37) is not completely determined by the symmetry group. The coefficients g_K have to be determined by the dynamics of the system, i.e., by diagonalizing the many-body Hamiltonian or by minimizing the projected energy.

Only in special cases, this additional diagonalization is not necessary. For example, if the intrinsic (symmetry-breaking) wave function $|\Phi\rangle$ is symmetric with respect to rotations around the intrinsic z-axis, i.e., if $\hat{J}_z|\Phi\rangle = K_0|\Phi\rangle$, then $\hat{P}^I_{MK}|\Phi\rangle = 0$ for $K \neq K_0$ and there is only

one coefficient g_{K_0}, which is determined by the normalization. A simple case is the intrinsic state $|\Phi\rangle_{K=0}$ of the ground state of an axially deformed even-even nucleus. Here we find the projected states

$$|\Psi^I_M\rangle = P^{\hat{I}}_{M0}|\Phi_{K=0}\rangle, \qquad (66)$$

which do obey Eq. (61),

Further, by integrating in Eq. (60) over the Euler angles α and γ, the generalized projector $\hat{P}^I_{MK}$ can be decomposed into three steps:

$$\hat{P}^I_{MK} \propto \delta(\hat{J}_z - M) \int_{-1}^{1} d\cos(\beta) d^{I*}_{MK}(\beta) e^{i\beta\hat{J}_y}\, \delta(\hat{J}_z - K).$$

We can now describe this result in two different ways:

1. In the first, the traditional language of the intrinsic and laboratory reference frames is used, whereupon to start with the projector, $P^K = \delta(\hat{J}_z - K)$ of Eq. (43), carries out a projection onto the quantum number K, corresponding to the component of the angular momentum $\hat{\mathbf{J}}$ along the intrinsic z-axis, then we have a rotation by the angle β around the y-axis from the z axis in the intrinsic system to the z-axis in the laboratory frame, and finally $P^M = \delta(\hat{J}_z - M)$ projects to an eigenstate with quantum number M in the laboratory frame.

2. In the second, one uses the notions of the symmetry-breaking and symmetry-restored states, whereupon the first operation projects out the symmetry-breaking state on the good quantum number K corresponding to the z quantization axis of a predefined reference frame. The second step projects on the good total-angular-momentum quantum number I, but it does that by a rotation along the y axis, and thus mixes again the previously restored projections of the angular momentum. Then, the third-step projector is required to restore the projection M on the z quantization axis of a predefined reference frame, and to give the fully symmetry-restored wave function.

The final wave function $|\Psi^I_M\rangle$ in Eq. (64) is a quantum-mechanical superposition of all these different orientations and, as usual in the generator coordinate method, the weight functions are related to the corresponding probabilities (Ring and Schuck, 1980).

It is important to emphasize, that the concept of generator coordinates, which corresponds here to the projection onto the subspaces determined by the symmetry group, deals only with the coordinates of the A particles in the corresponding wave functions in the intrinsic or in the laboratory frame, i.e., before or after the symmetry restoration. The collective coordinates, in this case the Euler angles, enter only in a parametric way. In

---

[3] It is better to call K additional quantum number than to call it projection of angular momentum on the intrinsic axis, which is the term frequently used. Indeed, states $\langle IK\alpha|$ are "bra" representations of "ket" states $|IM\alpha\rangle$, and both correspond to projections of angular momentum on the same predefined quantization axis.

none of these considerations one has to introduce "redundant" coordinates and no spurious states are involved. One stays, from the beginning to end, completely in the quantum-mechanical framework and no "requantization" is necessary. However, the results are not characterized by orbits in the collective subspace, but by probabilities corresponding to different orientations.

It needs to be added that there is a prize to pay as these calculations become relatively complicated. Therefore, although these concepts have been around since more than half a century, many of these calculations, in particular, those with realistic applications are possible only nowadays using modern computing resources (Bally *et al.*, 2014). Some of the applications still have to wait for more advanced facilities (Márquez Romero *et al.*, 2018).

3. Particle-number Projection

In close analogy to Eq. (43) the projection operator onto good particle-number is given by

$$\hat{P}^N = \frac{1}{2\pi} \int d\varphi \; e^{-i\varphi(\hat{N}-N)}. \qquad (67)$$

It corresponds to the group of rotations in gauge space.

$$\hat{R}(\varphi) = e^{-i\varphi\hat{N}}, \qquad d^N(\varphi) = \frac{1}{2\pi} e^{+i\varphi N}. \qquad (68)$$

The group is one-dimensional and therefore abelian. the collective coordinate is the gauge angle $g = \varphi$ and the generator is the particle number $I = N$.

Particle number projection, in particular in the BCS-case is relatively simple and it has been applied in the literature using different methods (Dietrich *et al.*, 1964; Egido and Ring, 1982a; Fomenko, 1970), in particular, also in the framework of approximate projections, see Sec. IV.

4. Parity Projection

The parity projection operator is connected to a discrete symmetry. It is similar to projection of spin-up and spin-down states and is written as (Egido and Robledo, 1991):

$$\hat{P}_p = \frac{1}{2}(1 + p\hat{\Pi}) \quad , \qquad (69)$$

where $p = \pm 1$ and $\hat{\Pi}$ is the standard parity operator which in the second quantization formalism is given by:

$$\hat{\Pi} = \exp\left\{ i\pi \sum_k{}' \; c_k^\dagger c_k \right\} \quad , \qquad (70)$$

where summation over k is restricted to negative-parity states. The above operator expression assumes that the basis configurations over which HF or HFB states are expressed have well defined parity quantum number. It is easy to check from the above operator expression that in case the total number of negative-parity states is even (odd) in the wave function, the above operator acting on the state is equal to $+1$ (-1). It can be also easily shown that the parity operator is a true projection operator, satisfying the following conditions:

$$\hat{P}_p^\dagger = \hat{P}_p \qquad , \qquad \hat{P}_p^2 = \hat{P}_p \qquad . \qquad (71)$$

C. Symmetry restoration of the HFB wave function

In most of the projection studies, one starts with broken-symmetry mean-field wave function $|\Phi\rangle$ of the HF or HFB type. The advantage of these states is that they can be written as generalized product states and Wick's theorem allows to evaluate the matrix elements of arbitrary many-body operators $\langle\Phi|\hat{O}|\Phi\rangle$ in terms of the matrix elements of the one-body densities

$$\rho_{nn'} = \langle\Phi|a_{n'}^\dagger a_n|\Phi\rangle \quad \text{and} \quad \kappa_{nn'} = \langle\Phi|a_{n'} a_n|\Phi\rangle. \qquad (72)$$

In addition the generalized Wick's theorem, see Appendix A, allows us to express matrix elements of the form $\langle\Phi|\hat{O}|\Phi'\rangle$ in terms of the corresponding transition densities (Balian and Brezin, 1969; Hara and Iwasaki, 1979; Onishi and Yoshida, 1966; Ring and Schuck, 1980).

1. Rotated Norm and Energy Kernels

In this section, we use a generic form of the projection operator (32)

$$\hat{P}^I = \int dg \, D^{I*}(g)\hat{R}(g), \qquad (73)$$

which represents several different projection operators discussed up to now. For the one-dimensional case, I represents directly the quantum number on which one projects. In the general case, I represents several quantum numbers, as for instance K_x, K_y, K_z for projection onto the linear momentum or I, M, K in the case of three-dimensional rotations.

Assuming that the Hamiltonian $\hat{H}$ commutes with the symmetry operator $\hat{R}(g)$, the projected energy is given by (Ring and Schuck, 1980)

$$E^I = \frac{\langle\Phi|\hat{H}\hat{P}^I|\Phi\rangle}{\langle\Phi|\hat{P}^I|\Phi\rangle} = \frac{\int dg \, D^{I*}(g)\langle\Phi|\hat{H}\hat{R}(g)|\Phi\rangle}{\int dg \, D^{I*}(g)\langle\Phi|\hat{R}(g)|\Phi\rangle} \quad . \qquad (74)$$

Defining the rotated HFB wave functions, as has been done in (Sheikh and Ring, 2000),

$$|g\rangle = \frac{\hat{R}(g)|\Phi\rangle}{\langle\Phi|\hat{R}(g)|\Phi\rangle} \quad \text{with} \quad |0\rangle = |\Phi\rangle \text{ and } \langle 0|g\rangle = 1, \qquad (75)$$

and two auxiliary functions of group elements, g,

$$x(g) = D^{I*}(g)\langle 0|g\rangle \quad \text{and} \quad y(g) = \frac{x(g)}{\int dg\, x(g)}, \quad (76)$$

we find

$$E^I = \int dg\, y(g)\langle 0|H|g\rangle. \quad (77)$$

Similar expressions can be found for other operators, such as the multipole operators (Dobaczewski *et al.*, 2009), and for electromagnetic transition matrix elements.

Standard expressions for the norm overlap are given in Appendix A, whereas those that do not explicitly employ transition densities, reader is referred to (Sheikh and Ring, 2000):

$$\langle \Phi|\hat{R}(g)|\Phi\rangle^2 = \det\left(R_g\rho^{-1}A_g\right). \quad (78)$$

Here R_g is the matrix representing of the group element g in the single-particle space and

$$A_g = \rho R_g \rho - \kappa R_g^* \kappa^*. \quad (79)$$

In Eq. (78) the norm overlap is defined only up to a sign ± 1. Several methods have been proposed in the literature to determine this sign (Bally and Duguet, 2018; Dönau, 1998; Hara *et al.*, 1982; Neergård and Wüst, 1983). As discussed in Appendix A, this problem does not show up, if one expresses the overlap in terms of Pfaffians (Bertsch and Robledo, 2012; González-Ballestero *et al.*, 2011; Robledo, 2009).

The matrix elements $\langle 0|H|g\rangle$ can be evaluated with the help of the generalized Wick's theorem, mentioned above. This means they depend in the same way on the one-body transition densities

$$\rho_{nn'}(g) = \langle 0|a_{n'}^\dagger a_n|g\rangle = \left(R_g\rho A_g^{-1}\rho\right)_{nn'}, \quad (80)$$

$$\kappa_{nn'}(g) = \langle 0|a_n a_n|g\rangle = \left(R_g\rho A_g^{-1}\kappa\right)_{nn'}, \quad (81)$$

$$\overline{\kappa}_{nn'}^*(g) = \langle 0|a_n^\dagger a_{n'}^\dagger|g\rangle = \left(R_g^*\kappa^* A_g^{-1}\rho\right)_{nn'} \quad (82)$$

as the matrix element $\langle 0|H|0\rangle$ depends on the normal one-body density matrix $\rho = \langle 0|a^\dagger a|0\rangle$, and pairing tensors $\kappa = \langle 0|aa|0\rangle$ and $\overline{\kappa}^* = \langle 0|a^\dagger a^\dagger|0\rangle$. It is important to note that we have expressed here all the matrix elements in terms of the intrinsic densities ρ and κ and the matrix elements of the representation, R_g.

As an example, let us consider a Hamiltonian with a two-body interaction of the form

$$\hat{H} = \sum_{nn'} e_{nn'} a_n^\dagger a_{n'} + \frac{1}{4} \sum_{nn'mm'} \overline{v}_{nn'mm'} a_n^\dagger a_{n'}^\dagger a_{m'} a_m \quad (83)$$

and obtain for the Hamiltonian matrix element

$$\langle 0|H|g\rangle = \text{Tr}\left((e\rho(g))\right.$$
$$+ \frac{1}{2}\text{Tr}\left(\Gamma(g)\rho(g)\right) - \frac{1}{2}\text{Tr}\left(\Delta(g)\overline{\kappa}^*(g)\right) \quad (84)$$

with the rotated fields

$$\Gamma_{nm}(g) = \sum_{n'm'} \overline{v}_{nn'mm'}\rho_{m'n'}(g)$$

$$\Delta_{nm}(g) = \frac{1}{2}\sum_{m'n'} \overline{v}_{nmn'm'}\kappa_{n'm'}(g) \quad (85)$$

In principle the evaluation of projected matrix elements is relatively straightforward. One only has to replace the normal density matrices ρ, κ, and κ^* by the transition densities $\rho(g)$, $\kappa(g)$, and $\overline{\kappa}^*(g)$ and integrate over the parameter space of the group. In practice, however, depending on the dimension of the single-particle space and the number of mesh-points in parameter space this can require a large computational effort, in particular, for triaxial nuclei. At each point g in parameter space one has to invert the large (often complex) matrix A_g (79) with the dimension of the single-particle space [see for instance (Yao *et al.*, 2014)].

As the Madrid group (Anguiano *et al.*, 2001) has shown, it may happen in regions of level-crossings that $\langle \Phi|\hat{R}(g)|\Phi\rangle$ vanishes in Eq. (78) at certain values of g. This leads to poles in certain parts of the Hamiltonian matrix element (84), for instance, in $\text{Tr}\left(\Gamma(g)\rho(g)\right)$, see discussion in Sec. VI.A.2. In all cases, where one uses a fixed Hamiltonian $\hat{H}$ and where one takes into account all the different terms, these poles cancel (Anguiano *et al.*, 2001). In other cases, however, where one uses different interactions in the pairing channel and in the HF-channel or where one neglects, for instance, the contributions of the Coulomb force to pairing etc., such poles can cause serious problems (Dobaczewski *et al.*, 2007). In Eq. (83), we considered only interactions without density dependence. Density-dependent interactions can cause additional problems, as we discuss in Sec. (VI).

2. Variation after projection

With the techniques discussed in the last section, it is relatively simple to calculate projected matrix elements for generalized product states such as HF or HFB wave functions $|\Phi\rangle$. This is usually called projection after variation, whereupon the symmetry is restored and the projected matrix elements of the Hamiltonian and other operators can be evaluated.

However, such a procedure violates the variation principle, because the projected energy does not correspond to a minimum of the projected energy surface. Therefore, the method of variation after projection has been proposed (Rouhaninejad and Yoccoz, 1966; Yoccoz, 1966; Zeh, 1965), where the mean-field wave function $|\Phi\rangle$ is determined by minimizing the projected energy surface, i.e., by solving the equation

$$\langle \delta\Phi|\hat{P}^I\hat{H}\hat{P}^I - E|\Phi\rangle = 0. \quad (86)$$

For the exact solution of this problem, following two methods have been proposed:

Gradient Method

A particularly powerful method to minimize the energy surface with respect to the product state is the gradient method, which has been introduced in (Mang *et al.*, 1976), and which has been applied for variation after projection in (Egido and Ring, 1982a,b). In this method, in the neighborhood of an arbitrary point $|\Phi_0\rangle$, the manifold of the HFB wave functions $|\Phi\rangle$ is parameterized by the Thouless theorem,

$$|\Phi\rangle \propto \exp(\sum_{k<k'} Z_{kk'}\alpha_k^\dagger \alpha_{k'}^\dagger)|\Phi_0\rangle, \qquad (87)$$

where operators $\alpha_k^\dagger$ are the quasiparticle operators with respect to the quasiparticle vacuum $|\Phi_0\rangle$, i.e., $\alpha_k|\Phi_0\rangle = 0$. The gradient of the projected energy with respect to parameters $Z_{kk'}$ is given by

$$\gamma_{kk'} = \frac{\partial E^I}{\partial Z_{kk'}^*}\bigg|_{Z=0} = \frac{\langle\Phi_0|\alpha_{k'}\alpha_k(\hat{H}-E^I)\hat{P}^I|\Phi_0\rangle}{\langle\Phi_0|\hat{P}^I|\Phi_0\rangle}. \quad (88)$$

These matrix elements can be evaluated using the generalized Wick's theorem, in a similar way as it is done for the average energy. Following the direction of steepest descent on this manifold by a step size of η, we obtain in the next step of the iteration, the following wave function

$$|\Phi_1\rangle \propto \exp(-\eta\sum_{k<k'}\gamma_{kk'}\alpha_k^\dagger\alpha_{k'}^\dagger)|\Phi_0\rangle. \qquad (89)$$

The resulting HFB coefficients of $|\Phi_1\rangle$ have to be orthogonalized [for details see (Egido and Ring, 1982a)]. Calculating the new projected energy E_1^I and changing the step size η in the next step accordingly, the minimum of the projected energy surface can be found without diagonalizing any matrix. This method is particularly useful, if one wants to minimize the energy surface with additional constraints. In this case the method of Lagrange multipliers is used, where the total gradient is projected onto the gradient along the hyper-surface determined by the constraining operator. The speed of convergence of this method can be considerably improved by using the conjugate gradient method (Egido *et al.*, 1995).

It is evident that the gradient method can only be applied for cases, where the final solution corresponds to a minimum in the energy surface. In all the applications of Covariant Density Functional Theory, the solution of the corresponding mean-field equations of motion do not correspond to a minimum, but rather to a saddle point on the energy surface, because on the manifold of product states formed by Dirac spinors, there is always the direction of mixing in negative energy solutions, which leads to lower energies. In practical applications with subsequent diagonalizations of the relativistic HFB Hamiltonian (Kucharek and Ring, 1991) this direction in

excluded by using the no-sea approximation for the calculations of the densities and currents in the next step of the iteration.

Projected HFB Equations

Within the HF and HFB theory, there exists a one-to-one correspondence between the product state $|\Phi\rangle$ and the corresponding one-body density matrices $\rho_{nn'}$ and $\kappa_{nn'}$ in Eq. (72). Therefore the HF Hamiltonian $\hat{h}$, which is diagonalized by the HF equations

$$\hat{h}|\varphi_k\rangle = \varepsilon_k|\varphi_k\rangle \qquad (90)$$

can be found as a derivative of the energy with respect to this density matrix

$$\hat{h}_{nn'} = \frac{\partial E}{\partial\rho_{n'n}}. \qquad (91)$$

In the HFB theory, the one-body density ρ is replaced by the Valatin density (Valatin, 1961)

$$\mathcal{R} = \begin{pmatrix} \rho & \kappa \\ -\kappa^* & 1-\rho^* \end{pmatrix}, \qquad (92)$$

and the HFB equations are derived as

$$\begin{pmatrix} h-\lambda & \Delta \\ -\Delta^* & -h^*+\lambda \end{pmatrix}\begin{pmatrix} U \\ V \end{pmatrix}_k = E_k\begin{pmatrix} U \\ V \end{pmatrix}_k \qquad (93)$$

where h is given by Eq. (81) and the pairing field is given by

$$\Delta_{nn'} = -\frac{\partial E}{\partial\kappa_{n'n}^*}. \qquad (94)$$

λ in Eq. (93) is the chemical potential, determined by the average particle number.

In order to derive projected HFB equations, we have to consider that the projected energy (74) also depends on the densities ρ and κ of the intrinsic wave function $|\Phi\rangle$. Therefore the optimal intrinsic wave function is found by a variation of the projected density with respect to the intrinsic densities ρ and κ. In full analogy to the case without projection, the variation leads to the projected HFB equations (Sheikh and Ring, 2000)

$$\begin{pmatrix} h^I-\lambda & \Delta^I \\ -\Delta^{I*} & -h^{I*}+\lambda \end{pmatrix}\begin{pmatrix} U \\ V \end{pmatrix}_k = E_k^I\begin{pmatrix} U \\ V \end{pmatrix}_k \qquad (95)$$

with

$$h_{nn'}^I = \frac{\partial E^I}{\partial\rho_{n'n}} \quad \text{and} \quad \Delta_{nn'}^I = -\frac{\partial E^I}{\partial\kappa_{n'n}^*}. \qquad (96)$$

In order to write down these quantities explicitly, we need the analytic form of the projected E^I in terms of the intrinsic densities ρ and κ and are given in Eqs. (78)–(82). The detailed expressions for HF and pairing fields have

been derived in (Sheikh *et al.*, 2002) and is not repeated here.

It needs to be mentioned that several other methods have been developed to perform the particle-number projection (Ring and Schuck, 1980) in the BCS case. In particular, the method of residuum integrals has been introduced to perform the exact particle-number projection (Dietrich *et al.*, 1964) before the variation. In this approach, the particle-number projected method is cast into a set of non-linear equations, which are similar in structure to those of BCS equations. It has been shown (Sheikh and Ring, 2000) that the projected pairing and the HF fields derived using the present projection method reduce to those derived in (Dietrich *et al.*, 1964) when using the canonical basis.

IV. APPROXIMATE PROJECTION METHODS

The general formalism of symmetry restoration, presented in the previous section, leads to expressions that involve multi-dimensional integrals of norm and Hamiltonian kernels over the symmetry group parameters, see Eq. (84). In the standard numerical approach these integrals are replaced with finite sums,[4] which entails evaluations of norm and Hamiltonian kernels for each mesh point in the multi-dimensional space of group parameters. For each mesh point, the overlap is evaluated using the Onishi or Pfaffian method and the Hamiltonian kernels are expressed in terms of the one-body rotated densities by employing the generalized Wick's theorem, see Appendix A. In general, the numerical cost of calculating one point of the projected integrand is somewhat larger than the cost of performing one iteration of the self-consistent method, required to determine the broken-symmetry state being projected.

Estimates of the number of mesh points vary a lot depending on the mass or deformation of the nucleus, and on the precision desired for the final results. On the one hand, for a weak symmetry breaking case, a larger number of eigenstates of the symmetry generators are mixed within the broken-symmetry state, and thus more mesh points are required to resolve them. On the other hand, conserved symmetries allow us to limit the integration domain and thus to decrease the number of mesh points. Typically, for a medium heavy nucleus with moderate deformation, about 10 integration points each are needed to project on good proton and neutron numbers, and about 50 integration points, to project on good angular momentum of an axial nucleus. Restoration of symmetry then requires a numerical expense somewhat larger

than that required to perform 5000 self-consistent iterations. It is evident that even with such a modest mesh size, the restoration of symmetries lead to numerical cost largely exceeding the typical 100 iterations required to converge the bare broken-symmetry state. For a triaxial state, where a three-dimensional integration over the Euler angles is needed, the number of integration points would increase to 1,25,00,000 and thus becoming unmanageable. Therefore, up to now, calculations of this type have been restricted to lighter systems only, see (Bally *et al.*, 2014).

In the early days of projection theory, well before the above *tour-de-force* achievements were envisioned and when the adequate computing power was not available, several approximate methods for symmetry restoration were proposed and implemented. Here we discuss in detail the most popular one, based on the so-called Lipkin method (Lipkin, 1960) or Kamlah expansion (Kamlah, 1968), along with the variant of the former one proposed by Nogami (Nogami, 1964). In fact, the Lipkin and Kamlah ideas were basically identical, although Kamlah did not apparently know about, and he did not cite the much earlier work of Lipkin.[5]

The main objective of both the approaches is to obtain approximate expressions for symmetry-projected energies and to employ them in the implementation of the variation-after-projection approach. However, the two approaches differ on the physical quantities to be described: Kamlah is primarily concerned with determining the projected energy, which is then varied; whereas Lipkin aims to model the entire spectrum of collective states related to a given broken symmetry. A bigger difference between them, is what Kamlah does and what Lipkin doesn't, is to consider the effects of collective motion brought about by the so-called pushing or cranking terms.

The baseline of the Lipkin and Kamlah approaches is the observation that the average values and matrix elements of operators calculated between symmetry-projected states always involve kernels of operators between symmetry-transformed states, Eq. (84). It is thus obvious that a meaningful approximation of the latter may lead to a useful approximation of the former.

Finally, we should stress the fact that although the Lipkin and Kamlah approaches are primarily concerned to identify the variation-after-projection symmetry-breaking state, they do not actually determine the projected state. For that, an explicit projection of the variation-after-projection symmetry-breaking state is always necessary. Only then one can calculate correct transition probabilities respecting all symmetry properties of the transition operators.

---

[4] An alternative method based on solving linear equations has recently been proposed in (Johnson and Jiao, 2019; Johnson and O'Mara, 2017).

[5] However, Kamlah did cite (Goodfellow and Nogami, 1966) that had cited (Lipkin, 1960).

A. The Lipkin method

The main idea of the Lipkin approach (Lipkin, 1960) can be formulated as a proposal to flatten the spectrum of projected energies E^I (Dobaczewski, 2009; Gao *et al.*, 2015a; Wang *et al.*, 2014),

$$E^I - K^I = const. \quad , \tag{97}$$

where

$$K^I = \frac{\langle \Phi | \hat{K} \hat{P}^I | \Phi \rangle}{\langle \Phi | \hat{P}^I | \Phi \rangle} \tag{98}$$

are average values of the so-called Lipkin operator, $\hat{K}$, evaluated between the projected states and the constant on the rhs of Eq. (97) does not depend on labels I of the projected states. Equivalently, as it is evident from Eq. (84), one can flatten the reduced energy kernels, i.e.,

$$\frac{\langle \Phi | \left(\hat{H} - \hat{K} \right) \hat{R}(g) | \Phi \rangle}{\langle \Phi | \hat{R}(g) | \Phi \rangle} = const. \quad , \tag{99}$$

where the constant on the rhs, which is the same constant as in Eq. (97), does not depend on the group element g.

How to find the Lipkin operator $\hat{K}$ that does the job as desired? The strategy is obvious, namely, since the quantum numbers I are related to the symmetry generators, we can build $\hat{K}$ as functions of the symmetry generators. For example:

- For the particle-number symmetry, projected energies depend on the number of particles, so $\hat{K}$ may depend on the particle-number operators, $\hat{N}$ and $\hat{Z}$, for neutrons and protons:

$$\hat{K} = \sum_{n+m>0} k_{nm} (\hat{N} - N_0)^n (\hat{Z} - Z_0)^m, \tag{100}$$

  where N_0 and Z_0 are numbers of protons and neutrons of the state we want to describe.

- For the translational symmetry, projected energies depend on total momenta, so $\hat{K}$ may depend on the components of the total momentum, $\hat{P}_x$, $\hat{P}_y$, and $\hat{P}_z$:

$$\hat{K} = \sum_{n+m+l>0} k_{nmk} \hat{P}_x^n \hat{P}_y^m \hat{P}_z^l. \tag{101}$$

- For the rotational symmetry, projected energies depend on total angular momentum, so $\hat{K}$ may depend on the components of the total angular momentum, $\hat{J}_x$, $\hat{J}_y$, and $\hat{J}_z$:

$$\hat{K} = \sum_{n+m+l>0} k_{nmk} \hat{J}_x^n \hat{J}_y^m \hat{J}_z^l. \tag{102}$$

- For the rotational symmetry and axial nucleus oriented along the z axis, projected energies depend on total angular momenta, so $\hat{K}$ may depend on the total angular momentum $\hat{\boldsymbol{J}}^2$:

$$\hat{K} = \sum_{m>0} k_m \left(\hat{\boldsymbol{J}}^2 - I(I+1) \right)^m, \tag{103}$$

  where I is the total angular momentum of the state we want to describe.

The main idea behind building the Lipkin operators is to have the best possible description of spectra E^I of projected energies in terms of averages of group generators K^I. We stress that we do not deal here with real spectra of the system, but with energies E^I of symmetry-conserving components $P^I | \Phi \rangle$ derived from the symmetry-breaking state $| \Phi \rangle$. In fact, among all the projected states, we are interested in the energy E^{I_0} and wave function $P^{I_0} | \Phi \rangle$ of only one of them. Of course, if the flattening (97) and (99) is perfect - this does not matter; however, if it is not perfect, we better do the best possible job for the one state I_0 that we want to describe. Then, the Lipkin operators constructed such that

$$K^{I_0} \equiv 0 \tag{104}$$

give us obviously

$$E^I - K^I = E^{I_0}. \tag{105}$$

In fact, for the examples of the Lipkin operators presented in Eqs. (100) and (103), condition (104) is fulfilled, whereas those in Eqs. (101) or (102) apply to states at rest ($\boldsymbol{P} = 0$) or non-rotating ($\boldsymbol{J} = 0$), respectively.

At this point, by evaluating Eq. (99) at $g = 0$, we obtain the "magic" Lipkin formula:

$$E^{I_0} = \langle \Phi | \hat{H} - \hat{K} | \Phi \rangle, \tag{106}$$

namely, the projected energy E^{I_0} can be obtained as an average value of $\hat{H} - \hat{K}$ calculated for the symmetry-breaking state $| \Phi \rangle$ *without performing any projection at all*. Of course, we can benefit from the magic formula only if we can find appropriate Lipkin operators that correctly flatten the spectrum, and the precision of it is dictated by the precision of the flattening.

Therefore, the main thrust of the method now lies in finding the numerical coefficients in Eqs. (100)–(103) that define the Lipkin operators in terms of the symmetry generators. Before going into details of specific applications, let us introduce a generic form of the Lipkin operator as a linear combination of different terms:

$$\hat{K} = \sum_{m=1}^{M} k_m \hat{K}_m. \tag{107}$$

Following the original idea of Peierls and Yoccoz (Peierls and Yoccoz, 1957), we now evaluate Eq. (99) at $M + 1$

group elements, g_i, for $i = 0, \ldots, M$, $g_0 = 0$, which leads to a set of linear equations that determine the Lipkin parameters k_m,

$$\sum_{m=0}^{M} A_{im} k_m = h_i, \qquad (108)$$

where we extended the list of symmetry generators by defining,

$$\hat{K}_0 \equiv \hat{1} \quad \text{and} \quad k_0 \equiv E^{I_0}. \qquad (109)$$

Then, coefficients in (108) are defined by the following reduced kernels:

$$A_{im} = \frac{\langle \Phi | \hat{K}_m \hat{R}(g_i) | \Phi \rangle}{\langle \Phi | \hat{R}(g_i) | \Phi \rangle}, \qquad (110)$$

$$h_i = \frac{\langle \Phi | \hat{H} \hat{R}(g_i) | \Phi \rangle}{\langle \Phi | \hat{R}(g_i) | \Phi \rangle}, \qquad (111)$$

and the Lipkin parameters can be obtained by inverting matrix A:

$$k_m = \sum_{i=0}^{M} A_{mi}^{-1} h_i. \qquad (112)$$

In doing so, we can always adjust the choice of group elements g_i so as to obtain a non-singular matrix A. It is noted here that one can simply ignore the value of k_0 given by Eq. (112). Indeed, since it is by definition (109) equal to E^{I_0}, one can always evaluate it from the magic Lipkin formula (106).

Based on the Peierls-Yoccoz prescription to determine the Lipkin parameters, one has to calculate a few overlap and energy kernels – the same ones that are required for the execution of the full projection, Eq. (84). Their number is, however, significantly smaller than that required for a full projection, and thus the Lipkin method is computationally much less intensive.

However, its true advantage manifests itself when we attempt to obtain the variation-after-projection solution, which, when executed exactly, leads to difficult programming and calculations, cf. Sec. III.C. On the other hand, variation of the projected energy obtained from the magic Lipkin formula (106) is as easy as a direct variation of the energy of the symmetry-breaking state. Clearly, the Lipkin method gives only the projected energy, whereas, if average values of other observables are to be calculated, the full projection has to be anyhow performed. Then, the Lipkin method allows for obtaining variation-after-projection results at the expense of a single projection-after-variation calculation, which still constitutes a substantial gain in computing time and efficiency.

One should stress one important aspect of the Lipkin method, namely, when varying state $|\Phi\rangle$ that appears in the magic formula (106) to obtain the variation-after-projection result, one should treat the Lipkin parameters

k_m as constants that do not undergo variation. Indeed, even if their values parametrically depend on $|\Phi\rangle$ through Eqs. (112) and (111), their role is to provide the best flattening of the final spectrum, so in principle, during variation they should be kept fixed and equal to the final variation-after-projection values. The algorithm that keeps them fixed at every iteration of the variation, and recalculates them after every step, yields the desired result once the convergence is reached.

B. The Lipkin-Nogami method

In a series of papers, Nogami and collaborators (Goodfellow and Nogami, 1966; Nogami, 1965; Nogami and Zucker, 1964; Nogami, 1964; Pradhan *et al.*, 1973) developed a variant of the Lipkin method that replaces the calculation of overlap and energy kernels by a calculation of several average values. This replacement can be derived by first rewriting Eqs. (99), (107), and (109) as

$$\langle \Phi | \left(\hat{H} - \sum_{m=0}^{M} k_m \hat{K}_m \right) \hat{R}(g) | \Phi \rangle = 0. \qquad (113)$$

Since the group operators $\hat{R}(g)$ are equal to the exponents of linear combinations of symmetry generators, it follows from Eq. (113) that

$$\langle \Phi | \left(\hat{H} - \sum_{m=0}^{M} k_m \hat{K}_m \right) \hat{K}_i | \Phi \rangle = 0. \qquad (114)$$

Lipkin parameters can be evaluated in analogous to how it is done in the original Lipkin approach (112):

$$k_m = \sum_{i=0}^{M} B_{mi}^{-1} l_i, \qquad (115)$$

but for

$$B_{im} = \langle \Phi | \hat{K}_m \hat{K}_i | \Phi \rangle, \qquad (116)$$

$$l_i = \langle \Phi | \hat{H} \hat{K}_i | \Phi \rangle. \qquad (117)$$

Had the Lipkin method been exact, the Lipkin-Nogami expressions would also be same, and would lead to exact results. Otherwise, the Lipkin and Lipkin-Nogami methods may give different results, and it is *a priori* difficult to say which one is superior. Nevertheless, if the calculation of kernels, and not only of the average values, is available, the Peierls-Yoccoz method is certainly easier to implement. Indeed, in case the Hamiltonian is a 2-body operator and the Lipkin operator is an n-body operator, the Peierls-Yoccoz method requires calculating kernels of these 2-body and n-body operators only, whereas the Lipkin-Nogami calls for calculating averages of $n+2$-body and $2n$-body operators. In spite of that, at second order ($n = 2$) and for the particle-number projection, the Lipkin-Nogami method has been applied quite widely, see Sec. IV.D.2.

C. The Kamlah method

The principal idea of the Kamlah expansion (Kamlah, 1968) is that the energy kernels can by efficiently expanded into a series of derivative operators $\mathcal{K}_m$ acting on overlap kernels:

$$\langle\Phi|\hat{H}\hat{R}(g)|\Phi\rangle = \sum_{m=0}^{M} k_m \mathcal{K}_m \langle\Phi|\hat{R}(g)|\Phi\rangle. \qquad (118)$$

This expansion is supposed to work best in the limit of strong symmetry breaking, for example, at large deformations. In this limit, the energy and overlap kernels are both strongly peaked near the diagonal of $g = 0$, and therefore, the expansion of the former in a series of derivatives of the latter may have a chance to converge rapidly.

Since for every continuous group, polynomials of symmetry generators $\hat{K}_m$ can always be represented by derivatives $\mathcal{K}_m$ with respect to the group parameters,

$$\hat{K}_m \hat{R}(g) \equiv \mathcal{K}_m \hat{R}(g), \qquad (119)$$

Kamlah expansion (118) is strictly equivalent to the Lipkin flattening condition (99) applied for the Lipkin operator of Eqs. (107) and (109). Since, in addition, Kamlah proposes to determine coefficients k_m by evaluating derivatives at $g = 0$, his method gives equations for k_m that are strictly equivalent to the Lipkin-Nogami method (114).

There are, nevertheless, two important differences. First, the Kamlah proposal involves variation of the projected energy (106) "as it is", i.e., a variation over symmetry-breaking states $|\Phi\rangle$ should also involve variation of k_m, see discussion in Sec. IV.D.2. Second, the Kamlah expansion may contain terms that are not invariants of the symmetry group, and therefore, they are not really within the realm of the Lipkin method. This latter property mostly relates to the so-called pushing and cranking terms discussed in detail in Sec. IV.D.1.

D. Applicability and Applications

The Lipkin, Kamlah, and Lipkin-Nogami methods, discussed in the previous sections, all rely on polynomial expansions of collective spectra or reduced kernels. This principal assumption creates two main limitations of these approaches. First, obviously, the expansions have to be carried out up to a sufficiently high order, see Sec. IV.D.3. And second, and most importantly, these methods cannot really be applied to spectra that have a non-analytical dependence on the quantum numbers. Unfortunately, the latter situation occurs in two physically meaningful cases, namely, when particle-numbers are restored in (semi)magic nuclei (Dobaczewski and Nazarewicz, 1993; Wang *et al.*, 2014) and when the

angular-momentum is restored in weakly-deformed systems (Gao *et al.*, 2015a).

1. First-order terms

The Fermi energy:
The simplest application of the Lipkin, Kamlah, or Lipkin-Nogami methods concerns the approximated restoration of the particle-number symmetry up to the first order in the particle number (100), i.e.,

$$\hat{K} = k_1(\hat{N} - N_0), \qquad (120)$$

where we can treat numbers of protons and neutrons separately. Then, the Lipkin-Nogami equations (115) and (117) give

$$k_0 = \frac{\langle\hat{H}\rangle\langle(\hat{N}-N_0)^2\rangle - \langle\hat{H}(\hat{N}-N_0)\rangle\langle\hat{N}-N_0\rangle}{\langle(\hat{N}-N_0)^2\rangle - \langle\hat{N}-N_0\rangle^2}, \quad (121)$$

$$k_1 = \frac{\langle\hat{H}(\hat{N}-N_0)\rangle - \langle\hat{H}\rangle\langle(\hat{N}-N_0)\rangle}{\langle(\hat{N}-N_0)^2\rangle - \langle\hat{N}-N_0\rangle^2}, \qquad (122)$$

where brackets $\langle\rangle$ denote average values calculated for the particle-number-symmetry-breaking state $|\Phi\rangle$. The variation-after-projection equation, which is derived from (106), now reads

$$\delta_\Phi E^{N_0} = 0 \qquad (123)$$

for

$$E^{N_0} = \langle\Phi|\hat{H} - k_1(\hat{N} - N_0)|\Phi\rangle. \qquad (124)$$

According to Lipkin's methodology, variation over $|\Phi\rangle$ has to be carried out at constant Lipkin coefficient k_1, and according to the Kamlah's methodology, expression for k_1 (122) should be inserted into (123) and then varied.

In this sense, at first order, the Lipkin-Nogami and Kamlah prescriptions lead to the same result. Moreover, the Lipkin coefficient k_1 can now be reinterpreted as a Lagrange multiplier λ_1, that is, as a Fermi energy, which has to be adjusted so as to obtain the correct average particle number. Then, the Lipkin-Nogami expressions (121) and (122) simplify tremendously, and give

$$k_0 = \langle\hat{H}\rangle, \qquad (125)$$

$$k_1 = \frac{\langle\hat{H}(\hat{N}-N_0)\rangle}{\langle(\hat{N}-N_0)^2\rangle}. \qquad (126)$$

The expression for k_0 is thus compatible with (124) and that for k_1 stems from (123), provided $\delta_\Phi|\Phi\rangle = (\hat{N} - N_0)|\Phi\rangle$ is an allowed variation.

In a similar way, we can evaluate the Lipkin expressions (112), which gives

$$k_0 = \frac{n_1(\phi_1)h(0) - n_1(0)h(\phi_1)}{n_1(\phi_1) - n_1(0)}, \qquad (127)$$

$$k_1 = \frac{h(\phi_1) - h(0)}{n_1(\phi_1) - n_1(0)}, \qquad (128)$$

where

$$n_m(\phi_i) = \frac{\langle\Phi|(\hat{N} - N_0)^m \exp(i\phi_i\hat{N})|\Phi\rangle}{\langle\Phi|\exp(i\phi_i\hat{N})|\Phi\rangle} \quad (129)$$

are reduced kernels of the shifted particle-number operator, evaluated at gauge angle ϕ_i, and $h(\phi_i) = h_i$ are the analogous reduced kernels of the Hamiltonian (111). Again it is beneficial to carry out variation (123) with the average particle number kept correct, $\langle\hat{N}\rangle = N_0$, which gives $n_1(0) = 0$. In this case, expression (127) reduces again to $k_0 = \langle\hat{H}\rangle$ and expression (128) stems from (123), provided the finite-difference derivatives are allowed as variations $\delta_\Phi|\Phi\rangle$.

We conclude, that the Lipkin, Lipkin-Nogami, and Kamlah symmetry restoration at first-order are completely equivalent to using Lagrange multipliers for adjusting average values of symmetry generators.

The pushing model and Thouless-Valatin mass:
For the restoration of translational symmetry, at first order the Lipkin operator reads,

$$\hat{K} = \sum_{n=x,y,z} k_{1n}(\hat{P}_n - P_{n0}) = \boldsymbol{k}_1 \cdot (\hat{\boldsymbol{P}} - \boldsymbol{P}_0), \quad (130)$$

where (101) is generalized to the case of a nucleus moving with the average total momentum $\boldsymbol{P}_0$. We note here that the lowest-order invariant of the translational group is equal to $\hat{\boldsymbol{P}}^2$, and therefore, the flattening of the spectrum requires using the second-order Lipkin operator, see Sec. IV.D.2. Therefore, the first-order model (130) rather pertains to the Kamlah approach.

Since components of the momentum operator $\hat{\boldsymbol{P}}$ commute, we can treat them independently. Then, following the derivations presented for the particle number, we conclude that the restoration of translational symmetry is, at first order, equivalent to performing minimization of the total energy, constrained to the given momentum $\boldsymbol{P}_0$,

$$E^{\boldsymbol{P}_0} = \langle\Phi|\hat{H} - \boldsymbol{v} \cdot (\hat{\boldsymbol{P}} - \boldsymbol{P}_0)|\Phi\rangle, \quad (131)$$

where the vector Lipkin coefficient $\boldsymbol{k}_1$ acquires interpretation of the Lagrange multiplier $\boldsymbol{v}$, i.e., of the velocity of the system.

For the translational symmetry, variation of the total energy $E^{\boldsymbol{P}_0}$ constrained to the momentum $\boldsymbol{P}_0$ is particularly simple. Indeed, suppose we have found the state $|\Phi_{\boldsymbol{P}_0=\boldsymbol{0}}\rangle$, which is at rest, $\langle\Phi_{\boldsymbol{P}_0=\boldsymbol{0}}|\hat{\boldsymbol{P}}|\Phi_{\boldsymbol{P}_0=\boldsymbol{0}}\rangle = \boldsymbol{0}$, and fulfills the variation-after-projection equation $\delta E^{\boldsymbol{P}_0=\boldsymbol{0}} = 0$ for $\boldsymbol{v} = \boldsymbol{0}$. Then, the Galilean symmetry,

$$\left[\hat{H}, \hat{\boldsymbol{R}}\right] = -\frac{i\hbar\hat{\boldsymbol{P}}}{Am}, \quad (132)$$

where $\hat{\boldsymbol{R}}$ is the center-of-mass coordinate and Am is the total mass of the system, allows us to boost state $|\Phi_{\boldsymbol{P}_0=\boldsymbol{0}}\rangle$ to momentum $\boldsymbol{P}_0$,

$$|\Phi_{\boldsymbol{P}_0}\rangle = \exp\langle\{\tfrac{i}{\hbar}\boldsymbol{P}_0 \cdot \hat{\boldsymbol{R}}\}|\Phi_{\boldsymbol{P}_0=\boldsymbol{0}}\rangle, \quad (133)$$

so that

$$\boldsymbol{P}_0 = \langle\Phi_{\boldsymbol{P}_0}|\hat{\boldsymbol{P}}|\Phi_{\boldsymbol{P}_0}\rangle, \quad (134)$$

$$\boldsymbol{v} = \frac{\boldsymbol{P}_0}{Am}, \quad (135)$$

$$E^{\boldsymbol{P}_0} = E^{\boldsymbol{P}_0=\boldsymbol{0}} + \frac{\boldsymbol{P}_0^2}{2Am}. \quad (136)$$

We see that the restoration of translational symmetry at first order, that is, the pushing model, correctly reproduces all classical-motion relations. In particular, from the analog of the Lipkin-Nogami expression (126) we obtain the velocity vector as,

$$\boldsymbol{v} = \frac{\langle\hat{H}(\hat{\boldsymbol{P}} - \boldsymbol{P}_0)\rangle}{\langle(\hat{\boldsymbol{P}} - \boldsymbol{P}_0)^2\rangle}, \quad (137)$$

which gives the mass

$$\mathcal{M}^{-1} = \frac{|\boldsymbol{v}|}{|\boldsymbol{P}_0|} = \frac{|\langle\hat{H}(\hat{\boldsymbol{P}} - \boldsymbol{P}_0)\rangle|}{\langle(\hat{\boldsymbol{P}} - \boldsymbol{P}_0)^2\rangle|\langle\hat{\boldsymbol{P}}\rangle|}, \quad (138)$$

that, in the translational case, correctly reproduces the true mass of the system, $\mathcal{M} = Am$ (Thouless and Valatin, 1962).

The cranking model and Thouless-Valatin moment of inertia:
Restoration of the rotational symmetry at first order leads to the so-called cranking model, which was introduced originally in a semiclassical time-dependent picture of a system rotating with constant angular velocity $\boldsymbol{\omega}$ around a fixed axis parallel to the angular momentum $\boldsymbol{J}$ (Inglis, 1954, 1956). This model was very successfully used in nuclear physics to describe a multitude of physical phenomena related to collective rotation (Bohr and Mottelson, 1998; Ring and Schuck, 1980). In this case, the Lipkin operator reads,

$$\hat{K} = \sum_{n=x,y,z} k_{1n}(\hat{J}_n - J_{n0}) = \boldsymbol{k}_1 \cdot (\hat{\boldsymbol{J}} - \boldsymbol{J}_0) \quad . \quad (139)$$

Since components of the angular-momentum operator $\hat{\boldsymbol{J}}$ do not commute, we cannot treat them independently. Eq. (139) has thus to be understood as corresponding to a nucleus having a fixed projection $J_0 = |\boldsymbol{J}_0|$ of the angular momentum on a quantization axis oriented along the Lipkin coefficient vector, $\boldsymbol{k}_1 = \boldsymbol{\omega}$. In systems with approximate axial symmetry along the z-axis, for instance, for the ground-state bands in well deformed even-even nuclei, the rotational axis is perpendicular to the symmetry axis and usually chosen along the x-axis. In this case, we have $J_0 = \langle J_x\rangle = \sqrt{I(I+1)}$ with integer values of I (for odd systems see (Ring *et al.*, 1974)). Different directions of $\boldsymbol{k}_1$ then mean a freedom of choosing an arbitrary direction of the quantization axis. This defines the so-called tilted-axis cranking model (Frauendorf, 2001;

Kerman and Onishi, 1981; Shi *et al.*, 2013), where the vector of the average angular momentum $\langle\hat{\boldsymbol{J}}\rangle$ is arbitrarily oriented with respect to the principal axes of the mass distribution of the rotational-symmetry-breaking state.

Following the derivations presented for the momentum operator, we conclude that the restoration of rotational symmetry is, at first order, equivalent to performing minimization of the total energy, constrained to the given projection of the angular momentum J_0,

$$E^{\boldsymbol{J}_0} = \langle\Phi|\hat{H} - \boldsymbol{\omega}\cdot(\hat{\boldsymbol{J}} - \boldsymbol{J}_0)|\Phi\rangle, \qquad (140)$$

where the vector Lipkin coefficient $\boldsymbol{k}_1$ acquires interpretation of the Lagrange multiplier $\boldsymbol{\omega}$, that is, of the angular velocity of the system.

The principal difference between translational and rotational symmetry is the fact that for rotations there is no analogue of the Galilean symmetry (132), and one cannot simply boost a non-rotating state to higher rotational frequencies without changing its structure. Indeed, with increasing rotational frequency, the quantum analogues of the classical Coriolis and centrifugal forces set in, and modify the state. Therefore, a constrained minimization of the total energy has now to be explicitly performed.

Recalling that the average momentum is exactly proportional to the translational velocity, Eq. (135), with a constant proportionality factor (mass). Although the average angular momentum $\langle\hat{\boldsymbol{J}}\rangle$ has to be parallel to the angular frequency $\boldsymbol{\omega}$ (Kerman and Onishi, 1981), the proportionality constant (moment of inertia) can vary along the rotational band. Therefore, we define two important *local*, that is, frequency-dependent characteristics of the band, which are called the first $\mathcal{J}^{(1)}$ (static) and the second $\mathcal{J}^{(2)}$ (dynamic) moments of inertia,

$$\mathcal{J}^{(1)}(\omega) = \frac{|\langle\hat{\boldsymbol{J}}\rangle(\omega)|}{\omega} \quad \text{and} \quad \mathcal{J}^{(2)}(\omega) = \frac{\mathrm{d}|\langle\hat{\boldsymbol{J}}\rangle(\omega)|}{\mathrm{d}\omega}, \qquad (141)$$

respectively.

In parallel with Eq. (138), the Lipkin expression allows us to determine the static moment of inertia,

$$\mathcal{J}^{(1)} = \frac{\langle(\hat{\boldsymbol{J}} - \boldsymbol{J}_0)^2\rangle|\langle\hat{\boldsymbol{J}}\rangle|}{|\langle\hat{H}(\hat{\boldsymbol{J}} - \boldsymbol{J}_0)\rangle|}. \qquad (142)$$

The dynamic moment of inertia is identical to this value only at $\omega = 0$. For all other values of ω, it corresponds to the Thouless-Valatin moment of inertia $\mathcal{J}^{(2)} = \mathcal{J}_{\mathrm{TV}}$ that can be derived in linear response theory (Thouless and Valatin, 1962).

Isocranking:
To perform restoration of the isospin symmetry at first order, Satuła and Wyss (Głowacz *et al.*, 2004; Satuła and Wyss, 2001a,b) introduced the so-called isocranking model, in which the Lipkin operator reads

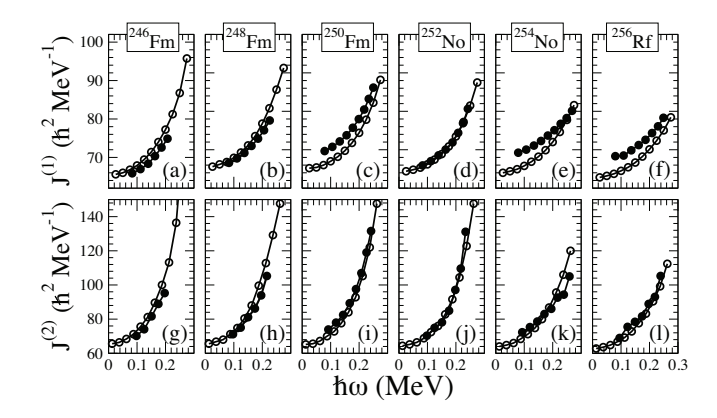$$\hat{K} = \sum_{n=x,y,z} k_{1n}(\hat{T}_n - T_{n0}) = \vec{k}_1 \circ (\hat{\vec{T}} - \vec{T}_0), \qquad (143)$$

FIG. 5 The kinematic $\mathcal{J}^{(1)}$ (top) and dynamic $\mathcal{J}^{(2)}$ (bottom) moments of inertia in ^{246}Fm, ^{248}Fm, ^{250}Fm, ^{252}No, ^{254}No, and ^{256}Rf as functions of the rotational frequency. Open circles show theoretical results whereas full dots denote experimental values. Reprinted figure with permission from (Shi *et al.*, 2014). Copyright 2014 by the American Physical Society.

where arrows denote vectors in the isospace (isovectors) and symbol "$\circ$" denotes their scalar product. Since components of the isospin operator $\hat{\vec{T}}$ do not commute, we cannot treat them independently. Thus Eq. (143) has to be understood as corresponding to a nucleus having a fixed projection $T_0 = |\vec{T}_0|$ of the isospin on the isoquantization axis oriented along the isovector Lipkin coefficient $\vec{k}_1$. Moreover, in even (odd) systems, projections T_0 can only equal to integer (half-integer) numbers. Different directions of $\vec{k}_1$ then mean a freedom of choosing an arbitrary direction of the isoquantization axis. The Lipkin coefficient $\vec{k}_1$ is interpreted as the isovector Fermi energy $\vec{\lambda}$ (Sato *et al.*, 2013; Sheikh *et al.*, 2014), which fixes the average values of components of the isospin $\langle\hat{\vec{T}}\rangle$.

We note that the standard definition of the isospin implies that its z component is equal to half of the neutron excess, $T_z = \frac{1}{2}(N - Z)$. Therefore, the z component of the isovector Fermi energy λ_z along with the standard isoscalar Fermi energy λ simply fix the neutron N and proton Z numbers. When the isocranking axis is tilted away from the z direction, one must use the formalism where proton and neutron components of single-particle states are mixed (Sato *et al.*, 2013; Sheikh *et al.*, 2014). Such a situation occurs when the isospin-symmetry-breaking terms are added to the nuclear Hamiltonian (Bączyk *et al.*, 2018). Figure 6 shows energies of states in ^{48}Cr isocranked to $\langle T_x\rangle = 0, 2, 4, 6$, and 8, while keeping $\langle T_z\rangle = 0$ (Sato *et al.*, 2013). We see that one obtains a perfectly rigid isorotating band (a sequence of states in ^{48}Cr with increasing isospin T). The obtained Thouless-Valatin moment of inertia then corresponds to the symmetry energy coefficient a_I in the symmetry energy, $E_I(N, Z) = \frac{1}{2}a_I(N - Z)/A$, i.e., to $a_I = 2A \times 1.39(2)/4 = 33.4(5)$ MeV.
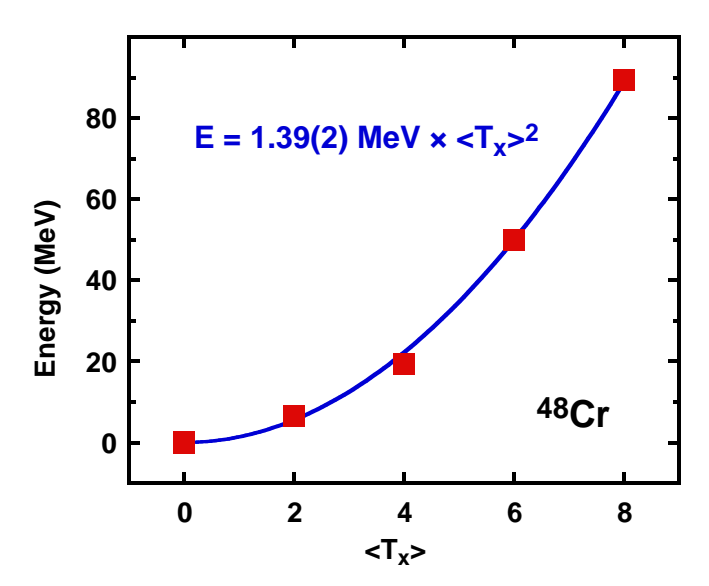
FIG. 6 (Color online) Excitation energies of ^{48}Cr isocranked to $\langle T_x \rangle = 0, 2, 4, 6,$ and 8 (squares) (Sato *et al.*, 2013). The solid line represents the parabolic fit.

2. Second-order terms

Although at first order the Lipkin or Kamlah approach provides correct understanding of the collective effects, including the proper determination of the collective mass, it does not really fulfil Lipkin's requirement of flattening the spectrum of projected states. Indeed, already from the example of the translational motion, we see that the main component of this dependence may rather be quadratic then linear. In this section, we thus examine the Lipkin operators expanded up to second-order terms in the symmetry generators. This allows us to model the spectra in terms of the quadratic Casimir operators of the corresponding symmetry groups.

Particle-number restoration:
The main focus of the Lipkin-Nogami method (Goodfellow and Nogami, 1966; Nogami, 1965; Nogami and Zucker, 1964; Nogami, 1964; Pradhan *et al.*, 1973) was up to now on the approximate restoration of the particle-number symmetry, whereby the Lipkin operator is postulated as,

$$\hat{K} = k_1(\hat{N} - N_0) + k_2(\hat{N} - N_0)^2. \qquad (144)$$

Assuming again that k_1 is always adjusted so as to obtain the correct particle number, $\langle \hat{N} - N_0 \rangle = 0$, the Lipkin (112) (Wang *et al.*, 2014) and Lipkin-Nogami (115) (Valor *et al.*, 1996) methods give, respectively,

$$k_2 = \frac{h(\phi_2) - k_1 n_1(\phi_2) - h(0)}{n_2(\phi_2) - n_2(0)}, \qquad (145)$$

and

$$\lambda_2 = \frac{\langle \hat{H}\Delta\hat{N}^2\rangle\langle\Delta\hat{N}^2\rangle - \langle\hat{H}\Delta\hat{N}\rangle\langle\Delta\hat{N}^3\rangle - \langle\hat{H}\rangle\langle\Delta\hat{N}^2\rangle^2}{\langle\Delta\hat{N}^4\rangle\langle\Delta\hat{N}^2\rangle - \langle\Delta\hat{N}^3\rangle^2 - \langle\Delta\hat{N}^2\rangle^3}. \qquad (146)$$

Here $\Delta\hat{N} \equiv \hat{N} - N_0$ is the shifted particle-number operator, $h(\phi_2)$ and $n_i(\phi_2)$ are the Hamiltonian (111) and shifted particle-number (129) kernels, and we used the traditional notation of $\lambda_2 \equiv k_2$ for the second-order Lipkin-Nogami coefficient. For an HFB vacuum $|0\rangle$, an alternative and equivalent expression for λ_2 was derived in (Sandhu and Rustgi, 1978) as

$$\lambda_2 = \frac{\sum_4 \langle 0|\hat{H}|4\rangle\langle 4|\hat{N}^2|0\rangle}{\sum_4 \langle 0|\hat{N}^2|4\rangle\langle 4|\hat{N}^2|0\rangle}, \qquad (147)$$

where $|4\rangle$ stands for all four-quasiparticle states. After evaluating all required matrix elements, one obtains (Flocard and Onishi, 1997; Stoitsov *et al.*, 2003)

$$\lambda_2 = \frac{4\mathrm{Tr}\Gamma'\rho(1-\rho) + 4\mathrm{Tr}\Delta'(1-\rho)\kappa}{8\left[\mathrm{Tr}\rho(1-\rho)\right]^2 - 16\mathrm{Tr}\rho^2(1-\rho)^2}, \qquad (148)$$

where the potentials

$$\Gamma'_{\mu\mu'} = \sum_{\nu\nu'} V_{\mu\nu\mu'\nu'}(\rho(1-\rho))_{\nu'\nu}, \qquad (149)$$

$$\Delta'_{\mu\nu} = \tfrac{1}{2}\sum_{\mu'\nu'} V_{\mu\nu\mu'\nu'}(\rho\kappa)_{\mu'\nu'}, \qquad (150)$$

can be calculated in full analogy to Γ and Δ by replacing the ρ and κ in terms of which they are defined by $\rho(1-\rho)$ and $\rho\kappa$, respectively. In the case of the seniority pairing interaction with strength G, Eq. (148) simplifies to

$$\lambda_2 = \frac{G}{4}\frac{\mathrm{Tr}(1-\rho)\kappa\,\mathrm{Tr}\rho\kappa - 2\,\mathrm{Tr}(1-\rho)^2\rho^2}{\left[\mathrm{Tr}\rho(1-\rho)\right]^2 - 2\,\mathrm{Tr}\rho^2(1-\rho)^2}, \qquad (151)$$

or explicitly in terms of the canonical-basis occupation factors (Pradhan *et al.*, 1973):

$$\lambda_2 = \frac{G}{4}\frac{\sum_{k>0}(u_k v_k^3)\sum_{k>0}(u_k^3 v_k) - \sum_{k>0}(u_k v_k)^4}{(\sum_{k>0}u_k^2 v_k^2)^2 - \sum_{k>0}(u_k v_k)^4}, \qquad (152)$$

where $k > 0$ denotes the summation over one state of each canonical pair.

Evaluation of the Lipkin coefficient k_2, as in Eq. 145, is fairly simple, see Sec. IV.D.3, but it was implemented only in (Wang *et al.*, 2014). A rigorous evaluation of the Lipkin-Nogami coefficient λ_2, Eq. (146) or (148), is for realistic Hamiltonians rather cumbersome, so it was rarely implemented in full, see, e.g., (Valor *et al.*, 1996). A practical workaround, which was used quite often, see, e.g., (Kortelainen *et al.*, 2010; Stoitsov *et al.*, 2007, 2003) was to use the seniority-pairing expression Eq. (151) with the effective strength $G \equiv G_{\mathrm{eff}} = -\frac{\bar{\Delta}^2}{E_{\mathrm{pair}}}$ determined from the pairing energy E_{pair} and the average pairing gap $\bar{\Delta}$.
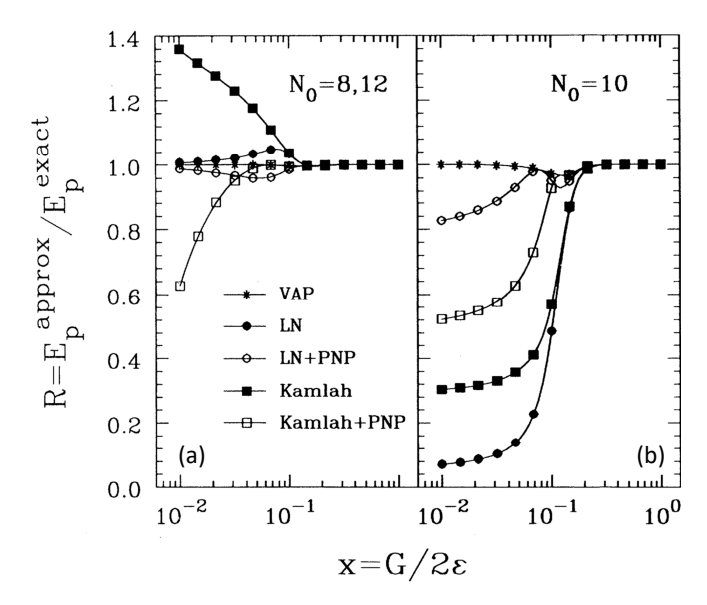
FIG. 7 (Color online) Pairing energies in the two-level model obtained in (Zheng *et al.*, 1992) within the variation after projection (VAP) (asterisks), Kamlah (full squares), and Lipkin-Nogami (full circles) approximations, relative to the exact values and plotted for $N_0=\Omega=10$ (right), and $N_0=\Omega\pm2$ (left). The energies resulting from the exact particle-number projection of Kamlah (open squares) and Lipkin-Nogami (open circles) states are shown for comparison. The critical value of x is $x_c=1/9$. Reprinted figure with permission from (Dobaczewski and Nazarewicz, 1993). Copyright 1993 by the American Physical Society.

Figure 7 shows comparison of the Lipkin-Nogami and Kamlah approaches within a simple solvable two-level model (Dobaczewski and Nazarewicz, 1993; Zheng *et al.*, 1992). In the strong-pairing regime, both approaches give excellent reproduction of the exact results, however, for the half-filled shell [Fig. 7(b)], at or below the critical pairing strength both fail. This is so because the kink in the dependence of the exact energies on the particle number, which is a characteristic feature of a shell gap, cannot be reproduced by the quadratic (Dobaczewski and Nazarewicz, 1993) or higher-order (Wang *et al.*, 2014) form of the Lipkin operator. Away from the shell gap [Fig. 7(a)], the Lipkin-Nogami approach works well for all pairing strengths, but the Kamlah approach fails below the critical pairing strength. This latter feature can be attributed to the fact that by exploiting errors of the approximation, the exact minimization over the Lipkin coefficient λ_2 brings the approximate projected energy below the exact result.

Peierls-Yoccoz mass:
For the translational symmetry, at second order, the general form of the Lipkin operator reads

$$\hat{K} = \boldsymbol{k}_1 \cdot (\hat{\boldsymbol{P}} - \boldsymbol{P}_0) + \sum_{n=x,y,z} k_{2n}(\hat{P}_n - P_{n0})^2. \quad (153)$$

As already discussed in Sec. IV.D.1, the first-order terms

define the pushing model, wherein the nucleus moves in space with average momentum $\boldsymbol{P}_0$ and velocity $\boldsymbol{v} \equiv \boldsymbol{k}_1$. This motion leads to an increase of energy that is quadratic in the momentum, and the corresponding proportionality coefficient is called the Thouless-Valatin mass (138), which is correctly equal to the translational mass mA.

The role of the Lipkin coefficients k_{2n} is different – they are meant to flatten the spectrum of energies projected on momentum eigenstates in the direction of $n = x$, y, or z. Their values thus characterize the momentum distributions within the translational-symmetry-breaking state, and have nothing to do with the physical motion of the system. This is particularly evident when we consider the state at rest, $|\Phi_{\boldsymbol{P}_0=\boldsymbol{0}}\rangle$, which can be obtained by simply conserving the time-reversal symmetry. This state does not move, so the Lipkin coefficients k_{2n} cannot describe inertia, which is the reaction of the system under boost.

Coefficients k_{2n} calculated for the $n = x$, y, or z directions can differ from one another (Gao *et al.*, 2015a). Indeed, along the longer or shorter principal axis of the mass distribution, the momentum distribution is narrower or wider, respectively, and the corresponding projected energy components can thus differ from one another.

Nevertheless, historically, quantities $\mathcal{M}_{\mathrm{PYn}} = \frac{1}{2}k_{2n}^{-1}$, corresponding to translational Lipkin coefficients k_{2n}, are called Peierls-Yoccoz (Peierls and Yoccoz, 1957) or Yoccoz (Ring and Schuck, 1980) masses. Assuming that those corresponding to the $n = x$, y, or z directions are independent from one another, they can be calculated in the Lipkin or Lipkin-Nogami approach, respectively, as:

$$k_{2n} \equiv (2\mathcal{M}_{\mathrm{PYn}})^{-1} = \frac{h(\phi_{2n}) - k_{1n}p_{1n}(\phi_{2n}) - h(0)}{p_{2n}(\phi_{2n}) - n_2(0)} \quad (154)$$

or

$$k_{2n} \equiv (2\mathcal{M}_{\mathrm{PYn}})^{-1}$$
$$= \frac{\langle\hat{H}\Delta\hat{P}_n^2\rangle\langle\Delta\hat{P}_n^2\rangle - \langle\hat{H}\Delta\hat{P}_n\rangle\langle\Delta\hat{P}_n^3\rangle - \langle\hat{H}\rangle\langle\Delta\hat{P}_n^2\rangle^2}{\langle\Delta\hat{P}_n^4\rangle\langle\Delta\hat{P}_n^2\rangle - \langle\Delta\hat{P}_n^3\rangle^2 - \langle\Delta\hat{P}_n^2\rangle^3}, \quad (155)$$

cf. Eqs. (145) or (146). Here $\Delta\hat{P}_n = \hat{P}_n - P_{n0}$ are shifted momentum operators for $n = x$, y, or z and $p_{in}(\phi_{2n})$ are their reduced kernels calculated at distances ϕ_{2n}.

For conserved time reversal, average values of all odd powers of momentum are equal to zero, and thus Eq. (155) reduces to

$$k_{2n} \equiv (2\mathcal{M}_{\mathrm{PYn}})^{-1} = \frac{\langle\hat{H}\hat{P}_n^2\rangle - \langle\hat{H}\rangle\langle\hat{P}_n^2\rangle}{\langle\hat{P}_n^4\rangle - \langle\hat{P}_n^2\rangle^2}. \quad (156)$$

In addition, if we consider a spherical nucleus, where the Lipkin coefficients corresponding to three directions $n = x$, y, or z are equal, and the Lipkin operator takes the
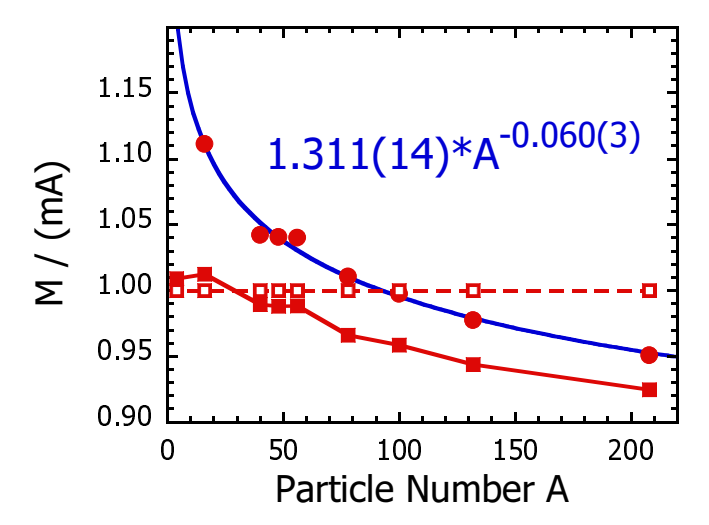
FIG. 8 (Color online) Exact masses ($M = mA$, open squares) and the Peierls-Yoccoz masses $M = \mathcal{M}_{\text{PY}}$, Eq. (157), calculated in doubly magic nuclei before (full circles) and after (full squares) including the Lipkin operator. Reprinted figure with permission from (Dobaczewski, 2009).

form $\hat{K} = k_2 \hat{\boldsymbol{P}}^2$, we then have

$$k_2 \equiv (2\mathcal{M}_{\text{PY}})^{-1} = \frac{\langle \hat{H}\hat{\boldsymbol{P}}^2 \rangle - \langle \hat{H} \rangle \langle \hat{\boldsymbol{P}}^2 \rangle}{\langle \hat{\boldsymbol{P}}^4 \rangle - \langle \hat{\boldsymbol{P}}^2 \rangle^2} . \qquad (157)$$

We see that equality of k_{2n} and k_2 requires independence of the three directions, $\langle \hat{P}_n^2 \hat{P}_m^2 \rangle = \langle \hat{P}_n^2 \rangle \langle \hat{P}_m^2 \rangle$ for $n \neq m$, which was assumed when deriving Eqs. (155) and (156). Further, within the Gaussian Overlap Approximation (Ring and Schuck, 1980), we have $\langle \hat{\boldsymbol{P}}^4 \rangle = 3\langle \hat{\boldsymbol{P}}^2 \rangle^2$, and Eq. (157) simplifies to

$$2k_2 \equiv (\mathcal{M}_{\text{PY}})^{-1} = \frac{\langle \hat{H}\hat{\boldsymbol{P}}^2 \rangle - \langle \hat{H} \rangle \langle \hat{\boldsymbol{P}}^2 \rangle}{\langle \hat{\boldsymbol{P}}^2 \rangle^2} . \qquad (158)$$

Figure 8 shows comparison of the Peierls-Yoccoz and Thouless-Valatin (exact) masses calculated in doubly magic nuclei. We see that the former are never equal to the latter, because they represent different quantities. Indeed, the Peierls-Yoccoz masses characterize the curvatures of energies projected from the symmetry-breaking states at rest, whereas the Thouless-Valatin masses characterize the increase of the energy when the symmetry-breaking states are boosted to non-zero momenta. In addition, the figure shows the Peierls-Yoccoz masses evaluated for energies minimized before and after including the Lipkin operator. One clearly sees that the self-consistent inclusion of the Lipkin correction does modify the curvatures of projected energies. In practice, however, differences between the Peierls-Yoccoz and Thouless-Valatin translational masses do not exceed 10% and vary smoothly with nuclear masses. More discussion can be found in (Bender et al., 2000; Dobaczewski, 2009).

Peierls-Yoccoz moment of inertia:
For the rotational symmetry, at second order, the Lipkin operator reads

$$\hat{K} = \boldsymbol{k}_1 \cdot (\hat{\boldsymbol{J}} - \boldsymbol{J}_0) + \sum_{n=x,y,z} k_{2n}(\hat{J}_n^2 - J_{n0}^2) . \qquad (159)$$

As already discussed in Sec. IV.D.1, the first-order terms define the cranking model, wherein the nucleus rotates in space with average angular momentum $\boldsymbol{J}_0$ and frequency $\boldsymbol{\omega} \equiv \boldsymbol{k}_1$. This motion leads to an increase of energy, which is (in deformed nuclei) approximately quadratic in the angular momentum, and the corresponding proportionality coefficient is called the Thouless-Valatin moment of inertia (142). On the other hand, the Lipkin coefficients k_{2n} are meant to flatten the spectrum of energies projected on angular momentum eigenstates. However, since the three components of the angular momentum do not commute, the three first-order and three second-order terms in the Lipkin operator (159) are not independent from one another. Moreover, in axial nuclei, the rotational symmetry is not fully broken, namely, the total angular momenta are mixed, but the projections of the angular momentum on the symmetry axis continue to be a good quantum numbers. In this case, the second-order Lipkin operator in the form of Eq. (103) is more appropriate.

Expressions for Peierls-Yoccoz moments of inertia can be obtained in full analogy to those for Peierls-Yoccoz masses, Eqs. (155)–(158). In particular, for a one-dimensional rotation of an axial nucleus about the x axis perpendicular to the symmetry axis, the analogue of Eq. (156) reads

$$(2\mathcal{J}_{\text{PY}})^{-1} = \frac{\langle \hat{H}\hat{J}_x^2 \rangle - \langle \hat{H} \rangle \langle \hat{J}_x^2 \rangle}{\langle \hat{J}_x^4 \rangle - \langle \hat{J}_x^2 \rangle^2} . \qquad (160)$$

Gao et al. (Gao et al., 2015a) performed calculations of the Thouless-Valatin (cranking) and Peierls-Yoccoz moments of inertia for axial ground states of even-even isotopes of erbium, see Fig. 9. As is well known (Bohr and Mottelson, 1998; Ring and Schuck, 1980), pairing correlations bring the cranking moments of inertia down by about a factor of two and remove peaks related to single-particle level crossings – these features are clearly visible in Fig. 9. On the other hand, the Peierls-Yoccoz moments of inertia appear to be fairly independent of the pairing correlations, that is, the angular-momentum contents of deformed states is not impacted by pairing.

Isospin:
Almost immediately after Nogami's work (Nogami, 1964), an analogous method has been suggested in the restoration of the isospin symmetry (Ghosh et al., 1975; Kissener and Münchow, 1966, 1967), whereupon the Lipkin operator,

$$\hat{K} = \vec{k}_1 \circ (\hat{\vec{T}} - \vec{T}_0) + k_2 \left(\hat{\vec{T}}^2 - T_0(T_0 + 1) \right), \qquad (161)$$
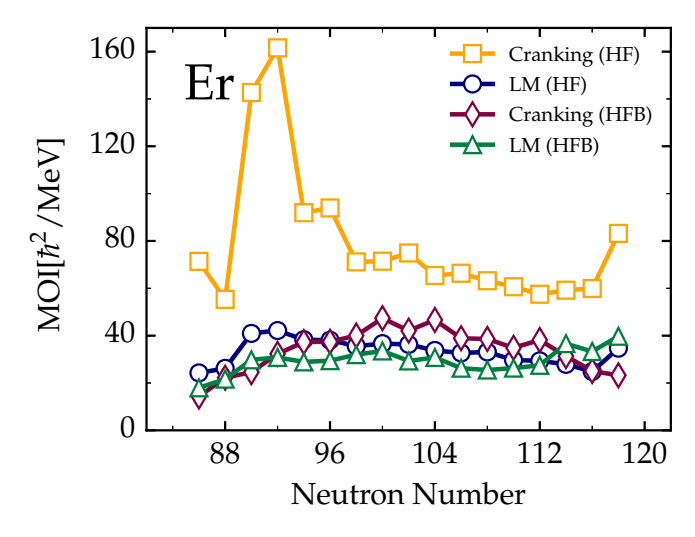
FIG. 9 (Color online) The Peierls-Yoccoz moments of inertia of erbium isotopes, obtained using the Lipkin method (LM), compared with the Thouless-Valatin (cranking) moments of inertia for axial states with pairing correlations included (HFB) or not included (HF) (Gao *et al.*, 2015a).
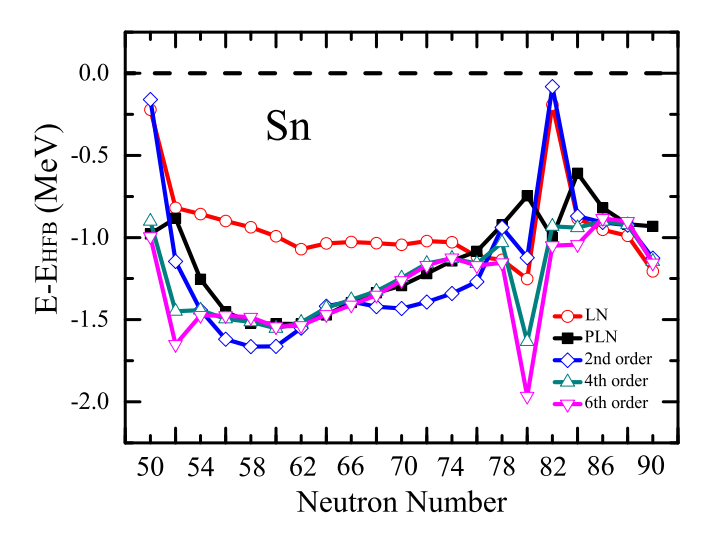

FIG. 10 (Color online) The Lipkin-Nogami (LN), Projected-Lipkin-Nogami (PLN), and Lipkin energies at 2nd, 4th, and 6th order relative to those obtained within the standard HFB method, calculated for the tin isotopes. Reprinted figure with permission from (Wang *et al.*, 2014). Copyright 2014 by the American Physical Society.

combines the isocranking term (143) with the second-order correction. Such approach, however, was later not too often employed, because the exact isospin restoration was early implemented (Caurier *et al.*, 1980a,b; Caurier and Poves, 1982) and is now efficiently used (Satuła *et al.*, 2016, 2009, 2010).

3. Higher-order terms

In the Lipkin approach or Kamlah expansion, higher-order terms were studied for the particle-number restoration. (Rodríguez *et al.*, 2005) introduced the so-called reduced variation-after-projection method, which aimed to improve second-order Lipkin-Nogami or Kamlah results. The proposed method reformulated the minimization of the Lipkin magic formula (106) for the 4th-order Lipkin operator,

$$\hat{K} = k_1(\hat{N} - N_0) + k_2(\hat{N} - N_0)^2 + k_4(\hat{N} - N_0)^4. \quad (162)$$

The minimization was, in fact, split into two separate phases: first the average value (106) was minimized for different *fixed* values of the Lipkin coefficients k_2 and k_4, with k_1 again used to adjust the average particle number, and second, the obtained energy as function of k_2 and k_4 was minimized over these parameters. This innovative approach thus treated the Lipkin coefficients as additional variational parameters, which allowed to adjust the second- and fourth-order fluctuations of the particle number. The authors showed that the second-order reduced variation-after-projection method was equivalent to the second-order Lipkin-Nogami method, however, the fourth-order reduced variation-after-projection

approach turned out to approximate the exact variation-after-projection results much more precisely.

The Lipkin method up to sixth order was implemented in (Wang *et al.*, 2014), see Fig. 10. This work showed that away from semi-magic nuclei, the Lipkin method converges already at 4th order, with the 6th order corrections bringing almost no change. Near the semi-magic nuclei, however, the non-analytical dependence of energy in function of the particle number did not allow for obtaining well converged results.

Finally, in (Wang *et al.*, 2018) the Lipkin operator was extended by taking into account the second-order cross-term, which depends on the product of neutron and proton particle numbers, $(\hat{N} - N_0)(\hat{Z} - Z_0)$. As shown in Fig. 11, the energy kernels in functions of the neutron and proton gauge angles can be very much tilted away from the axes when only one gauge angle is taken into account. Therefore, to reproduce the energy kernels by the kernels of the Lipkin operator, the latter must be augmented by the cross term. As it turns out, the introduction of the cross term does not impact the energy corrections very strongly, however, other observables can be affected much more.

V. PROJECTION METHODS IN SIMPLE NUCLEAR MODELS

A. The pairing-plus-quadrupole model

The basic objective of the projection methods is to include the many-body correlations beyond the mean-field level, and in order to treat them accurately, the best is to
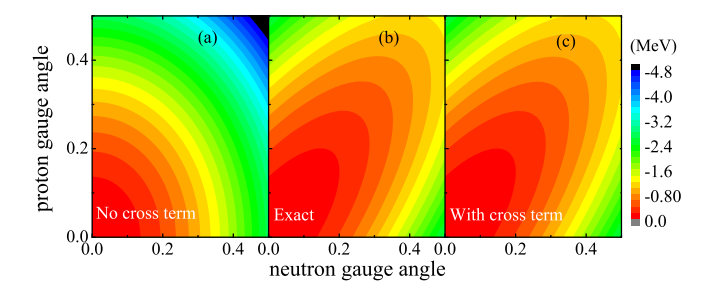
FIG. 11 (Color online) Reduced energy kernels $h(\phi_\nu, \phi_\pi) - h(0,0)$ calculated in ^{48}Cr as functions of the neutron and proton gauge angles (Wang *et al.*, 2018). Exact results (b) are compared with the Lipkin approximations without (a) and with (c) the cross term included.

perform them in the $\boldsymbol{r}$-space (Baye and Heenen, 1984). However, projection in the $\boldsymbol{r}$-space leads to solution of non-local potential problem, even with zero-range effective interaction. The non-local potential problem is quite prohibitive to solve even with the modern computing facilities. This has also to do with the fact that even the bare three-dimensional HFB problem is very difficult to solve in $\boldsymbol{r}$-space. Two-dimensional HFB equations have been solved in $\boldsymbol{r}$-space using the spline functions (Kegley Jr. *et al.*, 1996; Pei *et al.*, 2008) and there have been also attempts to solve the three-dimensional HFB problem using the multi-wavelet method (Pei *et al.*, 2014). As evident from these studies, the solution of the HFB equations in the $\boldsymbol{r}$-space become extremely complicated.

For the above reason, most of the application of projection methods have been carried out by expanding the single-particle wave functions in a finite basis. This leads to relatively simple matrix operations. The basis states, normally chosen, are solutions of harmonic oscillator or Woods-Saxon potentials. For 2D and 3D mean-field calculations, the oscillator bases has the advantage that these wave functions are separable in the coordinates x, y, z (in the triaxial case) or in $r_\perp, z, \varphi$ (in the axially symmetric case) and, therefore, it is very easy to use them by building deformed basis sets.

Through a careful choice of the basis deformation parameters, this allows us to reproduce, in a relatively small basis of roughly 20 major oscillator shells, the exact mean-field results of the system with sufficient accuracy, i.e., with roughly 500 keV in the total nuclear binding energies even for heavy nuclei (Dobaczewski *et al.*, 2002). However, for the application of projection methods, the use of a deformed basis leads to severe problems, as is also discussed in Sec. VI.A.1, because the basis violates the corresponding symmetry from the beginning. By this reason, all of the applications of angular momentum projection have been carried out in a spherical basis. Of course, no such problem occurs for the particle number projection, where one always starts with the usual single-particle basis.

In most of the realistic nuclear models, for instance, the density functional approach, the projection methods have been applied after variation and include correlations only partially beyond the mean-field level. Projection calculations before variation become exceedingly difficult, in particular, for the case of three-dimensional projection. These studies before variation have been performed with simpler model Hamiltonians using a few major oscillator shells around the Fermi surface.

The justification for using such a simpler approach is that the properties one is interested to describe using projection technique is to a large extent contained in the valence spaces. The pairing part of the effective interaction is dominated by single-particle states around the Fermi surface. Even the correlations leading to deformation are dominated by contributions from a valence space of a few major oscillator shells. It is known from several studies that states that are far above or below the Fermi surface do not contribute to the correlations beyond the mean-field level. This is clearly evident in the case of particle-number projection, where the states far from the Fermi surface have BCS occupations of either one or zero and, therefore, don't contribute to pairing correlations.

Such spaces are often too large for full configuration-interaction calculations, but still small enough even for sophisticated projection techniques. A famous case is the Baranger-Kumar space with the shells $N = 3, 4$ for protons and $N = 4, 5$ for neutrons for the description of the well deformed Rare Earth region. Its configuration space contains 72 neutron and 50 proton levels. This leads for mean-field calculations to matrices with dimension 72 and 50, which are easy to handle. On the other side in a configuration-interaction calculation in the M-scheme we have in the middle of the shells roughly 5×10^{34} configurations.

Of course, the model interaction has to be adjusted carefully to the underlying configuration space. If the interaction in such a valence space is properly chosen, much of the physics, in particular, the interplay between collective degrees of freedom and single-particle degrees of freedom can be well described in such a space, only global properties such as total binding energies or radii have to be treated in the full space. The applications are further simplified by the use of separable interactions. From the configuration-interaction calculations, one knows that an effective interaction in such a restricted space can be represented as a sum of terms separable in the *ph*-channel and in the *pp*-channel, i.e.,

$$\hat{V} = \frac{1}{2} \sum_\lambda \chi_\lambda \hat{Q}_\lambda^\dagger \hat{Q}_\lambda + \sum_\lambda G_\lambda \hat{P}_\lambda^\dagger \hat{P}_\lambda, \qquad (163)$$

where,

$$\hat{Q}_\lambda = \sum_{nn'} Q_{\lambda nn'} a_n^\dagger a_{n'}, \qquad \hat{P}_\lambda = \sum_{nn'} P_{\lambda nn'} a_n a_{n'} . \quad (164)$$

As in the shell model calculations, one starts with the Hamiltonian

$$\hat{H} = \hat{H}_0 + \hat{V}, \qquad (165)$$

where the doubly magic spherical core enters the calculations in terms of the single-particle energies ε_n in the operator

$$\hat{H}_0 = \sum_n \varepsilon_n a_n^\dagger a_n \qquad . \qquad (166)$$

The parameter of such models are the single-particle energies ε_n and the coupling constants χ_λ and G_λ.

In the configuration-interaction calculations with interactions derived from ab-initio calculations (Dufour and Zuker, 1996) one has found, in deriving separable representations of these effective forces, that the quadrupole part with $\lambda = 2$ plays the essential role in the ph-channel and the monopole part with $\lambda = 0$ dominates the pp-channel. These two parts do not depend much on the underlying bare nucleon-nucleon force, Therefore, it is easy to understand that the pairing plus quadrupole model, introduced in the sixties (Baranger and Kumar, 1968), has been pretty successful to describe the bulk of the important long-range correlations in nuclei in a very efficient way. Of course, it can be improved without great difficulties through the inclusion of additional separable terms, such as octupole ($\hat{Q}_3$) and hexadecapole ($\hat{Q}_4$) operators or the quadrupole pairing term $\hat{P}_2$. Some of the advantages of such models are:

(i) one works in a spherical basis which preserves, apart from translational invariance, all the symmetries;

(ii) the basis and the corresponding single-particle matrices are relatively small and, therefore, projection techniques can be applied easily;

(iii) if the parameters are carefully adjusted, one obtains excellent results which can be compared with the experimental data and the basic physics can be understood in this way.

Of course, such model have restrictions as quantities influenced by physics outside of the valence shells cannot be described. These include, most importantly, the total binding energy of the nucleus and also the phenomena driven by so-called intruder states coming from the excluded higher shells or coming from the core at large deformations. The fission process or superdeformed configurations belong to this category. There are also limitations for phenomena driven by special forces not considered in the model Hamiltonian, for instance, such parts of the tensor force which are not included in the phenomenologically adjusted single-particle energies.

In many applications of such models, additional simplifications are made with the neglect of certain terms, for instance, the exchange terms (Fock-terms) in the mean-field potential or the contributions of the pairing force to the mean-field potential and the contribution of the quadrupole force to the pairing field. With these further approximations, the energy acquires the following simple structure:

$$E = \langle \hat{H}_0 \rangle + \frac{1}{2}\chi \langle \hat{Q}^\dagger \rangle \langle \hat{Q} \rangle + G \langle \hat{P}^\dagger \rangle \langle \hat{P} \rangle, \qquad (167)$$

where $\hat{Q}$ is the quadrupole operator and $\hat{P}^\dagger = \sum_n a_n^\dagger a_{\bar{n}}^\dagger$ represents a Cooper pair coupled to angular momentum 0. The mean-field operator is

$$\mathcal{H} = \begin{pmatrix} \varepsilon + \beta Q - \lambda & \Delta \\ \Delta & -\varepsilon - \beta Q + \lambda \end{pmatrix}, \qquad (168)$$

with the quadrupole deformation β, the gap parameter Δ and the chemical potential λ. These parameters are determined through the self-consistent conditions

$$\beta = \chi \langle \hat{Q} \rangle \quad \text{and} \quad \Delta = G \langle \hat{P} \rangle \quad \text{and} \quad \langle \hat{N} \rangle_\lambda = N \quad . \qquad (169)$$

Since the pairing field is a multiple of the unity, the solution of the HFB-problem in this case is identical to the Nilsson + BCS calculation. This model has been extensively employed from sixties, not only for mean-field calculations, but has also been successfully applied for methods beyond mean field and, in particular, for projection techniques (Egido et $al.$, 1980).

As an example, we discuss below the particle number projection before the variation for the case of the pairing collapse with increasing angular momentum. In this case one starts with the number projected energy. Using the notation of Eq. (65), we have

$$E^N = \frac{\langle \hat{H}\hat{P}^N \rangle}{\langle \hat{P}^N \rangle} = \oint d\phi\, y(\phi) \langle 0|\hat{H}|\phi \rangle. \qquad (170)$$

Applying the Wick's theorem and neglecting the exchange terms one has

$$\langle 0|\hat{H}|\phi \rangle = \langle 0|\hat{H}_0|\phi \rangle + \frac{1}{2}\chi \langle 0|\hat{Q}^\dagger|\phi \rangle \langle 0|\hat{Q}^\dagger|\phi \rangle$$
$$+ G\langle 0|P^\dagger|\phi \rangle \langle 0|P|\phi \rangle, \qquad (171)$$

which indicates that one is left with the evaluation of the following single-particle terms:

$$\langle 0|\hat{H}_0|\phi \rangle = \mathrm{Tr}(\varepsilon \rho(\phi)), \quad \langle 0|\hat{Q}|\phi \rangle = \mathrm{Tr}(Q\rho(\phi)),$$
$$\text{and} \quad \langle 0|\hat{P}|\phi \rangle = \mathrm{Tr}(P\kappa(\phi)). \qquad (172)$$

Using the Thouless theorem for representing an arbitrary HFB-function in the vicinity of $|0\rangle$ (Thouless, 1960)

$$|z\rangle = e^{\hat{Z}}|0\rangle, \qquad (173)$$

where $\hat{Z} = \sum_{\mu\mu'} Z_{\mu\mu'} \beta_\mu^\dagger \beta_{\mu'}^\dagger$, one can also calculate the gradient with respect to the parameters $Z_{\mu\mu'}$

$$\partial_{\mu\mu'}|0\rangle := \partial_{Z_{\mu\mu'}}|z\rangle \Big|_{z=0} = \beta_\mu^\dagger \beta_{\mu'}^\dagger |0\rangle. \qquad (174)$$
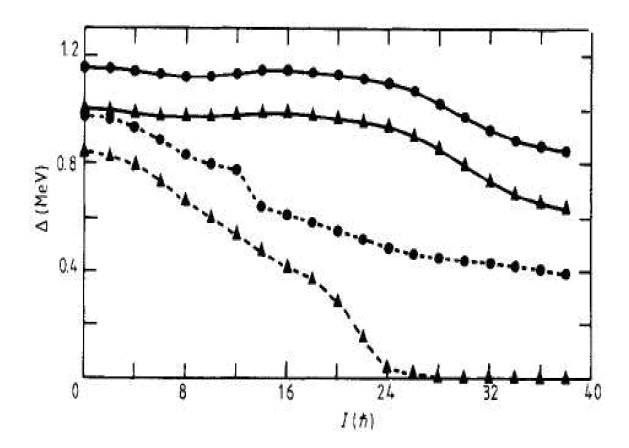
FIG. 12 Pairing correlations in ^{168}Hf as a function of angular momentum. Gap parameters for protons (circles) and neutrons (triangles) obtained by a variation after number projection (full curves) and by pure mean-field theory (dashed curves) [from (Mutz and Ring, 1984)]

FIG. 13 Energy surface in the β-γ plane for the nucleus ^{188}Os (a) without angular momentum projection and (b) with exact three-dimensional angular momentum projection. The units on the equipotential lines are in MeV [from (Hayashi *et al.*, 1984)]

FIG. 14 The shape of the energy surface along the line $\beta = 0.2$ for the nucleus ^{188}Os (a) without, with, and with approximate angular momentum projection [from (Hayashi *et al.*, 1984)]

In this case the gradient of the projected energy $\partial_{\mu\mu'} E^N$ can be easily evaluated in terms of the gradients of single-particle overlaps of the form

$$\partial_{\mu\mu'} \langle 0|\hat{Q}|\phi\rangle = \langle 0|\hat{Q}e^{i\phi\hat{N}}\beta_\mu^\dagger\beta_{\mu'}^\dagger|0\rangle. \qquad (175)$$

This allows to use the gradient method for the solution of variation after projection problem.

In these simple calculations one starts with a full Hamiltonian, but neglects certain terms in the evaluation of the projected energy, as for instance the Fock-term of the quadruple force, the contributions of the quadrupole force to the pairing channel and the contributions of the pairing force to the mean field. As we will discuss in detail in section VI.A.2 this can lead under certain circumstances to singularities in the energy surface (Anguiano *et al.*, 2001) and to large errors in such calculations. Therefore the results have to be checked very carefully in each case.

In Fig. 12, we show self-consistent cranking results for the pairing gap for protons and neutrons in the nucleus ^{168}Hf as a function of the average angular momentum, I calculated with and without number projection before the variation. Without projection, we observe in the neutron pairing collapse at spin $I = 24\hbar$. The proton gap is also somewhat quenched after $I = 10\hbar$. On the other hand, for the case of number projection the pairing correlations are reduced smoothly.

Angular momentum projection in triaxial systems is much more complicated. So far there are very few results for variation after projection. In most of the cases the variation of the angular momentum projected energy is restricted to a few external parameters as, for instance, deformation parameters. In this case, one needs for each deformation only to evaluate the projected energy in Eq. (170) after a constrained mean-field calcula-
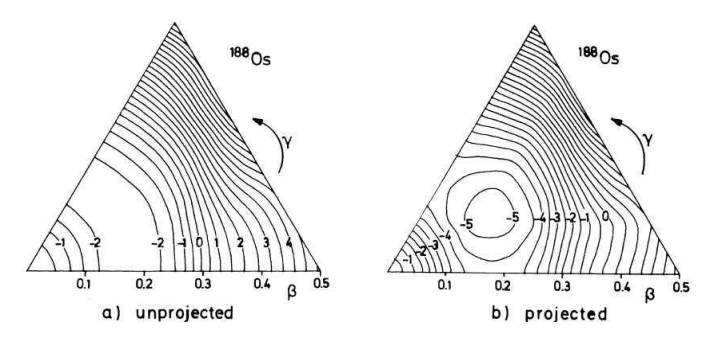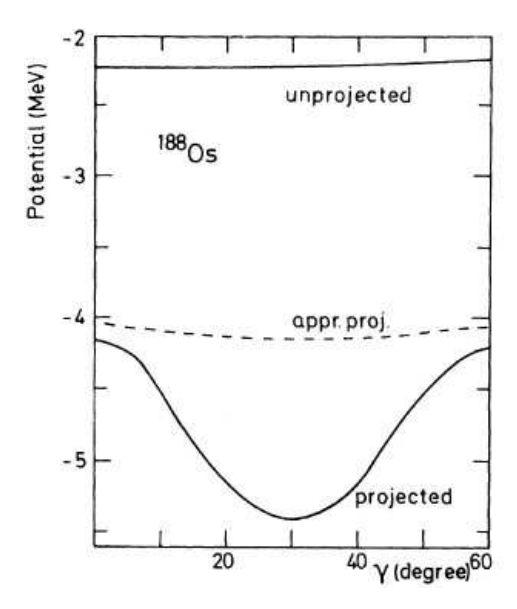
tion. This is considerably simpler than the evaluation of the projected gradient in each step of the iteration.

In Fig. 13, we show as an example [taken from (Hayashi *et al.*, 1984)], the energy surface of the nucleus ^{188}Os as a function of the Bohr quadrupole deformation parameters β and γ. The unprojected energy does not depend on the triaxiality γ, and a mean-field calculation without constraint would be relatively unstable. However, projection on the angular momentum $I = 0$ leads to a clear triaxially deformed minimum with $\gamma \approx 30°$.

In Fig. 14, we show the energy surface for the same nucleus ^{188}Os as a function of the triaxiality γ for fixed quadrupole deformation $\beta = 0.2$. As it was already visible in Fig. 13, the unprojected energy is rather flat in γ, whereas the projected energy has a pronounced minimum at $\gamma \approx 30°$. In addition, the approximate projected

energy is also shown in Fig. 14, where one has added to the unprojected energy the second order Kamlah correction, $-\langle 0|\Delta\hat{\mathbf{J}}^2|0\rangle/2\mathcal{J}_{\mathrm{PY}}$, with $\mathcal{J}_{\mathrm{PY}}$ being the Peierls-Yoccoz moment of inertia (160).

The Kamlah approximation is valid for the case of a strong symmetry breaking, i.e., when the overlap $\langle 0|R(\beta)|0\rangle$ is sharply peaked at the Euler angle $\beta = 0$, which is the case for axially symmetric shapes at $\gamma = 0$ and $\gamma = 60°$. Note that the Euler angle β in these two cases must be defined as an angle of rotation about the axis perpendicular to the symmetry axis. However, for triaxial shapes one has to apply the three dimensional rotation, see Sec. III.B.2, and the overlap is not really sharply peaked in the two remaining Euler angles α and γ,[6] Therefore, at $0° < \gamma < 60°$, the Kamlah approximation cannot be justified by the strong-symmetry-breaking argument. This is particularly conspicuous for γ near 0 or 60°, where the overlap becomes completely independent of α and γ.

Several advanced nuclear models have been developed based on the pairing plus quadrupole-quadrupole interaction and the projection theory. Here, we discuss the approach of triaxial projected shell model (TPSM) (Sheikh and Hara, 1999), which has been extensively employed in recent years to investigate the high-spin band structures in triaxial nuclei. In this method, intrinsic basis states are obtained by solving the triaxial Nilsson potential with the expected deformation values for the system under investigation. Explicit three-dimensional angular-momentum projection method is then employed to project out the states with good angular-momentum. Apart from the projected vacuum state, multi-quasiparticle states are also projected to the laboratory frame of reference in this approach. In the most recent version of the TPSM approach, for even-even systems, quasiparticle basis states employed are:

$$
\begin{aligned}
&\hat{P}^I_{MK}|\Phi\rangle; \\
&\hat{P}^I_{MK}\,\alpha^\dagger_{p_1}\alpha^\dagger_{p_2}|\Phi\rangle; \\
&\hat{P}^I_{MK}\,\alpha^\dagger_{n_1}\alpha^\dagger_{n_2}|\Phi\rangle; \\
&\hat{P}^I_{MK}\,\alpha^\dagger_{p_1}\alpha^\dagger_{p_2}\alpha^\dagger_{n_1}\alpha^\dagger_{n_2}|\Phi\rangle; \\
&\hat{P}^I_{MK}\,\alpha^\dagger_{n_1}\alpha^\dagger_{n_2}\alpha^\dagger_{n_3}\alpha^\dagger_{n_4}|\Phi\rangle; \\
&\hat{P}^I_{MK}\,\alpha^\dagger_{p_1}\alpha^\dagger_{p_2}\alpha^\dagger_{p_3}\alpha^\dagger_{p_4}|\Phi\rangle,
\end{aligned}
\tag{176}
$$

where $|\Phi\rangle$ is the vacuum state and $\alpha^\dagger_n$ ($\alpha^\dagger_p$) are neutron (proton) quasiparticle operators.

The projected basis of Eq. (176) is then used to diagonalize the shell model Hamiltonian consisting of pairing plus quadrupole-quadrupole terms. The QQ-force strength χ is adjusted such that the physical quadrupole

———

[6] The third Euler angle and nonaxial Bohr deformation are traditionally denoted by the same Greek symbol γ, so they can only be distinguished by the context in which they are used.

deformation β is obtained as a result of the self-consistent mean-field HFB calculation (Hara and Sun, 1995). The monopole pairing strength, G_M, is of the standard form

$$
G_M = (G_1 \mp G_2 \frac{N-Z}{A})\frac{1}{A}\,(\mathrm{MeV}), \tag{177}
$$

where $-(+)$ is neutron (proton).
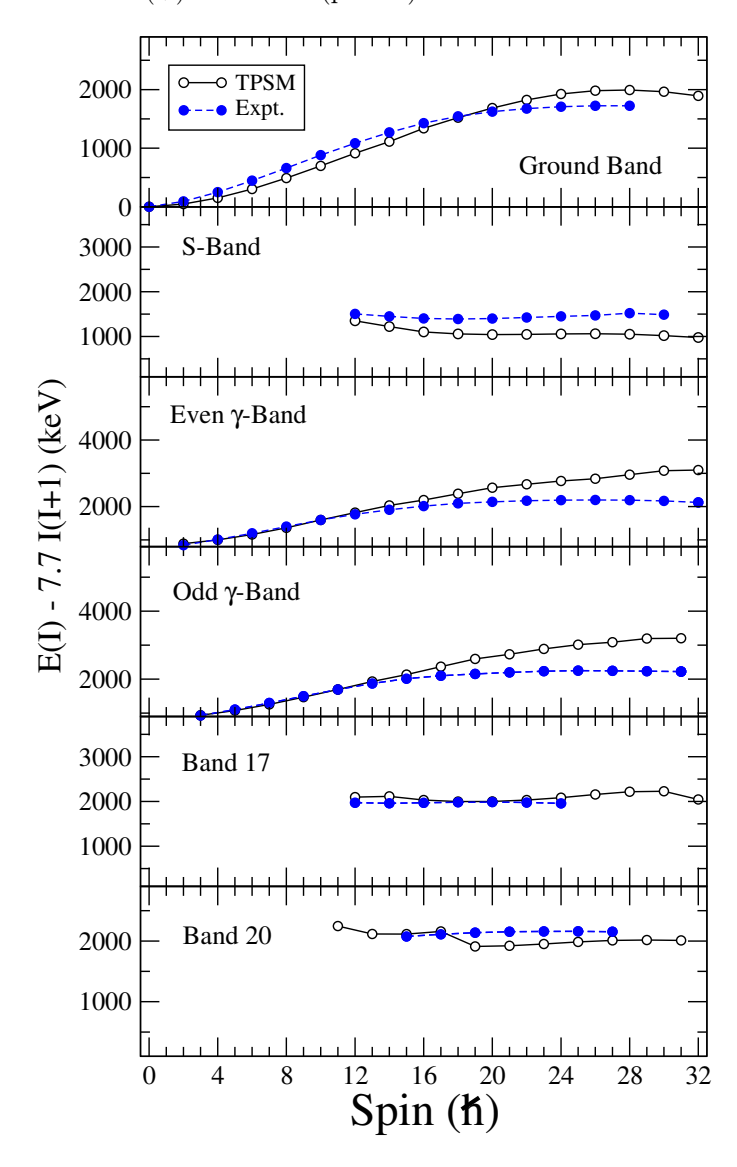
FIG. 15 (Color online) Comparison of the TPSM calculated and the measured excitation energies subtracted by a rigid core contribution for the band structures of ^{156}Dy. The comparison is made for the ground-state band, two-quasiparticle band (S-band), γ-band based on the ground-state (even-spin and odd-spin are shown separately) and the γ-band built on the S-band, denoted by Bands 17 and 20 for even- and odd-spin, respectively.

As an illustrative example, we present the TPSM results recently obtained in (Jehangir *et al.*, 2017) for the γ-vibrational bands based on quasiparticle excitations. The γ bands built on the ground-state band are well established in almost all regions of the periodic table. In the

TPSM approach, the $K = 0, 2, 4 \ldots$ states projected from the vacuum configuration lead to the ground-state, γ, $\gamma\gamma$, etc. bands. Similarly, for the two-quasiparticle configurations, projected $K = 1, 3, 5 \ldots$ states correspond to the aligned, γ, $\gamma\gamma$, etc. bands built on the two-quasiparticle configurations. As a matter of fact, projection from each quasiparticle configurations gives rise to the γ bands built on that configuration.

In (Sheikh *et al.*, 2009) it was shown that this feature could explain a long-standing puzzle in Ce and Ba region. The puzzle was that in some of these nuclei, two s-bands are observed with both of them having either positive (proton) or negative (neutron) g-factors. Normally, it is expected that for nuclei where neutron and proton Fermi surfaces are in close vicinity, one s-band would have neutron and the other one proton character. Both having the same structure is not expected and this problem had remained unresolved for quite some time.

Using the TPSM approach, in (Jehangir *et al.*, 2017) it was shown that the first s-band has the normal two-quasiparticle structure, whereas the second s-band is the γ band based on the parent two-quasiparticle state. Since this γ band has the same intrinsic structure as that of the parent band, both the s-bands are expected to have similar g-factors. Similar band structures were also identified in the $^{76-78}$Ge isotopes (Raju *et al.*, 2016).

More recently, γ band structures up to I=32 and several other excited structures were identified in ^{156}Dy. In the experimental work of (Majola *et al.*, 2015), it was conjectured that some of the excited band structures could be γ bands based on the two-quasiparticle excitations. Detailed TPSM calculations performed for this system in (Jehangir *et al.*, 2018) indicate that, indeed, excited band structures are γ bands built on the two-quasineutron configuration. This result was obtained through the analysis of branching ratios. A comparison of the TPSM results with the experimental data is illustrated in Fig. 15.

B. Projection in small configuration spaces

Over the years many applications to various projection methods have been carried out in relatively small configuration spaces and for light nuclei. This has been done in the first place by the reason, that many of these techniques require a considerable numerical effort and that it was or is impossible to apply them in large spaces and for heavy nuclei. A second reason was also the fact that exact configuration interaction calculations can be carried out in such small spaces, which allow a comparison of the projection methods with the exact solution in the corresponding space.

A variation after projection on particle number and angular momentum has been carried out already in the eighties by the Tübingen group (Schmid *et al.*, 1984a). This method has been called VAMPIR (variation af-

ter mean field projection in realistic model spaces). First it has been restricted to axially symmetric intrinsic HFB wavefunctions in the sd-shell and a phenomenological interactions adjusted to this space have been used. The results have been compared with configuration mixing calculations. At low spins the results are reasonable. However, in this approach the intrinsic wavefunctions obey time-reversal symmetry. This means that no alignment processes are taken into account and the resulting moments of inertia are too small. Such processes can be considered by mixing to the ground state band with projected two-quasiparticle configurations. This model (Schmid *et al.*, 1984b,c) has been called MONSTER (model handling many number- and spin-projected two-quasiparticle excitations with realistic interactions and model spaces). In Ref. (Hammaren *et al.*, 1985) a similar method has been used for odd-mass nuclei in the mass $A = 130$ region and the alignment processes are studied successfully. These configuration mixing of projected many-quasiparticle configurations are based on a fixed HFB function for the ground state. Changes in the deformation etc. cannot be included here. Therefore a new method has been developed by (Schmid *et al.*, 1986), the "excited VAMPIR". Here the intrinsic wavefunction for the yrast levels is determined in a first step. In the next step, for each angular momentum, a set of excited states is determined by new intrinsic wavefunctions, Schmidt-orthogonalized with respect to all the earlier solutions at this spin. Thus one successively constructs an optimal configuration space for the A-nucleon problem. Over the years all these methods have been applied in relatively small configuration spaces with realistic effective forces. They compare well with the corresponding exact configuration mixing calculations. For reviews see (Schmid and Grümmer, 1987; Schmid, 2004). The problem is, as in the case of the configuration mixing calculations, the determination of the effective interaction. It depends on the specific configuration space. In many cases one starts with a G-matrix and additional parameters are adjusted to experimental data. Modern applications also start from effective forces derived from *ab initio* calculations.

In Ref. (Gao *et al.*, 2015b) calculations with variation after projection on spin, isospin, and mass number have been carried out in the even-even nuclei in the sd-shell using the well known and successful USDB interaction, which was adjusted to configuration interaction calculations in this space (Brown and Richter, 2006). The binding energies turn out to be very close to the exact configuration interaction results. The differences are very small in cases, where the number of parameters in the projected wave functions is close or larger than the dimension of the configuration interaction space. For the opposite case one finds energy differences of up to 500 keV. Angular momentum projection is very important for these results. Calculations with angular momentum projection lead in

most of the cases to triaxial deformations of the intrinsic states. This is not the case for the calculation without J-projection. This is in agreement with systematic mean-field investigations with the Gogny-force without projection in large model spaces (Delaroche *et al.*, 2010).

Intrinsic wave functions with different deformations can be included in the Generator coordinate method. In Ref. (Gao and Horoi, 2009) this method is extended by adding at each deformation not only the lowest Hartree-Fock configuration, but in addition a large number np-nh configurations and projecting all these states on good angular momentum. This is a projected configuration interaction calculation. The results are compared with exact solutions for nuclei in the sd- and pf-shell and it is found that not only the energies, but also the quadrupole moments and the B(E2) transition probabilities are in very good agreement with the exact configuration interaction calculations in the spherical basis.

It is an interesting question, whether it is possible to define an intrinsic deformation for the exact wavefunctions in the laboratory frame obtained by configuration mixing calculations. In cases, where one finds good agreement between the projected states and the exact solution not only for the energy, but also for other operators, the projected mean field state is close to the exact solution and in such a case it is possible to define the intrinsic deformation of the exact wavefunction as the deformation of the intrinsic state in the projected theory. It turns out that in some cases the above mentioned calculations that the intrinsic deformation is not well determined, because the projected energy surfaces are very flat and the resulting projected wave functions are nearly identical, even if the intrinsic deformations are different.

The Monte-Carlo Shell Model of the Tokyo group (Otsuka *et al.*, 2001) is able to answer the above question. In a fixed configuration space it provides an exact solution identical to the conventional calculations mixing spherical configurations in an oscillator basis. Using the Hubbard-Stratonovich transformation (Hubbard, 1959; Stratonovich, 1958) the Monte-Carlo Shell Model uses a linear combination of angular momentum and parity projected intrinsic wavefunctions

$$|\Psi_M^{I\pi}\rangle = \sum_{\sigma K} c_\sigma P_{MK}^I P^\pi |\Phi(\sigma)\rangle \qquad (178)$$

where σ runs over a large number of intrinsic Slater-determinants $|\Phi(\sigma)\rangle$ determined by a stochastic Monte-Carlo sampling based on the Hamiltonian $\hat{H}$ and the coefficients c_σ are calculated by a diagonalization of $\hat{H}$. Each intrinsic state has a certain deformation and the sum of the coefficients $|c_\sigma|^2$ with a specific deformation determine the weight of the intrinsic deformation in the exact state $|\Psi_M^{I\pi}\rangle$. In principle one would not need the projection operators, because the important sampling would automatically lead to eigenstates with good quantum numbers, i.e., would automatically carry out the integration over the Euler angles and the summation over K. However, it turns out the calculations are much more stable and faster by using the projection operators. Technically, the 3-dimensional projection is possible because it is applied here in relatively small configuration spaces, including only a few oscillator shells as is usual in configuration mixing calculations. For recent reviews on modern extensions of this method to relatively large model spaces and to *ab initio* applications, the reader is referred to (Shimizu *et al.*, 2017, 2012).

VI. PROJECTION METHODS AND NUCLEAR DENSITY FUNCTIONAL THEORY

In many-body systems of condensed matter and atomic physics, the only interaction acting among the constituent particles is the simple Coulomb force. However, this is not the case in nuclear physics, where the complexity of the bare nucleon-nucleon force and strong in-medium effects lead us to consider phenomenological effective forces or relativistic Lagrangians to define the underlying intrinsic mean-field, see the reviews in (Bender *et al.*, 2003; Robledo *et al.*, 2019; Vretenar *et al.*, 2005). In nuclear physics, phenomenological zero range effective forces became quite popular in the sixties with the introduction of the Skyrme force (Skyrme, 1958). Soon after its introduction, it was realized that the contact three body force used to account for the saturation property of the nuclear force should be replaced by a phenomenological density-dependent two body term. Due to the zero range of the force, it is only meaningful for the particle-hole part of the nuclear force and pairing properties have to be described by a separate interaction. In the seventies, the zero range central part of Skyrme was replaced by a sum of finite range Gaussians in the Gogny force. The main advantage over the Skyrme force is that pairing properties are obtained from the same interaction and there is no need to introduce additional pairing terms. In the eighties, the birth of the nuclear relativistic mean-field models was witnessed, which start from a Lagrangian with nucleons described by Dirac spinors interacting through the exchange of scalar and vector mesons. In the classical limit, i.e., at the Hartree level, this leads to a local Dirac equation for the nucleons with self-consistent scalar and vector fields depending on various densities and currents. In addition, through the quantization of the spinor fields, a relativistic HFB theory has been derived for the description of pairing correlations in nuclei (Kucharek and Ring, 1991). However, it has been shown that in the relativistic case there is no possibility to employ the same interaction in the particle-hole and particle-particle channels. The very strong scalar and vector fields, closely connected to the spin-orbit splitting, lead to dramatically enhanced pairing and forbids it.

The aforementioned three frameworks are extensively used in the mean-field context to study many nuclear properties. The HF or HFB equations are traditionally solved by expanding on a complete and orthogonal basis, as for instance the harmonic oscillator or Woods-Saxon basis, or by using mesh techniques in the coordinate representation. The presence of density-dependent terms in the three schemes, containing the spatial density often raised to non-integer powers and sometimes of exponential form, imply that none of them can be obtained from mean-field average values of a Hamiltonian. Instead, the three can be considered as a special case of an energy density functional (EDF), where part of the functional is obtained from a two-body interaction (and therefore is quadratic in the densities) and the rest is purely phenomenological (with the aforementioned non-integer powers of the density or the density-dependent term of the Slater approximation to Coulomb exchange). These peculiarities of the traditional nuclear EDF lead to the following difficulties in implementing the methodology of symmetry restoration:

- The harmonic oscillator or Woods-Saxon basis are often adapted to the geometry of the problem and therefore break spatial symmetries like rotational and/or translational. This is also the case for the mesh representation of the wave functions. This symmetry breaking has to be taken into account in the formalism explicitly.

- The density-dependent term of the EDF is phenomenological and therefore it is not justified from first principles. As a consequence, one has to adopt some prescription to compute matrix elements of this density dependent term and the prescription chosen has to satisfy consistency requirements as discussed below.

- The use of separate interactions for the particle-hole and particle-particle channels lead to some difficulties related to self-energies and violation of the Pauli principle.

- Non-integer powers of the complex transition density have to be considered in the evaluation of the density dependent term, requiring pathways to choose among the possible branch-cuts in the complex plane.

The existence of these difficulties, and the fact that some of them are still not satisfactorily addressed, have slowed down the application of symmetry restoration techniques in nuclear structure with EDFs. To avoid these difficulties, there have been first attempts, very recently made, to generate EDFs directly from Hamiltonians (Bennaceur *et al.*, 2014, 2017; Sadoudi *et al.*, 2013). However, in spite of the difficulties encountered

in the traditional nuclear EDFs, numerous obtained results point to the necessity of symmetry restoration to improve both the qualitative and quantitative description of nuclear properties. Before discussing some of the achievements obtained within symmetry-restored calculations, we first present the difficulties encountered in the nuclear EDF framework.

A. Difficulties encountered in restoring symmetries with nuclear EDF

In this section, we discuss the four main problems faced by the implementation of symmetry restoration with nuclear EDF.

1. Basis not closed under the symmetry operation

Symmetry restoration requires the application of a symmetry operation (rotation, translation, etc) to an intrinsic wave function. Often, the single-particle basis used to characterize the intrinsic states is not closed under the symmetry operation and the "rotated" basis do not span the same subspace of the Hilbert space as the original basis. In the case of spatial rotations, this happens when a spherical harmonic oscillator basis does not contain all possible states in a major shell, or when oscillator lengths along different spatial direction are not the same, or when a Cartesian mesh is used in space representation. This is reason that most of the applications to-date are using spherical harmonic oscillator bases with sufficiently large numbers of complete major shells. This strategy increases the computational cost, and becomes impractical in some situations like fission, where the large variety of shapes involved would require a huge rotationally invariant bases. In addition, the strategy is not universal, as it cannot be applied, e.g., to the case of spatial translations as required in the restoration of translational and/or Galilean invariance (Rodríguez-Guzmán and Schmid, 2004; Rodríguez-Guzmán and Schmid, 2004; Schmid and Reinhard, 1991). To understand it, let us consider a simple model in one dimension where the basis contains just one single state $\varphi_0(x) = e^{-x^2}$ corresponding to the harmonic oscillator ground state with oscillator length of one Fermi. After translation $\varphi_0(x) \rightarrow \varphi_0(x - x_0) = e^{x_0^2} e^{-x^2} \sum_{k=0,\infty} \frac{(-2xx_0)^k}{k!}$ an infinite number of Gaussian wave functions $e^{-x^2} x^k$ is required to reconstruct the translated wave function. The situation does not improve if another basis, like Woods-Saxon or a discrete mesh in space (Baye and Heenen, 1984), is used.

A practical consequence of the above difficulty is that the traditional form of the generalized Wick's theorem, see Appendix A, cannot be used as it is implicitly assumes in its derivation (see, for instance, (Balian and Brezin, 1969)) that both HFB wave functions are ex-

panded in the same equivalent basis (spanning the same subspace). One way to circumvent this problem is to formally expand the original finite basis as to span the whole Hilbert space (Bonche *et al.*, 1990; Robledo, 1994). The new basis is the direct sum of the original single-particle basis (denoted by 1) plus the orthogonal complement required to cover the whole Hilbert space (basis 2). The extended U and V Bogoliubov amplitudes acquire a block diagonal form (i.e. they do not connect the two basis) and the block corresponding to basis 2 takes a simple form with an uniform occupancy of 0. The original generalized Wick's theorem can be applied, but in the final expressions the quantities referring to basis 2 have to be managed appropriately (Robledo, 1994) so as to refer to quantities defined in basis 1 only. In this way, an extended Wick's theorem is obtained and the main difference with respect to the traditional generalized Wick's theorem is that the overlap matrix between the two basis $\mathcal{R}_{11'}$ (1' refers to the "rotated" basis) enters now the expressions of the overlap

$$\langle \Phi_0 | \Phi_1 \rangle = \sqrt{\det(A) \det(\mathcal{R}_{11'})} \tag{179}$$

where the matrix A is given by

$$A = U_0^T \left(\mathcal{R}_{11'}^T \right)^{-1} U_1^* + V_0^T \left(\mathcal{R}_{11'} \right) V_1^* \tag{180}$$

Note the presence of $\left(\mathcal{R}_{11'}^T \right)^{-1}$ in the above expression, direct consequence of the fact that as basis 1 and 1' do not span the same Hilbert subspace, they cannot be connected by a unitary transformation (for which case $\left(\mathcal{R}_{11'}^T \right)^{-1} = \mathcal{R}_{11'}^*$). Further details, such as the contractions to be used in the generalized Wick's theorem, can be found in (Robledo, 1994).

2. Self-energy and Pauli principle

Reduced kernels of a two-body Hamiltonian between two HFB wave functions $|\Phi_0\rangle$ and $|\Phi_1\rangle$ can be expressed with the help of the generalized Wick's theorem, see Appendix A, in terms of the transition density matrix and pairing tensor as

$$\frac{\langle \Phi_0 | a_{k_1}^\dagger a_{k_2}^\dagger a_{k_4} a_{k_3} | \Phi_1 \rangle}{\langle \Phi_0 | \Phi_1 \rangle} = \left[\rho_{k_3 k_1}^{01} \rho_{k_4 k_2}^{01} - \rho_{k_4 k_1}^{01} \rho_{k_3 k_2}^{01} + \kappa_{k_1 k_2}^{01} \kappa_{k_3 k_4}^{10} \right], \tag{181}$$

where we identify three contributions: direct, exchange and pairing. As $\langle \Phi_0 | a_{k_1}^\dagger a_{k_2}^\dagger a_{k_4} a_{k_3} | \Phi_1 \rangle$ is a finite quantity, the right hand side of Eq. (181) must diverge when the overlap $\langle \Phi_0 | \Phi_1 \rangle$ vanishes.

The same argument applies to the transition density matrix,

$$\rho_{k_3 k_1}^{01} = \frac{\langle \Phi_0 | a_{k_1}^\dagger a_{k_3} | \Phi_1 \rangle}{\langle \Phi_0 | \Phi_1 \rangle}, \tag{182}$$

which must have a pole of the same degree as that of the Hamiltonian kernel. Therefore, in the right hand side of Eq. (181) there must be a cancellation of second order poles, so as to reduce the order of the pole in the products of transition densities and pairing tensors. The cancellation is a consequence of the Pauli exclusion principle and the nature of creation and annihilation operators. It represents a serious problem in the implementation of symmetry restoration with nuclear EDF as usually, for a given term of the interaction, some of the contributions (typically exchange or pairing) are not taken into account and, therefore, no such cancellation is possible. A typical example is the Coulomb force for which usually its direct term is fully considered, the exchange term is treated in the Slater approximation (Slater, 1951), and the pairing term is completely disregarded. In such cases and when the overlap becomes zero (or very small), the lack of cancellation leads to unphysical results.

These above difficulties were first noticed in (Tajima *et al.*, 1992). A simple recipe was given to keep using the generalized Wick's theorem, based on the regularization of the divergence by slightly modifying one of the wave functions. The regularization procedure was also used to subtract the singularity and to define "regularized" contributions for the direct, exchange and pairing terms. However, those "regularized" contributions are somehow arbitrary as they depend on the criteria used in the subtraction of the singularity (remember that subtracting infinity from infinity is an indeterminacy). In (Dönau, 1998), the problem was also discussed, raising serious doubts about the validity of calculations with the pairing plus quadrupole Hamiltonian (see Sec. V), where the exchange and pairing parts of the quadrupole-quadrupole force, as well as the direct and exchange parts of the pairing force, are all neglected.

In (Anguiano *et al.*, 2001) the same problem was discussed in the context of the particle-number projection with the Gogny force. In this study, the Coulomb exchange was treated in the Slater approximation and the Coulomb pairing field was neglected. In addition, the contribution of the spin-orbit potential to the pairing field was not taken into account either. As a consequence, a rather erratic behavior was observed in many calculated quantities. The use of variation after projection aggravated the problem, as the intrinsic state could minimize the energy using some of the unphysical terms. Due to the simple form of the overlaps involved in the particle-number projection, it was possible to trace back the problem to the occurrence of configurations with occupancy $v_k^2 = 1/2$ and gauge angles $\varphi = \pi/2$.

To illustrate the problem, let us compute the general matrix element of Eq. (181) with $|\Phi_1\rangle = \exp(-i\varphi\hat{N})|\Phi_0\rangle$ The transition density matrix and pairing tensor take a very simple form in the canonical basis of the Bogoliubov transformation where we can consider for the present purposes that the U and V amplitudes are diagonal in a

generalized sense (see (Mang, 1975b; Ring and Schuck, 1980) for details). If $a_k^\dagger$ represent the creation operators in the canonical basis of the HFB wave function $|\Phi_0\rangle$, we obtain

$$\frac{\langle\Phi_0|a_{k_1}^\dagger a_{k_2}^\dagger a_{k_4} a_{k_3} \exp(-i\varphi\hat{N})|\Phi_0\rangle}{\langle\Phi_0|\exp(-i\varphi\hat{N})|\Phi_0\rangle} = \frac{v_{k_1}^2 e^{-2i\varphi}}{u_{k_1}^2 + v_{k_1}^2 e^{-2i\varphi}} \cdot \frac{v_{k_2}^2 e^{-2i\varphi}}{u_{k_2}^2 + v_{k_2}^2 e^{-2i\varphi}} \left(\delta_{k_3 k_1}\delta_{k_2 k_4} - \delta_{k_4 k_1}\delta_{k_3 k_2}\right)$$
$$+ \frac{u_{k_1} v_{k_1}}{u_{k_1}^2 + v_{k_1}^2 e^{-2i\varphi}} \cdot \frac{u_{k_3} v_{k_3} e^{-2i\varphi}}{u_{k_3}^2 + v_{k_3}^2 e^{-2i\varphi}} \delta_{k_2 \bar{k}_1}\delta_{k_4 \bar{k}_3}. \qquad (183)$$

It is now easy to realize that for $\varphi = \pi/2$ ($e^{-i2\varphi} = -1$) and one of the states k satisfying $u_k^2 = v_k^2 = 1/2$, the denominators in this expression tend to zero. Taking into account that $\langle\Phi_0|\exp(-i\varphi\hat{N})\Phi_0\rangle = \prod_{k>0}(u_k^2 + v_k^2 e^{-2i\varphi})$, it is easy to notice that, as long as there is a single pole, or two poles but with $k_1 \neq k_2$ (or $k_3 \neq k_1$) the overlap in the numerator of the l.h.s. of Eq. (183) remains finite. The only problematic situation seems to happen for matrix elements of the form $\langle\Phi_0|a_k^\dagger a_{\bar{k}}^\dagger a_{\bar{k}} a_k \exp(-i\varphi\hat{N})|\Phi_0\rangle$. However, in this case, although each term of Eq. (183) by itself is divergent, the sum gives a finite contribution, namely $v_k^2 \cdot e^{-2i\varphi} \cdot \prod_{m>0, m\neq k}(u_m^2 + v_m^2 e^{-2i\varphi})$, which behaves properly when $v_k^2 = 1/2$ and $\varphi = \pi/2$. This means that, as long as all three terms of the Wick's factorization of Eq. (181), i.e., the direct, the exchange, and the pairing terms, are taken into account, no divergences appear in the particle-number projection formalism. This cancellation is also connected with the so-called "self interaction" problem (Perdew and Zunger, 1981): the sum of the three terms is required to give a zero contribution for a single-particle configuration. In this case, the two body energy must be zero as the particle cannot interact with itself (Lacroix *et al.*, 2009).

Note that the arguments given above are rather general, and thus they also apply to restoration of other symmetries like angular momentum (Zduńczuk *et al.*, 2007). They are also independent of the kind of force, or the kind of two body operator considered in the mean value. Obviously, the projected calculation of mean values of one-body operators are never affected by this problem. The "divergence" problem is nowadays one of the most serious problems in the implementation of symmetry restoration in the nuclear DFT framework, see results and discussions in (Bender *et al.*, 2009; Dobaczewski *et al.*, 2007; Duguet *et al.*, 2009, 2015; Hupin *et al.*, 2011). Attempts to renormalize the divergences have been made (Lacroix *et al.*, 2009; Satuła and Dobaczewski, 2014) but they only work for functionals containing densities raised to an integer power and they lack a clear renormalization criteria in the most general cases. This difficulty is the major reason for the recent interest in replacing EDFs by mean values of true Hamiltonians (Bennaceur *et al.*, 2014, 2017; Sadoudi *et al.*, 2013).

At this point the reader is probably wondering as to why there are so many successful applications of particle-number (and other types of) projection with EDFs that are prone to suffer from the above discussed singularity problem. The main reason is that these calculations are not variation after projection calculations, where the variational principle, if it leads to gaining of energy in the process, would drive the intrinsic state towards a vanishing-overlap situation. Moreover, in most of these calculations, the intrinsic state is determined using the approximate Lipkin-Nogami method, which is free from these problems, and the true particle number projection is carried out afterwards. In this case, except of the very unlikely event of hitting a pole in the matrix element, the results appear to be reasonable. Nevertheless, in general situations where the difficulties discussed above do not forbid performing explicit calculations, the results may be polluted by spurious contributions that are difficult to control or quantify.

3. Density-dependent prescription

Most of the EDF used nowadays include in one way or another a phenomenological density dependence. In the non-relativistic case, it is introduced to mock-up the saturation property of the nuclear interaction in a simple way. Although the saturation could also be obtained without any density dependence (Beiner *et al.*, 1975), this inevitably leads to an unrealistic low value for the effective mass (Davesne *et al.*, 2018). In the relativistic case, the saturation property is a relativistic effect due to the difference between the scalar density, the source of the attractive part of the force and the baryon density, the source of the repulsive part of the force. Here, the saturation can also be obtained without any density dependence (Walecka, 1974). Nonetheless, to obtain a realistic description of the nuclear incompressibility and surface properties, an additional density dependence is used in the coupling constants.

In both the cases, density-dependent forces are implemented in a state-dependent way, so that the density $\rho(\vec{r}) = \langle\Phi|\hat{\rho}(\vec{r})|\Phi\rangle$ is used to evaluate the HFB energy as-

sociated with the HFB wave function $|\Phi\rangle$. For most of the non-relativistic functionals the density-dependent contribution to the energy is strongly repulsive, it is usually proportional to $\delta(\vec{r}_1 - \vec{r}_2)$ (contact term) and depends on the intrinsic center of mass density $\rho((\vec{r}_1 + \vec{r}_2)/2)$ raised to some power α which is, in most of the cases, a non integer number (usually $1/3$, although $1/6$ is also a common choice). The typical form of the density-dependent part of functional reads

$$V_{DD}(\rho) = t_3(1 + x_0 P_\sigma)\delta(\vec{r}_1 - \vec{r}_2)\rho^\alpha(\frac{1}{2}(\vec{r}_1 + \vec{r}_2)).$$

When the variational principle is used to derive the HF or HFB equations, the density-dependent part has also to be varied, leading to the so-called rearrangement term in the mean field, which in the non-relativistic case is given by

$$\partial\Gamma_{ij} = \frac{1}{2}\sum\langle k_1 k_2|\frac{\delta V_{DD}}{\delta\rho_{ij}}|k_3 k_4\rangle\rho_{k_3 k_1}\rho_{k_4 k_2}. \qquad (184)$$

Given the strength of the density-dependent potential, this rearrangement term represents an important component of the HF or HFB mean field and it cannot be overlooked. It enters in the expressions of many quantities like chemical potentials, quasiparticle excitation energies, etc..

In the evaluation of symmetry-restored energies based on HFB intrinsic states, instead of the mean values of the HFB theory we have to consider kernels of the Hamiltonian between different HFB states. In the case of density-dependent forces, when evaluating the kernels, some kind of prescription has to be implemented for this term. It is noted that same problem arises in the implementation of the generator coordinate method.

There are a few fundamental requirements that can be used to guide the choice of the prescription:

- The projected energy has to be a real quantity.

- The projected energy has to remain invariant with respect to symmetry operations applied to the intrinsic state.

- In the strong deformation limit of the intrinsic state (see Sec. IV.C), the projected theory should reduce to the traditional mean-field approach with the constraint on the broken-symmetry quantum numbers, like the particle number or angular momentum, and then, the expression for the corresponding chemical potentials should be consistent with the one obtained for the rearrangement term included in the mean field.

Among various proposals made over the years (Bonche *et al.*, 1990; Duguet and Bonche, 2003; Rodríguez-Guzmán *et al.*, 2002b; Schmid, 2004; Valor *et al.*, 2000), we only comment on the two that are in vogue:

Mixed-density prescription:
The "mixed" or "overlap" density prescription, proposed already in early nineties (Bonche *et al.*, 1990) within the framework of the generator coordinate method, and extended to the symmetry restoration case in (Rodríguez-Guzmán *et al.*, 2002b; Valor *et al.*, 2000), employs the transition density,

$$\rho_{q,q'} = \langle\Phi(q)|\hat{\rho}|\Phi(q')\rangle/\langle\Phi(q)|\Phi(q')\rangle, \qquad (185)$$

in the evaluation of the Hamiltonian kernel

$$h(q, q') = \langle\Phi(q)|\hat{H}\{\rho_{q,q'}\}|\Phi\rangle(q')/\langle\Phi(q)|\Phi(q')\rangle. \qquad (186)$$

It is inspired by the contractions to be used in the generalized Wick's theorem to compute the Hamiltonian kernel for density-independent forces. It is also consistent with the result one would obtain had the density-dependent terms been derived from a true three-body (or many-body) operator. It satisfies all the consistency requirements mentioned above (Egido and Robledo, 2004; Rodríguez-Guzmán *et al.*, 2002b). However, since the transition density is in general a complex quantity, this prescription requires special attention when the density is raised to a non-integer power. Specifically, one cannot rely on how the powers of complex numbers are evaluated within a given programming language or compiler. Obviously, this prescription brings back all the problems associated with branch points and cuts on complex planes.

Projected-density prescription:
The density to be used in the density-dependent interaction is given by

$$\rho^P = \frac{\int dq dq' f^*(q) f(q')\langle\Phi(q)|\hat{\rho}|\Phi(q')\rangle}{\int dq dq' f^*(q) f(q')\langle\Phi(q)|\Phi(q')\rangle}, \qquad (187)$$

that is, the total projected energy is than given by

$$E^P = \frac{\int dq dq' f^*(q) f(q')\langle\Phi(q)|\hat{H}\{\rho^P\}|\Phi(q')\rangle}{\int dq dq' f^*(q) f(q')\langle\Phi(q)|\Phi(q')\rangle} \qquad (188)$$

This prescription produces a density-dependent term which is invariant under the broken symmetries if the f amplitudes are properly chosen. For instance, in the case of the rotational symmetry breaking a constant f leads to a density ρ^P which is spherically symmetric and because of this it has been advocated by some authors (Schmid, 2004).

The projected density prescription is highly inconsistent with the underlying intrinsic mean field (Robledo, 2010) when spatial symmetries like the parity or rotational invariance are under consideration. An example of the catastrophic consequences can be seen in Fig. 16 where the parity projected energy for the nucleus ^{224}Ra is plotted as a function of the octupole moment Q_{30} for the two prescriptions discussed here. For the projected density prescription, the projected energy continuously
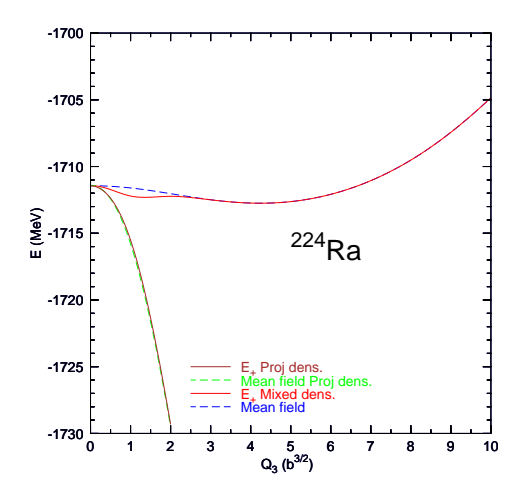
FIG. 16 (Color online) Various positive parity projected energies corresponding to different prescriptions for the density in the density dependent term of the Gogny force are plotted as a function of the axial octupole moment for the nucleus ^{224}Ra. The brown downsloping curve corresponds to the parity projected density prescription whereas the red curve corresponds to the mixed density prescription. The mean field energies corresponding to the two prescriptions are also plotted with dashed curves: blue for the mixed density prescription and green (on top of the brown curve) for the projected density prescription. Reprinted figures with permission from (Robledo, 2010). Copyright 2010 by the Institute of Physics.

decreases as the octupole moment is increased as a consequence of the mismatch between the projected density and the transition density. On the other hand, the use of the projected density in the case of particle number projection produces reasonable results. The Madrid group routinely uses an admixture of the two prescriptions, using the transition density but then using particle number projected wave functions. In addition, it has been shown (Valor *et al.*, 2000) in the framework of the Lipkin-Nogami prescription that the particle number projected density prescription leads to results which are very similar to those obtained using the "mixed density" prescription.

It is well known (Flocard and Onishi, 1997; Mang, 1975b; Ring and Schuck, 1980), that by using the Kamlah expansion (see Sect IV.C) it is possible to compute the particle number projected energy as an expansion in powers of $(\langle \hat{N} \rangle - N)$. The expansion is justified when the symmetry is strongly broken in the intrinsic wave function ($\langle \Delta \hat{N}^2 \rangle \gg 1$). In the first order, one obtains $E^N = \langle \Phi | (H - h_1(\hat{N} - N)) | \Phi \rangle$ for the projected energy. The parameter h_1 is given by $h_1 = \frac{\langle \hat{H} \Delta \hat{N} \rangle}{\langle \Delta \hat{N}^2 \rangle}$ and can be identified with the chemical potential λ of HFB. The minimum of the approximate particle number projected energy is obtained by minimizing $\langle \Phi | (H - h_1 \hat{N}) | \Phi \rangle$ with the constraint $\langle \Phi | \hat{N} | \Phi \rangle = N$. Thus, we recover the standard HFB mean-field procedure and justify the use

of the constraint. For density-dependent forces the expression for the chemical potential in the standard HFB has to be modified by adding to the Hamiltonian the rearrangement potential $\partial \hat{\Gamma} = \sum_{ij} \langle \frac{\delta H}{\delta \rho} \varphi_i^* \varphi_j \rangle c_i^\dagger c_j$. In order to maintain consistency between the projected theory and the underlying mean field, the prescription for the density-dependent term has to produce a parameter h_1 in the Kamlah expansion of the projected energy that also contains the rearrangement potential. As shown in (Robledo, 2007) this is only possible for the transition density.

The random phase approximation (Blaizot and Ripka, 1986; Ring and Schuck, 1980) for density-dependent forces (Blaizot and Gogny, 1977) requires also considering additional "rearrangement" terms in the residual interaction not present in the traditional, density-independent interaction, case. In fact, the residual interaction is obtained as the "second derivative" of the energy with respect to the generalized density (in the HFB case) justifying the mentioned rearrangement terms. On the other hand, the random phase approximation equation can be derived from the generator coordinate method (Jancovici and Schiff, 1964) if all the parameters of the Thouless transformation are used as generating coordinate. Therefore, this is another testing ground for the different prescriptions discussed above as the derivation of (Jancovici and Schiff, 1964) should produce the rearrangement terms discussed in (Blaizot and Gogny, 1977). As shown in (Robledo, 2007) this consistency in the derivation of the random phase approximation only holds for the transition density prescription.

4. Non integer powers of the density

The transition-density prescription requires to consider the transition density raised to some non-integer power. However, the transition density is a complex quantity, in general, and we are confronted with the problem of how to consider the evaluation of a non-integer power of a complex number. Given a complex number $z = |z|e^{i\varphi}$, the quantity z^α is not uniquely defined but is given by $z_n^{1/\gamma} = |z|^{1/\gamma} e^{i\varphi_n}$ with $n = 0, \ldots, \infty$ and $\varphi_n = \varphi/\gamma + 2\pi n/\gamma$. If γ is an integer m then $n = 0, \ldots, m-1$ and there are m possible roots. The choice of branch (i.e. the value of n) can have an enormous impact on the value of the matrix element as a consequence of the large positive value of the strength parameter of the density-dependent term.

In addition, in the symmetry restoration case, where integrals over the parameters of the symmetry group have to be carried out, the presence of branch cuts associated with the density-dependent part break the analyticity of the integrand and leads to spurious dependencies on the integration path in the complex plane of the symmetry group parameters. This issue has been discussed with a

great level of detail in (Dobaczewski *et al.*, 2007; Duguet *et al.*, 2009) in the simple case of particle number restoration. Similar problem is expected in the restoration of other symmetries. A few groups employ, as a partial solution to the problem, the particle-number-projected transition density discussed above, as this is a real quantity for diagonal terms. This choice, however is inconsistent with the underlying mean field and it belongs to the same category of projected densities that proved disastrous in the case of parity restoration (in fact, any spatial symmetry restoration) in (Robledo, 2010).

This above problem is still unsolved and represents a serious limitation in the applicability of the symmetry restoration and configuration mixing methodology with nuclear EDF. It is probably deeply connected with the differences in the descriptions of the quantum-mechanical many-body problem in the framework of wave functions and in density functional theory. In the first case one has wave functions, which extend over the entire space and are determined by boundary conditions. They have to preserve the symmetries of the system. In the second case one has only local densities, which depend only on the neighborhood of the interacting particles. They are not directly influenced by symmetries.

5. The future ahead

In recent years, the idea to give up phenomenological density-dependent terms in favor of real (multi-body) operators is becoming increasingly popular in non-relativistic density functional theory (Bennaceur *et al.*, 2014, 2017; Sadoudi *et al.*, 2013). The idea is to find a three-body interaction (not excluding higher order terms) that is able to mimic the saturation property induced by the density-dependent interaction. In this way, plain use of the generalized Wick's theorem is the only thing required to compute its contribution to the matrix element and all the issues related to zero norm overlaps, consequence of the violation of the Pauli principle, are also not present. The difficulty encountered with this approach is the large number of possible terms with their associated free parameters. In order to reduce the number of terms, several assumptions have been made, but so far, the three body interactions proposed are not very accurate in describing nuclear data. Another difficulty would be to extract a reasonable pairing field out of those multibody components of the interaction that would be presumably large and will require very precise cancellations.

On the other hand, the influence of the poles in the projected energy surfaces seem to be relatively narrow and in many applications, in particular in a projection after variation, they can be regularized by using a wider mesh in the integration over the various angles. In this way, the results depend on the choice of the discretization mesh, but at the end the numerical errors connected with such

procedures do not play an essential role, in particular for heavy nuclei. In any case, one finds in the literature many very successful applications of generator coordinate method and projection after variation (see below), where the impact of such poles in the physical observables do not spoil the physical interpretation.

B. Applications of symmetry restoration with nuclear EDFs

The importance of symmetry restoration in nuclear structure was noticed very early in nuclear physics but all the applications used very simple interactions and model spaces, for example, in the pairing plus quadrupole Hamiltonian which is made of separable interactions, both in the long and short range channels as to simplify the numerical treatment of the problem. Typical of this kind is the Projected Shell Model (Hara and Sun, 1995) where the mixing of angular momentum projected multi-quasiparticle excitations has proved to be very efficient in the description of high spin physics of deformed nuclei (Sun, 2016). Other approaches used shell model like effective interactions defined in a restricted configuration space involving a limited number of orbits. Among them we can mention the work developed by the Tübingen group using very sophisticated many body techniques involving mixing of configurations through projecting out mean-field intrinsic states obtained in a variation after projection framework (Schmid, 2004). We will not dwell on these approaches as we are more concerned with realistic nuclear energy density functionals. During the early years of the projection methods, the use of realistic effective interactions like that of Skyrme or Gogny families was at its infancy mostly due to computational limitations and therefore most of the applications focused on the implementation of mean-field computer codes or, at most, RPA codes using realistic effective interactions.

1. Non relativistic EDFs

The first application of symmetry restoration with an EDF possibly dates back to a work of Caurier and Grammaticos (Caurier and Grammaticos, 1977) where the projected spectrum of light nuclei was computed using several flavors of the Skyrme interaction. The limitation to light nuclei and small configuration spaces as well as the success of the mean-field approach over the whole nuclear periodic chart are the most likely reasons why this approach only become popular a couple of decades later.

A few years later Marcos et al (Marcos *et al.*, 1983) restored the parity symmetry broken in excited intrinsic configurations of ^{20}Ne using the BKN interaction. In this work the center of mass correction was also computed using symmetry restoration techniques. In the work (Bonche *et al.*, 1990), generator coordinate study of

a neutron deficient mercury isotope was carried out with Skyrme SIII using HFB mean field states. Although not a symmetry restoration paper, it is mentioned here because of the introduction of basic ideas like the mixed density prescription and the explicit form of the generalized Wick's theorem. Reflection symmetry restoration was also used along with the Gogny D1S interaction in (Egido and Robledo, 1991) to describe the physics of octupole deformation with HFB intrinsic states. Parity is a discrete symmetry with only two elements, a property that enormously simplifies the practical aspects of the calculations. Parity restoration has also been applied to cranking wave functions in order to study the emergence of octupole deformation at high spins in several rare earth and actinide nuclei (Garrote *et al.*, 1998, 1997). Also, projection of non axial intrinsic states has been performed in several mercury and lead isotopes in a generator coordinate context (Skalski *et al.*, 1993). Systematic calculations of the excitation energies, E3 transition strengths and ground state octupole correlation energies have been performed in a combined generator coordinate method and parity projection framework (Robledo, 2015a; Robledo and Bertsch, 2011b) with several flavors of the Gogny force, depicting the importance of the octupole degree of freedom and reflection symmetry breaking in nuclear structure.

Particle number restoration is another important application of symmetry restoration in nuclear structure as pairing correlations are known to be rather weak in atomic nuclei and therefore the use of an intrinsic mean field wave function (BCS or HFB wave function) is not easy to justify. Fluctuations on the order parameter associated with pairing correlations (for instance, the fluctuation on particle number $\langle \Delta N^2 \rangle$) as well as the corresponding gauge angle associated to particle number restoration are important ingredients for a proper description of pairing correlations in the weak regime of nuclear physics. As a consequence, a proliferation of particle number projected calculations is recently noted in the literature. Most of the applications use intrinsic states obtained from a HFB calculation, supplemented with the Lipkin Nogami procedure (see Sec. IV.B). The Lipkin Nogami method was proven to be equivalent to a restricted variation after projection where the particle number fluctuation $\langle \Delta N^2 \rangle$ is used as the variational parameter and an approximate first order formula for the projected energy (in the spirit of the Kamlah expansion, see Sect IV.C) is used instead of the exact result (Rodríguez *et al.*, 2005). Therefore, the Lipkin-Nogami is expected to capture most of the impact of the variation after projection on the intrinsic wave function, provided the approximate projected energy faithfully represents the exact one (Valor *et al.*, 1997). There are many examples of full variation after projection particle number projection calculations with the Gogny force, mostly in the framework of a particle number projected generator

coordinate method with restoration of additional symmetries. There are also early examples aimed to study high spin intrinsic states (Anguiano *et al.*, 2001) or to study the impact of particle number projection on the ground state correlation energy (Anguiano *et al.*, 2002). The effect of particle number projection on the moment of inertia of rotational bands was shown in (Anguiano *et al.*, 2001) to be quite large. The increase of pairing correlations due to the variation after particle number projection substantially decreases the moment of inertia, increasing thereby the excitation energy of rotational 2^+ states.

The first particle number projected calculation with Skyrme EDF was also in the generator coordinate method context and was carried out to analyze the structure of some Sr (Heenen *et al.*, 1993) or Pb isotopes (Heenen *et al.*, 2001). In (Stoitsov *et al.*, 2003), a mass table from proton to neutron dripline was generated with the SLy4 EDF and using volume pairing and implementing Lipkin Nogami method followed by a full particle number projection in order to capture the subtleties associated to pairing correlations in very neutron rich nuclei. The procedure has been implemented in a computer code that is publicly available (Stoitsov *et al.*, 2005). Similar calculations have been performed by the Brussels group in their quest for an accurate mass model (Samyn *et al.*, 2004).
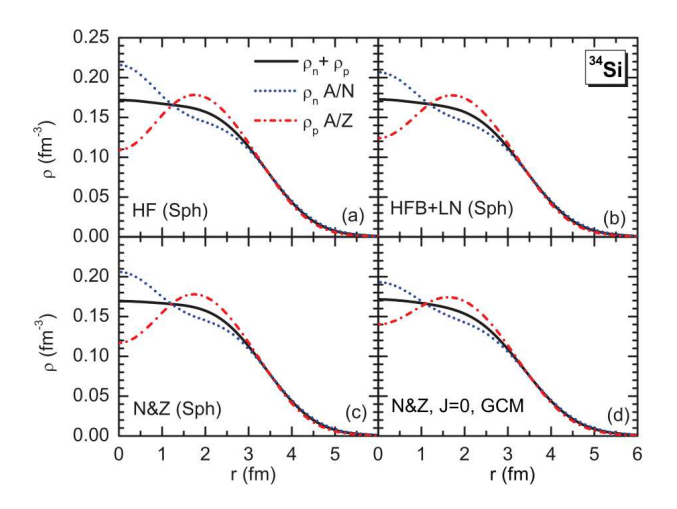
A full variation after projection particle number projection calculation with a Skyrme functional plus a zero range pairing force was carried out in (Stoitsov *et al.*, 2007) using the formulation of the particle number projection method of (Sheikh and Ring, 2000), solely involving functions of the standard density and the abnormal pairing tensor, see Sect III. The results are compared to the ones obtained with the Lipkin-Nogami method followed by a subsequent projection on particle number and a substantial improvement is observed, specially for magic or near magic nuclei.

Spontaneous symmetry breaking of rotational invariance is a defining characteristic of the nuclear interaction. It leads to the fruitful concept of nuclear deformation that allows us to explain a variety of phenomenology like, for instance, the ubiquitous existence of rotational bands that are essential to understand the structure of many high spin states. Most of nuclei in the Nuclear Chart are thought to present this property of rotational symmetry breaking in some of their quantum states, either the ground or excited states. Although it is possible to extract a lot of information out of the intrinsic deformed states by using the strong deformation limit [see (Mang, 1975b; Ring and Schuck, 1980)], the existence of weakly deformed states and/or the coexistence of different types of deformations in a limited range of energies requires the explicit restoration of the rotational symmetry. This is also the case in the calculation of electromagnetic transition strengths in weakly deformed nuclei (Robledo and Bertsch, 2012).

Restoration of angular momentum has been discussed in detail Sect III.B.2. Here we just want to remind the reader that the cumbersome three dimensional integration over the three Euler angles is replaced by a single one by assuming axial symmetry of the intrinsic state. This important simplification explains the early adoption of axial angular momentum projection.

Axial angular momentum projection along with particle number projection was first carried out in (Valor *et al.*, 2000) with several parameterizations of the Skyrme EDF. This paper, together with (Heenen *et al.*, 1993), contains a detailed description of the evaluation of operator matrix elements and different prescriptions for the density-dependent part of the interaction. Further applications include the study of the impact of the rotational energy correction in fission barriers (Bender *et al.*, 2004b) or the analysis of collective low lying structures in Kr (Bender *et al.*, 2006b) or Pb isotopes (Bender *et al.*, 2004a). Other applications include the study of bubble structures in ^{34}Si (Yao *et al.*, 2012) (see Fig 17) that shows the relevance of angular momentum projection in the passage of the intrinsic density (showing some sort of bubble structure) to the laboratory one (with a much less pronounced dip in the nuclear center).

Applications with the Gogny D1S energy density functional include the work (Rodríguez-Guzmán *et al.*, 2000a) where the erosion of the $N = 20$ magic number in the magnesium isotopic chain was addressed. The physics of super-deformation in sulfur isotopes was also analyzed (Rodríguez-Guzmán *et al.*, 2000c) in this framework. The calculations were further extended (Rodríguez-Guzmán *et al.*, 2002b, 2000b) to consider the generator coordinate method with the quadrupole degree of freedom as generating coordinate to explain more quantitative features of the deformation of Mg isotopes, including transition probabilities. The same calculations were carried out to analyze the $N = 28$ shell closure in (Rodríguez-Guzmán *et al.*, 2002a). Other applications of the same methodology including triple shape coexistence of neutron deficient lead isotopes was discussed in (Rodríguez-Guzmán *et al.*, 2004). Other applications include the calculation of mass tables of even-even nuclei including angular momentum projection restricted to axial symmetry plus particle number projection and including generator coordinate method for the axial quadrupole degree of freedom with Skyrme (Bender *et al.*, 2005, 2006a, 2008) or Gogny forces (Rodríguez *et al.*, 2015). Other large scale studies include the excitation energy of the collective 2^+ state and its $B(E2)$ transition strength to the ground state (Sabbey *et al.*, 2007) (see also (Rodríguez *et al.*, 2015) with the Gogny force). Applications of this methodology to the study of neutrino-less double beta decay are essential to extract relevant nuclear matrix elements in medium mass and heavy nuclei (Rodríguez and Martínez-Pinedo, 2010). In Fig 18 results for such matrix elements calculated with the Gogny force are compared
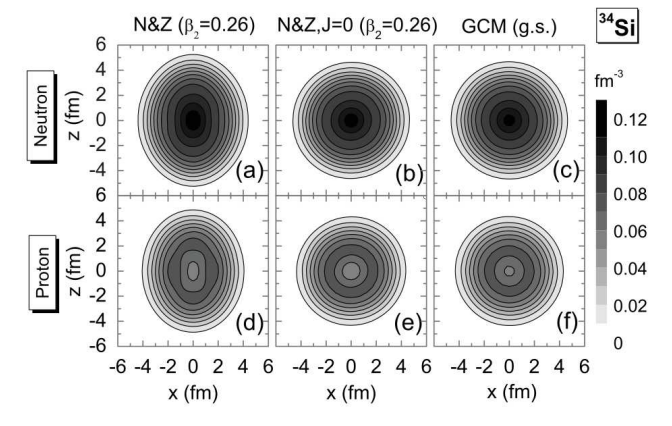

FIG. 17 (Color online) In the upper panels, the proton, neutron and total radial densities are plotted as a function of the radius r for four different types of calculations: a) pure HF imposing spherical symmetry b) HFB plus Lipkin-Nogami also imposing spherical symmetry c) Particle number projected density d) Particle number and angular momentum ($I = 0$) projected density obtained after generator coordinate method calculation using the quadrupole moment as generating coordinate. In the lower panels, contour plots of neutron and proton densities obtained using particle number projected wave functions obtained from a quadrupole deformed ($\beta_2 = 0.26$) intrinsic state (panels a) and d)); Panels b) and e), same as panels a) and d) but for particle number and angular momentum ($I = 0$) projected wave functions; the densities in panels c) and f) are obtained from generator coordinate method wave functions projected to good number of particles and angular momentum. Reprinted figures with permission from (Yao *et al.*, 2012). Copyright 2012 by the American Physical Society.

to results obtained with other interactions and (less sophisticated) methods.

The previous calculations were carried out under the assumption of reflection symmetry and therefore only positive parity states could be described. To describe negative parity states, intrinsic wave function with broken reflection symmetry is required. This is only pos-
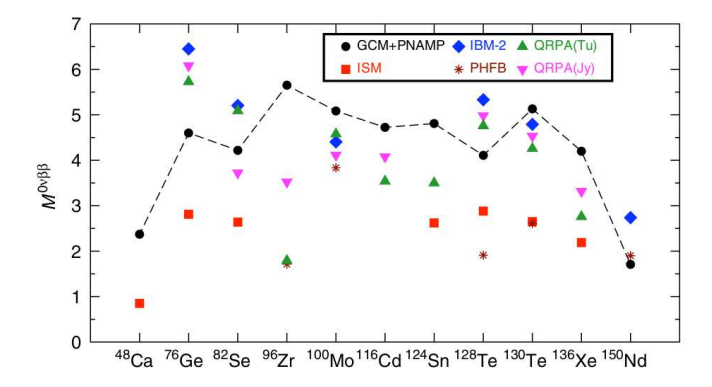
FIG. 18 Neutrinoless double beta decay matrix element for various nuclei of interest is computed with an angular momentum plus particle number projected generator coordinate method calculation with the Gogny D1S force. The results are compared with those of other approaches, showing a large uncertainty in the theoretical predictions. Reprinted figures with permission from (Rodríguez and Martínez-Pinedo, 2010). Copyright 2010 by the American Physical Society.

sible for a few octupole deformed nuclei in the actinide and rare earth regions, if only mean field intrinsic states and the projection after variation scheme are used. The number of nuclei accessible increases substantially if the intrinsic state is determined in the variation after projection scheme, irrespective of whether it is implemented exactly or in a restricted variational space (Robledo, 2015b; Robledo and Bertsch, 2011b). Another possibility is to perform a generator coordinate method calculation using the octupole degree of freedom as one of the collective coordinates. This approach has been followed in (Bernard et al., 2016; Bucher et al., 2017), where a combined angular momentum, parity and particle number projection of axially symmetric intrinsic states is carried out in a generator coordinate method framework with the Gogny force. The results obtained for rare earth nuclei around ^{144}Ba show a nice agreement with experiment. The physics of two octupole phonons can also be described consistently in this approach (Bernard et al., 2017).

Angular momentum projection of triaxial intrinsic states was first carried out in an early work by Caurier and Grammaticos (Caurier and Grammaticos, 1977) with the Skyrme SIII interaction. A restricted variation after projection was used with the radii and quadrupole moments as variational quantities. Moments of inertia obtained were a bit too high and different variants of the force were explored to improve the agreement with experimental data. A very small configuration space was used and therefore the applications were restricted to very light nuclei. Quite a few years later, Bonche et al (Bonche et al., 1991) used conveniently chosen combinations of intrinsic states oriented along different axis to carry out an approximate projection to $I = 0^+$ of triaxial intrinsic states. Full triaxial angular momentum projec-

tion was carried out with Skyrme interactions in (Baye and Heenen, 1984) but restricted to HF wave functions. The HF wave functions were expressed in a mesh in coordinate representation and special care how to define the rotation operator in that case was taken. In (Bender and Heenen, 2008) triaxial AMP plus particle number projection of HFB states was performed with Skyrme SLy4 for light nuclei. Additional configuration mixing using sets of configurations corresponding to different choices of the deformation parameters β and γ was also considered. The main conclusion is that the inclusion of triaxiality improves the description of rotational bands as compared to axial results. The calculations were subsequently extended to heavier systems in (Yao et al., 2013). Using the finite range Gogny forces, the technology to project triaxial states was developed in (Rodríguez and Egido, 2010) and applied to the study of ^{44}Si in (Rodríguez and Egido, 2011a) and to the waiting point nucleus ^{80}Zr in (Rodríguez and Egido, 2011b).

As discussed in Sec. III, there are two possible approaches when doing projection depending on how the intrinsic state is obtained: projection after or before variation. In the case of angular momentum projection and in the strong deformation limit (Beck et al., 1970; Mang, 1975b), the projection after variation leads to rotational bands with energies following the $I(I + 1)$ rule with the Peierls-Yoccoz moment of inertia (Peierls and Yoccoz, 1957; Yoccoz, 1957). On the other hand, variation after projection leads to the self-consistent cranking model with intrinsic states obtained from a constrained calculation on $\langle \hat{J}_x \rangle = \sqrt{I(I + 1)}$ (i.e. each angular momentum I has its own intrinsic state $|\varphi(I)\rangle$). The intrinsic states obtained in this approach break time-reversal invariance because J_x is a time-odd operator. The rotational band obtained in the variation-after-projection approach in the strong deformation limit (i.e. the cranking approach) also follows the $I(I + 1)$ rule, but this time with the Thouless-Valatin moment of inertia (Thouless and Valatin, 1962). Until recently, most of the angular momentum projected calculations were of the projection after variation type with intrinsic states preserving time-reversal invariance. As a consequence, the rotational bands obtained were stretched with respect to experiment by a typical factor of 1.4 (Li et al., 2012b; Rodríguez-Guzmán et al., 2002a), a consequence of implicitly using the Peierls-Yoccoz moment of inertia instead of the Thouless-Valatin one. In order to overcome this difficulty, the use of time-reversal breaking intrinsic states is required. Calculations with HFB cranking intrinsic states have been carried out with the Gogny force by Borrajo, Rodriguez et al in (Borrajo et al., 2015; Egido et al., 2016) [see also (Rodríguez, 2016) for an analysis of the different moments of inertia obtained in the different approaches]. In (Egido et al., 2016), collective and single-particle degrees of freedom were studied in the nucleus ^{44}S. Intrinsic wave functions $|\varphi(\beta, \gamma)\rangle_\omega$ of the HFB type
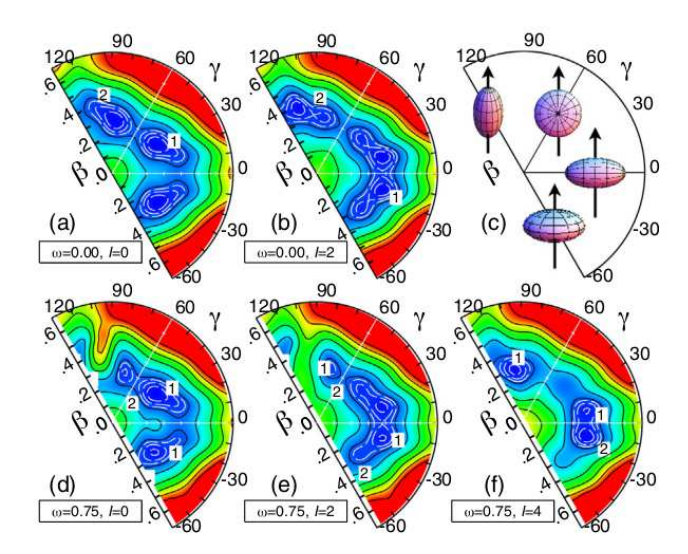
FIG. 19 Potential energy surfaces in the (β, γ) plane obtained by computing the projected energy of each of the intrinsic states obtained in a constrained cranked HFB calculation for different (β, γ) and ω values. Those states are used in a generator coordinate method calculation to obtain ground state and excited rotational bands in ^{44}S with the Gogny D1S force. The use of the cranking frequency ω as a generator coordinate improves the agreement with experiment substantially. Reprinted figure with permission from (Egido $et\ al.$, 2016). Copyright 2016 by the American Physical Society.

with quadrupole deformation parameters β and γ, and obtained at different angular frequencies ω were used in a configuration mixing calculation including projection to good particle number and angular momentum. The consideration of cranking states improves notably the description of moments of inertia and the inclusion of states with γ in the interval $-60 < \gamma < 120$ allows to consider two quasiparticle excitation like states which are present in the experimental spectrum of ^{44}S.

The use of the cranking frequency ω as a generator coordinate has also been considered in (Shimada $et\ al.$, 2015, 2016) with the Gogny D1S interaction but without particle number projection. In these calculations the intrinsic cranking state is rotated along a single axis, in contrast to the proposal of (Tagami and Shimizu, 2016) where intrinsic states are generated by using infinitesimal cranking frequencies ω_i but along the three cranking axis. This technique is well suited to describe γ bands and is applied to study these structures in ^{164}Er. Applications to wobbling motion in odd-A nuclei and to chiral doublet bands are presented in (Shimada $et\ al.$, 2018a) and in (Shimada $et\ al.$, 2018b). In the later three cases, no particle number projection is considered.

Cranked HF states were employed as early as in (Baye and Heenen, 1984) with a simple Skyrme like interaction (BKN+Coulomb). They were also used as intrinsic states in a full 3D angular momentum projection (Zduńczuk $et\ al.$, 2007) with the Skyrme SLy4 force in order to analyze band termination in nuclei around mass number 44.

Another situation requiring wave function breaking time reversal invariance is the description of odd mass nuclei. In addition, the blocking procedure has to be implemented to obtain the intrinsic HFB states. As a consequence of self-consistency, blocking the lowest quasiparticle states does not guarantee obtaining the lowest energy solutions and therefore several configurations have to be explored, increasing the computational cost accordingly. There is an additional issue that makes the description of odd nuclei more involved: the existence of zeros in the overlaps between rotated wave functions seem to be more likely than in the case of time-reversal preserving wave functions (Oi and Tajima, 2005). It is therefore to be expected that the problems mentioned before for density-dependent forces should be more relevant for odd mass nuclei. This consideration led (Bally $et\ al.$, 2014) to consider for their first projected calculation of an odd mass nucleus a Skyrme interaction which is fully derived from the Hamiltonian (Sadoudi $et\ al.$, 2013). The results for ^{25}Mg look reasonable, see Fig. 20 for the most important characteristics of the ground state band of this nucleus, in spite of the poor performance of SLyMR0 in other important aspects of nuclear structure. Surprisingly, the implementation with the density-dependent Gogny force (Borrajo and Egido, 2018; Borrajo $et\ al.$, 2015) does not lead to any apparent inconsistency in the Mg isotopes considered. Some results in heavier systems and for high spin states are discussed in (Shimada $et\ al.$, 2018a) for the Gogny D1S force.

Isospin symmetry is explicitly broken in the atomic nucleus due to the Coulomb interaction and the tiny differences observed in the different isospin channels of the nucleon-nucleon interaction originating from the different mass and charge of the u and d quarks. In addition, when working at the mean field level, isospin symmetry is also spontaneously broken by the mean field wave functions. Independently of the origin of the broken symmetry, working in a basis preserving isospin quantum numbers is advantageous to understand the impact of the different sources of isospin symmetry breaking in the nuclear wave function. The first application of isospin projection in a variation-after-projection framework was carried out in (Caurier and Poves, 1982) using a density-independent interaction with a Brink-Boecker central potential and applied to the study of Coulomb displacement energies. The projector operator is the same as in a full 3D angular momentum projection but the rotations take place in isospace (and therefore can be characterized by 2×2 matrices) simplifying thereby the treatment of the problem. Later, the formalism was applied to Skyrme functionals in (Satuła $et\ al.$, 2009, 2010, 2012) for the case of HF wave functions not mixing protons and neutrons at the single-particle level. This is particularly a
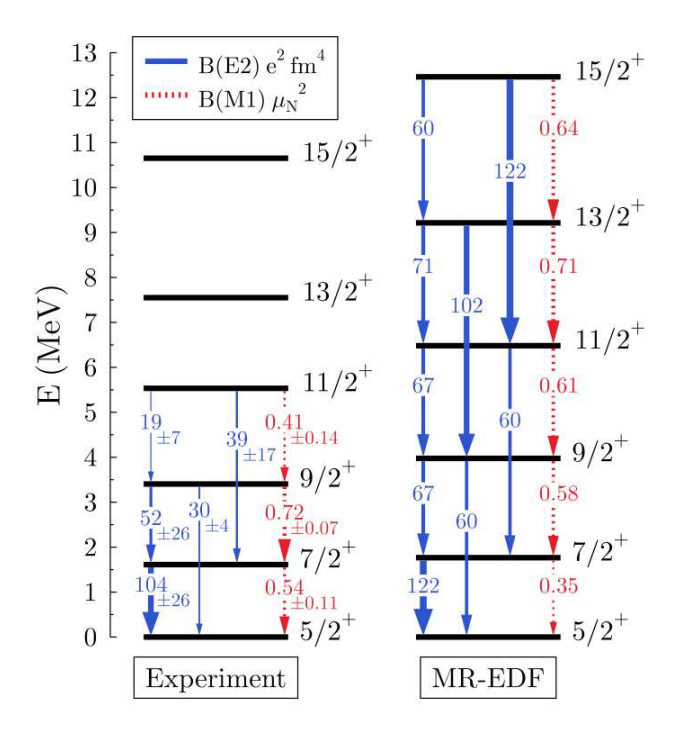
FIG. 20 (Color online) The excitation energies and transition strengths between the members of the ground state band of ^{25}Mg are compared with the experimental spectrum. The theory results are obtained from a calculation including angular momentum and particle number projection of intrinsic states breaking time reversal invariance. The density-independent SLyMR0 functional is used both for the particle-hole and the particle-particle channels to avoid all the difficulties associated to symmetry restoration and described in the text. Reprinted figure with permission from (Bally *et al.*, 2014). Copyright 2014 by the American Physical Society.

simple case, as the intrinsic HF wave function has a good T_z value and therefore the general projector reduces to a simple one dimensional integral as in axial symmetry angular momentum projection. The simplicity of rotations in isospace allows for analytical evaluation of most of the quantities involved in the evaluation of operator matrix elements. This allows to prove that even when the norm overlap is zero, the singularities are integrable.

The proper treatment of isospin related effects often involves the use of EDF mixing proton and neutron densities as well as cranking techniques in isospin (isocranking) (Sato *et al.*, 2013; Sheikh *et al.*, 2014) space. In this case a full "triaxial" projector with three Euler angles is required.

The traditional applications of symmetry restoration for EDF are combined with the use of the generator coordinate method with collective continuous coordinates (deformation parameters, pairing gaps, etc) so as to describe low energy collective states. An alternative is to use multi-quasiparticle excitations as discrete generating coordinates (like in the Projected Shell Model discussed

in V.A) to achieve flexibility in generating the correlated wave function. This approach is similar in spirit to the shell model, but contrary to this approach an intrinsic mean-field well adapted to the physics of the problem is used in the projected shell model, allowing for a restricted set of excitations to be considered for a faithful description of states. Both the projected shell model and the Shell Model employ restricted configuration spaces that require the introduction of a core as well as effective charges. Recently, a No Core Configuration Interaction method has been implemented along with the density-independent SV Skyrme interaction (Satuła *et al.*, 2016). The method is similar in spirit to the projected shell model but uses the full configuration space, removing the need for a core and/or effective charges. The present implementation of the No Core configuration interaction uses p-h excitations of Slater determinants projected to good angular momentum and isospin and has been used to study the excitation spectrum of several $N \approx Z$ nuclei as well as β decay matrix elements (Konieczka *et al.*, 2016, 2018). Also matrix elements of exotic processes exploring the physics beyond the Standard Model of particle physics have been analyzed.

2. Relativistic EDFs

The relativistic mean-field approach represents an alternative approach to describe the structure of the nucleus. Its main ingredient is the Dirac equation, which is used to determine the nucleon orbits. The potentials entering Dirac's equation are deduced in different ways depending on the version of the relativistic model used. In most of these models, the potentials experienced by nucleons depend upon several meson fields (Reinhard, 1989; Ring, 1996) which are determined through classical inhomogeneous Klein-Gordon equations, where the sources are given in terms of the nucleon densities and currents. The simplest version of this model (Walecka, 1974) cannot reproduce the right incompressibility of nuclear matter. Therefore a density dependence has been introduced by non-linear meson couplings (Boguta and Bodmer, 1977) or by an explicit density dependence of the meson-nucleon coupling constants (Lalazissis *et al.*, 2005).

In deformed nuclei the meson fields $\phi_i(\mathbf{r})$ are deformed. In order to restore symmetries one has to take them into account in a projection formalism going beyond mean field, i.e., the meson fields have to be quantized using creation and annihilation operators, $a^\dagger(\mathbf{r})$ and $a(\mathbf{r})$, obeying boson commutation relations. Slater determinants in fermion space correspond coherent states in boson space (see Chapt. 10 of (Ring and Schuck, 1980)). The total wave function of the system is therefore a product of a Slater determinant in Fermion space and a coherent state

in boson space

$$|\Psi\rangle \propto |\Phi\rangle \exp\left(\int d^3r \phi(\boldsymbol{r}) a^\dagger(\boldsymbol{r})\right)|0\rangle \quad . \qquad (189)$$

A variation of the corresponding energy with respect to the single-particle wave functions of the fermions and with respect to the meson fields $\phi(\boldsymbol{r})$ leads to the classical relativistic mean-field equations. For the angular momentum projection discussed in Sec. III.A.1 one needs the overlap integrals in Eq. 62 not only in the Fermion space, but also in the Boson space. The corresponding integrals in boson space for the norm and for the Hamiltonian can be found in (Balian and Brezin, 1969). However, because of the numerical complexity of Hamiltonian matrix elements with finite range interactions of Yukawa-type such calculations have not been carried out so far.

A simple way to bypass these problems is the relativistic point coupling models. Here the meson propagators with the large meson masses are expanded in momentum space up to second in q/m_ϕ and one ends up with a Lagrangian without mesons containing zero-range fermion interactions and zero range derivative terms in full analogy to the non-relativistic Skyrme functionals. The large repulsive density-dependent contact term is not needed in the relativistic case, but an additional density dependence for a good description of nuclear matter properties is introduced in the Lagrangian by either three- and four-body contact terms (Bürvenich et al., 2002; Niksic et al., 2008; Zhao et al., 2010) or by density-dependent coupling constants of the two-body contact terms (Niksic et al., 2008). Pairing correlations are considered by adding a contact interaction with parameters adjusted to the experimental data.

Point coupling models with many-body contact terms and without explicit density dependence were used in the mean-field + BCS approximation for beyond mean-field calculations with symmetry restoration (and configuration mixing) in (Nikšić et al., 2006a) with angular momentum projection of axially symmetric intrinsic states and also in (Nikšić et al., 2006b) with simultaneous angular momentum and particle number projection. Angular momentum projection was carried out after variation. The particle number was treated in the intrinsic state with the Lipkin-Nogami method (see Sec. IV.B) and after that an exact number projection has been carried out. In this way it was possible to provide a microscopic description the quantum-phase transition $X(5)$, which has been introduced in a group theoretical model (Iachello, 2001). It describes a transition from spherical to axially symmetric deformed intrinsic shapes and it is realized, e.g., in the chain of Nd-isotopes between the spherical nucleus ^{142}Nd and the axially deformed nucleus ^{152}Nd. At ^{150}Nd, a first order phase transition occurs and this nucleus has a very characteristic spectrum (see Fig.21), which can be described in the $X(5)$-model with only two phenomenological parameters. The same spectrum has
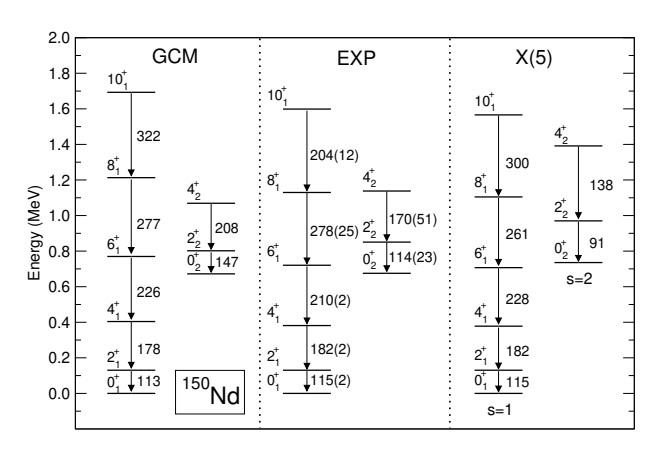

FIG. 21 The particle-number projected generator coordinate method spectrum of ^{150}Nd (left, compared with experiment (middle), and the $X(5)$-symmetry predictions (right). Reprinted figure with permission from (Niksic et al., 2007). Copyright 2007 by the American Physical Society.

been obtained in a fully microscopic relativistic mean-field calculation with subsequent angular momentum and number projection (Niksic et al., 2007). Only the 2^+ energy has to be slightly adjusted, because, as it has been discussed in the last section, the projection after variation does not break the time-reversal symmetry in the intrinsic states. The resulting spectrum is even better in agreement with experiment than the group-theoretical spectrum, which indicates that the nucleus ^{150}Nd is not exactly at the transition point of the $X(5)$-model. In the microscopic calculations, the transition rates are calculated in the full configuration space without effective charges and show excellent agreement with the experimental data.

This model based on covariant density functional was further extended to consider triaxial intrinsic states in (Yao et al., 2011, 2009, 2010), to reflection asymmetric ones in (Yao and Hagino, 2016; Yao et al., 2015b; Zhou et al., 2016) and to the admixture of projected two-quasiparticle configurations (Zhao et al., 2016) for the description of band-crossing phenomena in rotating nuclei. It also has been used to study nuclear matrix elements for $0\nu\beta\beta$ decay (Song et al., 2014; Yao et al., 2015a). In (Yao and Engel, 2016) the $0\nu\beta\beta$ decay of ^{150}Nd to ^{150}Sm is studied by including octupole correlations in the description of the ground and lowest lying 0^+ collective excited states. In Fig. 22 the result obtained for the nuclear matrix element corresponding to the $0^+_1 \to 0^+_1$ $0\nu\beta\beta$ transition is compared to the predictions not including octupole correlations as well as the predictions of other similar calculations with Gogny D1S (Rodríguez and Martínez-Pinedo, 2010). The inclusion of octupole correlations in the ground states of both mother and daughter nuclei reduces the value of $M^{0\nu}$ by 7 % but the reduction is not enough to reduce the discrepancies with non-relativistic calculations using a similar
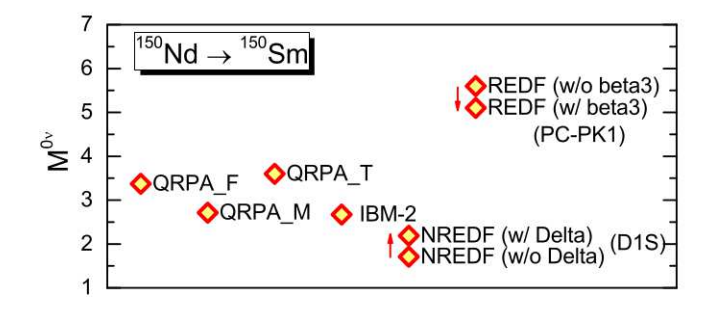
FIG. 22 Comparison of the nuclear matrix element of the $0\nu\beta\beta$ decay of the ground state of ^{150}Nd into ^{150}Sm obtained by different types of calculations. The inclusion of octupole correlations in the relativistic calculation has little impact on the matrix element value. Reprinted figure with permission from (Yao and Engel, 2016). Copyright 2007 by the American Physical Society.

framework and other calculations using the quasiparticle random phase approximation or the interacting boson model.

One of the advantages of relativistic PC models with many-body contact terms (Bürvenich *et al.*, 2002; Zhao *et al.*, 2010) is that phenomenological density-dependent terms are not required in order to obtain saturation, as is the case in the non-relativistic case. Therefore, these relativistic point coupling models are free from the difficulties mentioned in Sec. VI.A.4 and having to do with the non-analytical behavior of the density-dependent prescription used in the evaluation of EDF matrix elements. However, some words of caution are in order here: at the HF level, relativistic PC models with many-body contact terms leading to a polynomial density dependence can take into account all terms of the Hamiltonian such that the singularities cancel. In practice, the Fock terms, which are also of zero range, and which could be included, are usually neglected. The much more serious problem is, however, the pairing channel. As discussed before, because of the extremely large relativistic scalar and vector fields, one cannot use the same force in the HF and in the pairing channel (Kucharek and Ring, 1991). As a result, it is a common practice in the relativistic point coupling models to use a pairing interaction different from the one in the particle-hole channel and also to neglect the exchange contributions to the HF field. Therefore, the self-energy problems associated with the violation of Pauli principle are present in these calculations and cannot be easily avoided. The conclusion is that, as in most of the non-relativistic cases, the results obtained by symmetry restoration can contain some spurious contamination and their stability with respect to the parameters of the calculations have to be carefully checked.

C. Approximate projection for nuclear EDF

As we have seen in the last sections, the practical application of projection and configuration mixing methods for nuclear EDFs is quite successful. However, it is not only connected with conceptual problems, but also with extreme numerical efforts involved. Because of the large configuration spaces used in applications of universal density functional theory, it is even now extremely complicated to carry out a variation after projection of 3D angular momentum in heavy nuclei. Many of the applications are therefore restricted to light nuclei, where one has in principle also other methods such as configuration interaction calculations or coupled-cluster methods. Methods based on the mean-field approximation are assumed to work better in heavy systems, where other methods cannot be applied. Because of these difficulties one has developed approximate methods, which are tailored for heavy systems. They are based on the fact, that the overlap functions between two different Slater determinants $|q\rangle$ and $|q'\rangle$ are sharply peaked at $q = q'$. For heavy systems, the Gaussian overlap approximation is well justified. It has been shown (Giraud and Grammaticos, 1974; Haff and Wilets, 1973) that under these conditions one can derive a collective Hamiltonian in the variables q. It contains a potential energy $V(q) = \langle q|\hat{H}|q\rangle$, a kinetic term with microscopically derived inertia parameters and zero-point corrections (for details see (Libert *et al.*, 1999)). In the case of three dimensional angular momentum projection with the Euler angles one ends up with the Bohr-Hamiltonian for a rigid rotor in these variables (Une *et al.*, 1976), where angular momentum is automatically preserved. From the generator coordinate method ansatz for the parameters β and γ for quadrupole deformations one finds in this approximation the Bohr-Hamiltonian for collective β- and γ-vibrations. A similar collective Hamiltonian can also be derived from adiabatic time-dependent HF theory (Baranger and Vénéroni, 1978).

The advantage of above approximation is that one only has to solve the constrained mean-field equations on the energy surface characterized by the parameters q and to determine the expectation values of certain operators, e.g. $\langle q|\hat{H}|q\rangle$ or $\langle q|\hat{H}\hat{J}^2|q\rangle$. One avoids the complicated matrix elements and the problem of singularities connected with those.

In Fig. 23, we show the results of benchmark calculations (Yao *et al.*, 2014), where full three dimensional angular momentum and number projected generator coordinate method calculations are compared with experiment and with the results of the corresponding five dimensional collective Hamiltonian. The agreement between the two calculations for this complicated spectrum in the transitional nucleus ^{74}Kr is excellent. Having in mind, that the generator coordinate method calculations for this spectrum required 200 CPU hours with one pro-
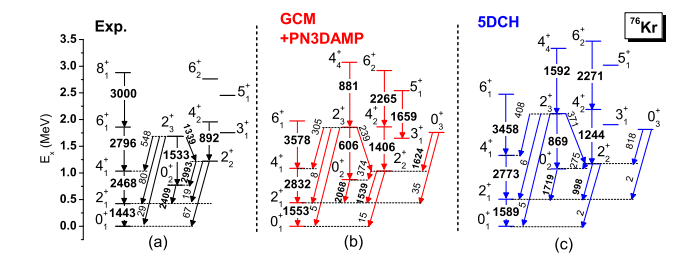
FIG. 23 Low-lying spectra and B(E2) values (in e^2 fm^4) of ^{76}Kr. Results from (b) the full relativistic generator coordinate method calculation with number and three dimensional angular momentum projection are compared with (c) 5DCH results and with (a) experimental data. Reprinted figure with permission from (Yao *et al.*, 2014). Copyright 2007 by the American Physical Society.

cessor, it is easy to understand that nowadays one finds many applications based on this approximation. Unfortunately, the method also has its downside as discussed in (Rodríguez *et al.*, 2015) with respect to negative values of zero point energy corrections.

VII. PROJECTION METHODS IN OTHER MESOSCOPIC SYSTEMS BEYOND ATOMIC NUCLEI

A. Physics framework

The last few decades have witnessed extraordinary advances in experimental techniques leading to the fabrication of mesoscopic and nanoscopic many-body systems with unparalleled control and diversity over the finite number of constituent particles, temperature, interparticle interactions, dimensionality, particle density, statistics (fermions versus bosons), and spin (Ellenberger *et al.*, 2006; Hanson *et al.*, 2007; Li *et al.*, 2017; Murmann *et al.*, 2015; Noguchi *et al.*, 2014; Serwane *et al.*, 2011; Tai *et al.*, 2017; Wineland *et al.*, 1987; Zürn *et al.*, 2012). Such manmade systems can be viewed as artificial atoms and molecules, and they offer unprecedented opportunities for generating and observing novel and exotic many-body states and phenomena, as well as for testing fundamental aspects of quantum physics that are beyond the reach of the natural chemical and condensed-matter systems. These nanosystems include two-dimensional semiconductor (Hanson *et al.*, 2007; Yannouleas and Landman, 2007) and graphene (Romanovsky *et al.*, 2009) quantum dots confining electrons and ultracold traps confining neutral atoms (Murmann *et al.*, 2015; Ramanathan *et al.*, 2011; Serwane *et al.*, 2011; Zürn *et al.*, 2012) or ions (Li *et al.*, 2017; Noguchi *et al.*, 2014; Wineland *et al.*, 1987) in a variety of trap shapes. Among the rich physics studied in these systems, one can mention Wigner molecules

(which extend Wigner crystals to the quantum regime), the connection to the fractional quantum Hall effect for high magnetic fields, Aharonov-Bohm phenomena and quantum space-time crystals in ring-shaped devices, wave function entanglement[7], Schrödinger-cat-state superpositions in strings of ultracold ions in linear traps, and the elucidation of the nature of correlations in assemblies of strongly repelling electrons (long-range Coulomb interaction) or strongly interacting neutral atoms with both an attractive or repulsive contact interaction. Areas of potential applications include quantum information and computing, improved electronic and photonic devices, atomic clocks, metrology, etc.

This section provides a pedagogical exposition of the essential aspects of symmetry breaking and symmetry restoration in mesoscopic systems beyond nuclei. It is hoped that this material will facilitate and motivate the reader to further explore the growing technical literature, which can only be described briefly here.

B. The microscopic many-body Hamiltonian

This chapter provides an outline of the application of symmetry-restoration methods to such mesoscopic systems beyond atomic nuclei. As usual in atomic and molecular physics, the $L - S$ coupling scheme is used and thus the restorations of the orbital angular momentum and spin are carried out independently of each other, whereas the restoration of the combined (orbital and spin) total angular momentum $\mathbf{J} = \mathbf{L} + \mathbf{S}$ ($J - J$ coupling) is pertinent in nuclei due to the strong spin-orbit interaction.

The spin-orbit coupling in atomic, molecular, and condensed-matter systems considered here is often weak compared to the corresponding coupling in nuclei. For example, the experimental particle magic numbers in metal clusters are 2, 8, 18, 20, 34, 40, 58, 92, ...(Knight *et al.*, 1984; Yannouleas and Landman, 1995), that is those for a spherical square well without spin-orbit modifications, unlike the nuclear case which has magic numbers 8, 20, 28, 50, 82, 126, ... (Goeppert Mayer, 1949; Haxel *et al.*, 1949).

The spin-orbit in condensed-matter systems (like quantum dots) is treated in two varieties i) the Rashba type (Bychkov and Rashba, 1984) and ii) The Dresselhaus type (Dresselhaus, 1955). The Rashba or Dresselhaus couplings can be included following the steps of restora-

---

[7] A pure state describing the quantum system of two or more particles is referred to as entangled if it is unfactorizable. A mixed state is entangled if it cannot be written as a mixture of factorizable pure states (Wootters, 1998); see also (Aspect, 2004; Eckert *et al.*, 2002) for additional background on the concept of entanglement.

A HIERARCHY OF APPROXIMATIONS

Restricted Hartree-Fock (RHF)
All spin and space symmetries are preserved
Single-particle densities: circularly symmetric
Each orbital is doubly/multiply occupied
Single Slater determinant (mean field)

Unrestricted Hartree-Fock (UHF)
Total-spin and space symmetries (rotational or parity) are broken
Repulsive: Different orbitals for different spins
Attractive: Each orbital doubly/multiply occupied
Solutions with lower point-group symmetry
Lower symmetry explicit in single-particle densities
Single Slater determinant (mean field)

Restoration of symmetry via projection techniques
Superposition of UHF Slater det.'s (beyond mean field)
sp-densities: circularly symmetric
Good total spin and angular momenta
Lower symmetry is HIDDEN (or EMERGENT)

Configuration interaction (EXACT)
Converged superposition of arbitrary-basis Slater det.'s
sp-densities: circularly symmetric
Good total spin and angular momenta
Lower symmetry is HIDDEN (or EMERGENT)

Total Energy

Correlations

FIG. 24 Synopsis of the method of hierarchical approximations, illustrating that symmetry breaking at the mean-field level (single Slater determinant) must be accompanied by a subsequent post-Hartree-Fock step of symmetry restoration yielding a linear superposition of UHF Slater determinants. The downward arrow on the left emphasizes that the total energy of the finite system is lowered with each successive step, approaching from above the exact configuration-interaction total energy; see Fig. 26 below for a simple example. The arrow on the right emphasizes that the steps beyond the restricted Hartree-Fock introduce correlations. [Reprinted with permission from (Yannouleas and Landman, 2007)].

tion of the spin and angular momentum broken symmetries. For an example of incorporating the Rashba and Dresselhaus spin-orbit couplings in the context of 2D quantum dots, see the configuration-interaction calculations in (Szafran *et al.*, 2009).

Symmetry restoration in electronic and atomic systems can be viewed as a particular step in the context of a multilevel hierarchical scheme, which produces a lower total energy at each step; see Fig. 24 that describes the successive levels in this hierarchy. One starts with the restricted Hartree Fock (RHF) whose wave function (a single determinant or permanent) preserves by construction all the symmetries of the many-body Hamiltonian; in particular, it imposes the spatial symmetries of the many-Hamiltonian on each individual HF orbital. The next level is an unrestricted Hartree Fock (UHF) whose single determinant (or permanent) allows for the breaking of some (or all) of the Hamiltonian symmetries in an appropriate range of the two-body interaction. In

this case, the UHF total energy is lower compared to the RHF one, but the UHF space orbitals do not reflect the space symmetries of the many-body Hamiltonian, a behavior that is often referred to as "Löwdin's symmetry dilemma" (Lykos and Pratt, 1963).

In a subsequent step, the broken symmetry in the UHF solutions is restored and the symmetry dilemma is resolved. This level produces a multi-determinantal (or multi-permanent) wave function by applying the projection-operator technique on the UHF single determinant (or permanent). This level, which is depicted as a single item in Fig. 24, consists of two substeps, namely the step of variation before projection and the step of variation after projection, see Sec. III. The variation-after-projection step produces lower energies in general, while the wave functions retain the same multi-determinantal structure as in the variation-before-projection step. The energy difference between these two projection variants decreases as the symmetry breaking becomes stronger. In the context of this section, an example of the variation-after-projection step is offered by (Romanovsky *et al.*, 2006, 2004) where the localized-particle orbitals [displaced Gaussians of Eq. (204) with variational parameters] were used to build an approximate UHF determinant for fermions (or permanent for bosons).

The final level corresponds to a configuration-interaction treatment which in principle provides the exact many-body energies and wave functions. The RHF and UHF are mean-field approximations; the restoration of symmetry and the configuration interaction are often referred to as beyond-mean-field approaches.

The many-body Hamiltonian describing N fermions or bosons confined in a two-dimensional geometry and interacting via a two-body potential $U(\mathbf{r}_1, \mathbf{r}_2)$ is given by

$$\mathcal{H} = \sum_{i=1}^{N} H_{sp}(i) + \sum_{i=1}^{N} \sum_{j>i}^{N} U(\mathbf{r}_1, \mathbf{r}_2). \qquad (190)$$

In Eq. (190), a variety of two-body interactions have been considered, i.e.,

(1) For electrons and ultracold ions the Coulomb repulsion,

$$U(\mathbf{r}_1, \mathbf{r}_2) = \frac{e^2}{\kappa |\mathbf{r}_i - \mathbf{r}_j|}, \qquad (191)$$

where κ is the dielectric constant of the material in the case of semiconductor quantum dots; for trapped ultracold ions, $\kappa = 1$. Beyond the familiar electrons, examples of trapped ultracold ions are: Be^+, Ca^+, and Yb^+.

(2) For ultracold trapped neutral atoms interacting via a Dirac-delta contact potential,

$$U(\mathbf{r}_1, \mathbf{r}_2) = g\delta(\mathbf{r}_i - \mathbf{r}_j), \qquad (192)$$

where the strength parameter g can take both negative (attractive interaction) and positive (repulsive interaction) values. Experimentally, this parameter can be

varied continuously from the attractive to the repulsive regime; see, e.g., (Brandt *et al.*, 2015; Zürn *et al.*, 2012). Examples of trapped neutral atoms are: ^{6}Li (fermionic) and ^{87}Rb (bosonic). In the case of ultracold atoms and molecules, dipole-dipole two-body interactions have also experimentally been realized. However, no symmetry-restoration investigations with dipolar interactions have been reported as yet.

The single-particle Hamiltonian in a perpendicular external field B is given by

$$H_{sp} = \frac{(\mathbf{p} - \eta\mathbf{A})^2}{2m} + V(x, y), \qquad (193)$$

where the external confinement is denoted by $V(x, y)$ and the vector potential $\mathbf{A}$ is given in the symmetric gauge by

$$\mathbf{A}(\mathbf{r}) = \frac{1}{2}\mathbf{B} \times \mathbf{r} = \frac{1}{2}(-By, Bx, 0). \qquad (194)$$

In the case of charged particles, a Zeeman interaction term is present leading to a splitting of the spin multiplets; it will be omitted in the following, but it can be easily added if needed. In the case of charged particles, $\mathbf{B}$ coincides with the natural magnetic field and $\eta = e/c$. For ultracold neutral atoms, $\mathbf{B}$ can be mimicked with artificial synthetic fields (Goldman *et al.*, 2014) or the fast rotation of the harmonic trap (Romanovsky *et al.*, 2006).

Unlike nuclear physics, the magnetic field plays an important role in finite two-dimensional systems like quantum dots, because of their relatively large spatial size. This allows the full range of orbital magnetic effects to be explored for magnetic fields that are readily attained in the laboratory (less than 40 T). In contrast, for natural atoms and molecules, magnetic fields of extremely large strength (i.e., larger than 10^5 T) are needed to produce novel phenomena related to orbital magnetism (beyond the perturbative regime). Such strong fields are known to occur only in astrophysical environments (e.g., on the surface of neutron stars) (Ruder *et al.*, 1994). A main orbital effect is the progressive spatial shrinking of the single-particle orbitals as the magnetic field increases; this behavior can be directly visualized from the analytic width λ [Eq. (205)] of the displaced Gaussian wave function given in Eq. (204). Another orbital effect is the acquisition of a Peierls phase factor [see again Eq. (204)]. These orbital effects are prerequisites behind the appearance of celebrated magnetic-field-dependent phenomena, like the Aharonov-Bohm effect and the formation of quantized Landau levels supporting integer and fractional quantum Hall effects.

The external potential confinement $V(x, y)$ can assume various parametrizations in order to model a single circular or elliptic quantum dot or ultracold confining trap, or a molecule-like double well. In the case of an elliptic confinement, one has

$$V(x, y) = \frac{1}{2}m^*(\omega_x^2 x^2 + \omega_y^2 y^2), \qquad (195)$$

which reduces to the circular confining potential when $\omega_x = \omega_y = \omega_0$. The appropriate parametrization of $V(x, y)$ in the case of a double well is more complicated. Often a parametrization based on a 2D version of a two-center oscillator with a smooth necking is used. Details of the double-well parametrization are described in (Li *et al.*, 2009; Yannouleas and Landman, 2002b).

C. Mean-field for fermions: The UHF self-consistent Pople-Nesbet equations

The UHF many-body wave function for N fermions is a single Slater determinant

$$\Psi_{\mathrm{UHF}}^N = \frac{1}{\sqrt{N!}}\det[\chi_1(\mathbf{x}_1), \chi_2(\mathbf{x}_2), \ldots, \chi_N(\mathbf{x}_N)], \quad (196)$$

where $[\chi_i(\mathbf{x})]$ are a set of N spin orbitals, with the index $\mathbf{x}$ denoting both the space and spin coordinates. We denote $\chi_i(\mathbf{x}) = \psi_i(\mathbf{r})\alpha$ for a spin-up fermion and $\chi_i(\mathbf{x}) = \psi_i(\mathbf{r})\beta$ for a spin-down one. As a result, the UHF determinants here are eigenstates of the projection of the total spin with eigenvalue $S_z = (N^\alpha - N^\beta)/2$, where $N^{\alpha(\beta)}$ denotes the number of spin up (down) fermions. However, these Slater determinants are not eigenstates of the square of the total spin, $\hat{\mathbf{S}}^2$, except in the fully spin polarized case.

To derive the Pople-Nesbet equations [see Ch 3.8 of (Szabo and Ostlund, 1989)], one minimizes the total energy $\langle\Psi_{\mathrm{UHF}}|\mathcal{H}|\Psi_{\mathrm{UHF}}\rangle$ by varying the spin orbitals $[\chi_i(\mathbf{x})]$ under the constraint that they remain *orthonormal*. Fermions with α (up) spin are described by one set of spatial orbitals $\{\psi_j^\alpha|j = 1, 2, \ldots, K\}$, while those with β (down) spin are described by a different set of spatial orbitals $\{\psi_j^\beta|j = 1, 2, \ldots, K\}$; of course one obtains the RHF result by requiring that $\psi_j^\alpha = \psi_j^\beta = \psi_j$.

Each UHF spatial orbital (the output of the Pople-Nesbet equations) is allowed to break the rotational symmetry. After projection (see Secs. VII.E and VII.F below), the projected many-body wave functions can have any magic total angular momentum L and total spin S (available for N particles). The broken-symmetry UHF determinant constructed with the Pople-Nesbet single-particle spin orbitals can be expressed as a linear superposition (many-body wave packet) of projected wave functions with different L's and S's.

Next, one introduces a set of basis functions $\{\varphi_\mu|\mu = 1, 2, \ldots, K\}$ (constructed to be *orthonormal* in our 2D case), and expands the UHF orbitals as

$$\psi_i^\alpha = \sum_{\mu=1}^K C_{\mu i}^\alpha \varphi_\mu \quad \text{and} \quad \psi_i^\beta = \sum_{\mu=1}^K C_{\mu i}^\beta \varphi_\mu, \qquad (197)$$

where $i = 1, 2, \ldots, K$. It is natural to form the basis set from the single-particle eigenstates of the confining external potential; this guaranties that the basis functions are orthonormal.

The Pople-Nesbet equations are a system of two coupled matrix eigenvalue problems resolved according to up and down spins,

$$\mathbf{F}^{\alpha\beta}\mathbf{C}^{\alpha} = \mathbf{C}^{\alpha}\mathbf{E}^{\alpha} \quad \text{and} \quad \mathbf{F}^{\beta\alpha}\mathbf{C}^{\beta} = \mathbf{C}^{\beta}\mathbf{E}^{\beta}, \qquad (198)$$

where $\mathbf{F}^{\alpha\beta(\beta\alpha)}$ are the Fock-operator *matrices* and $\mathbf{C}^{\alpha(\beta)}$ are the *vectors* formed with the coefficients in the expansions in Eq. (197). The *matrices* $\mathbf{E}^{\alpha(\beta)}$ are *diagonal* (Szabo and Ostlund, 1989). The coupling between the two UHF equations in Eq. (198) is given explicitly in the expressions for the elements of the Fock matrices below [Eqs. (200) and (201)].

Introducing the density matrices $\mathbf{P}^{\alpha(\beta)}$ for $\alpha(\beta)$ fermions,

$$P_{\mu\nu}^{\alpha} = \sum_{a}^{N^{\alpha}} C_{\mu a}^{\alpha}(C_{\nu a}^{\alpha})^{*} \quad \text{and} \quad P_{\mu\nu}^{\beta} = \sum_{a}^{N^{\beta}} C_{\mu a}^{\beta}(C_{\nu a}^{\beta})^{*},$$
$$(199)$$

where $N^{\alpha} + N^{\beta} = N$, the elements of the Fock-operator matrices are given by

$$F_{\mu\nu}^{\alpha\beta} = H_{\mu\nu} + \sum_{\lambda}\sum_{\sigma} P_{\lambda\sigma}^{\alpha}[(\mu\sigma|\nu\lambda) - (\mu\sigma|\lambda\nu)] + \sum_{\lambda}\sum_{\sigma} P_{\lambda\sigma}^{\beta}(\mu\sigma|\nu\lambda) \qquad (200)$$

$$F_{\mu\nu}^{\beta\alpha} = H_{\mu\nu} + \sum_{\lambda}\sum_{\sigma} P_{\lambda\sigma}^{\beta}[(\mu\sigma|\nu\lambda) - (\mu\sigma|\lambda\nu)] + \sum_{\lambda}\sum_{\sigma} P_{\lambda\sigma}^{\alpha}(\mu\sigma|\nu\lambda), \qquad (201)$$

where $H_{\mu\nu}$ are the elements of the single-particle Hamiltonian, and the interparticle interaction is expressed via the two-body integrals

$$(\mu\sigma|\nu\lambda) = \int d\mathbf{r}_1 d\mathbf{r}_2 \varphi_{\mu}^{*}(\mathbf{r}_1)\varphi_{\sigma}^{*}(\mathbf{r}_2)U(\mathbf{r}_1,\mathbf{r}_2)\varphi_{\nu}(\mathbf{r}_1)\varphi_{\lambda}(\mathbf{r}_2).$$
$$(202)$$

Of course, the Greek indices μ, ν, λ, and σ run from 1 to K.

The system of the two coupled UHF matrix equations in Eq. (198) is solved selfconsistently through iteration cycles. For obtaining the numerical solutions, a set of K basis states φ_i's that are chosen to be the product wave functions formed from the eigenstates of one-center (single trap) and/or two-center (Li *et al.*, 2009; Yannouleas and Landman, 2002b) (double well) one-dimensional oscillators along the Cartesian x and y axes.

The UHF equations preserve at each iteration step the symmetries of the many-body Hamiltonian, if these symmetries happen to be present in the input (initial) fermion density of the iteration. The input densities into the iteration cycle are controlled by the values of the $P_{\lambda\sigma}^{\alpha}$ and $P_{\lambda\sigma}^{\beta}$ matrix elements. For obtaining broken-symmetry UHF solutions, we have found that the choice $P_{\lambda\sigma}^{\alpha} = 1$ and $P_{\lambda\sigma}^{\beta} = 0$ usually produces broken-symmetry solutions (in the regime where symmetry breaking occurs).

Having obtained the selfconsistent solution, the total UHF energy is calculated as

$$E_{\text{UHF}} = \frac{1}{2}\sum_{\mu}\sum_{\nu}[(P_{\nu\mu}^{\alpha} + P_{\nu\mu}^{\beta})H_{\mu\nu} + P_{\nu\mu}^{\alpha}F_{\mu\nu}^{\alpha\beta} + P_{\nu\mu}^{\beta}F_{\mu\nu}^{\beta\alpha}].$$
$$(203)$$

An illustrative example of broken-symmetry UHF solutions is given in Fig. 25 for the case of $N = 9$ electrons in a parabolic quantum dot at $B = 0$. In the case of repulsive interactions [but also for high magnetic fields (Yannouleas and Landman, 2007)], the symmetry breaking results in particle localization and a lowering of the continuous rotational symmetry to a point-group one. The localized humps in the UHF densities in Fig. 25 result from the tendency of the particles to avoid each other due to their strong mutual repulsion. For high magnetic field, a similar localization effect is related to the shrinking of the space orbitals, as mentioned above.

Two UHF isomers of localized electrons, denoted as (2,7) and (1,8), are displayed in Fig. 25. Such nested polygonal-ring $(n_1, n_2, \ldots)$ isomers may compete with
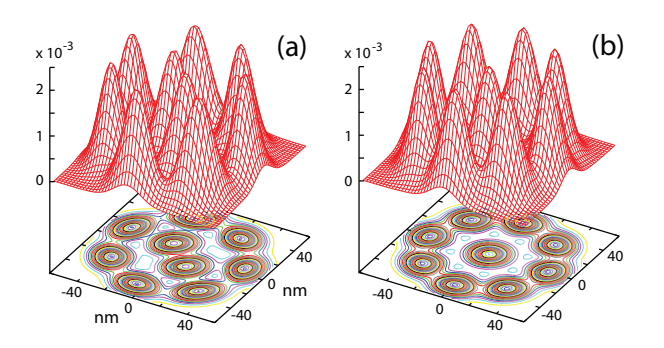

FIG. 25 UHF electron densities for two isomers in a parabolic quantum dot with $N = 9$ electrons and $S_z = 9/2$, exhibiting breaking of the circular symmetry at $R_W = 6.365$ [see Eq. (209)] and $B = 0$. (a) The (2,7) ground-state isomer with total energy 570.0093 meV. (b) The (1,8) first-excited isomer with total energy 570.2371 meV. The choice of the remaining parameters is: parabolic confinement $\hbar\omega_0 = 5$ meV, dielectric constant $\kappa = 3$, and effective mass $m^* = 0.067m_e$. Distances are in nanometers and the electron density in nm^{-2}.

each other in a similar way to the prolate and oblate nuclear shape deformations.

The localization of individual particles suggests a convenient and physically transparent approximation for the broken-symmetry mean-field solution by a Slater determinant Ψ^{MF} made out of non-orthogonal orbitals having the form of displaced Gaussian functions localized at positions $\mathbf{R}_j$, i.e.,

$$u(\mathbf{r}, \mathbf{R}_j) = \frac{1}{\sqrt{\pi}\lambda} \exp\left(-\frac{(\mathbf{r} - \mathbf{R}_j)^2}{2\lambda^2} - i\varphi(\mathbf{r}, \mathbf{R}_j; B)\right), \tag{204}$$

where λ is a potential variational parameter. For strong magnetic fields, one can take

$$\begin{aligned} \lambda &= \sqrt{\hbar/(M\Omega)}, \\ \Omega &= \sqrt{\omega_0^2 + \omega_c^2/4}, \end{aligned} \tag{205}$$

where $\omega_c = \eta B/M$ is the cyclotron frequency. The phase in Eq. (204) is due to the gauge invariance of magnetic translations (Peierls, 1933) and is given by $\varphi(\mathbf{r}, \mathbf{R}_j; B) = (xY_j - yX_j)/(2l_B^2)$, with $l_B = \sqrt{\hbar/(\eta B)}$ being the magnetic length.

D. Mean-field for spinless bosons

For spinless bosons, one can allow each particle to occupy a different space orbital $\psi_i(\mathbf{r}_i)$. We stress that this is a crucial point in the unrestricted versions of mean-field theory [in the fermionic UHF Pople-Nesbet equations, it is usually described as "different orbitals for different spins"; see, e.g., Fig. 26(b1)]. Employing different orbitals for each particle allows the description of particle localization in space, which is a prerequisite for the formation of Wigner molecules in the case of repulsive interparticle interactions.

Naturally, keeping the same space orbital and allowing only deformations of this orbital does break the rotational symmetry. However, this way one restricts the variational space to shape deformations only, akin to those associated with a central Nilsson-type potential in the case of attractive interparticle interactions .

The permanent

$$\Psi^N = \text{perm}[\psi_1(\mathbf{r}_1), ..., \psi_N(\mathbf{r}_N)] \tag{206}$$

serves as the many-body wave function of the unrestricted Bose-Hartree-Fock (UBHF) approximation.

The permanent of a matrix is an analog of a determinant where all the signs in the expansion by minors are taken as positive. For example, for a two by two matrix {{a,b},{c,d}}, the determinant is ad−bc, while the permanent is ad+bc.[8]

Wave function (206) reduces to the Gross-Pitaevskii form with the restriction that all bosons occupy the same orbital $\psi_0(\mathbf{r})$, i.e., $\Psi_{\text{GP}}^N = \prod_{i=1}^N \psi_0(\mathbf{r}_i)$. In this case, $\psi_0(\mathbf{r})$ is determined self-consistently at the restricted Bose-Hartree-Fock level via the equation (Esry, 1997)

$$\left[H_{sp}(\mathbf{r}_1) + (N-1)\int d\mathbf{r}_2 \psi_0^*(\mathbf{r}_2) U(\mathbf{r}_1, \mathbf{r}_2)\psi_0(\mathbf{r}_2)\right]\psi_0(\mathbf{r}_1)$$
$$= \varepsilon_0 \psi_0(\mathbf{r}_1). \tag{207}$$

Here $U(\mathbf{r}_1, \mathbf{r}_2)$ is the two-body interaction. The single-particle hamiltonian is given by $H_{sp}(\mathbf{r}) = -\hbar^2\nabla^2/(2m) + m\omega_0^2\mathbf{r}^2/2$, where ω_0 characterizes the harmonic confinement.

The boson statistics allows multiple particle occupation of a given orbital. As a result, the orbitals associated with two different bosons are not necessarily orthogonal, unlike the case of the spin-orbitals associated with two different fermions (that necessarily obey the Pauli exclusion principle). The inability to impose the orthogonality condition to all bosonic-particle pairs (i, j) results in a smaller number (only N) of Lagrange multipliers that can be used for the minimization of the total-energy mean-field functional compared to the fermionic case [with $N(N+1)/2$ Lagrange multipliers]. Thus, going beyond the Gross-Pitaevskii approach to the UHF level (i.e., using a permanent Ψ^N with different orbitals) results in a set of UBHF equations that are more complex compared to the fermionic Pople-Nesbet ones (Heimsoth and Bonitz, 2010; Romanovsky, 2006).

A simplification of the UBHF problem can be achieved by considering explicit analytic expressions for the space orbitals $\psi_i(\mathbf{r}_i)$. In particular, since for repelling bosons the particles must avoid occupying the same position in space in order to minimize their mutual repulsion, we take all the orbitals to be of the form of displaced Gaussians, namely we set $\psi_j(\mathbf{r}_i) = u(\mathbf{r}_i, \mathbf{R}_j)$.

For ultracold atoms or ions, rotating traps can be easily implemented. Such rotating traps can be handled theoretically by using the correspondence $\omega \to B$, where ω denotes the rotational frequency of the trap.

With the above choice of localized orbitals, the unrestricted permanent Ψ^N breaks the continuous rotational symmetry.

For both the cases of a contact potential and a Coulomb interaction, the resulting energy gain becomes substantial for stronger repulsion. Controlling this energy gain (the strength of correlations) is the ratio R between the strength of the repulsive potential and the

---

[8] Attention must be given to the normalization coefficient; for orthogonal orbitals, $\psi_i(\mathbf{r}_i)$, see Eq. (A1) in (Baksmaty *et al.*, 2007), and for non-orthogonal orbitals, see (Romanovsky, 2006).

zero-point kinetic energy. Specifically, for a 2D trap, one has

$$R_\delta = gm/(2\pi\hbar^2) \tag{208}$$

for a contact potential and

$$R_W = Z^2 e^2/(\hbar\omega_0 l_0) \tag{209}$$

for a Coulomb interaction, with $l_0 = \sqrt{\hbar/(m\omega_0)}$ being the characteristic harmonic-oscillator length. [The subscript W in the case of a Coulomb interaction stands for "Wigner", since the Coulomb crystallites in harmonic traps are finite-size analogs of the bulk Wigner crystal (Wigner, 1934).]

E. Restoration of broken 2D rotational symmetry

A stationary many-body state that preserves the total angular momentum, as well as the rotational symmetry of the 2D trap, can be projected out of the symmetry-broken Ψ^N by applying the projector operator $\mathcal{P}_L$,

$$\mathcal{P}_L = \frac{1}{2\pi}\int_0^{2\pi} e^{i\gamma(L-\hat{L})}d\gamma, \tag{210}$$

where $\hat{L} = \sum_{i=1}^N \hat{l}_i$, $i = 1, 2, \ldots, N$, and $\hbar\hat{L}$ is the *twodimensional* total angular-momentum operator. Then the projected many-body state is given (Ring and Schuck, 1980; Yannouleas and Landman, 2006a, 2007) by

$$\Phi_L^{\mathrm{PRJ}} = \frac{1}{2\pi}\int_0^{2\pi} d\gamma\,\Psi^N(\gamma)e^{i\gamma L}. \tag{211}$$

For the 3D case, see Sec. III.B.2.

$\mathcal{P}_L$ is analogous to the projector operators used in chemistry for molecular orbitals governed by point group symmetries (Cotton, 1990; Yannouleas and Landman, 2003a). Such projection operators are constructed through a summation over the characters of the molecular point group; the phases $e^{i\gamma L}$ are the characters of the rotational group in two dimensions (Hamermesh, 1962; Yannouleas and Landman, 2003a) and the operator $e^{-i\gamma\hat{L}}$ is the corresponding group generator of 2D rotations. Alternatively, Eq. (211) may be viewed as a linear superposition of all the (energy-degenerate) symmetry-broken states $\Psi^N(\gamma)$, azimuthally rotated by γ. Due to the rotational symmetry, the coefficients of this superposition, i.e., the phases $e^{i\gamma L}$, can be determined a priori, without the need to diagonalize a Hamiltonian matrix. In the absence of rotational symmetry, one can employ the more general wave functions according to the Hill-Wheeler-Griffin approach (Griffin and Wheeler, 1957; Hill and Wheeler, 1953).

The projected energies associated with the wave functions Φ_L^{PRJ}, are given (Ring and Schuck, 1980; Yan-

nouleas and Landman, 2007) by

$$E^{\mathrm{PRJ}}(L) = \int_0^{2\pi} h(\gamma)e^{i\gamma L}d\gamma \bigg/ \int_0^{2\pi} n(\gamma)e^{i\gamma L}d\gamma, \tag{212}$$

where $h(\gamma) = \langle\Psi^N(0)|\mathcal{H}|\Psi^N(\gamma)\rangle$, and the norm overlap $n(\gamma) = \langle\Psi^N(0)|\Psi^N(\gamma)\rangle$ enforces proper normalization of Φ_L^{PRJ}.

F. Combining spin and angular momentum restorations

When the fermions are not fully polarized, the symmetry-broken Pople-Nesbet UHF determinantal solutions do have the total spin projection S_z as good quantum numbers. However, the total spin $\hat{\mathbf{S}} = \hat{\mathbf{s}}_1 + \hat{\mathbf{s}}_2$ is not preserved. A simple example is the UHF determinant which describes the "singlet" ($S_z = 0$) ground state of two electrons in a parabolic quantum dot for $R_W = 2.40$ (and $B = 0$). Fig. 26(a) displays the azimuthally symmetric RHF electron density, which contrasts with the symmetry-broken UHF one displayed in Fig. 26(b2). Fig. 26(b1) displays the densities of the spin-up (left) and spin-down (right) localized orbitals that make up the UHF density and that are obtained by solving the Pople-Nesbet equations. Denoting these orbitals as $u(\mathbf{r})\alpha$ and $v(\mathbf{r})\beta$, the UHF determinant is written in a compact notation as

$$\Psi_{\mathrm{UHF}}(1, 2) = |u(1)\alpha(1)v(2)\beta(2)\rangle/\sqrt{2}. \tag{213}$$

From the determinant $\Psi_{\mathrm{UHF}}(1, 2)$, one can generate a singlet eigenstate of $\hat{\mathbf{S}}^2$ (with $S = 0$ eigenvalue) by applying the projection operator $\mathcal{P}_{\mathrm{spin}}^s \equiv 1 - \varpi_{12}$, where the operator ϖ_{12} interchanges the spins of the two electrons.

Thus the singlet state of the two localized electrons is given by the projected wave function,

$$\Phi_{\mathrm{spin}}^{\mathrm{PRJ}}(1, 2) \equiv \mathcal{P}_{\mathrm{spin}}^s \Psi_{\mathrm{UHF}}(1, 2) \propto$$
$$|u(1)\alpha(1)v(2)\beta(2)\rangle - |u(1)\beta(1)v(2)\alpha(2)\rangle. \tag{214}$$

In contrast to the single-determinantal wave functions of the RHF and UHF methods, the projected many-body wave function (214) is a linear superposition of two Slater determinants, and thus it is an entangled state representing a corrective (post-Hartree-Fock) step beyond the mean-field approximation. We note that the spatial reflection symmetry (parity) is automatically restored along with the spin symmetry (Fukutome, 1981). Furthermore, Eq. (214) has the form of a Heitler-London (Heitler and London, 1927) or valence bond (Szabo and Ostlund, 1989) wave function, familiar from the theory of the chemical bond of the natural H_2 molecule.

For the singlet state, one can generate appropriate projected wave functions by applying the product operator

$$\mathcal{O} \equiv \mathcal{P}_L \mathcal{P}_{\mathrm{spin}}^s, \tag{215}$$
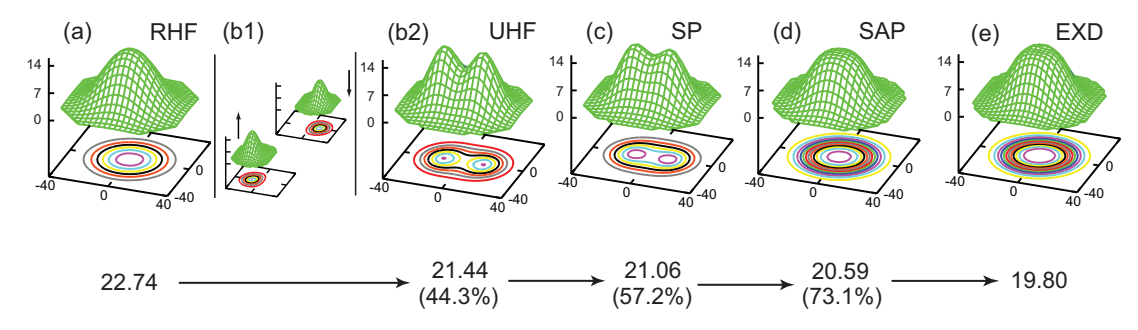
FIG. 26 Various approximation levels for the lowest singlet state of a field-free ($B = 0$) two-electron quantum dot with $R_W = 2.40$. The corresponding energies (in meV) are shown at the bottom of the figure. (a): Electron density of the RHF solution, exhibiting circular symmetry (due to the imposed symmetry restriction). The correlation energy, $E_{\text{corr}} = 2.94$ meV, is defined as the difference between the energy of the RHF state and the exact (EXD) solution [shown in frame (e)]. (b1) and (b2): The two occupied orbitals (modulus square) of the symmetry-broken "singlet" UHF solution (b1), with the corresponding total electron density exhibiting non-circular shape (b2). The energy of the UHF solution shows a gain of 44.3% of the correlation energy. (c): Electron density of the spin-projected singlet (SP), showing broken spatial symmetry, but with an additional gain of correlation energy. (d): the spin-and-angular-momentum projected state (SAP) exhibiting restored circular symmetry with a 73.1% gain of the correlation energy. The choice of parameters is: dielectric constant $\kappa = 8$, parabolic confinement $\hbar\omega_0 = 5$ meV, and effective mass $m^* = 0.067m_e$. Distances are in nanometers and the densities in 10^{-4} nm^{-2}. [Reprinted with permission from (Yannouleas and Landman, 2007)].

where the spin-projection operator $\mathcal{P}_{\text{spin}}^s$ produces the singlet wave function of Eq. (214), and then the angular-momentum operator $\mathcal{P}_L$ acts upon this two-determinant wave function. This double projection describes all the lowest-energy states [yrast band (Yannouleas and Landman, 2000a)] with good total angular momentum $L = 0, 2, 4, \ldots$. (The yrast-band states with odd values, $L = 1, 3, 5, \ldots$, are generated via a projection of the fully-polarized UHF state.)

The evolution of the ground-state ($L = 0$) electron densities according to the successive approximations, RHF, UHF, spin projection (SP), and combined spin and angular momentum projection (SAP) is illustrated in Fig. 26. The exact wave functions for two electrons in a parabolic confinement are available (Yannouleas and Landman, 2000a), and the corresponding ground-state electron density is plotted in Fig. 26(e). The successive lowering of the ground-state total energies is also displayed.

G. More on spin restoration

The literature of spin restoration in systems other than nuclei has a more complicated history compared to that of 2D angular momentum. Löwdin introduced a spin projection operator through the expression (Löwdin, 1955b)

$$\mathcal{P}_{\text{spin}}(S) \equiv \prod_{s' \neq S} \frac{\hat{\mathbf{S}}^2 - s'(s' + 1)}{S(S + 1) - s'(s' + 1)}, \qquad (216)$$

where the index s' runs over the quantum numbers associated with the eigenvalues $s'(s' + 1)$ of $\hat{\mathbf{S}}^2$ (in units of $\hbar^2$), with $\hat{\mathbf{S}}$ being the total spin operator. Apart from

a proportionality constant, for two electrons, the projection operator reduces to $\mathcal{P}_{\text{spin}}^{s,t} = 1 \mp \varpi_{12}$ (considered earlier), where the operator ϖ_{12} interchanges the spins of the two electrons; the upper (minus) sign corresponds to the singlet (s superscript), and the lower (plus) sign corresponds to the triplet (t superscript) state. For a larger number of electrons, N, a computationally practical implementation of Löwdin's spin projection formalism was recently discussed in (Pons Viver, 2018).

The operator $\mathcal{P}_{\text{spin}}(S)$ has been used (De Giovannini et al., 2007; Yannouleas and Landman, 2002b) to describe the energy spectra and wave functions of electrons in 2D quantum dots. However, for $N \geq 3$, there are multiple spin eigenfunctions for a given value S of the total spin, a fact that cannot be reproduced by the Löwdin operator which yields a single spin function. The spin multiplicities are given by the so-called branch diagram (Brandt et al., 2016; Li et al., 2009; Pauncz, 2000). For example, for $N = 3$ fermions, there are two spin eigenfunctions with $S = 1/2$. For a spin projection $S_z = 1/2$ and using the notation $\mathcal{S}(S, S_z; i)$ (where the index i is employed for the degeneracies), these spin eigenfunctions are

$$\sqrt{6}\mathcal{S}(\tfrac{1}{2}, \tfrac{1}{2}; 1) = 2|\uparrow\downarrow\uparrow\rangle - |\uparrow\uparrow\downarrow\rangle - |\downarrow\uparrow\uparrow\rangle, \qquad (217)$$

$$\sqrt{2}\mathcal{S}(\tfrac{1}{2}, \tfrac{1}{2}; 2) = |\uparrow\uparrow\downarrow\rangle - |\downarrow\uparrow\uparrow\rangle. \qquad (218)$$

For a larger number of fermions, the spin eigenfunctions can be specified by solving a Heisenberg Hamiltonian $H_H = \sum_{i,j} J_{ij}\hat{\mathbf{S}}_i \cdot \hat{\mathbf{S}}_j$ (Brandt et al., 2016; Li et al., 2009). Then using the fact that each fermion is associated with a localized space orbital, the spin primitives

$|\sigma_1\sigma_2\ldots\sigma_N\rangle$ can be transformed into determinants, thus generalizing (Dai *et al.*, 2007; Shi *et al.*, 2007) the two-fermion Heitler-London expression of Eq. (214).

Naturally, total spin restoration[9] can also be performed (Fukutome, 1981; Hashimoto, 1982; Igawa, 1995; Yannouleas and Landman, 2007) by using the projection-operator formulas that restore the 3D total angular momenta (see Sec. III.B.2).

H. Molecular symmetries of the UHF wave functions and magic angular momenta

The projected wave functions [Eq. (212)] have good total 2D angular momentum L, and the corresponding single-particle density is circular and azimuthally uniform. Thus any association of the wave function in Eq. (212) to a point-group symmetry (which corresponds to a single-particle density that is not azimuthally uniform) is counterintuitive. Despite this expectation, the trial wave functions in Eq. (211) do embody and reflect hidden (or emergent) molecular point-group symmetries similar to the case of natural molecules. Specifically, the C_N point-group symmetry of the "classical" crystalline configuration, which is accounted for through the kernel of symmetry-broken mean-field determinants (or permanents) Ψ^N, is reflected in the fact that the trial wave functions Φ_L^{PRJ} are identically zero except for a subset of *magic* angular momenta L_m.

For the simpler case of N repelling particles on a ring [i.e., a configuration $(0, N)$], the magic total angular momenta can be determined by considering the point-group symmetry operator $\hat{R}(2\pi/N) \equiv \exp(-i2\pi\hat{L}/N)$ that rotates on the ring simultaneously the localized particles by an angle $2\pi/N$. In connection to the state Φ_L^{PRJ}, the operator $\hat{R}(2\pi/N)$ can be invoked in two different ways, namely either by applying it on the "intrinsic" part $\check{\Psi}^N$ or the "external" phase factor $\exp(i\gamma L)$ (see Ch. 4-2c in (Bohr and Mottelson, 1998)). One gets in the case of fermions

$$\hat{R}(2\pi/N)\Phi_L^{\mathrm{PRJ}} = (-1)^{N-1}\Phi_L^{\mathrm{PRJ}}, \qquad (219)$$

from the first alternative and

$$\hat{R}(2\pi/N)\Phi_L^{\mathrm{PRJ}} = \exp(-2\pi Li/N)\Phi_L^{\mathrm{PRJ}}, \qquad (220)$$

from the second alternative. The $(-1)^{N-1}$ factor in Eq. (219) results from the fact that the $2\pi/N$ rotation is equivalent to exchanging $N-1$ rows in the Ψ^N determinant. Now if $\Phi_L^{\mathrm{PRJ}} \neq 0$, the only way that Eqs. (219)

and (220) can be simultaneously true is if the condition $\exp(2\pi Li/N) = (-1)^{N-1}$ is fulfilled. This leads to the following sequence of magic angular momenta,

$$L_m = kN; \quad k = 0, \pm 1, \pm 2, \pm 3, \ldots, \qquad (221)$$

for N odd, and

$$L_m = (k + \frac{1}{2})N; \quad k = 0, \pm 1, \pm 2, \pm 3, \ldots, \qquad (222)$$

for N even.

Because a permanent is symmetric under the interchange of two rows, the corresponding magic L_m's for spinless bosons are given by the sequence in Eq. (221) for both odd and even numbers of localized bosons.

Regarding the numerical aspects, the fact that Φ_L^{PRJ} is zero for non-magic L values results in the vanishing (within machine precision) of the normalization factor $\int_0^{2\pi} n(\gamma)e^{i\gamma L}d\gamma$ in Eq. (212).

The physics associated with magic-angular-momentum yrast states have been extensively explored in the literature of 2D quantum dots (Maksym, 1996; Maksym *et al.*, 2000; Ruan *et al.*, 1995; Seki *et al.*, 1996; Yannouleas and Landman, 2003b, 2006a, 2007). An important property is the enhanced energy stabilization (compared to the rest of the spectrum as described by configuration-interaction calculations) that they acquire in their neighborhood in the regime of strong interactions (i.e., for large R_W, R_δ, or large magnetic fields). Thus they are often characterized as "cusp" states in the literature of the lowest Landau level (Jain, 2007; Yannouleas and Landman, 2003b, 2004a). More importantly, they are precursors of the celebrated fractional quantum Hall effect bulk states (Jain, 2007; Yannouleas and Landman, 2003b, 2004a). The development of cusp states is portrayed in Fig. 27.

For magnetic-field-free systems, this energy stabilization leads to a separation of energy scales between the rotational the vibrational motions (formation of a near-rigid rotor), which is a familiar prerequisite in the formulation of nuclear effective field theories (Papenbrock and Weidenmüller, 2015). An example of such a separation of energy scales is portrayed in Fig. 28 for the case of two electrons in a parabolic 2D quantum dot.

In the above derivation, we considered fully polarized fermions only, that is cases when $S = S_z = N/2$, where S is the total spin and S_z is its projection. Consideration with this methodology of the other spin values $S_z < N/2$ is straightforward; it requires, however, restoration of both the total spin $\mathbf{S}^2$ and the total angular momentum. An explicit example for $N = 3$ fermions is discussed in (Yannouleas and Landman, 2003a).

I. Quantum dots

Advances in nanolithography and growth techniques have enabled the fabrication of small semiconductor devices with dimensions in the nanoscale range; they are

---

[9] Restoration of both the total spin $\hat{\mathbf{S}}$ and its projection S_z (in the case that the mean-field wave functions break both of these symmetries) has also been discussed in the context of chemistry (Fukutome, 1981).
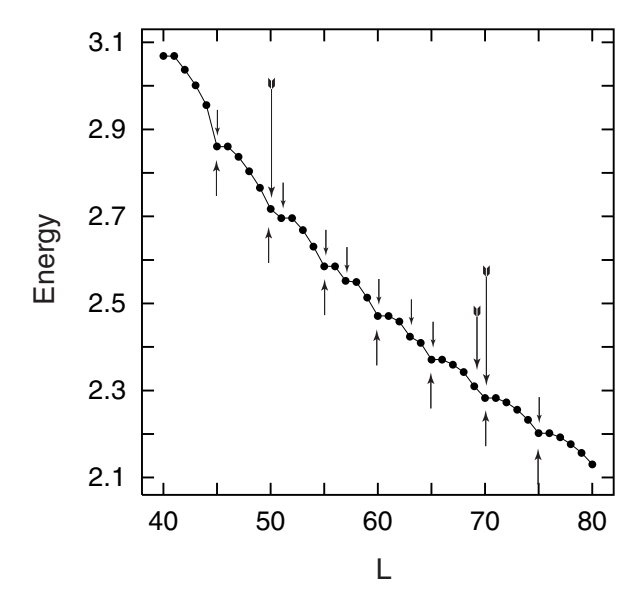
FIG. 27 Total interaction energy from configuration-interaction calculations as a function of the total angular momentum ($40 \leq L \leq 80$) for $N = 6$ electrons in high magnetic field. The upwards pointing arrows indicate the magic angular momenta corresponding to the classically most stable (1,5) polygonal ring arrangement of the Wigner molecule. The short downwards pointing arrows indicate successful predictions of the composite-fermion model. The medium-size downwards pointing arrow indicates a prediction of the CF model that fails to materialize as a magic angular momentum. The long downward arrows indicate magic angular momenta not predicted by the CF model. Energies in units of $e^2/\kappa l_B$, where κ is the dielectric constant. [Reprinted with permission from (Yannouleas and Landman, 2003b)].

FIG. 28 Spectra for a 2e quantum dot with $R_W = 200$. For each excitation band, the quantum numbers (N_0, M_0, n_0, m) are given at the bottom with $m = 0, 1, 2, ...$ (the levels for $m = 0$ and $m = 1$ are not resolved on the scale of the figure and appear as a thick line); only a few of the low lying rotational and vibrational states are shown, with the collective rovibrational behavior extending to higher excitations. Energies are in units of $\hbar\omega_0/2$.[Reprinted with permission from (Yannouleas and Landman, 2000a)].

known in the literature as quantum dots and they play a central role in the modern field of nanotechnology. Here we focus on two-dimensional electrostatically controlled quantum dots (Kouwenhoven *et al.*, 1997). Quantum dots are often referred to as "artificial atoms" (Kastner, 1993; Kouwenhoven and Marcus, 1998) due to their having a discrete single-particle spectrum arising from their finite size. Such a terminology invokes a 2D analogue of the physics of 3D electronic shells (whether closed or open) which is associated with the Mendeleev periodic table of natural elements (Kouwenhoven and Marcus, 1998). However, it was rather early realized (Yannouleas and Landman, 1999, 2000c, 2001, 2002a,b) through UHF calculations that the process of symmetry breaking is highly operative in 2D quantum dots [see also (Müller and Koonin, 1996)], unlike the case of natural atoms where the extent of spherical-symmetry breaking is minimal (Fertig and Kohn, 2000) due to the overwhelming Coulombic attraction from the central nucleus. As a result, the physics of 2D quantum dots overlaps substantially (Yannouleas and Landman, 2007) with the nuclear many-body problem, transposed however in the milli-eV (meV) energy range, instead of the mega-eV (MeV) range
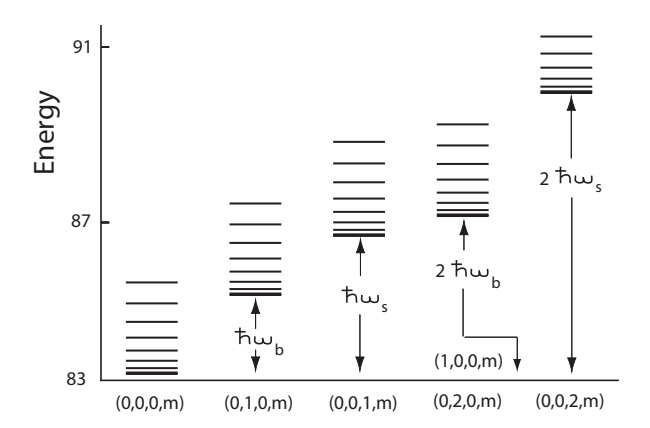
[see, e.g., (Ring and Schuck, 1980)] of natural atomic nuclei.

Naturally, there are several key differences between the physics of 2D quantum dots and that of atomic nuclei, which arise from the fact that the inter-particle interaction in quantum dots is repulsive, instead of attractive as in nuclei, and that quantum dots consist of one kind of fermions (electrons), instead of two kind of particles (protons and neutrons). As a result, symmetry breaking in quantum dots is associated with individual-electron localization in space in the intrinsic frame (leading to formation of mean-field crystalline configurations), rather than the familiar shape deformations of the nuclear central mean-field confining potential. Such mean-field crystalline configurations in quantum dots [see, e.g., Fig. 25] are referred to as "Wigner molecules" (Yannouleas and Landman, 1999). After restoration of the angular momentum symmetries, they are often referred to (Yannouleas and Landman, 2004b) as "rotating Wigner molecules" [10], exhibiting two special cases of "rotating electron molecules" (Yannouleas and Landman, 2003b)

———

[10] Note that the rotating-Wigner-molecule wave functions are stationary, exhibiting a time-independent single-particle density. The use of the term "rotating" here refers to the finite system having good quantum-mechanical total angular momenta, unlike a symmetry-broken crystalline UHF wave function. Consideration of the time-evolution of wave packets formed through the superposition of several rotating Wigner molecules (Yannouleas and Landman, 2017) leads to the concept of a quantum space-time crystal (Li *et al.*, 2012a; Wilczek, 2012; Yannouleas and Landman, 2017) and to phenomena of quantum mechanical revival (Eriksson *et al.*, 2018; Seideman, 1999; Yannouleas and Landman, 2017)

or "rotating boson molecules" (Romanovsky *et al.*, 2006). Localized corpuscular patterns arise also in symmetry-broken mean-field single-particle densities of lighter nuclei (Ebran *et al.*, 2013, 2017; Girod and Schuck, 2013; Ichikawa *et al.*, 2012); they are, however, associated with α-particle multi-nucleon clustering.

Starting with the early 2000's, the two-step methodology that combines symmetry breaking with subsequent symmetry restoration was employed extensively to investigate the physics of quantum dots. In particular, using the Löwdin projection for restoring the total spin, (Yannouleas and Landman, 2001) investigated the coupling and dissociation of two electrons in a double-well confinement (artificial H_2 molecule). It was found that, unlike the mean-field UHF result, restoration of the spin symmetry yields the correct result of a singlet ground state, with the triplet state being always an excited one. It was further shown that the projected wave functions have the structure of a Heitler-London or generalized valence-bond configuration. With increasing interdot barrier or increasing magnetic field, the double quantum-dot behavior resembles the physics of dissociation of a H_2 natural molecule. In addition to the spin restoration, the formation of a 2e rotating Wigner molecule was described in (Yannouleas and Landman, 2002b) by restoring simultaneously the total angular momentum in the case of two electrons confined in a parabolic (circularly symmetric) single-well quantum dot.

For the case of zero or low magnetic fields and using the two-step method, subsequent literature studied a larger number of electrons in parabolic quantum dots (in the range of $3 \leq N \leq 10$). An explicit demonstration that the projected ground-state wave function has a lower energy compared to the UHF one was given in (Mikhailov and Ziegler, 2002) for $N = 2 - 8$ fully spin-polarized electrons. For $N = 3$ electrons, a detailed analysis of the lower point-group symmetries of the UHF broken-symmetry molecular solutions and their influence upon the angular-momentum-restored wave functions has also been carried out (Yannouleas and Landman, 2003a). The richness of the physics embodied in the projected wave functions was illustrated in (Yannouleas and Landman, 2004b), where it was shown that the rotating Wigner molecule can attain two opposite limits depending on the parameters of the system. Namely the limit of a rigid 2D rotor is reached for strong Coulomb repulsion (e.g., $R_W = 200 >> 1$) in the absence of an applied magnetic field; the rotational spectrum (yrast band) in this case exhibits energy levels $\propto L^2$. An opposite limit of a hyper floppy rotor is reached for smaller $R_W \sim 10$, but very high magnetic field (the lowest-Landau-level regime); in this case the rotational energies (yrast band) have a $\mathcal{A}L + \mathcal{B}/\sqrt{L}$ dependence on the total angular momentum L. The limit of a 2D rigid rotor for $R_W \to \infty$ and low magnetic field was also demonstrated for the case of $N = 9$ and $N = 8$ ultracold ions confined in a 2D ring-shaped trap (Yannouleas and Landman, 2017). The limit of the 2D rigid-rotor rotational spectrum extracted in the papers above is reminiscent of the Kamlah expansion[11] in integer powers of L for strong symmetry breaking in rotating nuclei [see Sec. IV and (Ring and Schuck, 1980) Ch. 11.4.4]; in the present cases, however, only the dominant term $\propto L^2$ survives for $R_W \to \infty$.

Using broken-symmetry UHF solutions and following the Löwdin prescription for the total-spin projection [see Eq. (216)] in connection with the construction of spin eigenfunctions presented in (Smith Jr., 1964), the combined restoration of both total-spin and angular-momentum approach was applied in a systematic investigation (De Giovannini *et al.*, 2007, 2008) at zero and low magnetic field B of the properties of 2D parabolic quantum dots with up to $N = 12$ electrons. In particular for $B = 0$, it was confirmed that Hund's rules apply for weaker interaction with $R_W \leq 2$; for stronger interaction ($R_W > 4$), Hund's rules are violated signaling the dominance of a strong Wigner molecule (Yannouleas and Landman, 1999).

For completeness, we mention that collective modes associated with the spurious RPA states have been used to restore the broken rotational symmetry of UHF solutions in parabolic quantum dots. The case of $N = 2$ electrons was systematically studied (Birman *et al.*, 2013; Serra *et al.*, 2003). This RPA-based approach, however, becomes computationally prohibitive for larger N, due to the increasing number of RPA modes that are required.

The lowest Landau level: The symmetry-restoration methodology has also been successfully used to describe aspects of the many-body physics of few electrons in the lowest Landau level. This level forms at very large magnetic fields $B \to \infty$, and it consists exclusively of all single-particle levels $\propto r^l e^{il\phi} e^{-r^2/2\lambda_c^2}$ with zero radial nodes and arbitrary angular momentum l. These levels are degenerate with an energy $\hbar\omega_c/2$, where ω_c is the cyclotron frequency $\omega_c = \sqrt{eB/(m^*c)}$, and the magnetic length $\lambda_c = \sqrt{2\hbar/(m^*\omega_c)}$; see, e.g., the Appendix in (Yannouleas and Landman, 2007). By constructing a Slater determinant out of the displaced Gaussian orbitals in Eq. (204) (with $\lambda = \lambda_c$), and projecting out the good total angular momentum L using Eq. (211), one can derive analytic expressions for the rotating electron molecule (Yannouleas and Landman, 2002c) for any number N of fully spin-polarized electrons (i.e., with ($S = S_z = N/2$) and any L; for large magnetic fields, the

---

[11] The Kamlah expansion needs to be used in conjunction with the C_N Wigner-molecule lower symmetry; otherwise (Müller and Koonin, 1996) the multifaceted effects originating from the magic angular momenta are missed. Moreover in the lowest-Landau-level regime, use (Müller and Koonin, 1996) of the Kamlah expansion cannot reproduce the $1/\sqrt{L}$ energy component characteristic of the hyper-soft rotor (Li *et al.*, 2006; Yannouleas and Landman, 2004b).

electrons in the ground state are fully spin-polarized. Analytic expressions have been derived for both the cases of rotating electron molecules with $(0, N)$ (Yannouleas and Landman, 2002c) and $(1, N-1)$ (Yannouleas and Landman, 2003b) ring configurations. A numerical investigation of lowest-Landau-level rotating electron molecules exhibiting a configuration where the electrons are arranged in a configuration consisting of r concentric regular polygons $(n_1, n_2, \ldots, n_r, N = \sum_i^r n_i)$ was also presented (Yannouleas and Landman, 2004a). Corresponding analytic expressions for rotating bosonic molecules for N spinless bosons in the lowest Landau level in a doubling-ring configuration, (n_1, n_2) with $n_1 + n_2 = N$, were subsequently derived (Yannouleas and Landman, 2010).

Going beyond the rotating-electron or rotating-boson molecular states (which describe pure vibrationless rotations), a class of trial wave functions portraying combined rotations and vibrations of Wigner molecules associated with concentric polygonal rings was further introduced (Yannouleas and Landman, 2011). These trial functions, referred to as rovibrational molecular functions, are valid for both bosons and fermions and provide a correlated basis that spans the translationally invariant part of the lowest-Landau-level spectra for both the yrast and excited lowest-Landau-level states, and for both low and high angular momenta. As a result, the restoration of broken symmetry approach can describe the totality of the lowest-Landau-level states and not only the cusp states which are associated with ground states exhibiting magic angular momenta that are precursors of the fractional quantum Hall effect states.

A major subject in the lowest-Landau-level physics has been the emergence of actual broken-symmetry Wigner-solid crystal states. Such Wigner-solid crystals were expected to appear for smaller fractions $\nu \leq 1/5$. It was thus surprising that a Wigner-crystal regime was experimentally observed (Zhu et al., 2010) in the neighborhood of $\nu = 1/3$ in the case of very clean samples. An interpretation of these observations was achieved using linear superpositions (wave packets) of angular-momentum-restored wave functions (specifically the analytic ones of the rotating electron molecules). These superpositions involve summation over several cusp states with different magic angular momenta; they naturally break the rotational symmetry to exhibit explicitly the crystalline structure, without necessarily reverting back to the UHF level. The triggering agent for the pinning of the rotating Wigner molecule and the enforcing of symmetry breaking is the presence of residual impurities and disorder in the sample.

For non-fully spin polarized electrons, the symmetry restoration in the lowest Landau level must involve both the total spin S and the angular momentum L. Such combined S and L projection leading to spin-dependent rotating electron molecules with $S < N/2$ has been performed for $N = 4 - 5$ localized electrons in the lowest

Landau level (Dai et al., 2007; Shi et al., 2007). The combined spin and space projection has also been demonstrated for N lowest-Landau-level electrons confined in a ring geometry (Yang et al., 2008).

Of interest is the property that the edge states at zero-magnetic field in a circular graphene dot with a zigzag termination form a collection mimicking an lowest-Landau-level manifold; these edge states appear due to the existence of two valleys in the single-particle spectrum of the zero-mass Weyl-Dirac graphene electron. The formation of rotating Wigner molecules in this novel lowest-Landau-level manifold was investigated using both configuration interaction and projection techniques (Romanovsky et al., 2009; Wunsch et al., 2008).

J. Trapped ultracold ions and neutral atomic gases

The restoration of angular momentum has been employed (Romanovsky et al., 2004) to investigate systems with a finite number N of spinless neutral and charged bosons confined in a 2D harmonic trap. The broken-symmetry UHF-type orbitals were approximated as in Eq. (204), treating the positions and the widths of the displaced Gaussians as variational parameters (which corresponds to a variation-after-projection scheme). Wigner molecules were described for both neutral and charged bosons in the regime of strong interparticle repulsion. For the case of neutral bosons the Wigner-molecule regime corresponds to a process of 2D fermionization, when the strong repulsion keeps the particles away from each other overtaking the propensity of bosons to bunch together due to statistics. This fermionization behavior is well known for strongly repelling strictly 1D bosons (Girardeau, 1960); in two dimensions, it has also been recently further verified via exact numerical calculations for two interacting bosons (Mujal et al., 2018).

The system of N spinless bosons in *rotating* harmonic and toroidal traps has also been studied (Romanovsky et al., 2006) using angular-momentum restoration techniques. Fig. 29 illustrates the patterns in the single-particle particle and two-body conditional probabilities as the successive steps sketched in Fig. 24 are applied. The conditional probability is defined [see Sec. 1.5 in (Yannouleas and Landman, 2007)] as the probability for finding a particle at position $\mathbf{r}$ given that another particle is located (fixed) at a point $\mathbf{r}_f$. To be noted is the fact that the ground state has zero angular momentum only for small values of the rotational frequency ω (or equivalently the magnetic field B); for larger values of ω, the ground-state angular momentum increases in steps of N, which is the hallmark of the emergence of magic angular momenta.

An interesting application (Romanovsky et al., 2008) of the methodology of projection techniques is the restoration of the rotational symmetry starting from
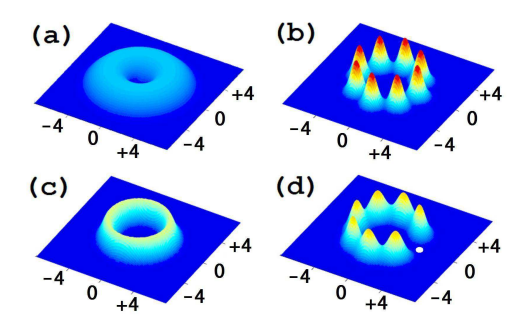
FIG. 29 Single-particle densities and conditional probability distributions for $N = 8$ bosons in a rotating toroidal trap of radius $r_0 = 3l_0$ with rotational frequency $\omega/\omega_0 = 0.2$ and $R_\delta = 50$. The confining potential has the form $V(\mathbf{r}) = \frac{\hbar\omega_0}{2}(r - r_0)^2/l_0^2$. (a) Gross-Pitaevskii single-particle density. (b) UBHF single-particle density exhibiting breaking of the circular symmetry. (c) Rotating-boson-molecule single-particle density exhibiting circular symmetry. (d) Conditional probability distribution for the rotating-boson-molecule wave function [PRJ wave function, see Eq. (211)] revealing the hidden point-group symmetry in the intrinsic frame of reference. The fixed (observation) point is denoted by a white dot. The rotating-boson-molecule ground-state angular momentum is $L_z = 16$. Lengths in units of l_0. The vertical scale is the same for (b), (c), and (d), but different for (a). [Reprinted with permission from (Romanovsky et al., 2006)].

broken-symmetry Gross-Pitaevskii solutions that describe vortices in rotating traps. In this case, the symmetry-restored many-body wave functions can be characterized as rotating vortex clusters. The presence of vortices is not visible in the single-particle densities of the rotating vortex clusters, which are homogeneous; to reveal the hidden vortices, one needs to employ the conditional probability distributions. The Gross-Pitaevskii vortex states are shown to be wave packets composed of such rotating-vortex-cluster states.

Finally, we mention that the restoration of angular-momentum (under the name of "continuous configuration-interaction") was applied (Alon et al., 2004) in the case of an attractive Bose gas on a ring. For strong attraction, the full-configuration-interaction method converges very slowly with the increasing dimension of the employed discrete single-particles basis, and thus the restoration of broken symmetry is advantageous yielding lower total energies compared to the nonconverged configuration-interaction ones.

K. Spin-projected UHF, Hubbard systems, and natural molecules

In addition to the description of novel strongly-correlated many-body phases and phenomena (Yannouleas and Landman, 2006a, 2007) for electrons in quantum dots and trapped ultracold neutral atoms and ions, the two-step method of symmetry breaking and symmetry restoration beyond nuclear physics is also being developed in the direction of a powerful computational approach that can rival in effectiveness the Kohn-Sham density-functional computational technique. This computational direction is mainly associated with the spin-projected UHF (restoration only of spin) in the context of condensed-matter Hubbard systems and natural molecules traditionally belonging to the field of chemistry. The specific approach used to restore the total spin is similar to that used for the 3D total angular momentum projection in nuclear physics (Ring and Schuck, 1980). This has definite practical advantages (Tsuchimochi and Van Voorhis, 2015) for large-scale computations compared to the prescription suggested by Löwdin (Löwdin, 1955b); however, see (Pons Viver, 2018). In this respect, we mention that, unlike the symmetry-restoration techniques, the single-determinantal Kohn-Sham density-functional formalism fails to provide a complete description of magnetic states (Kaplan, 2018), as well as to describe properly the regime of strong static correlation [when there are several competing degenerate states, as in dissociation processes and the formation of Wigner molecules; see, e.g., (Cohen et al., 2008; Yannouleas and Landman, 2006a, 2007)].

The Hubbard model (Hubbard, 1963) is widely used to describe strongly interacting electrons in periodic potentials (associated with natural ionic lattices in condensed-matter systems) and most recently ultracold atoms trapped in artificial optical lattices. The Hubbard model Hamiltonian for N fermions is given by

$$H = -t \sum_{<i,j>,\sigma} (c_{i,\sigma}^\dagger c_{j,\sigma} + c_{j,\sigma}^\dagger c_{i,\sigma}) + U \sum_{i=1}^{N} n_{i\uparrow} n_{i\downarrow}, \quad (223)$$

where $< i, j >$ denotes summation over nearest-neighbor sites and σ sums over the up ($\uparrow$) and down ($\downarrow$) spins, with $n_{i\sigma} = c_{i,\sigma}^\dagger c_{i,\sigma}$. The parameters t and U are the hopping parameter and the on-site repulsion, respectively.

In particular, following an early publication (Igawa, 1995), the method of restoration of spin symmetries has been applied with increasing numerical sophistication in the case of one-dimensional Hubbard chains (Rodríguez-Guzmán et al., 2013; Schmid et al., 2005; Tomita, 2004, 2009). Partially two-dimensional Hubbard geometries (e.g., 2×2 and 2×4 plaquettes) have also been studied (Rodríguez-Guzmán et al., 2012) using the spin-projected HF approach. Interestingly, it was shown that the exact ground-state in a four-site Hubbard plaquette can be recovered by the spin-projected wave function irrespective of the interaction strength (Leprévost et al., 2014). A combination of spin projection with Gutzwiller-type double-occupancy screening has been also applied to 2D Hubbard lattices (Wahlen-Strothman and Scuseria, 2016).

The restoration of the total-spin symmetry has been employed further to describe the ground-state corre-

lations and dissociation profiles of natural molecules (Jiménez-Hoyos *et al.*, 2012; Jiménez-Hoyos *et al.*, 2013; Scuseria *et al.*, 2011) familiar from quantum chemistry. Example of investigated systems are O_2, N_2, H_2O, $[Cu_2O_2]^{2+}$ core, etc. A projected coupled cluster theory is being also developed for both natural molecules and the Hubbard model. It was shown (Qiu *et al.*, 2017) that spin restoration via projection techniques significantly improves unrestricted coupled-cluster-method results while reimposing the required good quantum numbers.

L. Other electronic systems

In the early 1980's, it was discovered that the doubly-excited states of the Helium atom exhibit rovibrational spectra that reflect the formation of a highly nonrigid linear symmetric XYX "molecular" structure (Berry, 1989; Kellman and Herrick, 1980), where the X's stand for the two excited electrons and Y for the He nucleus. In addition to other methods (Berry, 1989), these rovibrational spectra and corresponding underlying collective wave functions were studied using the approach of 3D angular-momentum restoration (Iwai and Nakamura, 1989). Such molecular structures in highly excited atoms indicate that physical processes associated with symmetry breaking cannot be dismissed even in the case of natural atoms; they provide a bridge (Yannouleas and Landman, 2006a, 2007) to the regime of Wigner molecules in two-dimensional quantum dots.

Another notable application of projection techniques beyond nuclear physics is the use of a number-projection method [see Sec. VIII.A and (Rossignoli, 1995)] to calculate the canonical-ensemble, temperature-dependent free energy of metal clusters, in particular in describing temperature attenuation of electronic shell effects in ionization potentials, electron affinities, and fission fragmentation of poly-cationic and poly-anionic clusters (Yannouleas and Landman, 1997, 2000b; Yannouleas *et al.*, 2002).

Particle-number projection techniques have also been used to investigate the properties of superconducting metal grains (Fernández and Egido, 2003; Fernández and Egido, 2005).

Finally worth mentioning is the use of projection-operator techniques to describe the dynamic Jahn-Teller effect in natural molecules in the case of tunneling between equivalently distorted energy-minimum configurations of the adiabatic potential energy surface (Dunn *et al.*, 2012; Hallam *et al.*, 1992). Naturally, due to the very large masses of the ionic cores, the explicit symmetry-broken wave-packet state localized within a single minimum can be observed in cases when tunneling is suppressed (Bersuker, 2016). This is analogous to the observation of pinned classical Wigner crystals of trapped ultracold ions (Thompson, 2015; Yannouleas and Landman, 2017).

M. Other emerging directions

Relation to entanglement and quantum information theory: The emergence of modern quantum information theory is being built around exotic and counterintuitive theoretical concepts, such as entanglement (Aspect, 2004; Wootters, 1998) and quantumness (Modi *et al.*, 2012; Piani *et al.*, 2014), which reflect the complexity of the structure of the quantum wave functions (e.g., nonfactorizability in the case of two or more particles), or of quantum measurement. The symmetry-breaking mean-field solutions are at a disadvantage in this area; in passing, one can point out that they do not conserve the symmetries of the many-body Hamiltonian. In this context, it has been shown (Zeng *et al.*, 2014) that the broken-symmetry BCS wave function represents a class of wave functions where the required quantumness has been lost. It is noticeable that the lost quantumness [in the form of proper description for the concurrence (Wootters, 1998) and quantum discord (Ollivier and Zurek, 2001)] is restored simultaneously with the restoration of the particle number conservation in the projected BCS wave function.

Earlier, the ability of the total-spin, symmetry-restored wave function to describe properly the entanglement [in the form of concurrence and von Neumann entropy (Wootters, 1998)] for two electrons in a double quantum dot under the influence of an increasing magnetic field was also investigated in detail (Yannouleas and Landman, 2006a,b, 2007).

Time evolution in finite systems out of equilibrium: Apart from the small-amplitude harmonic vibrations, broken-symmetry wave functions (single determinants or permanents) fail to describe the proper time-evolution behavior when propagated in time with the corresponding mean-field Hamiltonian (Lichtner and Griffin, 1976; Yannouleas and Landman, 2017); see also Ch. 12.2.4, p. 498 in (Ring and Schuck, 1980). This drawback of the mean-field treatment of finite systems was earlier discussed in the framework of heavy-ion collisions in nuclear physics (Lichtner and Griffin, 1976). It is easily overcome by expressing the broken-symmetry wave function as a wave packet (superposition) of symmetry-restored wave functions and evolving independently in time (by multiplying by a time-dependent phase) each component of the wave packet. Using this approach, other symmetry-broken wave packets (different from the UHF solutions) can be envisaged that exhibit single-particle densities with controlled periodicities in both space and time, as was recently discussed in the framework of implementing a quantum space-time crystal of ultracold atoms or ions in a ring-shaped trap (Yannouleas and Landman, 2017). If the initial wave packet reproduces the UHF or

Gross-Pitaevskii broken-symmetry solution, revival and recurrence in-time behavior is generated (Eriksson *et al.*, 2018).

VIII. PROJECTED STATISTICS

The mechanism of symmetry breaking and restoration is not exclusive of quantum system described by pure states. It can also be used in the description of quantal statistical ensembles where, instead of dealing with pure states, one has to consider an ensemble of quantum states each of them weighted with a prescribed probability. In quantum mechanics, the formal treatment of statistical ensembles is similar to the one of pure quantum systems and it only requires to replace mean values of operators by traces over the whole Fock space "weighted" by a density matrix operator $\hat{D}$ responsible for the probability distribution. The form of this operator depends on the problem at hand but it is typically defined as an exponential where the exponent is the Hamiltonian plus some additional terms. When the problem is restricted to the mean-field level, the density matrix operator is the exponential of the one-body operator mean-field Hamiltonian. In the trace, all possible multi-quasiparticle excitations of the mean-field ground state are considered.

In those mean-field applications in nuclear physics that require the inclusion of pairing correlations, the density matrix operator to be used is the one of the grand canonical ensemble. This is required to accommodate the possibility of exchanging particles with the external "reservoir". When restricted to the mean-field approximation at finite temperature T, $\hat{D}$ is the exponential of the one body HFB hamiltonian H_{HFB} which is a quadratic form of creation and annihilation operators. This is an advantageous form for practical applications as it enormously simplifies the algebra. In this case, the density matrix operator can be viewed as the operator of a canonical transformation acting on the quasiparticle operators. To be more precise, in the HFB case $\hat{D}_{\mathrm{HFB}}$ is given by

$$\hat{D}_{\mathrm{HFB}} = \exp\left[\beta(\hat{H}_{\mathrm{HFB}} - \lambda\hat{N})\right] \qquad (224)$$

with $\beta = 1/(k_B T)$. The density matrix operator can be written in terms of single particle creation and annihilation operators using a shorthand notation,

$$\hat{D}_{\mathrm{HFB}} = \exp\left[\beta(c^\dagger\ c)(\mathcal{H} - \lambda\mathcal{N})\begin{pmatrix} c \\ c^\dagger \end{pmatrix}\right]. \qquad (225)$$

Here $\mathcal{H}$ is the traditional HFB matrix for the approximate one-body Hamiltonian in the single-particle basis representation and $\mathcal{N}$ is the corresponding quantity for the particle number operator. In the following we will denote $\mathcal{H}' = \mathcal{H} - \lambda\mathcal{N}$ The special form of $\hat{D}_{\mathrm{HFB}}$ implies the property

$$\begin{pmatrix} c \\ c^\dagger \end{pmatrix} \hat{D}_{\mathrm{HFB}} = \hat{D}_{\mathrm{HFB}} \exp[\beta\mathcal{H}'] \begin{pmatrix} c \\ c^\dagger \end{pmatrix} \qquad (226)$$

This identity allows one to compute any statistical trace by "jumping" with the statistical operator $\hat{D}_{\mathrm{HFB}}$ over the creation and annihilation operators to reach the appropriate place to use the cyclic invariance property of any trace

$$\mathrm{Tr}[AB\cdots YZ] = \mathrm{Tr}[ZAB\cdots Y] \qquad (227)$$

All these manipulations can be summarized in a theorem, dubbed Gaudin's theorem (Gaudin, 1960), which is the equivalent of Wick's theorem but for statistical ensembles. Like Wick's theorem, it allows us to write the trace of any operator times the HFB statistical density matrix as a contraction of the operator's matrix elements with the density and pairing tensors for the statistical ensemble. The demonstration of the theorem is rather straightforward (see (Gaudin, 1960) in a HF framework) and therefore we will sketch it here, for the convenience of the reader, in the most general HFB case. To alleviate the notation we start by defining the set of operators $a_\mu = (c_1, \ldots, c_N, c_1^\dagger, \ldots, c_N^\dagger)$ to write Eq. (226) in compact form

$$a_\mu \hat{D}_{\mathrm{HFB}} = \hat{D}_{\mathrm{HFB}} \sum_\nu \left(\exp[\beta\mathcal{H}']\right)_{\mu\nu} a_\nu. \qquad (228)$$

Assume now one wants to evaluate the statistical trace of the product of an even number p of creation and annihilation single-particle operators

$$\mathrm{Tr}[a_{\mu_1} a_{\mu_2} \cdots a_{\mu_p} \hat{D}_{\mathrm{HFB}}]. \qquad (229)$$

By anticommuting the a_{μ_1} to the right one obtains

$$\mathrm{Tr}[a_{\mu_1} a_{\mu_2} \cdots a_{\mu_p} \hat{D}_{\mathrm{HFB}}] = \qquad (230)$$
$$\{a_{\mu_1}, a_{\mu_2}\}\mathrm{Tr}[a_{\mu_3} \cdots a_{\mu_p} \hat{D}_{\mathrm{HFB}}]$$
$$-\{a_{\mu_1}, a_{\mu_3}\}\mathrm{Tr}[a_{\mu_2} \cdots a_{\mu_p} \hat{D}_{\mathrm{HFB}}]$$
$$+\cdots - \mathrm{Tr}[a_{\mu_2} \cdots a_{\mu_p} a_{\mu_1} \hat{D}_{\mathrm{HFB}}].$$

Using Eq. (228) to jump a_{μ_1} to the right of $\hat{D}_{\mathrm{HFB}}$ and using the cyclic invariance of the trace to bring a_{μ_1} back to the leftmost position, the last term can be written

$$\sum_{\nu_1} \left(\exp[\beta\mathcal{H}']\right)_{\mu_1,\nu_1} \mathrm{Tr}[a_{\nu_1} a_{\mu_2} \cdots a_{\mu_p} \hat{D}_{\mathrm{HFB}}] \qquad (231)$$

Now, moving it to the right hand side of Eq. (230) one gets

$$\sum_{\nu_1}(\mathbb{I} + \exp[\beta\mathcal{H}'])_{\mu_1,\nu_1} \mathrm{Tr}[a_{\nu_1} a_{\mu_2} \cdots a_{\mu_p} \hat{D}] = \qquad (232)$$
$$\{a_{\mu_1}, a_{\mu_2}\}\mathrm{Tr}[a_{\mu_3} \cdots a_{\mu_p} \hat{D}]$$
$$-\{a_{\mu_1}, a_{\mu_3}\}\mathrm{Tr}[a_{\mu_2} \cdots a_{\mu_p} \hat{D}]$$
$$+\cdots$$

This result tell us that we can evaluate the trace in Eq. (229) following the same rules of Wick's theorem but using the contraction

$$\text{Tr}[a_{\mu_1} a_{\mu_2} \hat{D}_{\text{HFB}}] = \sum_{\nu_2} \{a_{\nu_1}, a_{\mu_2}\} \left(\frac{\mathbb{I}}{\mathbb{I} + \exp[\beta \mathcal{H}']} \right)_{\nu_1 \mu_1} \tag{233}$$

instead of the traditional one. The simplicity of its formulation has made possible to establish in a simple way results that could, otherwise, be difficult to proof. This is the case, for instance, with a result concerning the generalized Wick's theorem, see Appendix A, for multi-quasiparticle overlaps which can be derived as the zero temperature limit of the corresponding Gaudin's result (Perez-Martin and Robledo, 2007).

A. Symmetry restoration at finite temperature

In the context of finite temperature or statistical ensembles, symmetry restoration means that the density matrix operator has to be able to select from all the states considered in the statistical trace only those with a given set of quantum numbers. The easiest way achieve this property is by sandwiching the statistical operator with the projector onto the required quantum numbers one wants to select. For instance, for particle number restoration we have to replace the density matrix operator $\hat{D}$ by

$$\hat{D}_N = \hat{P}^{N\dagger} \hat{D} \hat{P}^N. \tag{234}$$

For non-abelian symmetry groups, like the one of angular momentum projection the expression of the density matrix operator gets a bit more involved and the reader is referred to (Rossignoli and Ring, 1994) for the technical details. In general, the expression for $\hat{D}_N$ is rather involved, but it simplifies enormously if $\hat{D}$ is restricted to be the exponential of an one-body operator, as it is the case in the mean-field approximation to the exact $\hat{D}$. In the following and just to illustrate the method, we will restrict the discussion to the abelian case of particle number projection. The projector P^N is a linear combination of exponentials of one body operators. Therefore, $\hat{P}^{N\dagger} \hat{D}_{\text{HFB}} \hat{P}^N$ becomes a (very involved) linear combination of products of exponentials of one body operators. As in Eq. (225) those products are generators of canonical transformations

$$\hat{T}_1^{\dagger} \hat{T}_2^{\dagger} \begin{pmatrix} c \\ c^{\dagger} \end{pmatrix} \hat{T}_2 \hat{T}_1 = \exp(\mathcal{T}_1) \exp(\mathcal{T}_2) \begin{pmatrix} c \\ c^{\dagger} \end{pmatrix} \tag{235}$$

where $\mathcal{T}_i$ are matrices representing the one body operators in the exponents of $\hat{T}_i$. As a consequence of this property, Gaudin's theorem can still be used just replacing the $\exp[\beta \mathcal{H}']$ in Eq. 233 by the appropriate product of exponentials (see (Rossignoli and Ring, 1994) for details). The only difficulty in carrying out this program

is in the evaluation of the entropy, required to evaluate the free energy $F = H - TS$. The standard definition of the entropy involves the logarithm of the density matrix operator. In the standard mean-field approximation, this logarithm can be evaluated analytically and the final expression for the entropy in terms of quasi-particle energies is straightforward. Unfortunately, the projected density matrix can not be expressed in general as the exponential of an one-body operator and therefore the evaluation of the entropy becomes a very complicated task (Esebbag and Egido, 1993). In spite of these difficulties the use of projected statistics has proved to be advantageous over other techniques when applied in the spirit of projection after variation, that does not require the evaluation of the entropy (Fanto et al., 2017). The intrinsic difficulty associated with the sign ambiguity in the evaluation of the partition function has been addressed in (Fanto et al., 2017) in a time reversal preserving scenario and further generalized using the Pfaffian method (Robledo, 2009) to the more general case involving time reversal breaking intrinsic states (Fanto, 2017).

In quantum statistical mechanics it is possible to incorporate statistical fluctuations beyond the mean field by using path integral techniques. In the specific case when the interaction can be expressed as a combination of separable potentials, the Hubbard-Stratonovich trick (Hubbard, 1959) allows us to express the exact density matrix operator $\exp[\beta \hat{H}]$, which involves the two body Hamiltonian, as a path integral of exponentials of one body operators depending on an auxiliary field. The approximate evaluation of the path integral considering only the classical path, which is the one minimizing the classical action, leads to the mean-field result for the separable Hamiltonian. By going one step further and considering Gaussian fluctuations, the procedure leads to the static path approximation that also involves exponentials of one body operators. In this case, Gaudin's theorem can be used again which allows for an analytical evaluation of traces. This approach has proven to be very powerful in the evaluation of many quantities, like level densities but so far, the applications have been restricted to very simple Hamiltonians (Rossignoli et al., 1993) and there is no implementation using nuclear EDFs. In this framework, we can also mention the shell model Monte Carlo method (Koonin et al., 1997a,b; Lang et al., 1993) used to evaluate the partition function of nuclei with relatively large configuration spaces. The shell model Monte Carlo requires the use of particle number projection to carry out calculations in the more convenient canonical ensemble (Alhassid et al., 1999) and therefore this constitutes another field of application of the techniques discussed here. Recently, the use of particle number projection to carry out calculations in the canonical ensemble has also been explored in (Magnus et al., 2017).

B. Thermo-field dynamics

To finish this section, let us briefly mention an alternative to the traditional approach described above and known under the name of thermo-field dynamics. It consists in computing the traces of statistical operators by using mean values of pure states defined in an extended Fock space including twice the original degrees of freedom. This approach was introduced in the context of quantum field theory by Takahashi and Umezawa (Takahashi and Umezawa, 1996). In this approach, the statistical average of an operator $\hat{F}$ with probabilities p_n, given by

$$\langle \hat{F} \rangle_{\text{stat}} = \sum_n \langle n|\hat{F}|n \rangle p_n, \qquad (236)$$

is replaced by the mean value of $\hat{F}$ with the wave function

$$|\Phi\rangle = \sum_n \sqrt{p_n}|n\tilde{n}\rangle = \sqrt{p_1}|1\tilde{1}\rangle + \sqrt{p_2}|2\tilde{2}\rangle + \cdots \quad (237)$$

which is a linear combination of wave functions $|n\tilde{n}\rangle = |n\rangle \otimes |\tilde{n}\rangle$ defined in an extended Fock space which is the tensor product of the original Fock space with itself. The ket $|\tilde{n}\rangle$ represents a new set of states with identical characteristics as $|n\rangle$. In the extended Fock space all the operators are defined as $\hat{F} \otimes \mathbb{I}$ where $\mathbb{I}$ is the identity in the space spanned by $|\tilde{n}\rangle$. A new set of creation and annihilation single-particle operators $\tilde{c}_k^\dagger$ and $\tilde{c}_k$ satisfying fermion canonical commutation relations and anti-commuting with all the elements of the original $c_k^\dagger$ and c_k set is required too. An advantage of the formalism is that $|\Phi\rangle$ can be written as a HFB state, vacuum of a set of quasiparticles defined in terms of the $\tilde{c}_k^\dagger$, $\tilde{c}_k$, $c_k^\dagger$ and c_k by means of an appropriate BCS like transformation. Therefore, we can use verbatim all the zero temperature formalism developed before (including the generalized Wick's theorem) to restore symmetries but taking into account properly the doubling of the single-particle Fock space. It is not clear, however, if this method represents any advantage over the traditional one due to the doubling of matrix sizes. The procedure is analogous to the construction of statistical ensembles by taking the trace over a subsystem of the whole Hilbert space of a pure state density matrix operator. Applications to nuclear physics in the context of symmetry restoration are given in (Tanabe and Nakada, 2005) but only formal expressions are developed in the mentioned reference.

IX. SUMMARY, CONCLUSIONS, AND PERSPECTIVES

In recent years, research in mesoscopic many-body systems has witnessed a discernable progress with the development of the state-of-the-art models and methods. In particular, *ab initio* methods and mean-field theory based on effective interaction are now widely used to elucidate rich and fascinating properties of these quantum many-body systems. On the one hand, applications of the *ab initio* methods are still restricted to lighter systems only, whereas the mean-field approaches can be applied to investigate mesoscopic systems of any size. In particular, in nuclear physics, the density functional theory has been employed to investigate ground-state properties of all nuclear species predicted to exist in the Segré chart.

Spontaneous symmetry breaking mechanism, inherent to the mean-field based approaches, has played an important role in our understanding of many-body systems. For instance, in rotating nuclei, the breaking of rotational symmetry has led to the fundamental concept of deformation in nuclei. Nevertheless, the quantal fluctuations of the observables, absent in mean-field approaches, become quite important for mesoscopic systems.

To build quantal fluctuations on top of the mean-field solutions, several approaches have been developed. A powerful method to include these fluctuations is through the restoration of the broken symmetries. In the prelude section of this review, the spontaneous symmetry breaking mechanism was illustrated through three simple examples. The main purpose of the present review was to provide an overview of the recent developments and, more importantly, to bring to focus the bottlenecks in the application of symmetry-restoration methods.

The general formalism of symmetry restoration, whose origin can be traced in group theory and generator coordinate method, was laid out in Section III. There we distinguished between the symmetry restoration for abelian groups (particle number, linear momentum, parity), which have mathematical properties of projection operators, versus the symmetry restoration for non-abelian groups, as is the case of the rotational symmetry, relevant for the spatial coordinates, spin, or isotopic spin. In the later case, the symmetry-restoration operators do not obey properties of a projection operator, but they nevertheless project out the relevant symmetry quantum numbers. Further, we discussed the fact that the symmetry restoration can be performed either before minimization or after minimization of the energy functional. In the former approach, commonly referred to as variation after projection, symmetry breaking states (often called "intrinsic states") are determined by application of the variational principle on the projected energy (i.e., energy computed with the projected wave functions). In this procedure, different intrinsic states are obtained for different quantum numbers of the restored symmetry. In the latter approach, referred to as projection after variation, the intrinsic state is determined without consideration of the subsequent projection.

In general, implementation of the symmetry restoration is numerically quite challenging, especially in realistic applications where several quantum numbers need to be restored simultaneously, and calculations need to

be performed in the spirit of variation-after-projection method. Due to these numerical challenges, development of approximate projection methods have been actively pursued by exploiting the sharp character of the overlap kernel when the intrinsic state strongly breaks the underlying symmetry. This resulted in the development of popular methods of Lipkin-Nogami and Kamlah, and were discussed in Sec. IV. We showed that these methods lead to successful approximations, like the mean-field cranking model – a useful concept to understand the physics of rotational bands. Symmetry-restoration methods were also successfully applied to simple nuclear models, where the Hamiltonian is separable or the configuration spaces are limited to a few oscillator shells. These applications have been discussed in Sec. V.

Although the mechanism of symmetry restoration can be consistently formulated for systems described in terms of a Hamiltonian operator, this is not the case for the energy density functionals, which are commonly employed in nuclear physics to provide a description of low energy observables all over the nuclear Segré chart. The complexity of nuclear interaction, and in-medium effects that characterize many-body systems, required the introduction of phenomenological density-dependent interaction terms, for which symmetry-restoration methods cannot be uniquely defined. This is further aggravated when separate interactions are being considered in particle-particle and particle-hole channels. Recently, there have been several attempts to overcome these difficulties, but a satisfactory solution, covering both sources of problems, is still not available. A possible solution, which is being vigorously pursued, is to base the functionals on the Hamiltonian picture with explicit three-body terms. However, this approach is not yet sufficiently developed to give definite answers at this stage. Nevertheless, many symmetry restored calculations performed with present-day energy density functionals seem to provide reasonable and a consistent picture of low-energy nuclear phenomena, as was elucidated in Sec. VI. The results, however, should be taken with a pinch of salt as they might be contaminated with spurious effects.

Mesoscopic condensed matter systems and the physics of atoms and molecules, as well as assemblies of trapped ultracold ions and neutral atoms, are mostly free from the above mentioned difficulties as the interaction is often just the Coulomb or a contact interaction between the constituents of the system. Applications of symmetry restoration to those areas share many technical details with the ones in nuclear physics, but there are also clear differences like the fact that rotational symmetry restoration can be carried out separately for the spatial coordinates and the spin in condensed matter physics. Many applications have been presented where symmetry breaking and restoration represent an easy way to understand the complexity of the problem. Finally, we have demonstrated that the concept of symmetry restoration can be extended to the realm of quantum statistical mechanics where pure states are replaced by a set of quantum states with a prescribed probability distribution.

Based on the results presented in this work, it can be concluded that the method of symmetry restoration applied to mean-field wave functions provides a simple and fruitful mechanism to incorporate important dynamic correlations, while still using a simple framework of product wave functions. Furthermore, in this approach one stays within a fully quantum mechanical description from the beginning to end, and the classical picture of collective motion does not have to be invoked.

The generator coordinate method can be employed along with the symmetry restoration to provide a powerful framework to describe quantal fluctuations of relevant degrees of freedom around the mean-field values. In future, we expect development of more advanced configuration interaction approaches with symmetry projected states as the basic building blocks. For instance, projected multi-quasiparticle basis configurations can be constructed around the optimal mean-field, in the spirit of traditional shell model approach, to describe the physics of excited configurations and also to incorporate many-body correlations in the ground-state. The difference between configuration interaction and the traditional nuclear shell model is the use of symmetry-breaking basis states in the former case. The configuration interaction approach shall be a viable tool to have access to excited states in heavier systems as the particle or quasiparticle excitations required shall be quite low as compared to the spherical shell model approach, which employs spherical rather than the optimal mean-field.

X. ACKNOWLEDGMENTS

Appendix A: Overlaps and matrix elements between HFB states: the generalized Wick's theorem

The restoration of the symmetries broken by intrinsic HFB states requires to consider matrix elements of various operators between different HFB states. This is a rather general statement because the action of any operator belonging to the symmetry group on a given HFB state is again another HFB state. The origin of this property lies on the fact that the algebra of one-body operators can be used to provide a representation of any matrix Lie algebra (Gilmore, 2008). Therefore, the symmetry operations (which are members of the group spanned by the corresponding Lie algebra) are the exponential of one body operators and Thouless theorem (Mang, 1975a; Thouless and Valatin, 1962) applies.

The evaluation of the required matrix elements is best carried out with the help of the generalized Wick's theorem. The theorem, that can be derived in many different ways (Balian and Brezin, 1969; Bertsch and Robledo, 2012; Hara and Sun, 1995; Löwdin, 1955a; Onishi and Yoshida, 1966), states that the matrix elements of an arbitrary operator $\hat{O}$ between arbitrary, non orthogonal, HFB states $|\Phi_0\rangle$ and $|\Phi_1\rangle$

$$\frac{\langle\Phi_0|\hat{O}|\Phi_1\rangle}{\langle\Phi_0|\Phi_1\rangle} \tag{A1}$$

can always be written in terms of the sum of all possible two-quasiparticle contractions

$$\frac{\langle\Phi_0|\beta_\mu\beta_\nu|\Phi_1\rangle}{\langle\Phi_0|\Phi_1\rangle} = C_{\mu\nu} \tag{A2}$$

$$\frac{\langle\Phi_0|\beta_\mu\beta_\nu^\dagger|\Phi_1\rangle}{\langle\Phi_0|\Phi_1\rangle} = \delta_{\mu\nu} \tag{A3}$$

$$\frac{\langle\Phi_0|\beta_\mu^\dagger\beta_\nu^\dagger|\Phi_1\rangle}{\langle\Phi_0|\Phi_1\rangle} = 0 \tag{A4}$$

where the β_μ and $\beta_\mu^\dagger$ are annihilation and creation operators associated with $|\Phi_0\rangle$. The only non-trivial contraction is given in terms of the skew-symmetry matrix $C_{\mu\nu}$ which is the product of the inverse of $A = U_0^\dagger U_1 + V_0^\dagger V_1$ times $B = U_0^\dagger V_1 + V_0^\dagger U_1$, i.e.

$$C_{\mu\nu} = A^{-1}B. \tag{A5}$$

The U_0, V_0 and U_1, V_1 are the Bogoliubov transformation amplitudes of the corresponding HFB states. Using the generalized Wick's theorem we can write, for instance, one of the non-trivial matrix element entering the evaluation of the Hamiltonian matrix element as

$$\frac{\langle\Phi_0|\beta_\mu\beta_\nu\beta_\sigma\beta_\rho|\Phi_1\rangle}{\langle\Phi_0|\Phi_1\rangle} = C_{\mu\nu}C_{\sigma\rho} - C_{\mu\sigma}C_{\nu\rho} + C_{\mu\rho}C_{\nu\sigma} \tag{A6}$$

In the general case, where the matrix element of a product of n creation and annihilation quasiparticle operators

is required, the number of terms in the sum grows very quickly and is given by $(n-1)!!$. This is the so called combinatorial explosion problem (see (Hu *et al.*, 2014) for an example) that hampers applications where multi-quasiparticle excitations have to be considered. This difficulty can be avoided using the formulation of (Bertsch and Robledo, 2012) in terms of Pfaffians (see below).

The generalized Wick's theorem does not provide an expression for the overlap between the two HFB wave functions appearing in the denominator, but its determination is not difficult. Again, there are many derivations (Balian and Brezin, 1969; Hara and Sun, 1995; Onishi and Yoshida, 1966; Robledo, 2009) and even several different expressions for the overlap. The traditional formula (Onishi and Yoshida, 1966)

$$\langle\Phi_0|\Phi_1\rangle = \pm\sqrt{\det A} \tag{A7}$$

suffers from a sign indeterminacy that requires further consideration. The relevance of the sign of the overlap comes from the fact that it affects the sign of the integrand of the integrals characteristic of the symmetry restoration or configuration mixing methods. A wrong assignment of the sign even in a small integration interval can substantially change the value of the integral. The sign problem has been addressed in the past using different strategies like continuity arguments or determining pairwise degenerate eigenvalues of a general matrix (Neergård and Wüst, 1983). However, the use of techniques of fermion coherent states allows to avoid the sign problem by expressing the overlap in terms of the Pfaffian of a skew-symmetric matrix (Robledo, 2009). In the Pfaffian formulation the overlap is given by

$$\langle\Phi_0|\Phi_1\rangle = s_N \mathrm{pf}(\mathbb{M}) = s_N \mathrm{pf}\begin{pmatrix} M^{(1)} & -\mathbb{1} \\ \mathbb{1} & -M^{(0)*} \end{pmatrix} \tag{A8}$$

where the phase s_N depends on the dimensionality of the problem $s_N = (-1)^{N(N+1)/2}$. The skew-symmetric matrices $M^{(i)}$ are given in terms of the Bogoliubov amplitudes

$$M^{(i)} = (V_i U_i^{-1})^* \tag{A9}$$

It is important to note that the HFB wave functions in the overlap are not normalized but they satisfy $\langle 0|\Phi_i\rangle = 1$ instead. The Pfaffian of a skew-symmetric matrix is a quantity similar to the determinant and shares with it many properties. In fact it can be proven that it is somehow connected with the square of a determinant, justifying thereby the expression of Eq. (A7). The numerical evaluation of the Pfaffian can be carried out using the traditional algorithms of linear algebra with a cost similar to the one of the determinant (González-Ballestero *et al.*, 2011).

The quantities entering the contractions of the generalized Wick's theorem depend upon the inverse of the

U HFB amplitudes, which are not well defined quantities if the occupancies of the canonical basis orbitals are strictly one. In this case, some regularization procedure is required to render all the quantities well defined and useful formulas to deal with this problem can be found in (Bonche *et al.*, 1990; Robledo and Bertsch, 2011a; Tagami and Shimizu, 2012; Valor *et al.*, 2000). In those references the related problem of getting rid of the unoccupied (and therefore irrelevant) states is also addressed. In this case, the size of matrices can be drastically reduced with the subsequent impact on the computational cost. The extension of the theorem to consider HFB states expanded in different bases not spanning the same subspace of the total Hilbert space has been addressed in (Robledo, 1994; Valor *et al.*, 2000) and the consequences discussed in Sec. VI.A.1. The previous formulas could be used to evaluate overlaps between HF states, that can be considered as HFB states where the occupancies are strictly 0 or 1. Although the solutions already mentioned to treat this case are still valid, it is better to use the traditional formulas obtained specifically for Slater determinants (Löwdin, 1955b). The overlap between two Slater determinants $|A\rangle$ and $|B\rangle$ with N occupied distinct orbitals $|\varphi_i^A\rangle$ and $|\varphi_i^B\rangle$ is given by the determinant of the overlap matrix $(S_{AB})_{ij} = \langle\varphi_i^A|\varphi_j^B\rangle$

$$\langle A|B\rangle = \det S_{AB} \qquad (A10)$$

Wick's theorem also applies but with the contraction

$$\langle A|a_p^\dagger b_q|B\rangle = (S_{AB}^{-1})_{pq} \det S_{AB} \qquad (A11)$$

There is an additional caveat with the traditional form of the generalized Wick's theorem related to the case where the overlap of the two HFB wave functions is zero and therefore the contractions of the generalized Wick's theorem as given in Eq A2 are ill defined (in fact, divergent). This could be considered as a rare situation but it is indeed common in particle number projection or in other context involving cranking wave functions (Anguiano *et al.*, 2001; Oi and Tajima, 2005). The consequences of this failure of the generalized Wick's theorem have been discussed in many places (Anguiano *et al.*, 2001; Lacroix *et al.*, 2009) in the context of EDFs and is still an unresolved aspect of the theory that has to be further clarified. If the overlap $\langle\Phi_0|\hat{O}|\Phi_1\rangle$ is still required, a way to compute it is going to a sort of canonical basis (Lacroix *et al.*, 2009) or use the Pfaffian technique as discussed in (Bertsch and Robledo, 2012).

In applications involving statistical ensembles where traces with a density matrix operator are used instead of mean values it is possible to extend the ideas of the generalized Wick's theorem to those cases where the operator is multiplied by the exponential of a one body operator (a symmetry transformation or a Bogoliubov transformation). The corresponding expression is similar to the one of the generalized Wick's theorem in that it is given as

linear combination of contractions but the contractions are given by a different expression (see Sect VIII for a discussion).

REFERENCES

Alhassid, Y, S. Liu, and H. Nakada (1999), "Particle-number reprojection in the shell model monte carlo method: Application to nuclear level densities," Phys. Rev. Lett. **83**, 4265–4268.

Alon, O E, A. I. Streltsov, K. Sakmann, and L. S. Cederbaum (2004), "Continuous configuration-interaction for condensates in a ring," EPL **67**, 8.

Anguiano, M, J.L. Egido, and L.M. Robledo (2001), "Particle number projection with effective forces," Nuclear Physics A **696** (3), 467 – 493.

Anguiano, M, J.L Egido, and L.M Robledo (2002), "Mean-field based approaches to pairing correlations in atomic nuclei," Physics Letters B **545** (1), 62 – 72.

Aspect, A (2004), "John Bell and the second quantum revolution," foreword of *Speakable and unspeakable in quantum mechanics: J.S. Bell papers on quantum mechanics* (Cambridge University Press, New York).

Baksmaty, L O, C. Yannouleas, and U. Landman (2007), "Rapidly rotating boson molecules with long- or short-range repulsion: An exact diagonalization study," Phys. Rev. A **75**, 023620.

Balian, R, and E. Brezin (1969), "Nonunitary Bogoliubov transformations and extension of Wick theorem," Il Nuovo Cimento B (1965-1970) **64**, 37–55.

Bally, B, B. Avez, M. Bender, and P.-H. Heenen (2014), "Beyond mean-field calculations for odd-mass nuclei," Phys. Rev. Lett. **113**, 162501.

Bally, B, and T. Duguet (2018), "Norm overlap between many-body states: Uncorrelated overlap between arbitrary Bogoliubov product states," Phys. Rev. C **97**, 024304.

Baranger, M, and K. Kumar (1968), "Nuclear deformations in the pairing-plus-quadrupole model: (ii). discussion of validity of the model," Nucl. Phys. A **110**, 490.

Baranger, M, and M Vénéroni (1978), "An adiabatic time-dependent Hartree-Fock theory of collective motion in finite systems," Annals of Physics **114** (1), 123 – 200.

Bartlett, Rodney J (2010), "*Ab initio* DFT and its role in electronic structure theory," Mol. Phys. **108**, 3299–3311.

Baye, D, and P.-H. Heenen (1984), "Angular momentum projection on a mesh of cranked Hartree-Fock wave functions," Phys. Rev. C **29**, 1056–1068.

Beck, R, H. J. Mang, and P. Ring (1970), "Symmetry-conserving Hartree-Fock-Bogolyubov-theory and its application to collective nuclear rotation," Zeitschrift für Physik A Hadrons and nuclei **231** (1), 26–47.

Becke, Axel D (2014), "Perspective: Fifty years of density-functional theory in chemical physics," J. Chem. Phys. **140**, 18A301.

Beiner, M, H. Flocard, Nguyen Van Giai, and P. Quentin (1975), "Nuclear ground-state properties and self-consistent calculations with the Skyrme interaction: (I). Spherical description," Nuclear Physics A **238** (1), 29 – 69.

Bender, M, G. F. Bertsch, and P.-H. Heenen (2005), "Systematics of quadrupolar correlation energies," Phys. Rev. Lett. **94** (10), 102503.

Bender, M, G. F. Bertsch, and P.-H. Heenen (2006a), "Global

study of quadrupole correlation effects," Phys. Rev. C **73**, 034322.

Bender, M, G. F. Bertsch, and P.-H. Heenen (2008), "Collectivity-induced quenching of signatures for shell closures," Phys. Rev. C **78**, 054312.

Bender, M, P. Bonche, T. Duguet, and P.-H. Heenen (2004a), "Configuration mixing of angular momentum projected self-consistent mean-field states for neutron deficient pb isotopes," Phys. Rev. C **69**, 064303.

Bender, M, P. Bonche, and P.-H. Heenen (2006b), "Shape coexistence in neutron-deficient Kr isotopes: Constraints on the single-particle spectrum of self-consistent mean-field models from collective excitations," Phys. Rev. C **74**, 024312.

Bender, M, T. Duguet, and D. Lacroix (2009), "Particle-number restoration within the energy density functional formalism," Phys. Rev. C **79**, 044319.

Bender, M, P.-H. Heenen, and P. Bonche (2004b), "Microscopic study of ^{240}Pu: Mean field and beyond," Phys. Rev. C **70**, 054304.

Bender, M, P.-H. Heenen, and P.-G. Reinhard (2003), "Self-consistent mean-field models for nuclear structure," Rev. Mod. Phys. **75**, 121–180.

Bender, M, K. Rutz, P.-G. Reinhard, and J.A. Maruhn (2000), "Consequences of the center-of-mass correction in nuclear mean-field models," Eur. Phys. J. A **7** (4), 467–478.

Bender, Michael, and Paul-Henri Heenen (2008), "Configuration mixing of angular-momentum and particle-number projected triaxial Hartree-Fock-Bogoliubov states using the Skyrme energy density functional," Phys. Rev. C **78**, 024309.

Bennaceur, K, J. Dobaczewski, and F. Raimondi (2014), "New density-independent interactions for nuclear structure calculations," EPJ Web of Conferences **66**, 02031.

Bennaceur, K, A. Idini, J. Dobaczewski, P. Dobaczewski, M. Kortelainen, and F. Raimondi (2017), "Nonlocal energy density functionals for pairing and beyond-mean-field calculations," Journal of Physics G: Nuclear and Particle Physics **44** (4), 045106.

Bernard, Rémi N, Luis M. Robledo, and Tomás R. Rodríguez (2016), "Octupole correlations in the ^{144}Ba nucleus described with symmetry-conserving configuration-mixing calculations," Phys. Rev. C **93**, 061302.

Bernard, RN, Robledo L.M, and Rodríguez T.R. (2017), "Octupole correlations in a symmetry conserving framework," Acta Phys. Pol. B **48**, 249.

Berry, R S (1989), "How good is Niels Bohr's atomic model?" Contemporary Physics **30**, 1.

Bersuker, I B (2016), "Spontaneous symmetry breaking in matter induced by degeneracies and pseudodegeneracies," in *Adv. Chem. Phys.*, Chap. 3 (Wiley-Blackwell) p. 159.

Bertsch, G F, and L. M. Robledo (2012), "Symmetry restoration in Hartree-Fock-Bogoliubov based theories," Phys. Rev. Lett. **108**, 042505.

Birman, J L, R. G. Nazmitdinov, and V. I. Yukalov (2013), "Effects of symmetry breaking in finite quantum systems," Physics Reports **526**, 1.

Bączyk, P, J. Dobaczewski, M. Konieczka, W. Satuła, T. Nakatsukasa, and K. Sato (2018), "Isospin-symmetry breaking in masses of $N \approx Z$ nuclei," Physics Letters B **778**, 178 – 183.

Blaizot, JP, and D. Gogny (1977), "Theory of elementary excitations in closed shell nuclei," Nuclear Physics A **284** (3), 429 – 460.

Blaizot, JP, and G. Ripka (1986), *Quantum theory of finite systems* (MIT Press, Cambridge Mass.).

Boguta, J, and A. R. Bodmer (1977), "Relativistic calculation of nuclear matter and the nuclear surface," Nucl. Phys. A **292** (3), 413–428.

Bohr, Å, and B.R. Mottelson (1998), *Nuclear Structure* (World Scientific, Singapore, Vol. II).

Bonche, P, J. Dobaczewski, H. Flocard, and P.-H. Heenen (1991), "Generator coordinate method for triaxial quadrupole collective dynamics in strontium isotopes," Nuclear Physics A **530** (1), 149 – 170.

Bonche, P, J. Dobaczewski, H. Flocard, P.-H. Heenen, and J. Meyer (1990), "Analysis of the generator coordinate method in a study of shape isomerism in ^{194}Hg," Nuclear Physics A **510** (3), 466 – 502.

Borrajo, M, and J. Luis Egido (2018), "Symmetry conserving configuration mixing description of odd mass nuclei," Phys. Rev. C **98**, 044317.

Borrajo, Marta, Tomás R. Rodríguez, and J. Luis Egido (2015), "Symmetry conserving configuration mixing method with cranked states," Physics Letters B **746**, 341 – 346.

Brandt, B B, C. Yannouleas, and U. Landman (2015), "Double-well ultracold-fermions computational microscopy: Wave-function anatomy of attractive-pairing and Wigner-molecule entanglement and natural orbitals," Nano Lett. **15**, 7105.

Brandt, B B, C. Yannouleas, and U. Landman (2016), "Ultracold few fermionic atoms in needle-shaped double wells: Spin chains and resonating spin clusters from microscopic hamiltonians emulated via antiferromagnetic Heisenberg and t-J models," New J. Phys. **18**, 073018.

Brown, B Alex, and W. A. Richter (2006), "New "USD" Hamiltonians for the sd shell," Phys. Rev. C **74**, 034315.

Bucher, B, S. Zhu, C. Y. Wu, R. V. F. Janssens, R. N. Bernard, L. M. Robledo, T. R. Rodríguez, D. Cline, A. B. Hayes, A. D. Ayangeakaa, M. Q. Buckner, C. M. Campbell, M. P. Carpenter, J. A. Clark, H. L. Crawford, H. M. David, C. Dickerson, J. Harker, C. R. Hoffman, B. P. Kay, F. G. Kondev, T. Lauritsen, A. O. Macchiavelli, R. C. Pardo, G. Savard, D. Seweryniak, and R. Vondrasek (2017), "Direct evidence for octupole deformation in ^{146}Ba and the origin of large $E1$ moment variations in reflection-asymmetric nuclei," Phys. Rev. Lett. **118**, 152504.

Bürvenich, T, D. G. Madland, J. A. Maruhn, and P.-G. Reinhard (2002), "Nuclear ground state observables and QCD scaling in a refined relativistic point coupling model," Phys. Rev. C **65**, 044308.

Bychkov, Yu A, and E. I. Rashba (1984), "Properties of a 2D electron gas with lifted spectral degeneracy," JETP Lett. **39**, 78.

Caurier, E, and B. Grammaticos (1977), "Projected spectra of light nuclei with Skyrme interactions," Nuclear Physics A **279** (2), 333 – 346.

Caurier, E, A. Poves, and A. Zuker (1980a), "Hartree-Fock versus isospin projected Hartree-Fock in nuclei with neutron excess," Physics Letters B **96** (1), 11 – 14.

Caurier, E, A. Poves, and A. Zuker (1980b), "Isotope shifts and Coulomb displacement energies in calcium isotopes," Physics Letters B **96** (1), 15 – 18.

Caurier, Etienne, and Alfredo Poves (1982), "An isospin projected Hartree-Fock description of proton and neutron radii," Nuclear Physics A **385** (3), 407 – 429.

Nikšić, T, D. Vretenar, and P. Ring (2006a), "Beyond the

relativistic mean-field approximation: Configuration mixing of angular-momentum-projected wave functions," Phys. Rev. C **73**, 034308.

Nikšić, T, D. Vretenar, and P. Ring (2006b), "Beyond the relativistic mean-field approximation. II. Configuration mixing of mean-field wave functions projected on angular momentum and particle number," Phys. Rev. C **74**, 064309.

Cohen, A J, P. Mori-Sánchez, and W. Yang (2008), "Insights into current limitations of density functional theory," Science **321**, 792.

Cotton, F A (1990), *Chemical Applications of Group Theory* (Wiley, New York).

Dai, Z, J.-L. Zhu, N. Yang, and Y. Wang (2007), "Spin-dependent rotating Wigner molecules in quantum dots," Phys. Rev. B **76**, 085308.

Davesne, D, J. Navarro, J. Meyer, K. Bennaceur, and A. Pastore (2018), "Two-body contributions to the effective mass in nuclear effective interactions," Phys. Rev. C **97**, 044304.

De Giovannini, U, F. Cavaliere, R. Cenni, M. Sassetti, and B. Kramer (2007), "Spin and rotational symmetries in unrestricted Hartree-Fock states of quantum dots," New J. Phys. **9**, 93.

De Giovannini, U, F. Cavaliere, R. Cenni, M. Sassetti, and B. Kramer (2008), "Spin-projected unrestricted Hartree-Fock ground states for harmonic quantum dots," Phys. Rev. B **77**, 035325.

Delaroche, J-P, M. Girod, J. Libert, H. Goutte, S. Hilaire, S. Peru, N. Pillet, and G.F. Bertsch (2010), "Structure of even-even nuclei using a mapped collective Hamiltonian and the D1S Gogny interaction," Phys. Rev. C **81**, 014303.

Dietrich, Klaus, Hans J. Mang, and Jean H. Pradal (1964), "Conservation of particle number in the nuclear pairing model," Phys. Rev. **135**, B22–B34.

Dobaczewski, J, and W. Nazarewicz (1993), "Comment on "pairing correlations studied in the two-level model"," Phys. Rev. C **47**, 2418–2421.

Dobaczewski, J, W. Nazarewicz, and M.V. Stoitsov (2002), "Nuclear ground-state properties from mean-field calculations," Eur. Phys. J. A **15** (1-2), 21.

Dobaczewski, J, W. Satuła, B.G. Carlsson, J. Engel, P. Olbratowski, P. Powałowski, M. Sadziak, J. Sarich, N. Schunck, A. Staszczak, M. Stoitsov, M. Zalewski, and H. Zduńczuk (2009), "Solution of the Skyrme-Hartree-Fock-Bogolyubov equations in the Cartesian deformed harmonic-oscillator basis.: (VI) HFODD (v2.40h): A new version of the program," Computer Physics Communications **180** (11), 2361 – 2391.

Dobaczewski, J, M. V. Stoitsov, W. Nazarewicz, and P.-G. Reinhard (2007), "Particle-number projection and the density functional theory," Phys. Rev. C **76**, 054315.

Dobaczewski, Jacek (2009), "Lipkin translational-symmetry restoration in the mean-field and energy–density-functional methods," Journal of Physics G: Nuclear and Particle Physics **36** (10), 105105.

Dönau, F (1998), "Canonical form of transition matrix elements," Phys. Rev. C **58**, 872–877.

Dresselhaus, G (1955), "Spin-orbit coupling effects in Zinc Blende structures," Phys. Rev. **100**, 580.

Dufour, Marianne, and Andrés P. Zuker (1996), "Realistic collective nuclear hamiltonian," Phys. Rev. C **54**, 1641–1660.

Duguet, T, M. Bender, K. Bennaceur, D. Lacroix, and T. Lesinski (2009), "Particle-number restoration within the energy density functional formalism: Non viability of terms

depending on non integer powers of the density matrices," Phys. Rev. C **79**, 044320.

Duguet, T, M. Bender, J. P. Ebran, T. Lesinski, and V. Somà (2015), "Ab initio-driven nuclear energy density functional method," The European Physical Journal A **51** (12), 162.

Duguet, T, and P. Bonche (2003), "Density dependence of two-body interactions for beyond-mean-field calculations," Phys. Rev. C **67**, 054308.

Dunn, J L, A. J. Lakin, and I. D. Hands (2012), "Manifestation of dynamic Jahn-Teller distortions and surface interactions in scanning tunnelling microscopy images of the fullerene anion C_{60}^-," New J. Phys. **14**, 083038.

Ebran, J-P, E. Khan, T. Nikšić, and D. Vretenar (2013), "Localization and clustering in the nuclear Fermi liquid," Phys. Rev. C **87**, 044307.

Ebran, J-P, E. Khan, T. Nikšić, and D. Vretenar (2017), "Localization and clustering in atomic nuclei," Journal of Physics G: Nuclear and Particle Physics **44** (10), 103001.

Eckert, K, J. Schliemann, D. Bruß, and M. Lewenstein (2002), "Quantum correlations in systems of indistinguishable particles," Annals of Physics (New York) **299**, 88.

Edmonds, A R (1957), *Angular Momentum in Quantum Mechanics* (Princeton University Press).

Egido, J L, and L M Robledo (1991), "Parity-projected calculations on octupole deformed nuclei," Nucl. Phys. A **524** (1), 65 – 87.

Egido, J L, and L. M. Robledo (2004), "Angular momentum projection and quadrupole correlations effects in atomic nuclei," Extended Density Functionals In Nuclear Structure Physics **641**, Wilhelm & Else Heraeus Fdn.

Egido, J Luis, Marta Borrajo, and Tomás R. Rodríguez (2016), "Collective and single-particle motion in beyond mean field approaches," Phys. Rev. Lett. **116**, 052502.

Egido, JL, J. Lessing, V. Martin, and L.M. Robledo (1995), "On the solution of the Hartree-Fock-Bogoliubov equations by the conjugate gradient method," Nuclear Physics A **594** (1), 70 – 86.

Egido, JL, H.-J. Mang, and P. Ring (1980), "Selfconsistent treatment of excited rotational bands in deformed nuclei," Nucl. Phys. A **334** (1), 1.

Egido, JL, and P. Ring (1982a), "Symmetry conserving Hartree-Fock-Bogoliubov theory: (I). On the solution of variational equations," Nuclear Physics A **383** (2), 189 – 204.

Egido, JL, and P. Ring (1982b), "Symmetry-conserving Hartree-Fock-Bogoliubov theory: (II). Number-projected cranked Hartree-Fock-Bogoliubov calculations in the rare earth region," Nuclear Physics A **388** (1), 19 – 36.

Ellenberger, C, T. Ihn, C. Yannouleas, U. Landman, K. Ensslin, D.C. Driscoll, and A.C. Gossard (2006), "Excitation spectrum of two correlated electrons in a lateral quantum dot with negligible zeeman splitting," Phys. Rev. Lett. **96**, 126806.

Eriksson, G, J. Bengtsson, E. Ö. Karabulut, G. M. Kavoulakis, and S. M. Reimann (2018), "Finite-size effects in the dynamics of few bosons in a ring potential," J. Phys. B: At. Mol. Opt. Phys. **51**, 035504.

Esebbag, C, and J.L. Egido (1993), "Number projected statistics and the pairing correlations at high excitation energies," Nuclear Physics A **552** (2), 205 – 231.

Esry, B D (1997), "Hartree-Fock theory for Bose-Einstein condensates and the inclusion of correlation effects," Phys. Rev. A **55**, 1147.

Fanto, P (2017), "Projection after variation in the

finite-temperature Hartree-Fock-Bogoliubov approximation," Phys. Rev. C **96**, 051301.

Fanto, P, Y. Alhassid, and G. F. Bertsch (2017), "Particle-number projection in the finite-temperature mean-field approximation," Phys. Rev. C **96**, 014305.

Fernández, M A, and J. L. Egido (2003), "Generalized BCS ansatz for pairing correlations in superconducting grains," Phys. Rev. B **68**, 184505.

Fernández, M A, and J. L. Egido (2005), "Pairing correlations in finite systems: from the weak to the strong fluctuations regime," Eur. Phys. J. B – Condensed Matter and Complex Systems **48**, 305.

Fertig, H A, and W. Kohn (2000), "Symmetry of the atomic electron density in Hartree, Hartree-Fock, and density-functional theories," Phys. Rev. A **62**, 052511.

Flocard, H, and N. Onishi (1997), "On the restoration of symmetry in paired fermion systems," Annals of Physics **254** (2), 275 – 327.

Fomenko, V N (1970), "Projection in the occupation-number space and the canonical transformation," J. Phys. A **3**, 8.

Frauendorf, Stefan (2001), "Spontaneous symmetry breaking in rotating nuclei," Rev. Mod. Phys. **73**, 463–514.

Fukutome, H (1981), "Unrestricted Hartree-Fock theory and its applications to molecules and chemical reactions," Int. J. Quantum Chem. **20**, 955.

Gao, Y, J. Dobaczewski, and P. Toivanen (2015a), "Approximate restoration of translational and rotational symmetries within the lipkin method," arXiv:1511.02814 [nucl-th].

Gao, Zao-Chun, and Mihai Horoi (2009), "Angular momentum projected configuration interaction with realistic Hamiltonians," Phys. Rev. C **79**, 014311.

Gao, Zao-Chun, Mihai Horoi, and Y. S. Chen (2015b), "Variation after projection with a triaxially deformed nuclear mean field," Phys. Rev. C **92**, 064310.

Garrote, E, J. L. Egido, and L. M. Robledo (1998), "Fingerprints of reflection asymmetry at high angular momentum in atomic nuclei," Physical Review Letters **80** (20), 4398–4401.

Garrote, E, J.L. Egido, and L.M. Robledo (1997), "A microscopic study of the octupole degree of freedom at high angular momentum," Physics Letters B **410** (2), 86 – 94.

Gaudin, Michel (1960), "Une démonstration simplifiée du théorème de Wick en mécanique statistique," Nuclear Physics **15** (Supplement C), 89 – 91.

Ghosh, MK, A. Goswami, and S.R. Majumdar (1975), "Self-consistent orthonormalization and the BCS treatment of the charge-independent pairing correlation," Phys. Rev. C **12**, 1650–1658.

Gilmore, R (2008), *Lie Groups, Physics, and Geometry: An Introduction for Physicists, Engineers and Chemists* (Cambridge University Press).

Girardeau, M (1960), "Relationship between systems of impenetrable bosons and fermions in one dimension," J. Math. Phys. **1**, 516.

Giraud, B, and B. Grammaticos (1974), "Energy surfaces, collective potentials and collective inertia parameters," Nucl. Phys. A **233**, 373 – 384.

Girod, M, and P. Schuck (2013), "α-Particle clustering from expanding self-conjugate nuclei within the Hartree-Fock-Bogoliubov approach," Phys. Rev. Lett. **111**, 132503.

Głowacz, S, W. Satuła, and R. A. Wyss (2004), "Cranking in isospace," The European Physical Journal A - Hadrons and Nuclei **19** (1), 33–44.

Goeppert Mayer, M (1949), "On closed shells in nuclei. II," Phys. Rev. **75**, 1969.

Goldman, N, G. Juzeliūnas, P. Öhberg, and I.B. Spielman (2014), "Light-induced gauge fields for ultracold atoms," Rep. Prog. Phys. **77**, 126401.

Goldstone, J (1961), "Field theories with « superconductor » solutions," Il Nuovo Cimento (1955-1965) **19** (1), 154–164.

González-Ballestero, C, L.M. Robledo, and G.F. Bertsch (2011), "Numeric and symbolic evaluation of the pfaffian of general skew-symmetric matrices," Computer Physics Communications **182** (10), 2213 – 2218.

Goodfellow, JF, and Y. Nogami (1966), "On the superconductivity approximation for the nuclear pairing interaction," Canadian Journal of Physics **44** (6), 1321–1327.

Griffin, J J, and J. A. Wheeler (1957), "Collective motions in nuclei by the method of generator coordinates," Phys. Rev. **108**, 311.

Gulshani, P (2011), "Derivation of microscopic unified Bohr-Mottelson rotational model," Nuclear Physics A **852** (1), 109 – 126.

Haff, P K, and L. Wilets (1973), "Microscopic theory of nuclear collective motion," Phys. Rev. C **7**, 951–968.

Hallam, L D, C. A. Bates, and J. L. Dunn (1992), "Symmetry-adapted states for $T(X)(e+t_2)$ Jahn-Teller systems," Journal of Physics: Condensed Matter **4**, 6775.

Hamermesh, M (1962), *Group Theory and its Application to Physical Problems* (Addison-Wesley, Reading, MA).

Hammaren, E, K. W. Schmid, F. Grümmer, A. Faessler, and B. Fladt (1985), "Microscopic description of odd-mass nuclei in the mass A = 130 region," Nucl. Phys. A **437** (1), 1 – 46.

Hanson, R, L. P. Kouwenhoven, J. R. Petta, S. Tarucha, and L. M. K. Vandersypen (2007), "Spins in few-electron quantum dots," Rev. Mod. Phys. **79**, 1217.

Hara, K, A. Hayashi, and P. Ring (1982), "Exact angular momentum projection of cranked Hartree-Fock-Bogoliubov wave functions," Nuclear Physics A **385** (1), 14 – 28.

Hara, K, and S. Iwasaki (1979), "On the quantum number projection: (I). General theory," Nucl. Phys. A **332**, 61 – 68.

Hara, K, and Y. Sun (1995), "Projected shell model and high-spin spectroscopy," International Journal of Modern Physics E **04** (04), 637–785.

Hara, Kenji (1967), "Number-conserving approach to the pairing-force model: (i). almost-degenerate model," Nucl. Phys. A **95** (2), 385 – 419.

Hashimoto, K (1982), "Unrestricted Hartree-Fock wave functions approximating lowlying covalent states of ring π systems," Int. J. Quantum Chem. **22**, 397.

Haxel, O, J. H. D. Jensen, and H. E. Suess (1949), "On the "Magic Numbers" in nuclear structure," Phys. Rev. **75**, 1766.

Hayashi, A, K. Hara, and P. Ring (1984), "Existence of triaxial shapes in transitional nuclei," Phys. Rev. Lett. **53**, 337–340.

Heenen, P-H, P. Bonche, J. Dobaczewski, and H. Flocard (1993), "Generator-coordinate method for triaxial quadrupole dynamics in Sr isotopes (II). Results for particle-number-projected states," Nuclear Physics A **561** (3), 367 – 386.

Heenen, P-H, A. Valor, M. Bender, P. Bonche, and H. Flocard (2001), "GCM analysis of the collective properties of lead isotopes with exact projection on particle numbers," The European Physical Journal A - Hadrons and Nuclei **11** (4), 393–402.

Heimsoth, M, and M. Bonitz (2010), "Interacting bosons beyond the Gross-Pitaevskii mean field," Physica E **42**, 420.

Heitler, H, and F. London (1927), "Wechselwirkung neutraler atome und homöopolare bindung nach der quantenmechanik," Z. Phys. **44**, 455.

Hill, D L, and J. A. Wheeler (1953), "Nuclear constitution and the interpretation of fission phenomena," Phys. Rev. **89**, 1102.

Hohenberg, P, and W. Kohn (1964), Phys. Rev. **136**, B864.

Hu, Qing-Li, Zao-Chun Gao, and Y.S. Chen (2014), "Matrix elements of one-body and two-body operators between arbitrary HFB multi-quasiparticle states," Physics Letters B **734**, 162 – 166.

Hubbard, J (1959), "Calculation of partition functions," Phys. Rev. Lett. **3**, 77–78.

Hubbard, J (1963), "Electron correlations in narrow energy bands," Proceedings of the Royal Society of London A: Mathematical, Physical and Engineering Sciences **276**, 238.

Hupin, Guillaume, Denis Lacroix, and Michael Bender (2011), "Formulation of functional theory for pairing with particle number restoration," Phys. Rev. C **84**, 014309.

Iachello, F (2001), "Analytic description of critical point nuclei in a spherical-axially deformed shape phase transition," Phys. Rev. Lett. **87**, 052502.

Ichikawa, T, J. A. Maruhn, N. Itagaki, K. Matsuyanagi, P.-G. Reinhard, and S. Ohkubo (2012), "Existence of an exotic torus configuration in high-spin excited states of ^{40}Ca," Phys. Rev. Lett. **109**, 232503.

Igawa, A (1995), "A method of calculation of the matrix elements between the spin projected nonorthogonal Slater determinants," Int. J. Quantum Chem. **54**, 235.

Inglis, D R (1954), "Particle derivation of nuclear rotation properties associated with a surface wave," Phys. Rev. **96**, 1059–1065.

Inglis, D R (1956), "Nuclear moments of inertia due to nucleon motion in a rotating well," Phys. Rev. **103**, 1786–1795.

Iwai, M, and H Nakamura (1989), "Generator-coordinate representation of the O(4) supermultiplets of doubly excited states," Phys. Rev. A **40**, 2247.

Jain, J K (2007), *Composite Fermions* (Cambridge University Press, New York).

Jancovici, B, and D.H. Schiff (1964), "The collective vibrations of a many-fermion system," Nuclear Physics **58**, 678 – 686.

Jehangir, S, G.H. Bhat, J.A. Sheikh, S. Frauendorf, S.N.T. Majola, P.A. Ganai, and J.F. Sharpey-Schafer (2018), "Quasiparticle and γ-band structures in ^{156}Dy," Phys. Rev. C **97**, 014310.

Jehangir, S, G.H. Bhat, J.A. Sheikh, R. Palit, and P.A. Ganai (2017), "Intrinsic properties of high-spin band structures in triaxial nuclei," Nuclear Physics A **968**, 48 – 70.

Jiménez-Hoyos, C A, Th. M. Henderson, Takashi Tsuchimochi, and G. E. Scuseria (2012), "Projected Hartree-Fock theory," J. Chem. Phys. **136**, 164109.

Jiménez-Hoyos, C A, R. Rodrí-guez-Guzmán, and G. E. Scuseria (2013), "Multi-component symmetry-projected approach for molecular ground state correlations," J. Chem. Phys. **139**, 204102.

Johnson, Calvin W, and Changfeng Jiao (2019), "Convergence and efficiency of angular momentum projection," Journal of Physics G: Nuclear and Particle Physics **46** (1), 015101.

Johnson, Calvin W, and Kevin D. O'Mara (2017), "Projection of angular momentum via linear algebra," Phys. Rev.

C **96**, 064304.

Jones, R O (2015), "Density functional theory: Its origins, rise to prominence, and future," Rev. Mod. Phys. **87**, 897–923.

Kamlah, A (1968), "An approximation for rotation-projected expectation values of the energy for deformed nuclei and a derivation of the cranking variational equation," Zeitschrift für Physik A Hadrons and nuclei **216** (1), 52–64.

Kaplan, I G (2018), "Symmetry properties of the electron density and following from it limits on the KS-DFT applications," Molecular Physics **116**, 658.

Kastner, M A (1993), "Artificial atoms," Phys. Today **46**, 24.

Kegley Jr., D R, V. E. Oberacker, M. R. Strayer, A. S. Umar, and J. C. Wells (1996), "Basis Spline Collocation Method for Solving the Schrödinger Equation in Axillary Symmetric Systems," J. Comput. Phys. **128** (1), 197.

Kellman, M E, and D. R. Herrick (1980), "Ro-vibrational collective interpretation of supermultiplet classifications of intrashell levels of two-electron atoms," Phys. Rev. A **22**, 1536.

Kerman, A K (1961), "Pairing forces and nuclear collective motion," Ann. Phys. (N.Y.) **12** (2), 300 – 329.

Kerman, AK, and N. Onishi (1981), "Nuclear rotations studied by the time-dependent variational method," Nuclear Physics A **361** (1), 179 – 191.

Kissener, H-R, and L. Münchow (1966), "A note on the linear Bogoliubov transformation for proton-neutron correlations," Physics Letters **19** (8), 665 – 667.

Kissener, HR, and L. Münchow (1967), "Comparison of projected BCS solutions with exact ones for charge-independent ($J = 0, T = 1$) pairing interaction," Physics Letters B **25** (8), 493 – 496.

Knight, W D, K. Clemenger, W. A. de Heer, W. A. Saunders, M. Y. Chou, and M. L. Cohen (1984), "Electronic shell structure and abundances of Sodium clusters," Phys. Rev. Lett. **52**, 2141.

Kohn, W, and L. J. Sham (1965), "Self-consistent equations including exchange and correlation effects," Phys. Rev. **140**, A1133–A1138.

Konieczka, M, P. Bączyk, and W. Satuła (2016), "β-decay study within multireference density functional theory and beyond," Phys. Rev. C **93**, 042501.

Konieczka, M, M. Kortelainen, and W. Satuła (2018), "Gamow-teller response in the configuration space of a density-functional-theory–rooted no-core configuration-interaction model," Phys. Rev. C **97**, 034310.

Koonin, S E, D. J. Dean, and K. Langanke (1997a), "Results from shell-model monte carlo studies," Annual Review of Nuclear and Particle Science **47** (1), 463–504.

Koonin, SE, D.J. Dean, and K. Langanke (1997b), "Shell model monte carlo methods," Physics Reports **278** (1), 1 – 77.

Kortelainen, M, T. Lesinski, J. Moré, W. Nazarewicz, J. Sarich, N. Schunck, M. V. Stoitsov, and S. Wild (2010), "Nuclear energy density optimization," Phys. Rev. C **82**, 024313.

Kouwenhoven, L, and C. Marcus (1998), "Quantum dots," Phys. World **11**, 35.

Kouwenhoven, L P, C.M. Marcus, P.L. McEuen, S. Tarucha, R. M. Westervelt, and N. S. Wingreen (1997), "Electron transport in quantum dots," in *Mesoscopic Electron Transport,* L. L. Sohn, L. P. Kouwenhoven, and G. Schön (eds), NATO ASI Series (Series E: Applied Sciences), vol 345, p. 105 (Springer, Dordrecht).

Kucharek, H, and P. Ring (1991), "Relativistic field theory

of superfluidity in nuclei," Z. Phys. A **339** (1), 23–35.

Lacroix, D, T. Duguet, and M. Bender (2009), "Configuration mixing within the energy density functional formalism: Removing spurious contributions from nondiagonal energy kernels," Phys. Rev. C **79**, 044318.

Lalazissis, G A, T. Nikšić, D. Vretenar, and P. Ring (2005), "New relativistic mean field interaction with density dependent meson couplings," Phys. Rev. C **71**, 024312.

Lamme, HA, and E. Boeker (1968), "Exact and approximate angular momentum projection for light nuclei," Nuclear Physics A **111** (3), 492 – 512.

Lang, G H, C. W. Johnson, S. E. Koonin, and W. E. Ormand (1993), "Monte carlo evaluation of path integrals for the nuclear shell model," Phys. Rev. C **48**, 1518–1545.

Leprévost, A, O. Juillet, and R. Frésard (2014), "Exact ground state of strongly correlated electron systems from symmetry-entangled wave-functions," Annalen der Physik **526**, 430.

Li, H K, E. Urban, C. Noel, A. Chuang, Y. Xia, A. Ransford, B. Hemmerling, Y. Wang, T. Li, H. Häffner, and X. Zhang (2017), "Realization of translational symmetry in trapped cold ion rings," Phys. Rev. Lett. **118**, 053001.

Li, T, Z.-X. Gong, Z.-Q. Yin, H. T. Quan, X. Yin, P. Zhang, L.-M. Duan, and X. Zhang (2012a), "Space-time crystals of trapped ions," Phys. Rev. Lett. **109**, 163001.

Li, Ying, C. Yannouleas, and U. Landman (2009), "Artificial quantum-dot Helium molecules: Electronic spectra, spin structures, and Heisenberg clusters," Phys. Rev. B **80**, 045326.

Li, Yuesong, C. Yannouleas, and U. Landman (2006), "From a few to many electrons in quantum dots under strong magnetic fields: Properties of rotating electron molecules with multiple rings," Phys. Rev. B **73**, 075301.

Li, Zhipan, T. Niksic, P. Ring, D. Vretenar, Jiangming Yao, and Jie Meng (2012b), "Efficient method for computing the Thouless-Valatin inertia parameters," Phys. Rev. C **86**, 034334.

Libert, J, M. Girod, and J.-P. Delaroche (1999), "Microscopic descriptions of superdeformed bands with the Gogny force: Configuration mixing calculations in the A=190 mass region," Phys. Rev. C **60**, 054301.

Lichtner, P C, and J. J. Griffin (1976), "Evolution of a quantum system: Lifetime of a determinant," Phys. Rev. Lett. **37**, 1521.

Lipkin, H J (1956), "On the description of collective motion by the use of superfluous co-ordinates," Suppl. Nouvo Cim. **3**, 1147.

Lipkin, H J (1958), "Center-of-mass motion in the nuclear shell model," Phys. Rev. **110**, 1395–1397.

Lipkin, H J, A. de Shalit, and I. Talmi (1955), "On the description of collective motion by th use of superfluous co-ordinates," Il Nuovo Cimento (1955-1965) **2** (4), 773–798.

Lipkin, Harry J (1960), "Collective motion in many-particle systems: Part 1. The violation of conservation laws," Annals of Physics **9** (2), 272 – 291.

Lipkin, Harry J (1961), "Collective motion in many-particle systems: Part II. Treatment of coupled systems," Annals of Physics **12** (3), 452 – 462.

Löwdin, Per-Olov (1955a), "Quantum theory of many-particle systems. I. Physical interpretations by means of density matrices, natural spin-orbitals, and convergence problems in the method of configurational interaction," Phys. Rev. **97**, 1474–1489.

Löwdin, Per-Olov (1955b), "Quantum theory of many-particle systems. III. Extension of the Hartree-Fock scheme to include degenerate systems and correlation effects," Phys. Rev. **97**, 1509–1520.

Lykos, P, and G. W. Pratt (1963), "Discussion on the Hartree-Fock approximation," Rev. Mod. Phys. **35**, 496.

Magnus, Wim, Lucien Lemmens, and Fons Brosens (2017), "Quantum canonical ensemble: A projection operator approach," Physica A: Statistical Mechanics and its Applications **482**, 1 – 13.

Majola, S N T, D. J. Hartley, L. L. Riedinger, J. F. Sharpey-Schafer, J. M. Allmond, C. Beausang, M. P. Carpenter, C. J. Chiara, N. Cooper, D. Curien, B. J. P. Gall, P. E. Garrett, R. V. F. Janssens, F. G. Kondev, W. D. Kulp, T. Lauritsen, E. A. McCutchan, D. Miller, J. Piot, N. Redon, M. A. Riley, J. Simpson, I. Stefanescu, V. Werner, X. Wang, J. L. Wood, C.-H. Yu, and S. Zhu (2015), "Observation of γ vibrations and alignments built on non-ground-state configurations in ^{156}Dy," Phys. Rev. C **91**, 034330.

Maksym, P A (1996), "Eckardt frame theory of interacting electrons in quantum dots," Phys. Rev. B **53**, 10871.

Maksym, P A, H. Imamura, G. P. Mallon, and H. Aoki (2000), "Molecular aspects of electron correlation in quantum dots," J. Phys.: Condens. Matter **12**, R299.

Mang, H J, B. Samadi, and P. Ring (1976), "On the solution of constrained Hartree-Fock-Bogolyubov equations," Zeitschrift für Physik A Atoms and Nuclei **279** (3), 325–329.

Mang, Hans-Jörg (1975a), "The self-consistent single-particle model in nuclear physics," Phys. Rep. **18** (6), 325.

Mang, HJ (1975b), "The self-consistent single-particle model in nuclear physics," Physics Reports **18** (6), 325 – 368.

Marcos, S, H. Flocard, and P.H. Heenen (1983), "Influence of left-right asymmetry degrees of freedom in self-consistent calculations of 20Ne," Nuclear Physics A **410** (1), 125 – 136.

Márquez Romero, A, J. Dobaczewski, and A. Pastore (2018), "Symmetry restoration in the nuclear-DFT description of proton-neutron pairing," arXiv:1812.03927 [nucl-th].

Marshalek, E R, and J. Weneser (1969), "Nuclear rotation and the random-phase approximation," Ann. Phys. (N.Y.) **53** (3), 569 – 624.

Messud, Jérémie (2013), "Alternate, well-founded way to treat center-of-mass correlations: Proposal of a local center-of-mass correlations potential," Phys. Rev. C **87**, 024302.

Mikhailov, S, and K. Ziegler (2002), "Floating Wigner molecules and possible phase transitions in quantum dots," Eur. Phys. J. B **28**, 117.

Modi, K, A. Brodutch, H. Cable, T. Paterek, and V. Vedral (2012), "The classical-quantum boundary for correlations: Discord and related measures," Rev. Mod. Phys. **84**, 1655.

Mujal, P, A. Polls, and B. Juliá-Díaz (2018), "Fermionic properties of two interacting bosons in a Two-Dimensional harmonic trap," Condens. Matter **3**, 9.

Müller, H-M, and S. E. Koonin (1996), "Phase transitions in quantum dots," Phys. Rev. B **54**, 14532.

Murmann, S, A. Bergschneider, V. M. Klinkhamer, G. Zürn, Th. Lompe, and S. Jochim (2015), "Two fermions in a double well: Exploring a fundamental building block of the Hubbard model," Phys. Rev. Lett. **114**, 080402.

Mutz, U, and P Ring (1984), "On the pairing collapse in nuclei at high angular momenta," Journal of Physics G: Nuclear Physics **10** (2), L39.

Nambu, Yoichiro (1960), "Axial vector current conservation in weak interactions," Phys. Rev. Lett. **4**, 380–382.

Neergård, K, and E. Wüst (1983), "On the calculation of matrix elements of operators between symmetry-projected Bogoliubov states," Nuclear Physics A **402** (2), 311 – 321.

Niksic, T, D. Vretenar, G. A. Lalazissis, and P. Ring (2007), "Microscopic description of nuclear quantum phase transitions," Phys. Rev. Lett. **99**, 092502.

Niksic, T, D. Vretenar, and P. Ring (2008), "Relativistic nuclear energy density functionals: adjusting parameters to binding energies." Phys. Rev. C **78**, 034318.

Nogami, Y (1965), "On the superconductivity theory of the nuclear pairing interaction," Physics Letters **15** (4), 335 – 337.

Nogami, Y, and I.J. Zucker (1964), "A note on the pairing interaction in nuclei," Nuclear Physics **60** (2), 203 – 208.

Nogami, Yukihisa (1964), "Improved superconductivity approximation for the pairing interaction in nuclei," Phys. Rev. **134**, B313–B321.

Noguchi, A, Y. Shikano, K. Toyoda, and S. Urabe (2014), "Aharonov bohm effect in the tunnelling of a quantum rotor in a linear paul trap," Nat. Commun. **5**, 3868.

Oi, M, and N. Tajima (2005), "Nodal lines in the cranked HFB overlap kernels," Physics Letters B **606** (1), 43 – 51.

Ollivier, H, and W. H. Zurek (2001), "Quantum discord: A measure of the quantumness of correlations," Phys. Rev. Lett. **88**, 017901.

Onishi, Naoki, and Shiro Yoshida (1966), "Generator coordinate method applied to nuclei in the transition region," Nuclear Physics **80** (2), 367 – 376.

Otsuka, T, M. Honma, T. Mizusaki, N. Shimizu, and Y. Utsuno (2001), "Monte Carlo shell model for atomic nuclei," Prog. Part. Nucl. Phys. **47** (1), 319 – 400.

Papenbrock, T, and H. A. Weidenmüller (2015), "Effective field theory of emergent symmetry breaking in deformed atomic nuclei," J. Phys. G: Nucl. Part. Phys. **42**, 105103.

Pauncz, R (2000), *The Construction of Spin Eigenfunctions: An Exercise Book* (Kluwer Academic/Plenum Publishers, New York).

Pei, J, M. Stoitsov, G. Fann, W. Nazarewicz, N. Schunck, and F. Xu (2008), "Deformed coordinate-space Hartree-Fock-Bogoliubov approach to weakly bound nuclei and large deformations," Phys. Rev. C **78** (6), 064306.

Pei, J C, G. I. Fann, R. J. Harrison, W. Nazarewicz, Yue Shi, and S. Thornton (2014), "Adaptive multi-resolution 3D Hartree-Fock-Bogoliubov solver for nuclear structure," Phys. Rev. C **90** (2), 024317.

Peierls, R (1933), "Zur Theorie des Diamagnetismus von Leitungselektronen," Zeitschrift für Physik **80** (11), 763–791.

Peierls, R E, and J Yoccoz (1957), "The collective model of nuclear motion," Proceedings of the Physical Society. Section A **70** (5), 381.

Perdew, J P, and Alex Zunger (1981), "Self-interaction correction to density-functional approximations for many-electron systems," Phys. Rev. B **23**, 5048–5079.

Perez-Martin, S, and L.M. Robledo (2007), "Generalized Wick's theorem for multiquasiparticle overlaps as a limit of Gaudin's theorem," Phys. Rev. C **76**, 064314.

Piani, M, V. Narasimhachar, and J. Calsamiglia (2014), "Quantumness of correlations, quantumness of ensembles and quantum data hiding," New J. Phys. **16**, 113001.

Pons Viver, M (2018), "The practical implementation of Löwdin's method for spin projection," Int. J. Quantum Chem. **119** (4), e25770.

Pradhan, HC, Y. Nogami, and J. Law (1973), "Study of approximations in the nuclear pairing-force problem," Nuclear Physics A **201** (2), 357 – 368.

Qiu, Y, Th. M. Henderson, J. Zhao, and G. E. Scuseria (2017), "Projected coupled cluster theory," J. Chem. Phys. **147**, 064111.

Raju, M Kumar, P. V. Madhusudhana Rao, S. Muralithar, R. P. Singh, G. H. Bhat, J. A. Sheikh, S. K. Tandel, P. Sugathan, T. Seshi Reddy, B. V. Thirumala Rao, and R. K. Bhowmik (2016), "Observation of a γ band based on a two-quasiparticle configuration in ^{70}ge," Phys. Rev. C **93**, 034317.

Ramanathan, A, K. C. Wright, S. R. Muniz, M. Zelan, III W. T. Hill, C. J. Lobb, K. Helmerson, W. D. Phillips, and G. K. Campbell (2011), "Superflow in a toroidal Bose-Einstein condensate: An atom circuit with a tunable weak link," Phys. Rev. Lett. **106**, 130401.

Reinhard, P G (1989), "The relativistic mean-field description of nuclei and nuclear dynamics," Reports on Progress in Physics **52** (4), 439.

Ring, P (1996), "Relativistic mean field theory in finite nuclei," Progress in Particle and Nuclear Physics **37**, 193 – 263.

Ring, P, H.J. Mang, and B. Banerjee (1974), "Theoretical investigation of rotational bands in odd-mass nuclei," Nucl. Phys. A **225** (1), 141–156.

Ring, P, and P. Schuck (1980), *The Nuclear Many-Body Problem* (Springer-Verlag).

Robledo, L M (1992), "Characterization of octupole correlations in the lipkin model," Phys. Rev. C **46**, 238–243.

Robledo, L M (1994), "Practical formulation of the extended Wick theorem and the Onishi formula," Phys. Rev. C **50**, 2874–2881.

Robledo, L M (2009), "Sign of the overlap of Hartree-Fock-Bogoliubov wave functions," Phys. Rev. C **79**, 021302.

Robledo, L M (2010), "Remarks on the use of projected densities in the density-dependent part of Skyrme or Gogny functionals," Journal of Physics G: Nuclear and Particle Physics **37** (6), 064020.

Robledo, L M (2015a), "Ground state octupole correlation energy with effective forces," Journal of Physics G: Nuclear and Particle Physics **42** (5), 055109.

Robledo, L M (2015b), "Mean-field studies of time reversal breaking states in super-heavy nuclei with the Gogny force," AIP Conference Proceedings **1681** (1), 030016, http://aip.scitation.org/doi/pdf/10.1063/1.4932260.

Robledo, L M, and G. F. Bertsch (2011a), "Application of the gradient method to hartree-fock-bogoliubov theory," Phys. Rev. C **84**, 014312.

Robledo, L M, and G. F. Bertsch (2011b), "Global systematics of octupole excitations in even-even nuclei," Phys. Rev. C **84**, 054302.

Robledo, L M, and G. F. Bertsch (2012), "Electromagnetic transition strengths in soft deformed nuclei," Phys. Rev. C **86**, 054306.

Robledo, L M, T R Rodríguez, and R R Rodríguez-Guzmán (2019), "Mean field and beyond description of nuclear structure with the gogny force: a review," Journal of Physics G: Nuclear and Particle Physics **46** (1), 013001.

Robledo, Luis M (2007), "Particle number restoration: its implementation and impact in nuclear structure calculations," International Journal of Modern Physics E **16** (02), 337–351.

Rodríguez, Tomás R (2016), "Precise description of nuclear spectra with Gogny energy density functional methods,"

Eur. Phys. J. A **52** (7), 190.

Rodríguez, Tomás R, Alexander Arzhanov, and Gabriel Martínez-Pinedo (2015), "Toward global beyond-mean-field calculations of nuclear masses and low-energy spectra," Phys. Rev. C **91**, 044315.

Rodríguez, Tomás R, J. L. Egido, and L. M. Robledo (2005), "Restricted variation after projection and the Lipkin-Nogami methods," Phys. Rev. C **72**, 064303.

Rodríguez, Tomás R, and J. Luis Egido (2010), "Triaxial angular momentum projection and configuration mixing calculations with the Gogny force," Phys. Rev. C **81**, 064323.

Rodríguez, Tomás R, and J. Luis Egido (2011a), "Configuration mixing description of the nucleus ^{44}S," Phys. Rev. C **84**, 051307.

Rodríguez, Tomás R, and J. Luis Egido (2011b), "Multiple shape coexistence in the nucleus ^{80}Zr," Physics Letters B **705** (3), 255 – 259.

Rodríguez, Tomás R, and Gabriel Martínez-Pinedo (2010), "Energy density functional study of nuclear matrix elements for neutrinoless $\beta\beta$ decay," Phys. Rev. Lett. **105**, 252503.

Rodríguez-Guzmán, R, J. L. Egido, and L. M. Robledo (2002a), "Quadrupole collectivity in $N \approx 28$ nuclei with the angular momentum projected generator coordinate method," Phys. Rev. C **65**, 024304.

Rodríguez-Guzmán, R, J.L. Egido, and L.M. Robledo (2000a), "Angular momentum projected analysis of quadrupole collectivity in ^{30,32,34}Mg and ^{32,34,36,38}Si with the Gogny interaction," Physics Letters B **474** (1), 15 – 20.

Rodríguez-Guzmán, R, J.L. Egido, and L.M. Robledo (2002b), "Correlations beyond the mean field in magnesium isotopes: angular momentum projection and configuration mixing," Nuclear Physics A **709** (1), 201 – 235.

Rodríguez-Guzmán, R, C. A. Jiménez-Hoyos, R. Schutski, and G. E. Scuseria (2013), "Multireference symmetry-projected variational approaches for ground and excited states of the one-dimensional Hubbard model," Phys. Rev. B **87**, 235129.

Rodríguez-Guzmán, R, K. W. Schmid, C. A. Jiménez-Hoyos, and G. E. Scuseria (2012), "Symmetry-projected variational approach for ground and excited states of the two-dimensional Hubbard model," Phys. Rev. B **85**, 245130.

Rodríguez-Guzmán, R R, J. L. Egido, and L. M. Robledo (2000b), "Description of quadrupole collectivity in $N \simeq 20$ nuclei with techniques beyond the mean field," Phys. Rev. C **62** (5), 054319.

Rodríguez-Guzmán, R R, J. L. Egido, and L. M. Robledo (2000c), "Properties of the predicted superdeformed band in ^{32}S," Phys. Rev. C **62**, 054308.

Rodríguez-Guzmán, R R, J. L. Egido, and L. M. Robledo (2004), "Beyond mean field description of shape coexistence in neutron-deficient pb isotopes," Physical Review C **69** (5), 054319.

Rodríguez-Guzmán, R R, and K. W. Schmid (2004), "Spherical Hartree-Fock calculations with linear-momentum projection before the variation," The European Physical Journal A - Hadrons and Nuclei **19** (1), 45–59.

Rodríguez-Guzmán, RR, and KW Schmid (2004), "Spherical Hartree-Fock calculations with linear-momentum projection before the variation," The European Physical Journal A-Hadrons and Nuclei **19** (1), 61–75.

Romanovsky, I (2006), Ph.D. Thesis, *Novel properties of interacting particles in small low-dimensional systems* (Georgia Institute of Technology).

Romanovsky, I, C. Yannouleas, L. O. Baksmaty, and U. Landman (2006), "Bosonic molecules in rotating traps," Phys. Rev. Lett. **97**, 090401.

Romanovsky, I, C. Yannouleas, and U. Landman (2004), "Crystalline boson phases in harmonic traps: Beyond the Gross-Pitaevskii mean field," Phys. Rev. Lett. **93**, 230405.

Romanovsky, I, C. Yannouleas, and U. Landman (2008), "Symmetry-conserving vortex clusters in small rotating clouds of ultracold bosons," Phys. Rev. A **78**, 011606.

Romanovsky, I, C. Yannouleas, and U. Landman (2009), "Edge states in graphene quantum dots: Fractional quantum Hall effect analogies and differences at zero magnetic field," Phys. Rev. B **79**, 075311.

Rossignoli, R (1995), "Canonical and grand-canonical partition functions and level densities," Phys. Rev. C **51**, 1772.

Rossignoli, R, A. Ansari, and P. Ring (1993), "Projected statistics and level densities," Phys. Rev. Lett. **70**, 1061–1064.

Rossignoli, R, and P. Ring (1994), "Projection at finite temperature," Annals of Physics **235** (2), 350 – 389.

Rouhaninejad, H, and J. Yoccoz (1966), "Champ self-consistent et methode de projection," Nucl. Phys. **78** (2), 353 – 368.

Ruan, W Y, Y. Y. Liu, C. G. Bao, and Z. Q. Zhang (1995), "Origin of magic angular momenta in few-electron quantum dots," Phys. Rev. B **51**, 7942(R).

Ruder, H, G. Wunner, H. Herold, and F Geyer (1994), *Atoms in Strong Magnetic Fields* (Springer, Berlin).

Sabbey, B, M. Bender, G. F. Bertsch, and P.-H. Heenen (2007), "Global study of the spectroscopic properties of the first 2^+ state in even-even nuclei," Phys. Rev. C **75**, 044305.

Sadoudi, J, M Bender, K Bennaceur, D Davesne, R Jodon, and T Duguet (2013), "Skyrme pseudo-potential-based EDF parametrization for spuriousity-free MR EDF calculations," Physica Scripta **2013** (T154), 014013.

Sakurai, J J (1994), *Modern Quantum Mechanics* (Addison-Wesley Publishing Company), p. 281.

Samyn, M, S. Goriely, M. Bender, and J. Pearson (2004), "Further explorations of Skyrme-Hartree-Fock-Bogoliubov mass formulas. III. Role of particle-number projection," Phys. Rev. C **70** (4), 044309.

Sandhu, T S, and M. L. Rustgi (1978), "Lipkin-Nogami method using effective Yale interaction," Phys. Rev. C **17**, 796–799.

Sato, K, J. Dobaczewski, T. Nakatsukasa, and W. Satuła (2013), "Energy-density-functional calculations including proton-neutron mixing," Phys. Rev. C **88**, 061301.

Satuła, W, P. Bączyk, J. Dobaczewski, and M. Konieczka (2016), "No-core configuration-interaction model for the isospin- and angular-momentum-projected states," Phys. Rev. C **94**, 024306.

Satuła, W, and J. Dobaczewski (2014), "Simple regularization scheme for multireference density functional theories," Phys. Rev. C **90**, 054303.

Satuła, W, J. Dobaczewski, W. Nazarewicz, and M. Rafalski (2009), "Isospin mixing in nuclei within the nuclear density functional theory," Phys. Rev. Lett. **103**, 012502.

Satuła, W, J. Dobaczewski, W. Nazarewicz, and M. Rafalski (2010), "Isospin-symmetry restoration within the nuclear density functional theory: Formalism and applications," Phys. Rev. C **81**, 054310.

Satuła, W, J. Dobaczewski, W. Nazarewicz, and T. R. Werner (2012), "Isospin-breaking corrections to superallowed fermi β decay in isospin- and angular-momentum-

projected nuclear density functional theory," Phys. Rev. C **86**, 054316.

Satuła, Wojciech, and Ramon Wyss (2001a), "Microscopic structure of fundamental excitations in $N = Z$ nuclei," Phys. Rev. Lett. **87**, 052504.

Satuła, Wojciech, and Ramon Wyss (2001b), "Rotations in isospace: A doorway to the understanding of neutron-proton superfluidity in $N = Z$ nuclei," Phys. Rev. Lett. **86**, 4488–4491.

Schmid, K W, T. Dahm, J. Margueron, and H. Müther (2005), "Symmetry-projected variational approach to the one-dimensional hubbard model," Phys. Rev. B **72**, 085116.

Schmid, K W, and F. Grümmer (1987), "Large-scale nuclear structure studies," Rep. Prog. Phys. **50** (6), 731.

Schmid, K W, F. Grümmer, and Amand Faessler (1984a), "Hartree-fock-bogoliubov theory with spin and number projection before the variation: An application to 20Ne and 22Ne," Nucl. Phys. A **431** (2), 205–229.

Schmid, K W, F. Grümmer, and Amand Faessler (1984b), "Nuclear structure theory in spin- and number-conserving quasiparticle configuration spaces: First applications," Phys. Rev. C **29** (1), 308–323.

Schmid, K W, F. Grümmer, and Amand Faessler (1984c), "Nuclear structure theory in spin- and number-conserving quasiparticle configuration spaces: General formalism," Phys. Rev. C **29** (1), 291–307.

Schmid, K W, F. Grümmer, M. Kyotoku, and A. Faessler (1986), "Selfconsistent description of non-yrast states in nuclei: The excited VAMPIR approach," Nucl. Phys. A **452** (3), 493 – 512.

Schmid, KW (2004), "On the use of general symmetry-projected Hartree-Fock-Bogoliubov configurations in variational approaches to the nuclear many-body problem," Progress in Particle and Nuclear Physics **52** (2), 565 – 633.

Schmid, KW, and P.-G. Reinhard (1991), "Center-of-mass projection of Skyrme-Hartree-Fock densities," Nuclear Physics A **530** (2), 283 – 302.

Scuseria, G E, C. A. Jiméez-Hoyos, Th. M. Henderson, K. Samanta, and J. K. Ellis (2011), "Projected quasiparticle theory for molecular electronic structure," J. Chem. Phys. **135**, 124108.

Seideman, T (1999), "Revival structure of aligned rotational wave packets," Phys. Rev. Lett. **83**, 4971.

Seki, T, Y. Kuramoto, and T. Nishino (1996), "Origin of magic angular momentum in a quantum dot under strong magnetic field," J. Phys. Soc. Jpn. **65**, 3945.

Serra, Ll, R. G. Nazmitdinov, and A. Puente (2003), "Symmetry breaking and the random-phase approximation in small quantum dots," Phys. Rev. B **68**, 035341.

Serwane, F, G. Zürn, T. Lompe, T. B. Ottenstein, A. N. Wenz, and S. Jochim (2011), "Deterministic preparation of a tunable few-fermion system," Science **332**, 336.

Sheikh, J A, N. Hinohara, J. Dobaczewski, T. Nakatsukasa, W. Nazarewicz, and K. Sato (2014), "Isospin-invariant Skyrme energy-density-functional approach with axial symmetry," Phys. Rev. C **89**, 054317.

Sheikh, J A, P. Ring, E. Lopes, and R. Rossignoli (2002), "Pairing correlations and particle-number projection methods," Phys. Rev. C **66**, 044318.

Sheikh, JA, G.H. Bhat, R. Palit, Z. Naik, and Y. Sun (2009), "Multi-quasiparticle γ-band structure in neutron-deficient Ce and Nd isotopes," Nuclear Physics A **824** (1), 58 – 69.

Sheikh, JA, and K. Hara (1999), "Triaxial projected shell model approach," Phys. Rev. Lett. **82**, 3968.

Sheikh, JA, and P. Ring (2000), "Symmetry-projected Hartree-Fock-Bogoliubov equations," Nuclear Physics A **665** (1), 71 – 91.

Shi, C, G. S. Jeon, and J. K. Jain (2007), "Composite fermion solid and liquid states in two component quantum dots," Phys. Rev. B **75**, 165302.

Shi, Yue, J. Dobaczewski, and P. T. Greenlees (2014), "Rotational properties of nuclei around ^{254}No investigated using a spectroscopic-quality Skyrme energy density functional," Phys. Rev. C **89**, 034309.

Shi, Yue, C. L. Zhang, J. Dobaczewski, and W. Nazarewicz (2013), "Kerman-Onishi conditions in self-consistent tilted-axis-cranking mean-field calculations," Phys. Rev. C **88**, 034311.

Shimada, Mitsuhiro, Yudai Fujioka, Shingo Tagami, and Yoshifumi R. Shimizu (2018a), "Rotational motion of triaxially deformed nuclei studied by the microscopic angular-momentum-projection method. I. Nuclear wobbling motion," Phys. Rev. C **97**, 024318.

Shimada, Mitsuhiro, Yudai Fujioka, Shingo Tagami, and Yoshifumi R. Shimizu (2018b), "Rotational motion of triaxially deformed nuclei studied by the microscopic angular-momentum-projection method. ii. chiral doublet band," Phys. Rev. C **97**, 024319.

Shimada, Mitsuhiro, Shingo Tagami, and Yoshifumi R. Shimizu (2015), "Angular momentum projected multi-cranked configuration mixing for reliable calculation of high-spin rotational bands," Progress of Theoretical and Experimental Physics **2015** (6), 063D02.

Shimada, Mitsuhiro, Shingo Tagami, and Yoshifumi R. Shimizu (2016), "Realistic description of rotational bands in rare earth nuclei by the angular-momentum-projected multicranked configuration-mixing method," Phys. Rev. C **93**, 044317.

Shimizu, Noritaka, Takashi Abe, Michio Honma, Takaharu Otsuka, Tomoaki Togashi, Yusuke Tsunoda, Yutaka Utsuno, and Tooru Yoshida (2017), "Monte Carlo shell model studies with massively parallel supercomputers," Phys. Scr. **92**, 063001.

Shimizu, Noritaka, Takashi Abe, Yusuke Tsunoda, Yutaka Utsuno, Tooru Yoshida, Takahiro Mizusaki, Michio Honma, and Takaharu Otsuka (2012), "New-generation Monte Carlo shell model for the K computer era," Prog. Theor. Exp. Phys. **2012**, 01A205.

Skalski, J, P.-H. Heenen, P. Bonche, H. Flocard, and J. Meyer (1993), "Octupole correlations in superdeformed mercury and lead nuclei: A generator-coordinate method analysis," Nuclear Physics A **551** (1), 109 – 124.

Skyrme, T H R (1958), "The effective nuclear potential," Nucl. Phys. **9** (4), 615 – 634.

Slater, J C (1951), "A simplification of the Hartree-Fock method," Phys. Rev. **81**, 385–390.

Smith Jr., V H (1964), "Construction of exact spin eigenfunctions," J. Chem. Phys. **41**, 277.

Song, L S, J. M. Yao, P. Ring, and J. Meng (2014), "Relativistic description of nuclear matrix elements in neutrinoless double-beta decay," Phys. Rev. C **90**, 054309.

Stoitsov, M V, J. Dobaczewski, R. Kirchner, W. Nazarewicz, and J. Terasaki (2007), "Variation after particle-number projection for the Hartree-Fock-Bogoliubov method with the Skyrme energy density functional," Phys. Rev. C **76**, 014308.

Stoitsov, M V, J. Dobaczewski, W. Nazarewicz, S. Pittel, and D. J. Dean (2003), "Systematic study of deformed nuclei at

the drip lines and beyond," Phys. Rev. C **68**, 054312.

Stoitsov, MV, J. Dobaczewski, W. Nazarewicz, and P. Ring (2005), "Axially deformed solution of the Skyrme-Hartree-Fock-Bogolyubov equations using the transformed harmonic oscillator basis. the program HFBTHO (v1.66p)," Computer Physics Communications **167** (1), 43 – 63.

Stratonovich, R L (1958), Sov. Phys. Dokl. **2**, 458.

Sun, Yang (2016), "Projection techniques to approach the nuclear many-body problem," Physica Scripta **91** (4), 043005.

Szabo, A, and N. S. Ostlund (1989), *Modern Quantum Chemistry* (McGraw-Hill, New York).

Szafran, B, M. P. Nowak, S. Bednarek, T. Chwiej, and F. M. Peeters (2009), "Selective suppression of Dresselhaus or Rashba spin-orbit coupling effects by the Zeeman interaction in quantum dots," Phys. Rev. B **79**, 235303.

Tagami, Shingo, and Yoshifumi R. Shimizu (2012), "Efficient method to perform quantum number projection and configuration mixing for most general mean-field states," Progress of Theoretical Physics **127** (1), 79–115.

Tagami, Shingo, and Yoshifumi R. Shimizu (2016), "Infinitesimal cranking for triaxial angular-momentum-projected configuration-mixing calculations and its application to the γ vibrational band," Phys. Rev. C **93**, 024323.

Tai, M E, A. Lukin, M. Rispoli, R. Schittko, T. Menke, D. Borgnia, Ph. M. Preiss, F. Grusdt, A. M. Kaufman, and M. Greiner (2017), "Microscopy of the interacting Harper-Hofstadter model in the two-body limit," Nature **546**, 519.

Tajima, N, H. Flocard, P. Bonche, J. Dobaczewski, and P.-H. Heenen (1992), "Generator coordinate kernels between zero- and two-quasiparticle BCS states," Nuclear Physics A **542** (3), 355 – 367.

Takahashi, Yasushi, and Hiroomi Umezawa (1996), "Thermo Field Dynamics," International Journal of Modern Physics B **10** (13n14), 1755–1805.

Tanabe, K, and H. Nakada (2005), "Quantum number projection at finite temperature via thermofield dynamics," Phys. Rev. C **71**, 024314.

Thompson, R C (2015), "Ion Coulomb crystals," Contemporary Physics **56**, 63.

Thouless, D J (1960), "Stability conditions and nuclear rotations in the Hartree-Fock theory," Nucl. Phys. **21**, 225.

Thouless, D J, and J. G. Valatin (1962), "Time-dependent Hartree-Fock equations and rotational states of nuclei," Nucl. Phys. **31**, 211.

Tomita, N (2004), "Many-body wave functions approximated by the superposition of spin-projected nonorthogonal Slater determinants in the resonating Hartree-Fock method," Phys. Rev. B **69**, 045110.

Tomita, N (2009), "Visualization of quantum fluctuations by superposition of optimized nonorthogonal Slater determinants," Phys. Rev. B **79**, 075113.

Tsuchimochi, T, and T. Van Voorhis (2015), "Time-dependent projected Hartree-Fock," J. Chem. Phys. **142**, 124103.

Une, Tsutomu, Akitsu Ikeda, and Naoki Onishi (1976), "Collective Hamiltonian in the generator coordinate method with local gaussian approximation," Prog. Theor. Phys. **55**, 498.

Valatin, J G (1961), "Generalized Hartree-Fock method," Phys. Rev. **122**, 1012–1020.

Valor, A, J.L. Egido, and L.M. Robledo (1996), "Approximate particle number projection for finite range density dependent forces," Phys. Rev. C **53**, 172–175.

Valor, A, J.L. Egido, and L.M. Robledo (1997), "A new approach to approximate symmetry restoration with density dependent forces: The superdeformed band in ^{192}Hg," Physics Letters B **392** (3), 249 – 254.

Valor, A, P.-H. Heenen, and P. Bonche (2000), "Configuration mixing of mean-field wave functions projected on angular momentum and particle number: Application to ^{24}Mg," Nuclear Physics A **671** (1), 145 – 164.

Varshalovich, DA, A.N. Moskalev, and V.K. Khersonskii (1988), *Quantum Theory of Angular Momentum* (World Scientific, Singapore).

Villars, F (1957), "The collective model of nuclei," Annu. Rev. Nucl. Sci. **7**, 185–230.

Villars, F, and G. Cooper (1970), "Unified theory of nuclear rotations," Ann. Phys. (N.Y.) **56** (1), 224 – 258.

Vretenar, D, A. V. Afanasjev, G.A. Lalazissis, and P. Ring (2005), "Relativistic hartree-bogoliubov theory: static and dynamic aspects of exotic nuclear structure," Phys. Rep. **409**, 101.

Wahlen-Strothman, J M, and G. E. Scuseria (2016), "Biorthogonal projected energies of a Gutzwiller similarity transformed Hamiltonian," J. Phys. Cond. Matt. **28**, 485502.

Walecka, J D (1974), "A theory of highly condensed matter," Ann. Phys. (N.Y.) **83** (2), 491 – 529.

Wang, XB, J. Dobaczewski, and M. Kortelainen (2018), to be submitted to Journal of Physics G.

Wang, XB, J. Dobaczewski, M. Kortelainen, L.F. Yu, and M.V. Stoitsov (2014), "Lipkin method of particle-number restoration to higher orders," Phys. Rev. C **90**, 014312.

Wigner, E (1934), "On the interaction of electrons in metals," Phys. Rev. **46**, 1002.

Wilczek, F (2012), "Quantum time crystals," Phys. Rev. Lett. **109**, 160401.

Wineland, D J, J. C. Bergquist, Wayne M. Itano, J. J. Bollinger, and C. H. Manney (1987), "Atomic-ion Coulomb clusters in an ion trap," Phys. Rev. Lett. **59**, 2935–2938.

Wootters, W K (1998), "Entanglement of formation of an arbitrary state of two qubits," Phys. Rev. Lett. **80**, 2245.

Wunsch, B, T. Stauber, and F. Guinea (2008), "Electron-electron interactions and charging effects in graphene quantum dots," Phys. Rev. B **77**, 035316.

Yang, N, J.-L. Zhu, and Z. Dai (2008), "Rotating Wigner molecules and spin-related behaviors in quantum rings," J. Phys.: Condens. Matter **20**, 295202.

Yannouleas, C, and U. Landman (1995), "Electronic shell effects in triaxially deformed metal clusters: A systematic interpretation of experimental observations," Phys. Rev. B **51**, 1902.

Yannouleas, C, and U. Landman (1997), "Electronic entropy, shell structure, and size-evolutionary patterns of metal clusters," Phys. Rev. Lett. **78**, 1424.

Yannouleas, C, and U. Landman (1999), "Spontaneous symmetry breaking in single and molecular quantum dots," Phys. Rev. Lett. **82**, 5325.

Yannouleas, C, and U. Landman (2000a), "Collective and independent-particle motion in two-electron artificial atoms," Phys. Rev. Lett. **85**, 1726.

Yannouleas, C, and U. Landman (2000b), "Decay channels and appearance sizes of doubly anionic gold and silver clusters," Phys. Rev. B **61**, R10587.

Yannouleas, C, and U. Landman (2000c), "Formation and control of electron molecules in artificial atoms: Impurity and magnetic-field effects," Phys. Rev. B **61**, 15895.

Yannouleas, C, and U. Landman (2001), "Coupling and dis-

sociation in artificial molecules," The European Physical Journal D - Atomic, Molecular, Optical and Plasma Physics **16** (1), 373–380.

Yannouleas, C, and U. Landman (2002a), "Magnetic-field manipulation of chemical bonding in artificial molecules," International Journal of Quantum Chemistry **90** (2), 699–708.

Yannouleas, C, and U. Landman (2002b), "Strongly correlated wavefunctions for artificial atoms and molecules," Journal of Physics: Condensed Matter **14** (34), L591.

Yannouleas, C, and U. Landman (2002c), "Trial wave functions with long-range Coulomb correlations for two-dimensional N-electron systems in high magnetic fields," Phys. Rev. B **66**, 115315.

Yannouleas, C, and U. Landman (2003a), "Group theoretical analysis of symmetry breaking in two-dimensional quantum dots," Phys. Rev. B **68**, 035325.

Yannouleas, C, and U. Landman (2003b), "Two-dimensional quantum dots in high magnetic fields: Rotating-electron-molecule versus composite-fermion approach," Phys. Rev. B **68**, 035326.

Yannouleas, C, and U. Landman (2004a), "Structural properties of electrons in quantum dots in high magnetic fields: Crystalline character of cusp states and excitation spectra," Phys. Rev. B **70**, 235319.

Yannouleas, C, and U. Landman (2004b), "Unified description of floppy and rigid rotating Wigner molecules formed in quantum dots," Phys. Rev. B **69**, 113306.

Yannouleas, C, and U. Landman (2006a), "Electron and boson clusters in confined geometries: Symmetry breaking in quantum dots and harmonic traps," Proc. Natl. Acad. Sci. USA **103**, 10600 (Special Feature).

Yannouleas, C, and U. Landman (2006b), "Symmetry breaking and Wigner molecules in few-electron quantum dots," phys. stat. sol. (a) **203**, 1160.

Yannouleas, C, and U. Landman (2007), "Symmetry breaking and quantum correlations in finite systems: Studies of quantum dots and ultracold Bose gases and related nuclear and chemical methods," Rep. Prog. Phys. **70**, 2067.

Yannouleas, C, and U. Landman (2010), "Quantal molecular description and universal aspects of the spectra of bosons and fermions in the lowest Landau level," Phys. Rev. A **81**, 023609.

Yannouleas, C, and U. Landman (2011), "Unified microscopic approach to the interplay of pinned-Wigner-solid and liquid behavior of the lowest Landau-level states in the neighborhood of $\nu = \frac{1}{3}$," Phys. Rev. B **84**, 165327.

Yannouleas, C, and U. Landman (2017), "Trial wave functions for ring-trapped ions and neutral atoms: Microscopic description of the quantum space-time crystal," Phys. Rev. A **96**, 043610.

Yannouleas, C, U. Landman, Bréchignac, C., Ph. Cahuzac, B. Concina, and J. Leygnier (2002), "Thermal quenching of electronic shells and channel competition in cluster fission," Phys. Rev. Lett. **89**, 173403.

Yao, J M, M. Bender, and P.-H. Heenen (2013), "Systematics of low-lying states of even-even nuclei in the neutron-deficient lead region from a beyond-mean-field calculation," Phys. Rev. C **87**, 034322.

Yao, J M, and J. Engel (2016), "Octupole correlations in low-lying states of ^{150}Nd and ^{150}Sm and their impact on neutrinoless double-β decay," Phys. Rev. C **94**, 014306.

Yao, J M, and K. Hagino (2016), "Anharmonicity of multi-octupole-phonon excitations in 208Pb: analysis with multi-reference covariant density functional theory and subbarrier fusion of 16O+208Pb," Phys. Rev. C **94**, 011303.

Yao, J M, K. Hagino, Z. P. Li, J. Meng, and P. Ring (2014), "Microscopic benchmark-study of triaxiality in low-lying states of 76kr," Phys. Rev. C **89**, 054306.

Yao, J M, H. Mei, H. Chen, J. Meng, P. Ring, and D. Vretenar (2011), "Configuration mixing of angular-momentum-projected triaxial relativistic mean-field wave functions. II. Microscopic analysis of low-lying states in magnesium isotopes," Phys. Rev. C **83**, 014308.

Yao, J M, J. Meng, P. Ring, and D. Pena Arteaga (2009), "Three-dimensional angular momentum projection in relativistic mean-field theory," Phys. Rev. C **79**, 044312.

Yao, J M, J. Meng, P. Ring, and D. Vretenar (2010), "Configuration mixing of angular-momentum-projected triaxial relativistic mean-field wave functions," Phys. Rev. C **81**, 044311.

Yao, J M, L. S. Song, K. Hagino, P. Ring, and J. Meng (2015a), "Systematic study of nuclear matrix elements in neutrinoless double-beta decay with a beyond-mean-field covariant density functional theory," Phys. Rev. C **91**, 024316.

Yao, J M, E. F. Zhou, and Z. P. Li (2015b), "Beyond relativistic mean-field approach for nuclear octupole excitations," Phys. Rev. C **92**, 041304.

Yao, Jiang-Ming, Simone Baroni, Michael Bender, and Paul-Henri Heenen (2012), "Beyond-mean-field study of the possible "bubble" structure of ^{34}Si," Phys. Rev. C **86**, 014310.

Yoccoz, J (1957), "On the Moments of Inertia of Nuclei," Proc. Phys. Soc. A **70** (5), 388.

Yoccoz, J (1966), Varenna Lectures **36**, 474.

Zduńczuk, H, W. Satuła, J. Dobaczewski, and M. Kosmulski (2007), "Angular momentum projection of cranked Hartree-Fock states: Application to terminating bands in $A \sim 44$ nuclei," Phys. Rev. C **76**, 044304.

Zeh, HD (1965), "Symmetry violating trial wave functions," Z. Phys. **188**, 361.

Zeng, G-M, L.-A. Wu, and H.-J. Xing (2014), "Symmetry restoration and quantumness reestablishment," Sci. Rep. **4**, 6377.

Zhao, P W, Z. P. Li, J. M. Yao, and J. Meng (2010), "New parametrization for the nuclear covariant energy density functional with a point-coupling interaction," Phys. Rev. C **82**, 054319.

Zhao, P W, P. Ring, and J. Meng (2016), "Configuration interaction in symmetry conserving covariant density functional theory," Phys. Rev. C **94**, 041301.

Zheng, D C, D. W. L. Sprung, and H. Flocard (1992), "Pairing correlations studied in the two-level model," Phys. Rev. C **46**, 1355–1363.

Zhou, En-fu, Jiangming Yao, Zhipan Li, Jie Meng, and Peter Ring (2016), "Anatomy of molecular structures in 20Ne," Phys. Lett. B **753**, 227–231.

Zhu, H, Y. P. Chen, P. Jiang, L. W. Engel, D. C. Tsui, L. N. Pfeiffer, and K. W. West (2010), "Observation of a pinning mode in a Wigner solid with $\nu = 1/3$ fractional quantum Hall excitations," Phys. Rev. Lett. **105**, 126803.

Zürn, G, F. Serwane, T. Lompe, A. N. Wenz, M. G. Ries, J. E. Bohn, and S. Jochim (2012), "Fermionization of two distinguishable fermions," Phys. Rev. Lett. **108**, 075303.